UAB
Universitat Autònoma de Barcelona

NIR LIGHT CONTROLLED RELEASE OF Pt(II) BY MEANS OF UPCONVERSION NANOPARTICLES

Marc Ricard Batten Vera
PhD in Chemistry
PhD Thesis
2023

Supervisors:
Dr. Pau Bayón
Dr. Oscar Palacios

UAB
Universitat Autònoma de Barcelona

NIR LIGHT CONTROLLED RELEASE OF Pt(II) BY MEANS OF UPCONVERSION NANOPARTICLES

Marc-Ricard Batten Vera

PhD Thesis

Ph. D. in Chemistry

2023

Supervisors:

Dr. Pau Bayón Rueda

Dr. Òscar Palacios Bonilla

Manuscript presented to obtain the PhD Degree by Marc-Ricard Batten Vera

Marc-Ricard Batten Vera

With the approval of the supervisors of the Doctoral Thesis, Dr. Pau Bayón Rueda and Dr. Òscar Palacios Bonilla

ACKNOWLEDGEMENTS

sé que arribaràs lluny a la vida, gràcies per totes les xerrades, les tonteries i riures que ens hem fet, hem de seguir igual. Dani Torralba, el cuñado, el que té el rècord d' hores treballant el laboratori, estic molt content d'haver pogut compartir aquests anys de doctorat amb tu, et vaig conèixer abans del doctorat i ara som molt amics, ets una persona impressionant, espero que hagis gaudit igual que jo del nostre temps treballant junts, el nostre humor especial (el teu costat em ric molt), les festes, sopars i més, gràcies per tota la teva ajuda, aguantar-me de les meves queixes i ànims en acabar la tesi. Roger, ets una gran persona, m'ha encantat treballar amb tu i gràcies per totes l'ajuda i xerrades que hem tingut. De les últimes persones en entrar en el laboratori Aleix Quintana, el model, no sé com t'ho fas, però tot el que fas, ho fas amb elegància, llàstima no haver compartit tan de temps amb tu, però tot el temps que he passat el teu costat m'ho he passat molt bé, espero que puguem seguir quedant i tenir més moments divertits.

Xavier Baami, Josep Gutierrez, Joana Daussà i Gustavo López, tots vosaltres sou grans treballadors, aquest treball també s'ha pogut realitzar gràcies a la vostra ajuda, espero que us vagi molt bé el vostre futur i estiguem en contacte. Voldria agrair a tots el TFGs que han passat pel laboratori: David Pla, Ainoa Castaño, Arnau, Raul, Pablo, Robert hem gaudit de molt bons moments el laboratori

M' agradaria agrair també a Sergio Jurado, Gisela Cabré, Rubén, Amanda per tots els moments que hem passat junts, sopars, xerrades, i ajuda, he sigut afortunat de poder treballar amb vosaltres.

Del laboratori d' inorgànica, l'altra part del grup, vull començar per la Gloria, ets tan bona persona, m'has ajudat tan, gràcies per tots els consells, per animar-me i totes les xerrades. Quim, vull que sàpigues que ets una persona increïble, t'admiro molt, m'has transmès tans coneixements, sempre disposat a ajudar-me, gràcies per tot. Mario, amb tu m'he fet un fart de riure, amb els teus acudits i sempre has estat disposat ajudar-me tot. Fatima, lots of encouragement to finish, it is hard but you will get it because I know you are a very hard worker, thanks for all the talks.

Vull seguir agraint la resta de gent orgànica. Cris, m'has ajudat i animat molt, conèixer-te ha sigut de les millors coses que m'han passat, gràcies per tots els moments divertits i els que tindrem, ets una gran persona i hem de seguir gaudint junts. Albert Gallego, vaig conèixer el teu pare abans que tu, ell és un grande, però tu estàs a un level més alt, m'ho passo tan bé el teu costat, totes les festes, xerrades, sopar, Vinya Rock, vull dir-te que ets una gran persona i que sé que si segueixes amb aquesta actitud arribaràs molt lluny, vull que seguim quedant per poder explicar més anècdotes. Axel, la meva parella del calendari 2024, som la parella més sexy que hi ha i ho saps, no hem pogut estar molt de temps junts, perquè quan tu començaves, jo ja acabava, però vull que seguim quedant per sopar, casa rural, etc. Perquè m'ho passo molt bé el teu costat. Marc Villabona i Arnau, gràcies per tota l' ajuda que m'heu proposionat, tots els ànims i coneixements que m'heu donat, us estic molt agraït. Granados, la Autònoma ha fet el millor fitxatge que existeix, gràcies per aguantar totes les meves queixes i animar-me a seguir endavant.

Guillem Fernández, Carolina Gascó, Kevin Reyes, Laura Parejo, Ferran, Salabert, Joel, gràcies per tots els moments divertits, tots els ànims, sopars, dinars, cases rurals, etc. El vostre costat m'ho he passat molt bé.

Anna Broto, estic molt agraït perquè sense la teva motivació que donaves, els teus ànims, totes les xerrades, els cafès, berenars, esmorzars, etc. No hauria pogut acabar aquesta tesi, has sigut un peça clau. Ànims amb el postdoc, sé que ets una gran persona que arribarà molt lluny. Adrià Crespo, espero que et vagi molt bé el postdoc, t'agreixo tots els esmorzars i cafès que hem fet junts. Totes les xerrades i bons moments, encara ens devem una birra que hem de fer recorda. Una promesa és una promesa.

Els biòlegs Sergi Rodriguez i David Montpeyó, m'heu ajudat tan i m'heu transmès tans coneixements. Moltes gràcies per tota l'ajuda que m'heu donat, de treure el temps d'on sigui per mi, ja que sempre aneu superenfeinats i per aguantar-me perquè sé que soc un "pesado".

Els analítics Rodry, Anna, Elena i Mireia gràcies per ajudar-me durant la tesis, per animar-me, pels cafès que hem fet junts, sopars i totes les birres, espero que us vagi molt bé tot. Me gustaría agradecer toda la gente de Portugal: Daniela, eres la mejor persona que conozco, gracias por toda la ayuda, por tus conocimientos, todos los Kinder Buenos, McFlurrys,

me lo pase muy bien a tu lado, espero que te vaya muy bien todo. Tatiana y Lina, sois muy buena gente, me divertí mucho a vuestro lado, que buenos momentos me he llevado con vosotras, espero que os vaya muy bien todo. A toda la gente del grupo 3C's muchas gracias por la ayuda en mi estancia. Fernando Maturi gracias por toda la ayuda con el láser, aunque parecía que los experimentos no iban bien, gracias a tus ánimos y ayuda el final lo conseguimos. Jaime, David, Silvia, Cos, Fernando, Jone, Adri, Valeria, Iraitz y toda la gente que conocí muchas gracias por todas las cervezas al Mercado Negro, las fiestas, excursiones y todos los buenos momentos, disfruté mucho de la estancia a Portugal gracias a vosotros, tenemos de volver a vernos.

Marc, Agustí, Anna, Cris, Sergi, Xavi sou el meu grup del màster i encara que estem separats i quedem poc, sempre m'ho passo molt bé el vostre costat, gràcies pels ànims tots aquests anys. Jaume, vam començar el doctorat junts i cada cop ens hem anat unint més, ets un gran amic i t'estic agraït per tots els cafès que hem fet junts, la teva ajuda, els teus ànims, ara te n'aniràs als Estats Units, et trobaré a faltar, però sé que t'espera un gran futur. Carla, també et volia agrair-te tota la teva ajuda, ets la millor professora que conec, m'has ajudat molt i preocupat per la tesis, espero algun dia poder-te tornar-te tots els favors que et dec, moltes gràcies per tot, ets la millor!!

Masin, Jordi, Alex, Alexia, Anna, Albert, Bernat, Pinto, David heu de saber que vosaltres heu sigut molt clau en aquesta etapa, si hagués de dir totes les coses bones que penso de cada un de vosaltres, aquests agraïments s'allargarien a moltes pàgines. Tots vosaltres sou imprescindibles a la meva vida, no us canviaria per res del món, hem tingut tans bons moments junts, tantes aventures, vull que seguim igual o millor. Us estic agraït per tots els ànims, ajuda, bons moments que hem viscut. Sense vosaltres no hauria pogut acabar aquest doctorat, gràcies per estar sempre el meu costat.

Ara voldria agrair a la gent més important que tinc el meu costat, tota la gent de Calella: Baños, Eloi, Xai, Hagen, Manel, Marc, Mesa, Robert, Aitor, Nuria (també t'incloc el grup encara que no siguis de Calella) i Miki. No sé com dir-vos que us estic agraït per tot el que feu per mi, encara que no sigueu químics, sempre heu estat el meu costat i m'heu donat suport amb tot, sense vosaltres no hauria arribat tan lluny. Són tans anys d' amistat que sé que acabarem junts per sempre, vull que sapigueu que aquesta tesi és tan vostre com meva, perquè sense vosaltres al meu costat no s'hauria pogut fer aquest treball. VISCA CALELLA, LA DE VERDAD!!!!

Martina fa poc vas entrar a la meva vida i, des de llavors, has demostrat ser una persona increïble. Sempre estàs disposada a ajudar-me a qualsevol moment. Has estat la font de la meva força i esperança, ajudant-me a veure claredat quan tot semblava perdut en aquesta fase final de la tesis. Amb tu el meu costat, aquest final d'etapa no ha estat tan difícil. Em considero afortunat de tenir-te al meu costat i estic emocionat per començar una nova etapa al teu costat.

Finalment a la meva família: Guillem, Patrick, mama i nana després de tans anys aguantant-me de saber quan acabaré la tesis, us haig de dir que ja s'està acabant. Us estimo molt, hem passat moments difícils però una cosa s'ha de dir, sempre hem estat junts. Sempre m'heu animat amb tot, us heu preocupat de com m'anava el doctorat, m'heu ensenyat a no rendir-me. Us vull dir que aquest logro és tan meu com vostre. Tinc una sort de teniu-vos, ara vindrà una nova etapa i la farem junts com tot.

TABLE OF CONTENTS

Table of Contents

Abstract

Cancer chemotherapy is limited by severe side effects due to unspecific cytotoxicity activity of currently used therapies, especially Pt(II)-based drugs. In order, to minimize these unwanted effects, several approaches relying on the use of light to activate the drugs have been taken. This methodology is a promising strategy to selectively activate cytotoxicity drugs at their site of action and thus to improving the tolerability and safety of chemotherapy. However, the majority of Pt(II) photosensitive anticancer compounds respond to short wavelengths, which damage healthy cells and have low penetration depths in tissues. The use of upoconversion nanoparticles (UCNPs) to locally transform near infrared (NIR) light into higher energy radiation at the desired site allows overcoming this issue. The use of these systems permits reducing systematic toxicity, increasing the cellular uptake and improving therapeutic effect while reducing undesirable side effects.[1]

In this work, a platform that contains two new Pt(II)-photosensitive complexes anchored to UCNPs has been developed. These complexes were shown to be stable in the dark and activated by UV-light. They were combined with $LiYF_4$; Yb^{3+}, Tm^{3+} UCNPs, which upon absorption of NIR light generate UV upconverted emission, thus activating the Pt(II)-complexes. In order to improve the solubility of the platform in aqueous media these UCNPs were coated with poly(ethyleneglycol)-methyl-eher-ocatadecyl-amine (mPEG-ODA). Irradiation with the more penetrating NIR-light, which is less energetic than UV and visible light, may provoke less damage in the treated tissues.

This new platform exhibits the same Pt(II) release after irradiating with either UV or NIR-light corroborating the quantitative light conversion. Furthermore, this nanosystem increased the cytotoxicity significantly in A375 melanoma cancer cells after exposure to 980 nm radiation. The achieved–results indicate that the proposed nanoplatform provides a new tool to use UCNPs combined with Pt(II)-photoresponsive to generate interesting platforms for photoactivated chemotherapy application using NIR-light.

ABBREVIATIONS

Abbreviations

5CNU	5-cyanouracil
APTES	(3-Aminopropyl) triethoxysilane
bpy	Bipyridine
CD	Circular Dichroism
CDDP	cisplatin
CT	charge transfer
cur	curcumin
DACH	1,2-diaminocyclohexane
DLS	Dynamic light scattering
DMF	Dimethylformamide
DMSO	Dimethyl sulfoxide
DNA	deoxyribonucleic acid
dox	doxorubicin
EDX	Energy-dispersive X-Ray
en	ethylenediamine
ESA	Excited state absorption
ESI	Electrospray ionization
ETU	Energy transfer upconversion
EWG	Electron withdrawing group
GSH	Glutathione
HBTU	Hexafluorophosphate Benzotriazole Tetramethyl Uronium
HOBt	hydroxybenzotriazole
HPPH	2-(1-Hexyloxyethyl)-2-devinyl pyropheophorbide-a
IC$_{50}$	Half maximal inhibitory concentration
ICP-MS	Inductively coupled plasma mass spectrometry
ICP-OES	Inductively coupled plasma optical emission spectroscopy
LC	Ligand-centred
LMCT	Ligand-to-metal charge transfer
MA	Methylamine
MC	Metal centred
MLCT	Metal-to-ligand charge transfer
mPEG	Poly(ethylene glycol) methyl ether
MTT	[3-(4,5-Dimethylthiazol-2-yl)-2,5-Diphenyltetrazolium Bromide]
NAMPT	Nicotinamide phosphoribosyltransferase
nap	naproxen

Abbreviations

NIR	Near Infrared	**WHO**	World Health Organization
OAc	Acetoxy group	**XRD**	X-Ray Diffraction
ODA	Octadecylamine		
_o_-NB	_orto_-Nitrobenzyl		
PA	photoavalanche		
PACT	Photoactivated chemotherapy		
PBS	Phosphate buffer saline		
PDT	Photodynamic therapy		
PEG	Polyethylene Glycol		
Phen	Phenyl		
Phena	Phenanthroline		
PPG	Photolabile Protecting Group		
PS	Photosensitiser		
PTT	Photothermal therapy		
Py	Pyridine		
ROS	Radical oxygen species		
STEM	Scanning Transmission Electron Microscopy		
TEMPO	(2,2,6,6-Tetramethylpiperidin-1-yl)oxyl		
THF	Tetrahydrofuran		
UCNPs	Upconversion nanoparticles		
UV	Ultraviolet		
Vis	Visible		

STRUCTURE INDEX

Structure Index
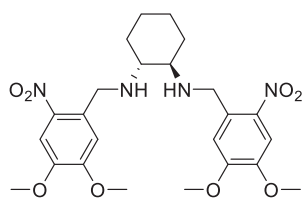
L1
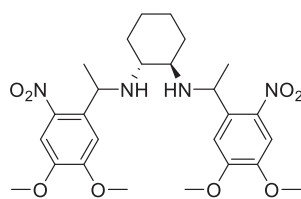
L2

C1

C2

1

2

3

4

5

6

7

8

9

10

9
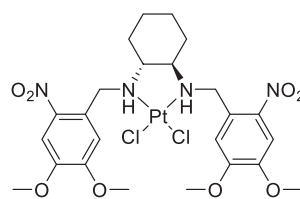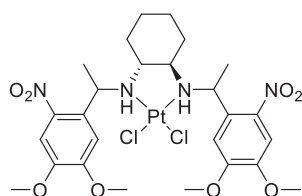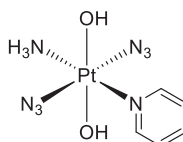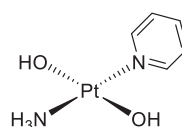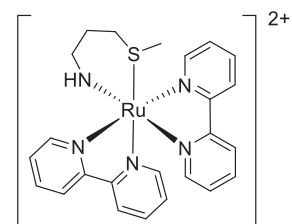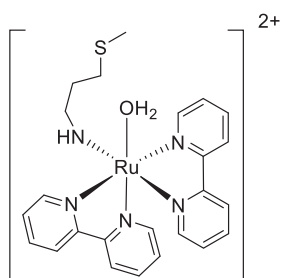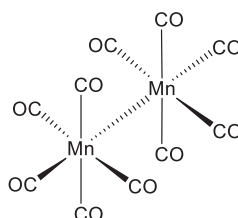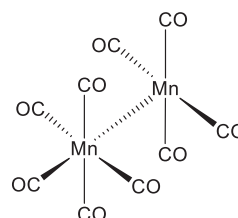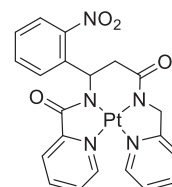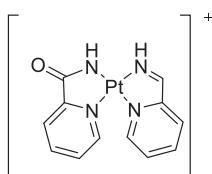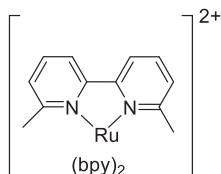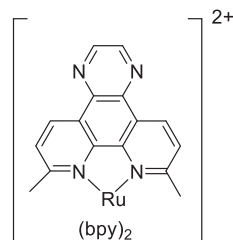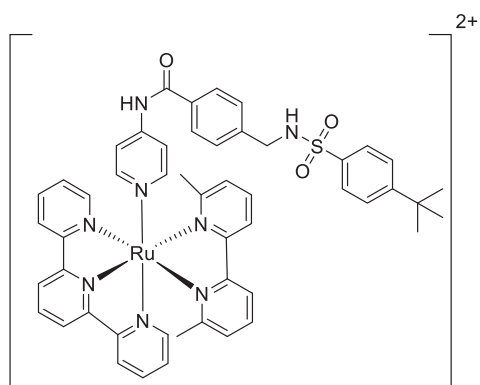
11
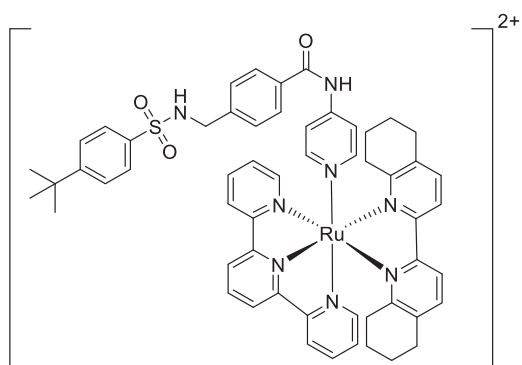
12
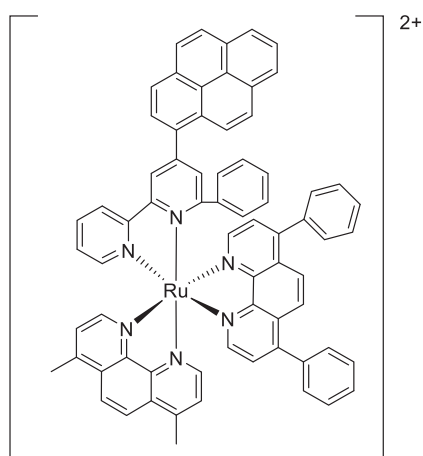
13
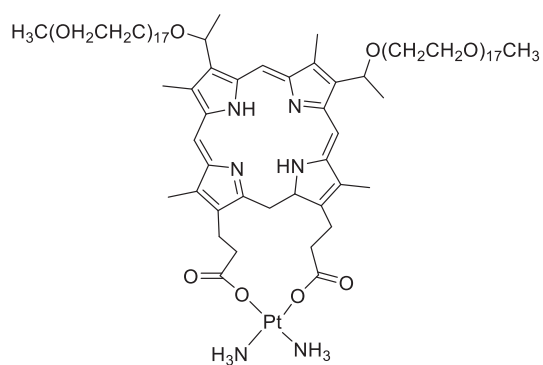
14
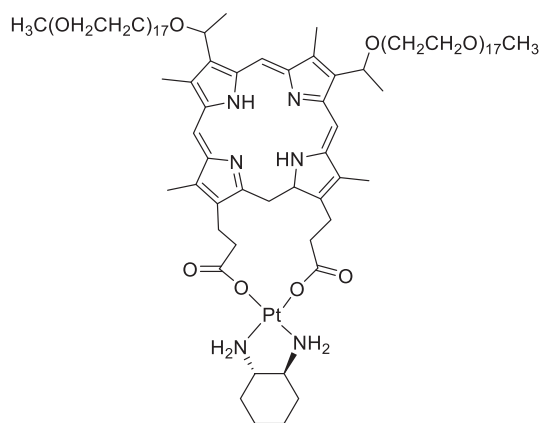
15
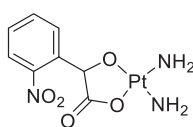
16
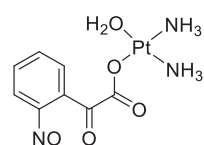
17
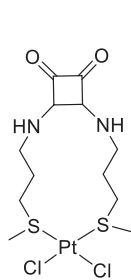
18
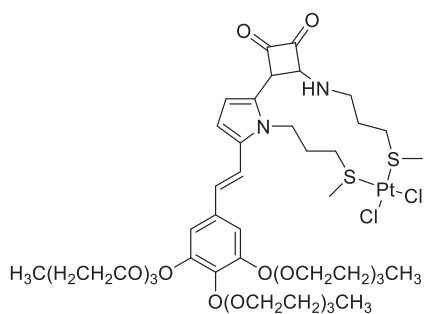
19
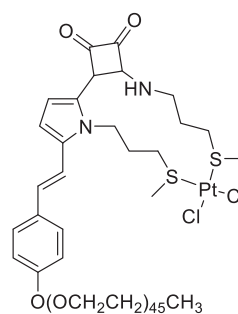
20
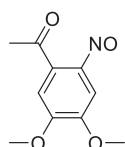
21
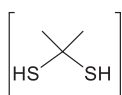
22
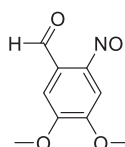
23
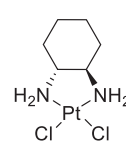
24
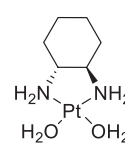
25
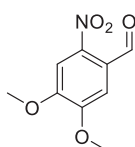
26
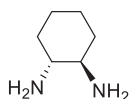
(±)-27
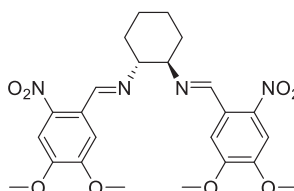
28
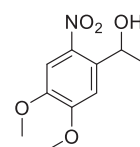
29
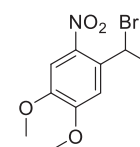
30

31

32

33

34

35

36

37

11
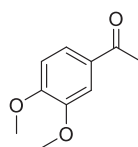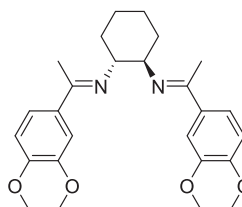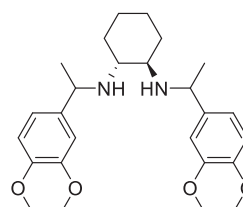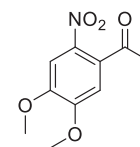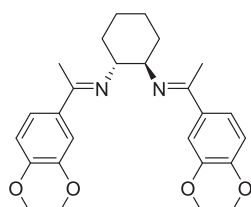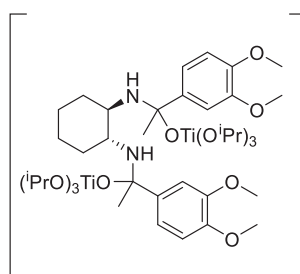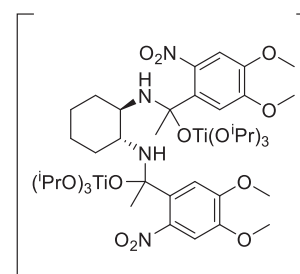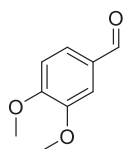
38
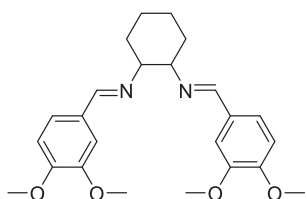
39
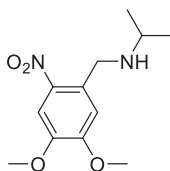
40
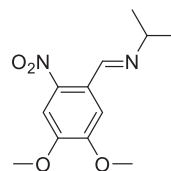
41

42
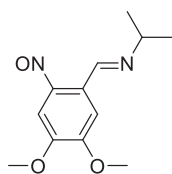
43
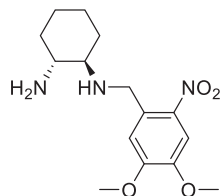
44
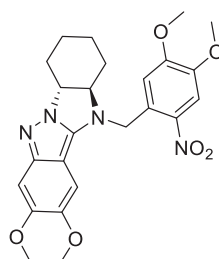
45
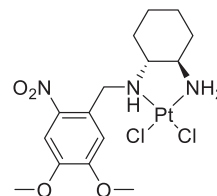
46
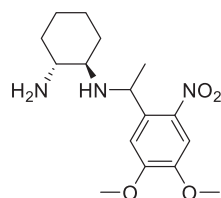
47
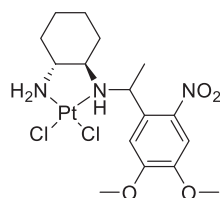
48

CHAPTER 1

GENERAL INTRODUCTION

1. General Introduction

1.1 Cancer

Cancer is a group of diseases that involves the growth of abnormal cells that can start in almost any organ or tissue in the body and can invade or spread to other parts of the body (metastasis), which is the leading cause of death in cancer. Human cells usually growth and divide until they reach their limit. When a normal cell becomes damaged or "old", it is naturally programmed to die, this process is called *apoptosis.* In contrast, cancer cells grow and reproduce without control. This uncontrolled growth of cell leads to form a tumour.[1]

The meaning of tumour is not the same as cancer. There are two types of tumours depending on the type of cells involved:[2,3]

- Benign tumours: These types of tumours are noncancerous but contain abnormal cells. They usually develop slowly and does not invade other body tissues.
- Malignant tumours: The cancerous tumours grow and spread rapidly to other body tissues through bloodstream (metastasis).

Cancer is the result of a genetic disease caused by a mutation of the deoxyribonucleic acid (DNA) and consequently an uncontrolled proliferation of cells.[4] This change can transform a normal cell into a cancerous cell. These abnormal cells are characterized by the follow hallmarks:[4,5]

- Maintain proliferative signalling.
- Evade growth suppressors.
- Activate invasion and metastasis.
- Enable replicative immortality.
- Induce angiogenesis.
- Resist to cell death (*apoptosis*)

Cancer is the second leading cause of death worldwide, after cardiovascular diseases, and responsible for approximately 9.6 million deaths, or one in six deaths, in 2018. There are about a hundred types of cancer, being the most common in men: lung, prostate, colorectal, stomach and liver cancer. On the other hand, the most common ones in women are: breast, colorectal, lung, cervical and thyroid cancer.[6] Lung cancer is the leading cause of cancer deaths worldwide followed by liver, colorectal, stomach and breast cancer.[7]

Chemotherapy, radiotherapy and surgery are the most common techniques for treating tumours.[8] Nowadays, immunotherapy has become the fourth treatment option for tumours.[9] Each treatment is used depending on the type of cancer and its location. Often, these techniques are combined to improve their efficacy.[10,11]

Surgery and radiotherapy are the main therapy when the disease is at the early stage.[10]

Cancer surgery is the most effective treatment, as it involves removing the tumour from the tissue using manual and instrumental techniques.[12] Many solid cancers have been successfully treated by surgical excision of the tumour.[13, 14] However, this approach cannot be used to treat metastatic tumours.[11]

Cancer radiotherapy use ionising radiation (X-ray, gamma rays) to kill malignant cells by damaging DNA.[15] Nevertheless, this radiation also affects surrounding healthy tissues. For this reason, this treatment has severe limitations.[16]

Immunotherapy is a treatment that involves the administration of a very personal and specific drug that helps the immune system of the body to recognise and attack the cancer cells. This therapy has some limitations because it cannot be applied to all types of cancer.[17, 18]

Chemotherapy is the most widely applied anticancer therapy that consists in the administration of a drug. The chemotherapeutic agent, with specific concentrations and administration, reaches the tumour and can prevent the division of the cells, causing their death. This treatment is mostly used for cancer in advanced stages.[19,20]

1.1.1. Cancer chemotherapy

Cancer chemotherapy is a crucial remedy to treat solid tumours, involving the administration of cytotoxic chemicals with the aim of destroying or, at least, reduce the malignant tumour and preventing it from proliferating.[21]

The German scientist Paul Ehrlich was the founder of inorganic chemotherapy, whose research was based on using alkylating agents to treat various diseases. He developed a cure against the syphilis using an inorganic compound called Arsephamine.[22,23] The use of chemotherapy to treat cancer began in the mid-20th century, after the Second World War.[23,24]

Before chemotherapy, X-Ray was mainly used to treat cancer. In 1943, Gilman discovered that the mustard gas which was used in wars to incapacitate the enemy and contaminate the battlefield, formed an alkylating agent that prevent DNA replication and produced a decrease in white blood cells concentration. Between 1946 and 1948, nitrogen

mustard was clinically applied to treat lymphoma, becoming the first anti-cancer drug in chemotherapy. [23–25] Since then, new anticancer agents have been applied in chemotherapy including alkylating agents, antimetabolites, nitrosoureas, antitumour antibiotics, topoisomerase inhibitors, antimitotic, and corticosteroids (**Figure 1.1**). Among all these medicines, the most notably were 5-fluoroacil (1957), methotrexate (1958) and cisplatin (1971). [26]

In the 1970s a breakthrough in cancer treatment was the appearance of adjuvant therapies that consist of applying chemotherapy treatment after surgery or radiotherapy.[26] This combination was crucial because it reduced the chances of the patient relapsing back into cancer. Furthermore, many anti-cancer medications with different mechanism were combined to increase the efficacy of the treatment.[21]

Nowadays, research is still underway to develop more effective and selective anticancer agents. To this end, special interest is being placed on the use of metallodrugs and, due to the efficiency of drugs such as cisplatin and its derivatives, current research is focusing especially on platinum-based metal complexes.
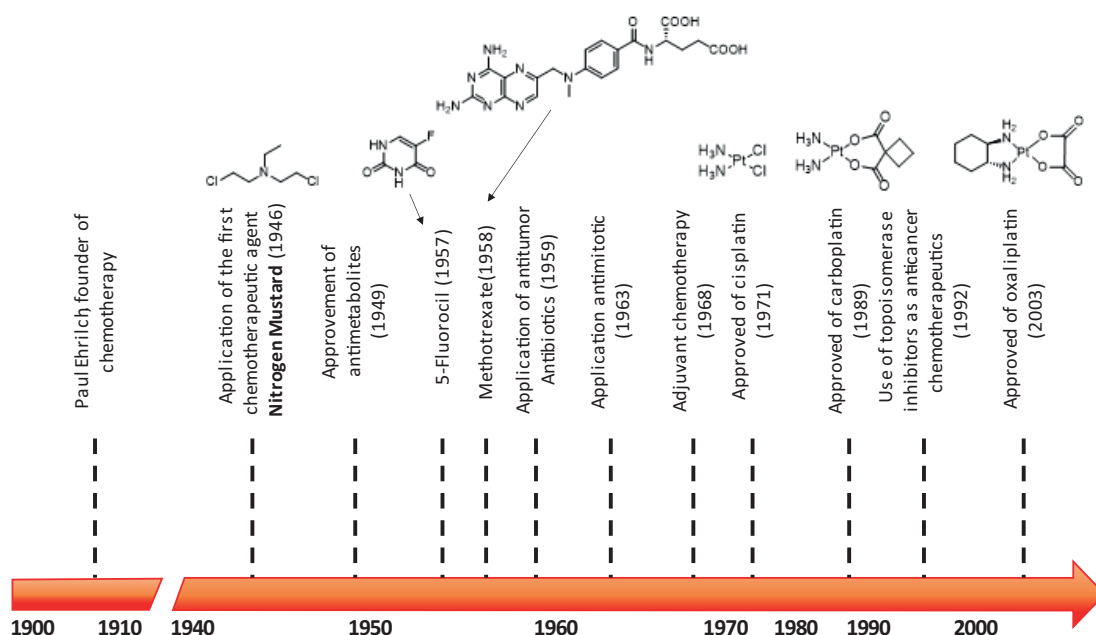
Figure 1.1: The evolution of cancer chemotherapy since the 1900s[26]

1.1.1.1. Pt(II) anticancer drugs in chemotherapy

Since 1950's cytotoxic drugs have been used as the standard anti-cancer treatment. These drugs work by damaging DNA and interfering with their metabolism preventing cancer cells from growing and dividing, leading to *apoptosis*.[27]

Since the discovery of the anticancer activity of cisplatin or *cis*-diamminedichloroplatinum (CDDP) by Barnnet E. Rosenberg and colleagues, a new pathway of cancer treatment was unlocked using metal complexes to inhibit tumours.[28] Cisplatin and its derivates are still used in more than 50% of treatments for cancer patients in the clinic. Specifically, CDDP is the most widely used platinum complex in chemotherapy for ovarian, testicular, lung, breast, bladder, neck cancer and brain tumours. In 1964 Barnnet E. Rosenberg discovered the anti-cancer activity of CDDP through an electrochemical experiment.[29] The experiment consisted of applying current to *E. Coli* bacteria using platinum electrodes, which led to the cessation of bacteria division. Investigating of the cause of this growth inhibition led to the conclusion that a platinum complex formed on an electrode was responsible. This complex was later identified as CDDP. In 1971, patients were treated for the first time with cisplatin, and in 1978, the US Food and Drug Administration (FDA) approved its use in various cancer treatments.[30]

After the successful use of CDDP in the treatment of a variety of cancer, several other metal-complexes have been described as potential anticancer agents and some of them have reached their clinical use. Complexes containing different metals as Platinum, Palladium, Rhodium, Ruthenium, Copper, Iron and Gold have been employed.[31,32] These complexes have several advantages in comparison with other potential drugs, such as structure stability, structural variety (linear, square planar, octahedral) and kinetical stablility.[33] However, they are toxic and difficult to degrade, therefore they can cause apoptosis through oxidative stress in normal cells, but also DNA damage or alteration of enzymes or protein functions.[34]

Although the mechanism of action of cisplatin is not entirely clear, there are several hypotheses. The most accepted is that CDDP enters the cell through the copper transporter CTR1 or by passive diffusion (**Scheme 1.1**). Once inside the cell, CDDP undergoes a hydrolysis process. Chlorido ligands are replaced by H_2O during this process named aquation. This ligand-exchange is more likely to occur in the cytoplasm, where the chloride concentration is low ($\approx$ 20 mM), rather than in the bloodstream, where the chloride concentration is high ($\approx$ 100 mM). Once the diaquo-complex is formed, it can interact with *S*-containing molecules (i.e. metallothionein and glutathione) as well as covalently bind to DNA, as the positive charge of the complex is attracted to the negative charge mainly of the N_7 of the imidazole ring of guanine and adenine bases. When Pt binds to DNA they both form an adduct that can take two forms: interstrand crosslinks, which binds to two guanine nucleotides on the same strand, or intrastrand crosslinks, which bind to two guanines separated by one or more bases in a same strand. These adducts can initiate the *apoptosis* process.[30,35–37]
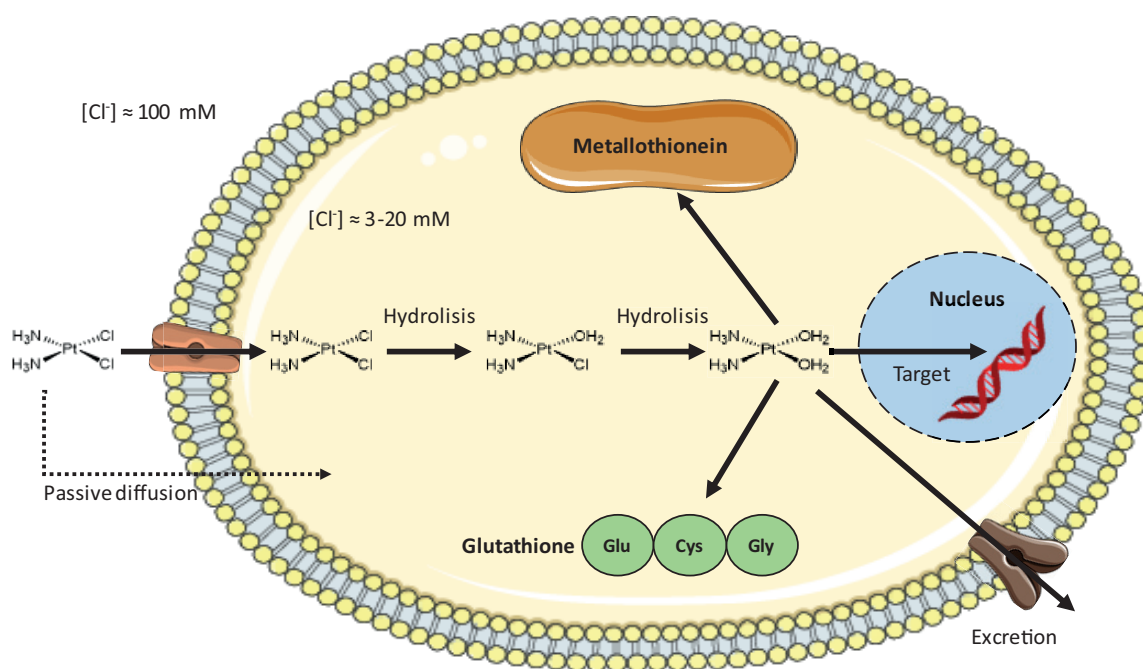
Scheme 1.1: Mechanism of action of CDDP by interaction with DNA as well as other S-containing molecules (metallothionein and glutathione).

The application of CDDP is limited due to several undesired side effects: the development of cancer cell resistance against the drug, low cell selectivity, and other associated side effects, such as kidney damage, nausea, vomiting, and bone marrow suppression.[38] Several mechanisms of CDDP resistance have been described, such as DNA-adduct repair, increased CDDP-glutathione complex due to Pt-S bond formation, reduced cellular accumulation of cisplatin due to lower cell uptake and increased cell efflux.[39]

Two new Pt(II)-complexes oxaliplatin ([Oxalate(2-)-O,O'][1R,2R-cyclohexanediamine-N,N']platinum(II)) and carboplatin (*cis*-diammine[1,1-cyclobutanedicarboxylato(2-)-O,O']platinum(II)) (**Figure 1.2**) were clinically approved against the disease with fewer side effects than CDDP.[40] Cisplatin, carboplatin and oxaliplatin are complexes with square-planar structures conformation about a central Pt(II) ion. All three also have two amino ligands as "non-leaving groups" that form stronger interactions with Pt(II) and "two leaving groups" (chlorides or carboxylates) that finally allow the Pt(II)-DNA adducts formation. In comparison with cisplatin, carboplatin and oxaliplatin show slower kinetics in the hydrolysis process and, moreover, their corresponding aquo-complexes are more stable. These two facts lead a decrease in their side effects.

Cisplatin   **Carboplatin**   **Oxaliplatin**
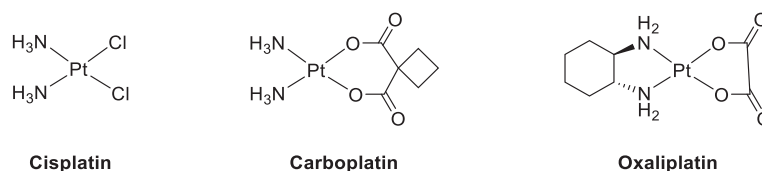
Figure 1.2: Structure of the anticancer Pt(II)-complexes clinically used in cancer treatment.

Carboplatin and cisplatin have the same mechanism of action. The difference between them is that carboplatin does not present nephrotoxicity and neurotoxicity. Carboplatin is commonly used in ovarian cancer.[41]

On the other hand, oxaliplatin, unlike the other two Pt(II)-complexes, after aquation, the resulting Pt(II)-diaminocyclohexane (DACH) complex forms an adduct with DNA which shows a greater degree of inhibition and cytotoxicity. It is believed that because DACH is a bulker ligand, it helps to have higher activity and avoids DNA repair by preventing the binding of repairing proteins. Oxaliplatin is commonly used in patients with colorectal metastases.[42]

Apart of these three Pt(II)-anticancer complexes which are in clinically use against cancer in all over the word, there are three additional Pt(II) anticancer drugs that are clinically approved in specific countries: nedaplatin, lobaplatin and heptaplatin (**Figure 1.3**).[43]

Nedaplatin   **Heptaplatin**   **Lobaplatin**
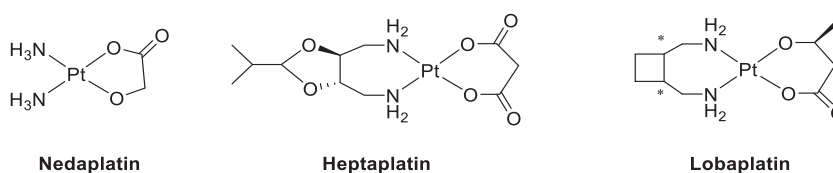
Figure 1.3: Structure of Pt(II)-anticancer drugs clinically approved in specific countries.

As all the above mentioned, these Pt(II) drugs also provoke unwanted side effect. Since they reach all tissues when administrated to patients. To overcome this drawback several new strategies are being proposed using new drugs (prodrugs) that allow the activation in an externally controlled manner by a specific stimulus such as light, ionising radiation, sonodynamic or heat.[44–47] Some alternatives consist in using prodrugs that are not toxic to cells, but easily activated with an external stimulus, such as pH, hypoxia, ultrasounds, or light. External stimuli need to be spatially and temporally precise, and light is the easiest stimulus to control.[48]

1.1.2. Phototherapy in cancer

Light has been used in medicine for thousands of years, dating back to ancient Egypt, China, and India, to treat different skin diseases, which combined the ingestion of plants with the sunlight for different treatments.[49,50] In modern times, the Danish physician Niels Fiensen

developed phototherapy, using red light to cure smallpox, and, ultraviolet light to cure tuberculosis, for which he won the Nobel Prize, in 1903.[51] Since then, light has been used for treatments in various fields of medicine.

In cancer treatment, the most studied phototherapies are:

- Photodynamic therapy (PDT): It uses non-toxic photosensitisers (PS) that are activated by visible light (Vis) and generate cytotoxicity through the formation of singlet oxygen ($^1O_2$) and other reactive oxygen species (ROS) to induce *apoptosis* in cancer cells.[52,53]

- Photothermal therapy (PTT): Near Infrared (NIR) light is used to irradiate the desired tissues. As a response, the sensitive administered drugs emit heat, producing thermal decomposition of cancer cells and therefore provoking their death. The most investigated materials for this therapy are inorganic nanomaterial such as gold, palladium or copper sulphides, and carbon nanoparticles.[54,55]

- Photoactivated chemotherapy (PACT): This therapy is similar to PDT but with the advantage that PACT does not require the presence of oxygen. It is based on the use of prodrugs, this is a drug linked to a photocaging agent that helps the releasing of the active drug when it is irradiated with light.[56,57]

These therapies have received great attention because of their minimal invasiveness, high temporal and spatial controllability, negligible side effects and because they do not produce drug resistance.[58]

1.1.2.1 Photodynamic therapy (PDT)

1.1.2.1.1. Mechanism of action

PDT is a cancer treatment that uses light and oxygen to activate the anticancer drug that has been implied in the clinic for the past few decades.[59,60] PDT was discovered by Schwartz and Lipson in the 1960s with the synthesis of hematoporphyrin derivates that have a high cytotoxic effect against tumours.[61] Since then, numerous new photosensitisers have been discovered to treat various types of cancers.[61] The application of PDT in clinical treatments has been successful employed against different types of cancer, such as skin, prostate, and bladder cancer.[62]

PDT consists of 3 essential components: photosensitiser (PS), light, and oxygen. The PDT process involves two procedures (**Scheme 1.2**): First, the patient receives a drug that is inactive or has low activity in the dark, called photosensitiser. After the time delay, which is the time between the administration of PS and the start of illumination, the drug is excited by

irradiating the tissue at a specific wavelength. This activates the drug and lead it to act as a photocatalyst which transfers an electron to oxygen to form radicals and superoxide (PDT type I) or can convert the triplet oxygen ($^3O_2$) into a singlet oxygen ($^1O_2$), which is cytotoxic to cells (PDT type II) (**Scheme 1.3**).[63.64] This process is called radical oxygen species (ROS) generation.[65] These species are cytotoxic, induce hyper-stress, and can damage proteins, membranes, and DNA. The advantages of this treatment consist in having fewer side effects, being minimally invasive, having higher selectivity for cancer cell death, and including less drug resistance.[66]
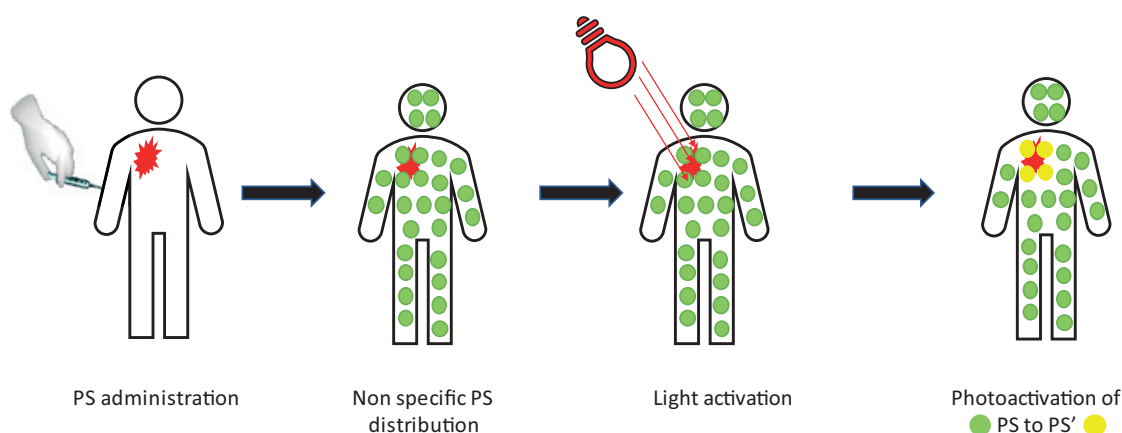
Scheme 1.2: Schematic representation of PDT treatment. The PS is administred to the patient and with a specific light, the PS is activated producing ROS that causes the death of the tumour.
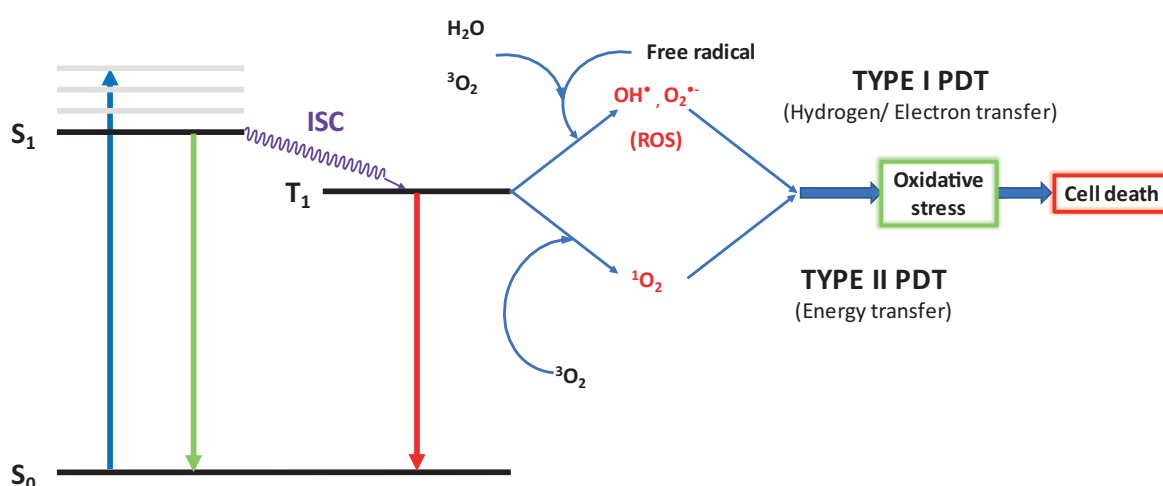
Scheme 1.3: Photoactivation process illustrated by a Modified Jablonski Diagram. The PS is excited from its ground singlet state (S_0) to its excited singlet state (S_1) when absorbs light. Via intersystem crossing (ISC) the PS is relayed to its excited triplet state (T_1), which can undergo Type I reaction which forms radicals or induces Type II reactions, transferring its energy to a molecule of oxygen ($^3O_2$) to form singlet oxygen ($^1O_2$)

1.1.2.1.2 Photosensitisers

The first-generation of PSs were the hematoporphyrin and their derivates, which were prepared for the treatment of cancer (**Figure 1.4**). However, they had significant disadvantages, such as cytotoxicity without the need of light irradiation (in the dark), short wavelength absorption, high half-life leading to the accumulation of the drug in normal tissue.[60,67] After decades of research, the first photosensitiser clinically approved for use in PDT was Photofrin® in 1993, which is a derivate of Hematoporphyrin.[68]

First-Generation PSs

Hematoporphyrin
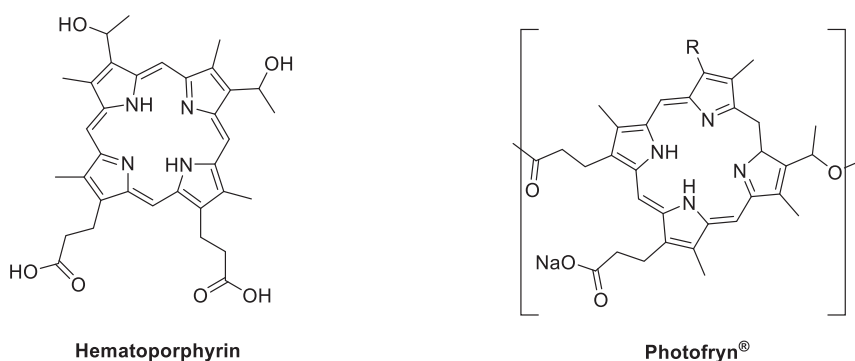
Photofryn®

Figure 1.4.: Structures of Hematoporphyrin and Photofryn® from the First-Generation PSs for PDT

To overcome these side effects, a second generation of PSs were developed (**Figure 1.5**). New PSs based on porphyrin and chlorin structures were proposed. These PSs exhibit absorption at higher wavelengths (around 650 nm), increased the tissue selectivity and accelerated excretion of the drug from the body. The second generation of PSs was more effective than the first generation. However, the drawback of this generation is the low water solubility.[60,67,69]

Second-Generation PSs

5'- Aminolevulinic acid

Bacteriochlorin

HPPH

Foscan®

Figure 1.5: Examples of the structures for the second-generation PSs in PDT: 5'- Aminolevulinic acid, bacteriochlorin, 2-(1-Hexyloxyethyl)-2-devinyl pyropheophorbide-a (HPPH), Foscan®

The objective of the third-generation is to develop new photosensitisers to overcome the secondary effects of the second-generation ones; more soluble in water and higher selectivity toward tumour tissues. These PSs maintain the conjugation of the second-generation and are intended to bind biological motifs such as amino acids, peptides, antibodies, carbohydrates or encapsulate them in carriers such as liposomes, micelles, etc.[69–71]

1.1.2.1.3. Metal-complexes for PDT

In recent years, the development of new metal complexes used as PS in PDT has generated great interest. Metal compounds have been shown to be more stable and phototoxic than organic drugs.[68] Furthermore, transition metals have good photophysical properties, making it easy to reach their excited states through light.[72]

Organic PS usually exhibits a π-π* and n-π* molecular electronic transition when they are excited. Also, metal complexes present more allowed transitions such as metal centred (MC) (*i.e.* d-d transitions), charge transfer (CT) (*i.e.* metal-to-ligand charge transfer (MLCT), ligand-to-metal charger transfer (LMCT) and ligand-centred (LC) transitions.[72] The advantage of these transitions is that they can be achieved by means of excitation to triplet excited state

easily due to the efficient intersystem crossing promoted by the metal ion, which has the benefit of a longer lifetime, increasing the probability of the photochemical reaction to occur. Furthermore, this will facilitate the efficiency of both type I and II PDT.[72,73] Today, some metal-containing complexes have been clinically applied, and others are in clinical trials (**Figure 1.6**):

Rostaporfin
Purlytin®

Motexafin, Lutetium
Lutrin®, Antrin®

Sulfonated Aluminium Phtaclocyanine
Photosens®

Padeliporfin, WST09
TOOKAD®

Padeliporfin, WST11
TOOKAD® soluble

TLD-1433
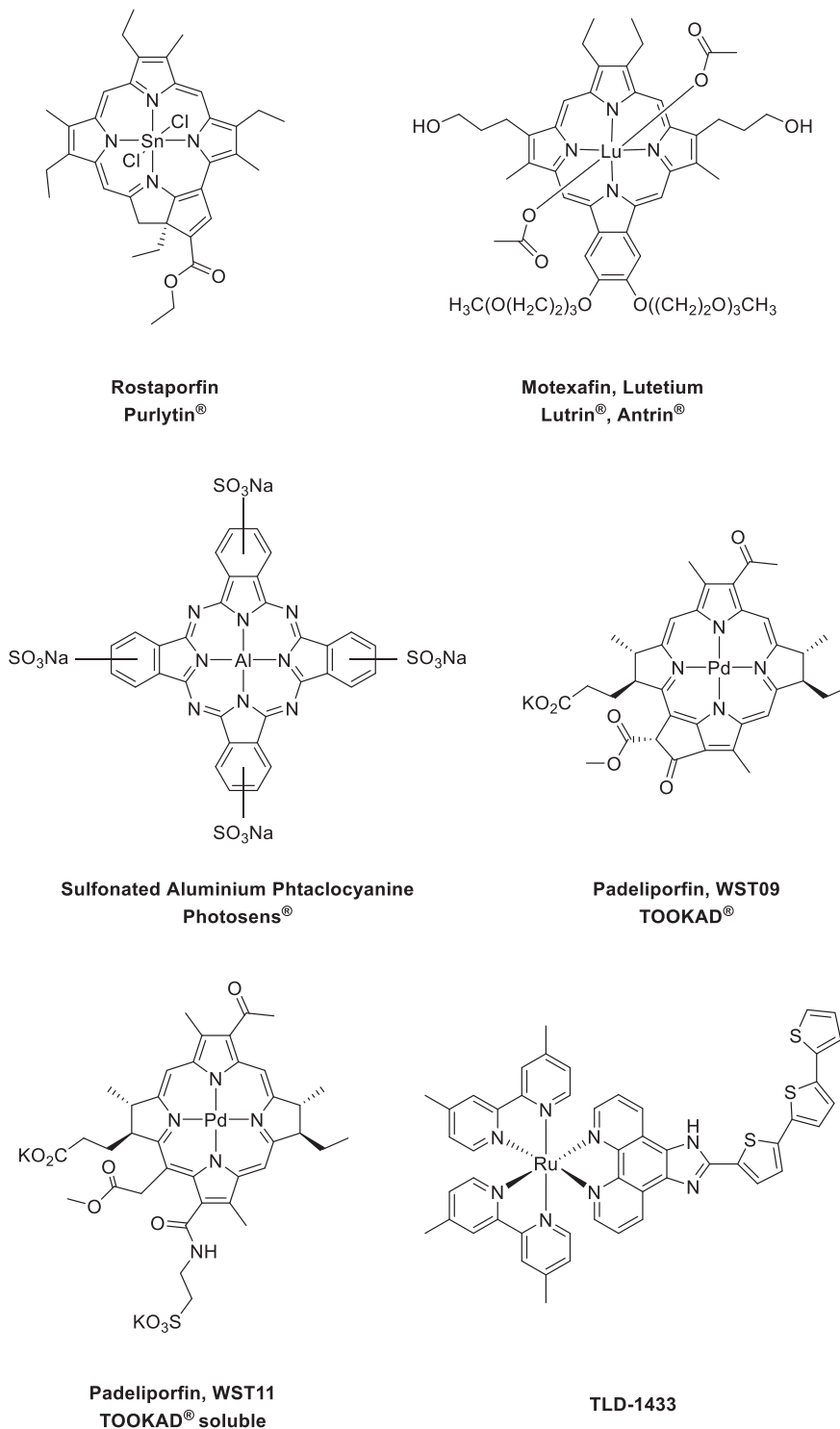
Figure 1.6: Structures of metal-containing PSs in PDT clinical trials

Purlytin®, Lutrin® and Antrin® are currently undergoing clinical trials in the United States, but they have not been approved yet.[74,75] However, Photosens® and TOOKAD® soluble have been clinically approved. The first is approved in Russia to treat lung, liver, breast, skin, and gastrointestinal cancers and, the second one is approved in Mexico, Israel and 31 countries European Countries to treat prostate cancer.[76,77]

TLD1433 was the first photosensitive drug in clinical trial which instead of having a porphyrin-type ligand, contains pyridine-type ligand linked to Ru(II).[78] Ru(II)-photosensitisers are generating great interest for their photochemical properties. Ruthenium complexes also exhibit excellent solubility, high cellular uptake, photostability and the ability to produce ROS.[56]

Apart from this compounds, other transition metals are also being investigated for PSs in PDT such as Ir,[79] Os,[80] Pt[81] and Re[82] due to their physiochemical properties.

Despite the improvement of photosensitisers, PDT is a technique with several limitations because of its dependence on the generation of ROS: Firstly, the small diffusion distance of ROS (>20 nm). Furthermore, this therapy is restricted by the light excitation of the drug, as it is limited by the depth of light and moreover it is oxygen-dependent. This technique is not appropriate for solid tumours since they present hypoxic conditions (low oxygen concentrations).[64,83, 84]

1.1.2.2 Photoactivated chemotherapy (PACT)

1.1.2.2.1 Mechanism of action

Photoactivated chemotherapy (PACT) is an alternative treatment to overcome the limitations of traditional anticancer compounds and PDT. PACT has the advantage that the activation mechanism is not oxygen-dependent, whereas PDT requires the presence of oxygen. This technique can be used specially against solid tumours in hypoxic microenvironments.[85,86]

The idea of photoactivation was introduced by Morrison *et al.* in the 1990s using the Rhodium complex *cis*-[Rh(phen)$_2$Cl$_2$]Cl. When this complex was degraded by ultraviolet light (UV), the metallic photoproduct so generated was able to bind DNA.[87] The concept of photoactivated chemotherapy was introduced by Sadler *et al.*[50] who defined it as a therapy in which the prodrug does not have any cytotoxicity in the dark but when it is irradiated at the corresponding wavelength, chemical changes occur in the prodrug that form a new component with high biological activity.[50]

There are different approaches in PACT (**Scheme 1.4**):[50, 88]

- Photoinduced electron transfer: Photoreduction of the metal centre by light that produces the dissociation of the axial ligands, the most common reductions are Pt(IV) to Pt(II)[89] or Co(III) to Co(II).[90]

- Photosubstitution: When irradiated with light, the ligands are replaced by molecules of the solvent, typically water. The most common complexes are based on Ru(II),[91] Rh(III),[87] Ir(III),[92] and Re(I).[93]

- Bioactive ligand release: Irradiation with light releases small bioactive molecules such as NO and CO.[94]

- Ligand photocleavage: When the drug is irradiated, it can produce a photomodification of the ligand acting as a photoswitch or photocage.[95]
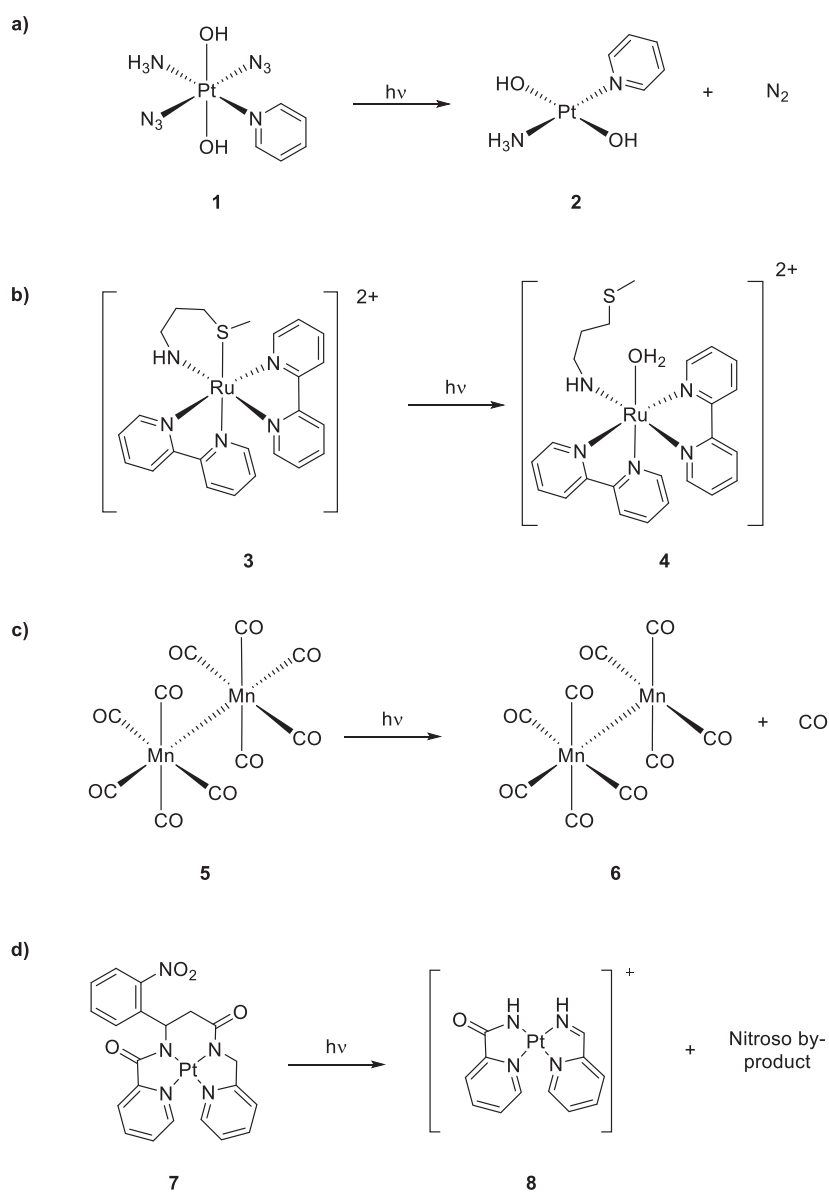
Scheme 1.4: Examples of the different approaches in PACT a) Photoinduced electron transfer,[89] b) Photosubstitution,[91] c) Bioactive ligand release,[94] and d) Ligand photocleavage[95]

Different metals have generated great interest to be able to apply in PACT: Ti (IV),[96] V (IV),[97] Cr (III),[98] Mn (VI),[99] Fe (III),[100] Ru (II),[101] Co (III),[102] Rh (III),[103] Rh (II),[104] Ir (III),[92] Re(I),[93] Pt (II),[105] Pt (IV).[106] Among these examples Pt(IV) and Ru(II) are those more investigated.

1.1.2.2.2. Ru(II)-photoresponsive complexes

The physicochemical properties of Ru(II)-complexes have drawn attention for their potential application in biomedicine. As an example, the Ru(II)-compound, TLD1433 is currently undergoing clinical trials as anticancer drug.

Ru(II)-complexes under investigation for use in PACT have an octahedral structure and follow a ligand substitution photomechanism. This mechanism is explained through the corresponding aquo complex binding to DNA, similar to the mechanism of CDDP.[107]

In 2004, Turro and co-workers published that the complex $[Ru(bpy)_2(NH_3)_2]^{2+}$ when irradiated near UV light, formed the corresponding aquo-complex, by water substitution. This photoproduct was later covalently attached to DNA thus being one of the first examples of photoactivatable Ru(II)-complexes.[108] In 2011, $[Ru(bpy)_2(5CNU)_2]^{2+}$ (5CNU = 5-cyanouracil),a Ru(II)-compound with cytotoxic ligands was discovered. The complex is a derivative of the anticancer drug 5-Fluorouracil. When the compound was irradiated with visible light, 5CNU were released and the phototoxicity increased, as both the ligand and the newly formed Ru are cytotoxic.[109]

$[Ru(bpy)_2(NH_3)_2]^{2+}$ *cis*-$[Ru(bpy)_2(5CNU)_2]^{2+}$ **9**

10   **11**   **12**
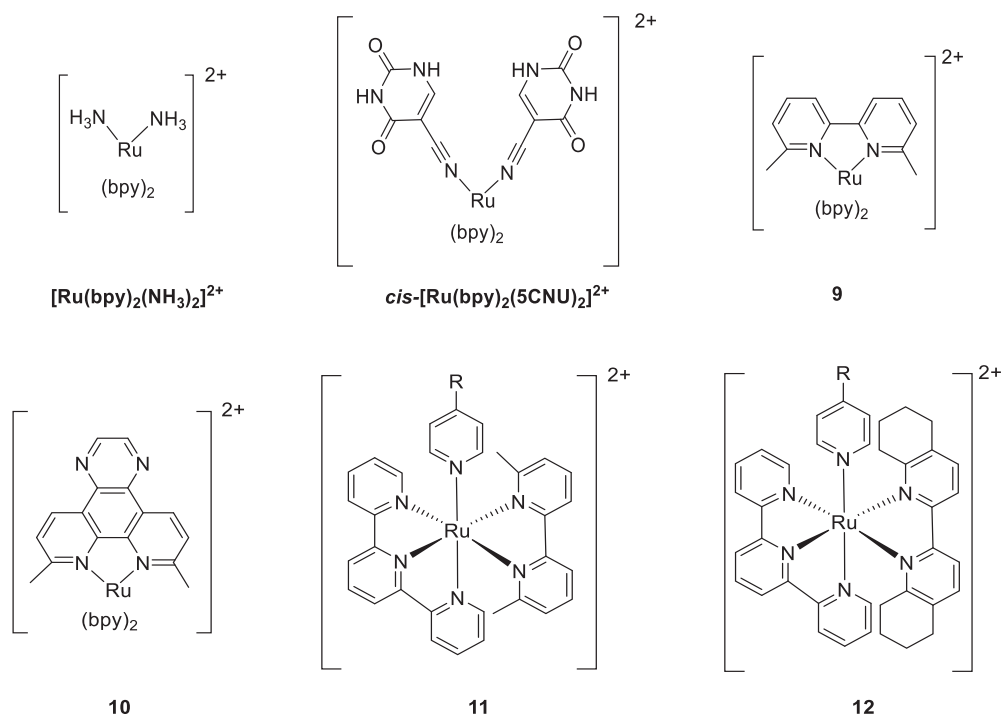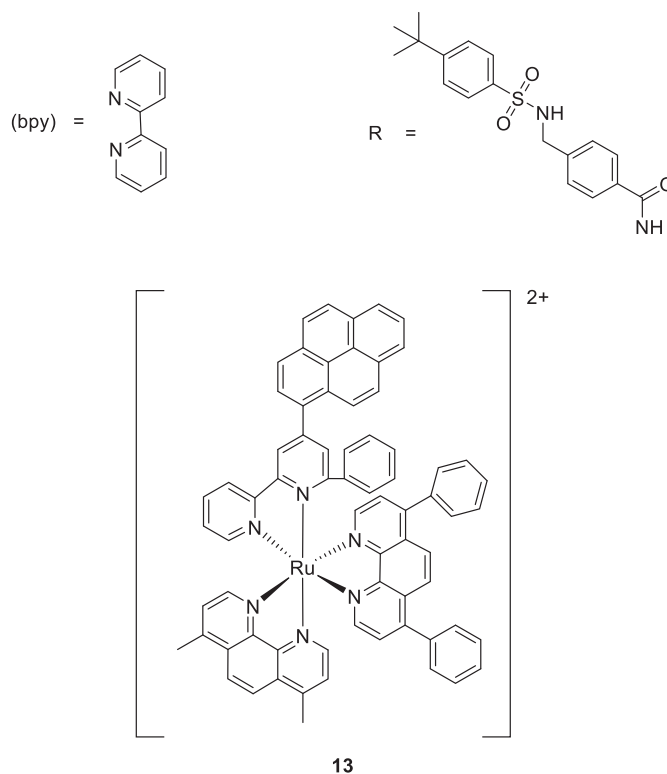
Figure 1.7: Some relevant examples of photoactivatable Ru(II)-complexes drugs[108-111]

In the following year, Glazer *et al.* reported two new Ru(II)-bypyridyno-type complexes that exhibited photoreactions under visible light (Λ_{exc} > 450 nm). These compounds were **9** and **10** (**Figure 1.7**) which released a bidentate ligand, 6,6'-dimethyl-2,2'-bipyridinde for **9** and 1,10-phenanthroline for **10** and formed the same Ru(II)-photoproduct complex $[Ru(bpy)_2]^{2+}$. Both photosensitisers were tested with HL60 leukaemia and A549 lung cell lines, and it was found that they increased the cytotoxicity after being activated by light.[110]

Recently, Bonnet and co-workers discovered two new Ru(II)-compounds that could be activated at 628 nm.[111] Both Ru(II)-photosensitive drugs (**11** and **12** in **Figure 1.11**) contain cytotoxic nicotinamide phosphoribosyltransferase (NAMPT) as photocage. Cytotoxicity was studied against A549, MCF-7 and A431 cell lines, where complex **12** proved to be a good PACT candidate.

Also, some studies demonstrate that some Ru(II)-complexes can be used for either PACT or PDT.[101,112,113] One example is complex **13**, which can be activated through NIR light by two photon excitation to form $^1O_2$ or the ligand dissociation, exhibiting cytotoxicity.[114]

1.1.2.2.3. Pt(IV)-photoresponsive complexes

The photochemical properties of Pt(IV) began to be applied in the mid-19th century in the photography field.[106] Pt(IV) are good candidates for PACT because they tend to follow

photodecomposition mechanism when irradiated.[115] These complexes are stable in the dark (low cytotoxic activity) and tend to be stable in physiological media, but they can easily be photoreduced to Pt(II)-complex, which is the active species (with high cytotoxic activity). This means that the leaving ligand can play also an important role in their reactivity.[115]

Bednarski and co-workers[116,117] developed the first photoactivatable Pt(IV)-complexes, which were [PtCl$_2$I$_2$(en)$_2$]. This Pt(IV)-complex was irradiated at 400 nm, and the photoproducts obtained were able to bind DNA and prevent cell division. However, the complex was no stable in the dark. To increase its stability, the chlorido ligands were replaced by OH, Acetoxy (OAc), and OSO$_2$CH$_3$ as ligands. All complexes were irradiated under visible light (>375 nm). The results published show that [Pt(OSO$_2$CH$_3$)$_2$I$_2$(en)] exhibited good solubility but with a small percentage of Pt-DNA binding. Also, [Pt(OH)$_2$I$_2$(en)] followed a photosubstitution mechanism where a new Pt(IV)-complex photoproduct was produced, which was neither cytotoxic. Besides, [Pt(OAc)$_2$I$_2$(en)] in the absence of GSH, underwent photoreduction mechanism where Pt(II)-complex photoproducts were formed and covalently bind to DNA. However, in presence of GSH, the Pt(IV)-complex was already reduced prior to irradiation (**Figure 1.8**).

[Pt(Cl)$_2$I$_2$(en)]   **[Pt(OH)$_2$I$_2$(en)]**   **[Pt(OAc)$_2$I$_2$(en)]**   **[Pt(MsO)$_2$I$_2$(en)]**
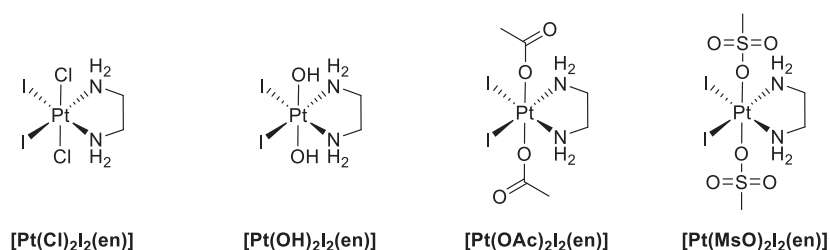
Figure 1.8: First generation diiodo photoactivable Pt(IV) drugs synthesised by Bednarski group[116,117]

A few years later, Sadler and co-workers[118,119] reported that Pt(IV)-diaminodiazido were inert in the dark and could be activated under light irradiation (**Figure 1.9**). The first diazido-Pt(IV)-complex photosensitisers were *cis-, trans*-[Pt(en)(N$_3$)(OH)$_2$] and *cis, trans, cis*-[Pt(N$_3$)(OH)$_2$(NH$_3$)$_2$] which were stable in the dark and presented a higher toxicity than cisplatin when irradiated with light.

cis, trans-
[Pt(en)(N$_3$)$_2$(OH)$_2$]

cis, trans, cis-
[Pt(N$_3$)$_2$(OH)$_2$(NH$_3$)$_2$]

trans, trans, trans-
[Pt(N$_3$)$_2$(OH)$_2$(NH$_3$)$_2$]

trans, trans, trans-
[Pt(N$_3$)$_2$(OH)$_2$(NH$_3$)(MA)]

trans, trans, trans-
[Pt(N$_3$)$_2$(OH)$_2$(Py)$_2$]

trans, cis-
[Pt(2,2'-Bpy)(OAc)$_2$(N$_3$)$_2$]

trans, cis-
[Pt(Phen)(OAc)$_2$(N$_3$)$_2$]
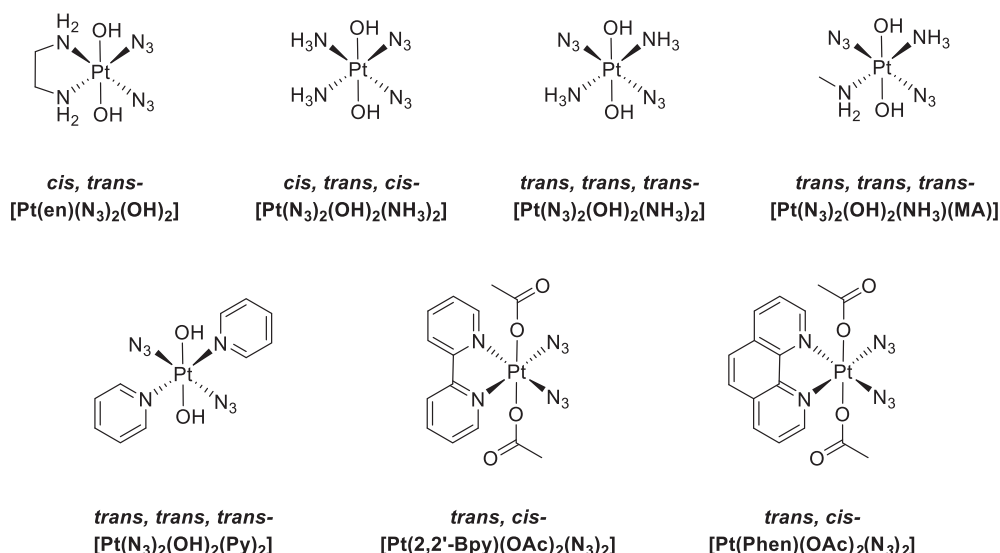
Figure 1.9: Second generation photoactivatable diazido-Pt(IV) complexes synthesised by Sadler and co-workers[118,119]

By changing the configuration, as was the case for the *trans, trans, trans-*[Pt(N$_3$)(OH)$_2$(NH$_3$)$_2$] solubility, absorption and importantly cytotoxicity were improved.[120] Furthermore, changing the ligand to an aliphatic amine as for (*trans-, trans-, trans-*[Pt(N$_3$)$_2$(OH)$_2$(NH$_3$)(MA)])[121] or substituting NH$_3$ for pyridine (Py) as for (*trans-, trans-, trans-*[Pt(N$_3$)$_2$(OH)$_2$(Py)$_2$]) resulted in even more photocytotoxic.[122]

Also, the Pt(IV)-complex absorbed at a longer wavelength when the compound had a π-conjugated bidentate diimine as ligand, as in the two cases of *trans, cis-*[Pt(2,2'-bpy)(OAc)$_2$(N$_3$)] and *trans, cis-*[Pt(Phen)(OAc)$_2$(N$_3$)] [123]

Despite the recent development of Pt(IV)-anticancer complexes for PACT, none of them have entered in clinical trials yet.

1.1.2.2.4. Pt(II)-photoresponsive complexes

In contrast to Pt(IV) and Ru(II) complexes, Pt(II)-compounds present a square planar structure. In addition, these Pt(II)-photosensitisers can also follow mechanisms of ligand photo-cleavage or photodissociation of the ligand.

On the one hand, when irradiated with light, the photodissociation Pt(II)-complexes cause a modification of the ligand that changes the molecule form becoming biologically active (**Scheme 1.4**). On the other hand, other type of photoactivated Pt(II)-complexes can release a photolabile ligand when irradiated (**Scheme 1.4**).

One of the first examples of photoactivatable Pt(II)-complexes was reported by Brunner and co-workers.[124] Different hematoporphyrin attached to Pt(II) were synthesised. Among 35 Pt(II)-compounds, when irradiated with visible light (λ = 600-730 nm), only **14** and **15** were water soluble and increased cytotoxicity against TCC-SUP and J82 transitional bladder cancer cell lines. These two photosensitive complexes contain polyethylene glycol (PEG) as functional group linked to hematoporphyrin, and when exposed to light, the antitumor activity increased.

In 2006, Brabec, *et al.* demonstrated that transplatin, in the dark, did not exhibit cytotoxicity, but upon UV irradiation, the complex loses the chloride ligands and form an adduct with the DNA, thus improving its cytotoxicity.[125] Lately, a similar effect was reported with carboplatin when it was irradiated with UV-light.[126]

Recently, Patra and co-workers[127] have published two new Pt(II)-complexes that could be used in both PACT and PDT: [Pt(DACH)(nap)Cl] and [Pt(DACH)(nap)$_2$] (nap = naproxen) (**Figure 1.10**). When irradiated with UV-light, these complexes release nap, which generates ROS, and the Pt(II)-complex photoproduct binds to DNA and causes cell death.

A new visible light photoactivated Pt(II)-complex has been synthesised containing a curcumin (cur) unit as dissociative ligand (**Figure 1.10**). The complex [Pt(cur)(NH$_3$)$_2$]NO$_3$ reported by Chakravarty and co-workers[128] did not exhibit cytotoxicity in the dark, but upon irradiation with visible light, the curcumin ligand is released, forming the corresponding diamminoplatinum(II) photoproduct, which interacts with DNA causing cell death. This work is one of the first examples of ligand photodissociation in Pt(II)-complexes activated with visible light.

14   15   transplatin

R = (CH₂CH₂O)₁₇CH₃

[Pt(DACH)(nap)₂]   [Pt(cur)(NH₃)₂]NO₃

X =

[Pt(DACH)(nap)Cl]
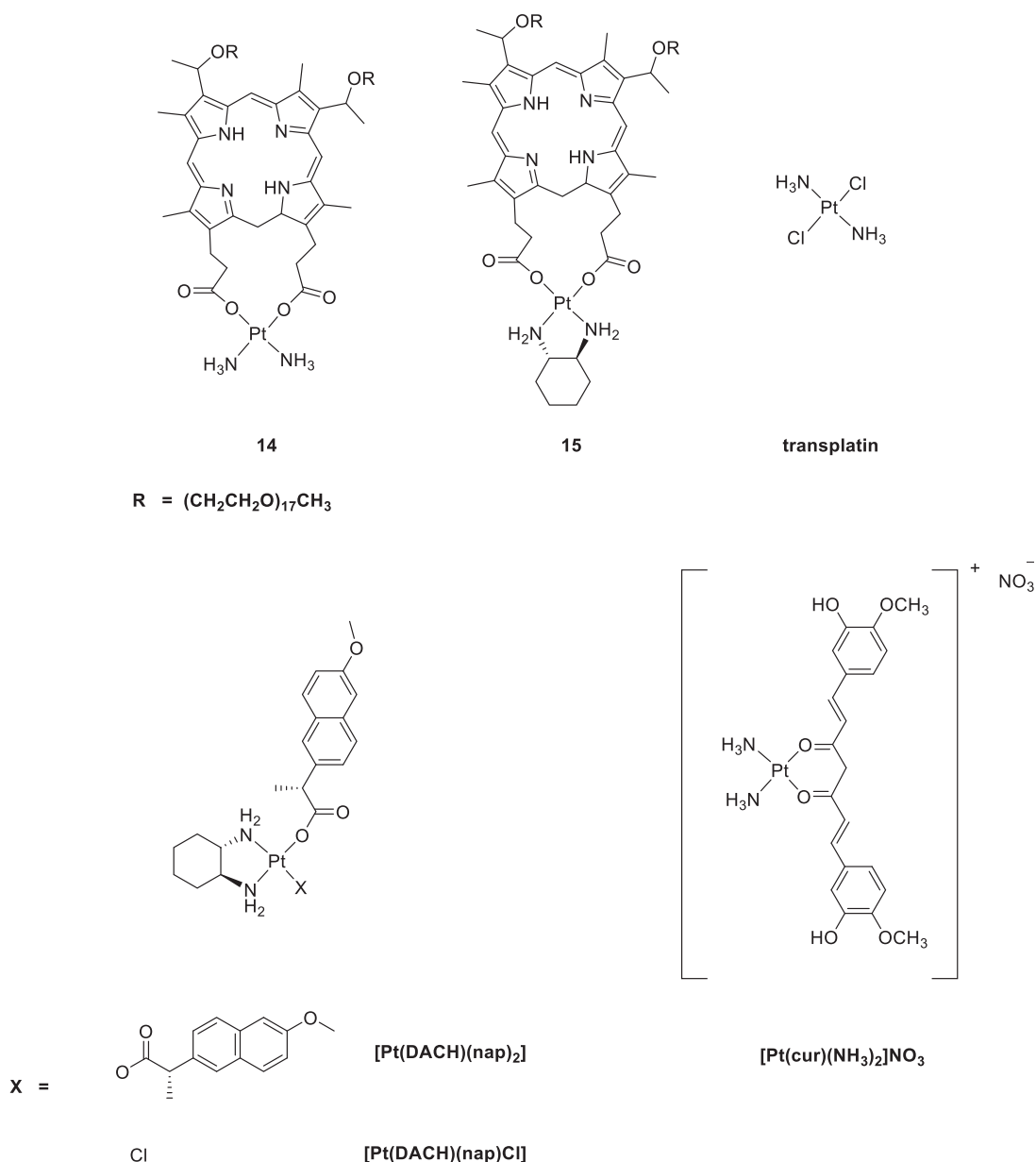
Figure 1.10: Relevant examples of photodissociative Pt(II)-complexes in PACT

Various other examples of ligand photodissociation have been furtherly described. Pt(II)-photoactivatable complexes can also be activated by means of photocaging ligands. One of the most widely used photocages in biology is *o*-nitrobenzyl type, which, when irradiated with UV-light, undergoes a photochemical fragmentation process that release an *o*-nitrosophenyl moiety as the biologically active molecule. Franz and co-workers[95] synthesised a new Pt(II)-complex bonded to a ligand (**7**) that contains a nitrophenyl group (**Scheme 1.5**). This compound did not show toxicity towards MCF-7 breast cancer cell line in the dark but exhibited phototoxicity after irradiating with UV-light, which produced the photodegradation of the ligand and formed the active complex and nitroso by-products that induced cell death.
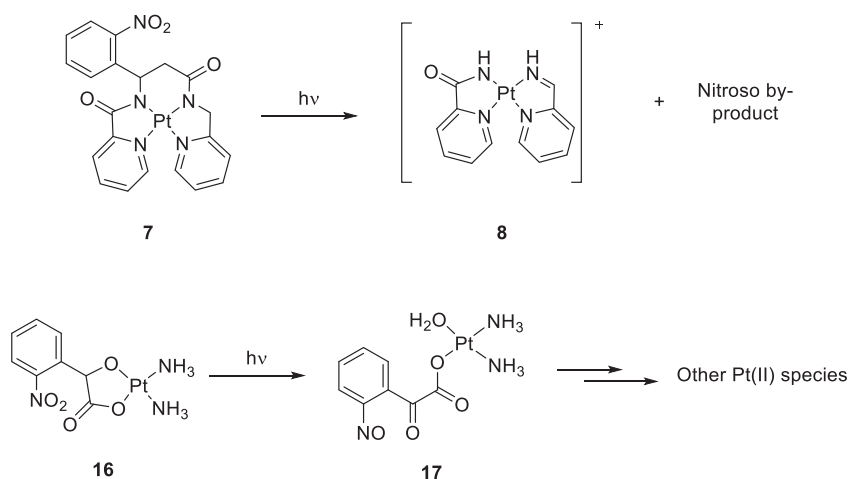
Scheme 1.5: Two relevant examples of photodissociation Pt(II)-complexes containing a nitrobenzyl group to applicate in PACT

Another Pt(II)-photosensitiser (**16**) was synthesised by the Guo group,[129] which was bound to a ligand containing a nitrobenzyl group and hydroxyl groups (**Scheme 1.5**). Upon irradiation with UV-light, the nitrophenyl group was reduced to nitrosophenyl and the hydroxide groups were oxidised to carbonyl group, giving rise to the Pt(II)-photoproduct, which was more cytotoxic in front of breast cancer MCF-7 cells than before irradiation.

Our group has also synthesised photoactivatable Pt(II) complexes based on squaramide. In 2018, a new squaramide-based Pt(II) complex was reported to exhibit differential photoreactivity when irradiated under UV-light in hypoxic and normoxic media. Moreover, this complex exhibited phototoxicity against HeLa cells in hypoxic medium.[105] These results suggest that squaramide-based Pt(II)-complexes could act as a new kind of PACT photocage. In 2022, two improved squaramide-based Pt(II)-complexes (**18** and **19**) were reported to be more water soluble and absorbed blue light. In addition, both complexes showed a significant increase in cytotoxicity after irradiation against three cell lines (HeLa, A2780, A2780cis) which was caused by forming ROS species or interacting with DNA. These results suggest that these complexes could be applied as dual PACT and PDT agents.[130]
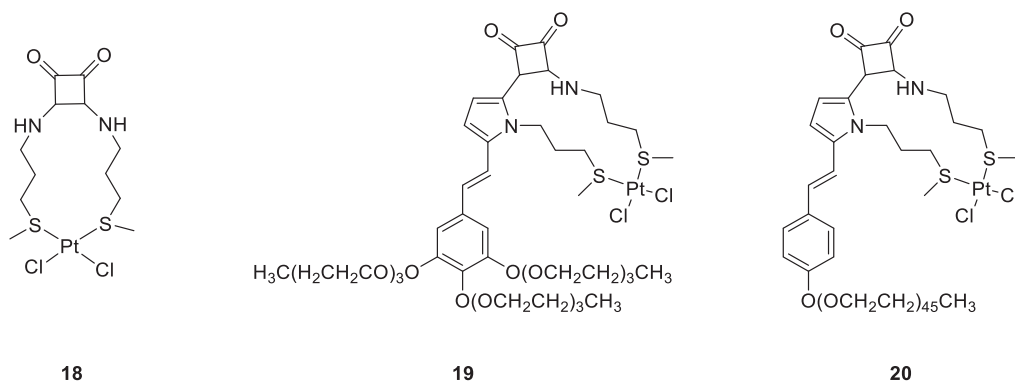
Figure 1.12: Some examples of the squaramide-based Pt(II) complexes synthesised in our group

However, one major challenge in the of PDT and PACT is the limited tissue penetration of the photosensitisers. These photosensitisers require light in the UV-Vis region to be activated, which has low penetration due to light scattering with the biomolecules and can produce phototoxicity, especially UV light.[131] Furthermore, synthesising photosensitisers that absorb in the visible light requires the use of π-conjugated motives, which can result in tough synthesis and finally in solubility issues in biological media. To overcome this challenge, efforts have been made to develop molecules that can absorb in lower energy regions, as the near infrared (NIR) (700 – 1000 nm), where the light is more penetrating (**Figure 1.13**).

However, the energy associated with irradiation at the NIR wavelengths is usually not sufficient to activate photosensitisers. An alternative to this problem is the use of two-photon irradiation with which sufficient energy is achieved for the excitation of the photosensitiser. Nevertheless, this technique requires a pulsed laser to excite small areas, which limits its application.[132]
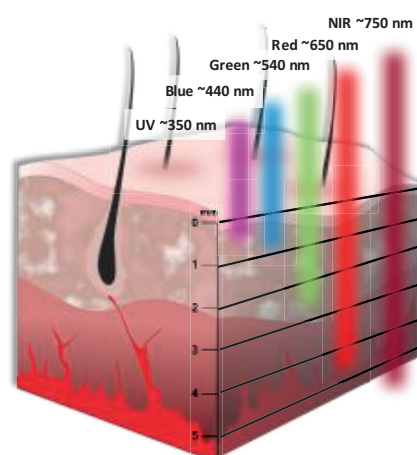
Figure 1.13: Deep penetration scheme of each light scale where the most penetrating light is NIR and the least penetrating is UV

In short, by using UV irradiation it is possible to excite the photosensitisers, but this radiation is harmful to any cell (even healthy ones) and also has little penetration. By decreasing the energy of the radiation (NIR), even though there is an improvement of penetrability and also is not harmful by itself to the cells, in general, the energy apply is not sufficient to activate the photosensitisers. Faced this dilemma, a very convenient solution would be to be able to provide the photosensitisers with a component that, when irradiated in the NIR range, would emit UV irradiation, which could therefore activate UV-responsible photosensitisers, but by means of irradiation in the NIR range. This approach led us to consider the exploitation of the upconversion phenomena. [133,134]

1.2. Upconversion nanoparticles

According to Stokes' law, a fluorescent light emitter absorbs photons of higher energy light and emits photons with lower energy light.[135] In contrast, upconversion is a process in which the molecule can absorb two or more photons of low energy light (long wavelength) and emit higher energy light (short wavelength), following the so-called antistokes effect.[136] Lanthanide-doped materials have special optical and magnetic properties, including upconversion which is an important optical property. Specifically, in recent years, it has been shown that upconversion nanoparticles (UCNPs), composed by lanthanides doped with other lanthanides, can convert NIR light to UV light.[137]

In 1966, Auzel proposed the first concept of upconversion transfer working with Yb^{3+}-Er^{3+} couple, which could emit green light upon irradiation with NIR. By increasing the upconversion efficiency, blue light emission using a Yb^{3+}-Tm^{3+} couple was achieved.[138] Since then, the upconversion process has been further investigated with different materials and applications in nanotechnology[139] and biomedicine.[140]

Most of the UCNPs are composed by three components: a host material, a sensitizer, and an activator.[141] The host material must be chemically stable and transparent in both absorption and emission range to avoid interfering with the upconversion process. Moreover, it must have a low phonon energy (low frequency vibrations of the lattice) to avoid excited energy loss in the upconversion process and form a crystalline lattice around the dopants to ensure the maximum efficacy of the upconversion (distance, position, and coordination). The best host materials with these properties are oxides and halides. While oxides are chemical stable, they have high phonon energy. Bromide and Iodide have a very low phonon energy but tend to absorb water from the environment, which limits their application. However, fluorides have been proven to be the best candidates as they have low phonon energy and are chemically stable.[142] $NaYF_4$ has been one of the most efficient host matrix for the upconversion process.[135]

The sensitizers absorb the light and transfer the excited energy to the emitter; therefore, their absorbance does not have to be coupled with the emission to be achieved with the upconversion process. It is important that they have a large absorption cross-section (high probability of absorbing the incident radiation) and long excited state lifetime. The most commonly used ions used as sensitizers are Yb^{3+} and Nd^{3+} because of their absorption at NIR light.[143]

The activators or emitters are the ions that receive the excited energy transferred by the sensitizer ion. These ions exhibit a low and constant energy difference between orbitals, like a ladder of energy levels, to facilitate the energy transfer and in particular, they have a long

lifetime in the upconversion states. The common activators ions for UCNPs are Tm^{3+}, Er^{3+} and Ho^{3+}.[144]

The upconversion process can be divided into three types depending on the mechanism: Excited state absorption (ESA), energy transfer upconversion (ETU) and photoavalanche (PA) **Scheme 1.6**.[135,145]

- ESA: Is a single ion process. First, some photons are excited form the ground state to the metastable E1 level when the absorbed energy is resonant with the transition from the ground state to the excitation level E1. Secondly, a pump photon is incised which has a resonant energy at the transition from E1 to E2 allowing the ion to be excited to E2, thus producing an upconversion emission.

- ETU: This process occurs between two or more ions. The ions are excited to metastable energy level through pumped photons. Thanks to the interaction between the two ions, an energy transfer will take place at that moment. One of the two ions will relax to the ground state, emitting energy to the other ion, which will be excited to a higher energy level and produce an upconversion emission when it is relaxed to the ground state.

- PA: In this mechanism the ion starts off excited at a slightly higher energy level than E2 (E2'). First, the electron is relaxed to the E2 energy level. Second, an energy transfer occurs when the electron is relaxed to E1, exciting another electron from E0 to E1, giving two electrons at E1. One of them is excited at E3, absorbing radiation, and when it is relaxed to E1 again, another energy transfer occurs, which excites two other electrons from E0 to E1. The radiation that is resonant to the energy gap between E1 and E3 can excite the electrons from E1 to E3. When this process is repeated many times, the number of electrons occupying the E3 energy level increases, leading a relaxation to E0, and producing an upconversion emission.
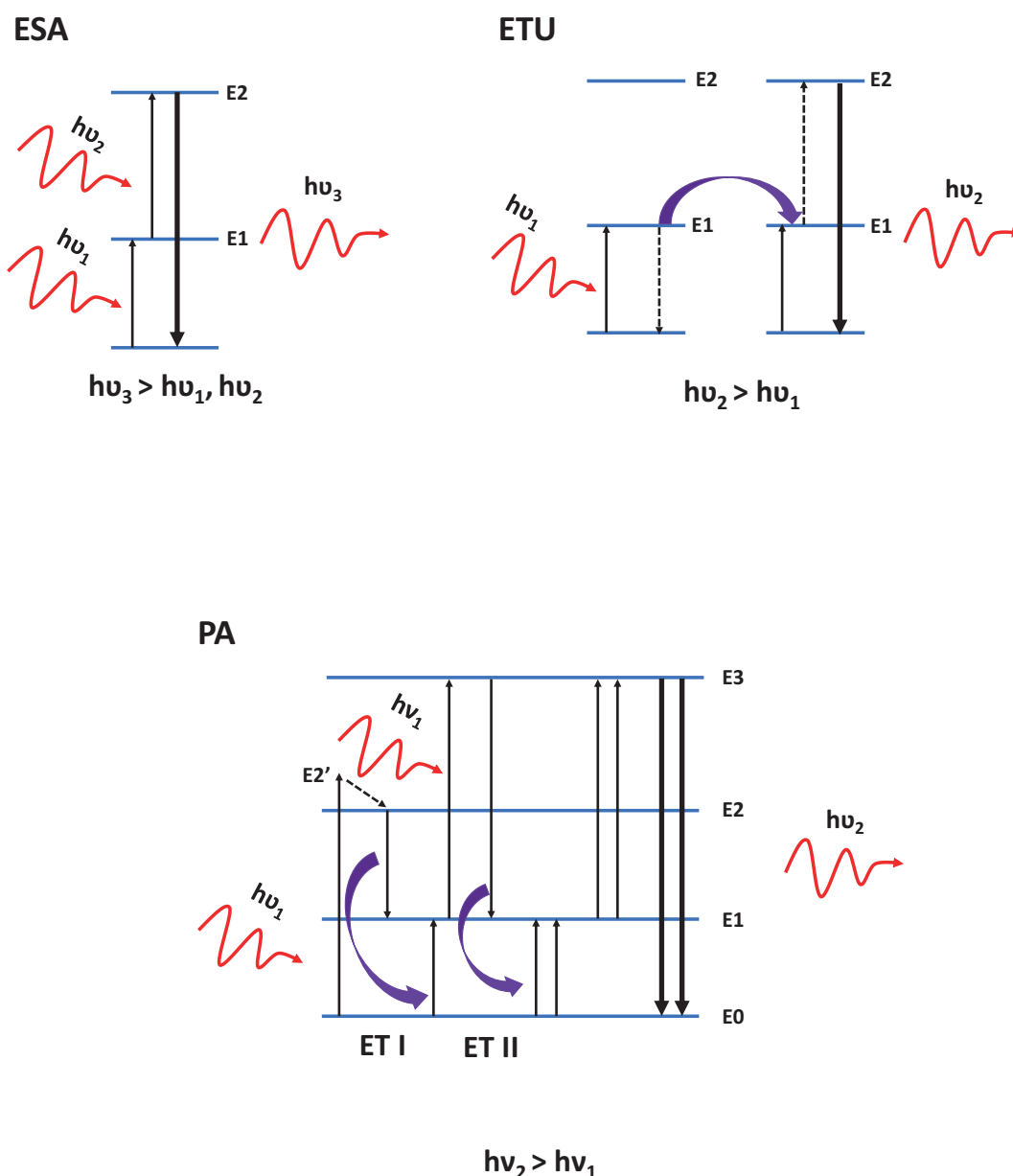
Scheme 1.6: Different types of mechanisms for upconversion process: ESA, ETU, PA

Upconversion nanoparticles (UCNPs) have been attracting attention in biomedical applications because they can absorb NIR light, which is more penetrating and less toxic to tissues, and emit at different wavelength (NIR, visible light and UV-light).[20,131] They also offer a number of advantages such as resistance to photodegradation after irradiation, low cytotoxicity and high photostability,[146] which have been employed in biological imaging (*in vitro*[147] and *in vivo*[148]), biological sensing/detection,[149] development of point-of-care devices,[150] and drug delivery for cancer therapy.[151]

1.2.1.UCNPs in cancer treatment

UNCPs devices in cancer therapy can activate drugs with NIR light. The major photosensitisers can be activated by UV-visible light, which have lower penetration because the light can be scattered by biomolecules in the organism.[152] However, if a platform is formed where PS is associated with UCNPs, the UCNPs can absorb NIR light and emit visible or UV light, activating PS (**Figure 1.14**).

UV

UV

NIR

Coating   UCNPs   UV-PS (Inactive form)   PS' (Active form)
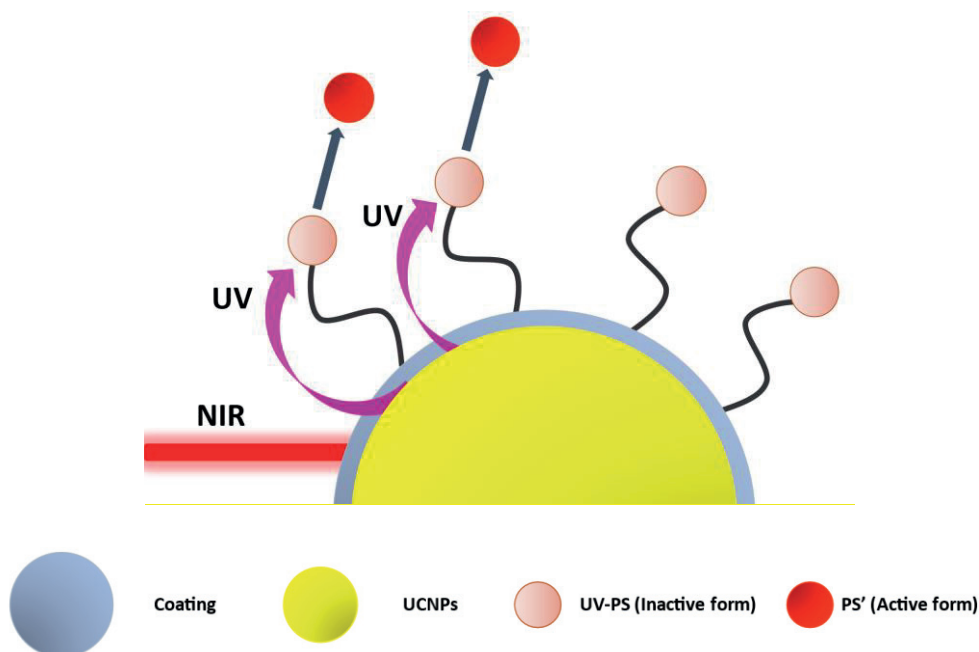
Figure 1.14: Schematic illustration of NIR light activation of the prodrug through upconversion to UV light via luminescent nanoparticles

In 2007, Scholfield and co-workers published the first system using UCNPs that can be applied in photodynamic therapy. UCNPs were coated with a layer of silica and doped ~~them~~ with merocyanine as a photosensitiser. This strategy consisted of using radiation at 974 nm which is absorbed by the UCNPs which in response, emit at 574 nm, thus activating the photosensitiser that interacts with oxygen to generate singlet oxygen ($^1O_2$) species. This new system was applied to an *in vitro* study with the MCF-7/AZ breast cancer cell line, where cell death was observed when cells were exposed to NIR light, while in the dark, the cells survived.[153]

Since then, more studies have been published using systems containing UCNPs and PS.[154–156] Liu and co-workers[152] published the first study about PDT *in vivo* with UCNPs system. The work consists of introducing the Chlorin e6 (Ce6) photosensitiser in the UCNPs ($NaYF_4$; Yb^{3+}; Er^{3+}) coating. This new system produced singlet oxygen when irradiated with NIR-light. An *in vitro* study of the UCNPs and the photosensitiser was carried out with 4T1 murine breast

cancer cell lines. This experiment showed that this UCNPs-Ce6 entered the cell, causing cell death after irradiating at 980 nm. Following these results, subsequent *in vivo* studies in mice were carried out. The experiments were done in three different ways, one was injecting UNCPs-Ce6 only irradiating with NIR, another was just injecting UCNPs-Ce6 and finally, the last one was irradiating with NIR. It was observed that only the combination of the UCNPs-system with light prevented the growth of the mouse tumour. With this work they demonstrated that UCNPs could be applied in PDT for cancer therapy.

Following this example, other publications have reported using coated UCNPs with photosensitisers to apply in PDT.[134,157] Furthermore, studies with metal-complexes have also been carried out. In 2007, Zhang group designed a platform that loaded the photosensitiser complex Ru(bpy)$_3$ (Λ_{exc} = 450 nm) to the NaYF$_4$; Yb^{3+}; Tm^{3+} UCNPs coated with silica. This platform was able to generate $^1O_2$ by irradiating with Visible light (excitation of Ru(bpy)$_3$) or with NIR light (excitation of the UCNPs). This was the first example of using the UCNPs strategy to activate the metal complex for PDT.[158]

In addition, this system has also been published for use in PACT. The first approach to activate a photoactivatable metal-complex through UCNPs for PACT was reported by Zhang and co-workers. They developed a strategy that released the bioactive molecule NO by irradiating with NIR light which involves coating the NaYF$_4$; Yb^{3+}; Tm^{3+} UCNPs with [Fe$_4$S$_3$(NO)$_7$]$^-$ salt. As demonstrated, the salt was able to release NO by photodegradation by means of upconversion of NIR to visible light.[159] This offered the possibility that this strategy could be implemented in PACT. Furthermore, CO release from *trans*-Mn(bpy)(PPh$_3$)$_2$(CO)$_2$ was also studied using the same system.[160]

In 2013, the Lin's group[161] developed UV-photoactivated PS by the use of a Pt(IV) complex ([Pt(N$_3$)$_2$(NH$_3$)(py)(O$_2$CCH$_2$CH$_2$COOH)$_2$] (**DPP**)) and combined with the UNCPs (NaYF$_4$; Yb^{3+}; Tm^{3+} surrounded by a NaGdF$_4$; Yb^{3+} shell) within a PEG coating. This new platform released more Pt(II) under both UV and NIR irradiation than in the dark at pH = 7.4 and 5.5, thus indicating good stability. In addition, *in vitro* tests were performed on HeLa cancer cells irradiating under the UV and NIR region, and in the dark, demonstrating that the system can be activated by UV as well as by upconversion with NIR with similar results. Moreover, this platform was applied in mice with liver cancer tumour cell line H22 in which the platform **DPP**/UCNPs/PEG was injected and studied in three different groups: dark, UV-irradiation and NIR-irradiation, as well as two extra group without the platform, one irradiated with NIR-light and the other without irradiation (control). The group that inhibited the tumour the most was the one injected with **DPP**/UCNPs/PEG and irradiated with NIR-light, rather than UV, demonstrating that NIR-light is more penetrating than UV. This was the first time that this

strategy was studied *in vitro* and *in* vivo using a photoactivatable metal-complex. This new platform could be an alternative method of phototherapy for cancer which is activated by NIR irradiation and can also be applied in hypoxic conditions.

Other Pt(IV) complexes photoactivatable by UCNPs have also been studied.[162–166] In addition to Pt(IV)-compounds, examples have also been published with photoactivatable Ru(II)-complexes. Salassa and co-workers[167] published the first example of photoactivating Ru(II)-complex with NIR-light through UCNPs. The strategy consisted in photodegradating the *cis*-[Ru(bpy)$_2$(py)$_2$][Cl]$_2$ through the visible emission from the UCNPs when irradiated with NIR-light, thus photodissociating the pyridine and forming the corresponding aquo-adduct as active form.

Later, more examples were described using this strategy. The Wu's group[168] reported the same strategy with *cis*-[Ru(bpy)$_2$(P(CH$_3$)$_3$)(APTES)][PF$_6$]$_2$ (Λ_{exc} = 453 nm). The Ru(II)-compound and doxorubicin (dox) were loaded onto mesoporous silica coated UCNPs, when irradiated with NIR light, released *cis*-[Ru(bpy)$_2$(P(CH$_3$)$_3$)(H$_2$O)][PF$_6$]$_2$ and doxorubicin. Cytotoxicity was assessed against HeLa cells. It turned out that in the dark, there was no cytotoxicity, but under NIR irradiation, the cell viability decreased, which was shown to be due to the activation of the drug and not by the overheating caused by the laser. This demonstrated that using the strategy of activating Ru(II)-photoactivatable complexes with NIR-light by UCNPs was also effective in *in vitro* studies and could be applied biomedically. Further studies on UCNPs-assisted photolysis of Ru(II)-compounds with NIR-light, including *in vivo* studies, have been also carried out.[169–171]

Activating metal complexes with NIR light for biomedical application is a big challenge. As seen in these studies, the strategy of applying nanodrugs delivery using UCNPs to activate the photoactivatable metal complex is proving to be of great interest. However, to the best of our knowledge, no example of activating a phototherapeutic Pt(II)-complex using the UNCPs-containing platform has yet been issued.

1.3 References

1. Very Well Health https://www.verywellhealth.com/cancer-cells-vs-normal-cells-2248794 [Accessed November 2023]

2. Cancer Research UK https://www.cancerresearchuk.org/about-cancer/what-is-cancer/how-cancer-starts/cancer-cells [Accessed November 2023]

3. Health line https://www.healthline.com/health/cancer [Accessed November 2023]

4. Hanahan, D. & Weinberg, R. A. Hallmarks of Cancer: The Next Generation. *Cell* **2011**, *144*, 646-674 https://doi.org/10.1016/j.cell.2011.02.013

5. Hanhan, D. & Winberg, R. A. The Hallmarks of Cancer. *Cell* **2000,** *100*, 57-70 https://doi.org/10.1016/s0092-8674(00)81683-9

6. WHO (World Health Organization), https://www.who.int/health-topics/cancer#tab=tab_1 [Accessed September 2021]

7. Chung, L.; Tang, S.; Wu, Y.; Yang, K.; Huang, H.; Sun, G.& Sun, K. Platinum-based combination chemotherapy triggers cancer cell death through induction of BNIP3 and ROS, but not autophagy. *J. Cell Mol. Med.* **2020**, *24*, 1993-2003 https://doi.org/10.1111/jcmm.14898

8. Li, S.; Tan, L. & Meng, X. Nanoscale Metal-Organic Frameworks: Synthesis, Biocompatibility, Imaging Applications, and Thermal and Dynamic Therapy of Tumors. *Adv. Funct. Mater.* **2020**, *30*, 1908924 https://doi.org/10.1002/adfm.201908924

9. Mittal, D.; Gubin, M. M.; Schreiber, R. D. & Smyth, M. J. New insights into cancer immunoediting and its three component phases — elimination, equilibrium and escape. *Current Opinion of Immunology* **2014,** *27,* 16-25 https://doi.org/10.1016/j.coi.2014.01.004

10. Chang, A. G. & Wong, D. J. Chemotherapy: Where we have been and where we are going. *Cancer Sensistizing Agents for Chemostherapy* **2020**, *9*, 17-38 https://doi.org/10.1016/B978-0-12-820679-9.00002-5

11. Ahmad, E.; Ali, A.; Fatima, M. T.; Nimisha; Apurva; Kumar, A.; Sumi, M. P.; Sattar, R. S. A.; Mahajan, B. & Saluja, S. S. Ligand decorated biodegradable nanomedicine in the treatment of cancer. *Pharmacological Research* **2021,** *167*, 105544 https://doi.org/10.1016/j.phrs.2021.105544

12. Cancer. Net https://www.cancer.net/navigating-cancer-care/how-cancer-treated/surgery/what-cancer-surgery [Accessed August 2021]

13. Najafi, M.; Maijdpoor, J.; Toolee, H.; Mortezaee, K.; The current knowledge concerning solid cancer and therapy. *Journal of Biochemical and Molecular Toxicology* **2021,** *35,* e22900 https://doi.org/10.1002/jbt.22900

14. Matzner, P.; Sandbank, E.; Neeman, E.; Zmora, O.; Gottumukkala, V. & Ben-Eliyahu, S. Harnessing cancer immunotherapy during the unexploited immediate perioperative period. *Nature Reviews. Clinical Oncology* **2020**, *17*, 313-326 https://doi.org/10.1038/s41571-019-0319-9

15. National Cancer Institute https://www.cancer.gov/about-cancer/treatment/types/radiation-therapy [Accessed August 2021]

16. Damyanov, C. A.; Maslev, I. K.; Pavlov, V. S. & Avramov, L. Conventional Treatment of Cancer Realities and Problems. *Annals of Complementary and Alternative Medicine* **2018**, *1*, 1002 https://doi.org/10.1038/s41571-019-0319-9

17. Igarashi, Y. & Sasada, T. Cancer Vaccines: Toward the Next Breakthrough in Cancer Immunotherapy. *Journal of Immunology Research* **2020,** *2020*, 5825401 https://doi.org/10.1155/2020/5825401

18. Chaudhuri, D.; Suriano, R.; Mittelman, A. & Tiwari, R. Targeting the Immune System in Cancer. *Current Pharmaceutical Biotechnology* **2009**, *10*, 166-184 https://doi.org/10.2174/138920109787315114

19. Senapati, S.; Mahanta, A. K.; Kumar, S.& Mati, P. Controlled drug delivery vehicles for cancer treatment and their performance. *Signal Transduction and Targeted Therapy* **2018,** *3*, 1-19. https://doi.org/10.1038/s41392-017-0004-3

20. Meng, Z.; Wei, F.; Wang, R.; Xia, M.; Chen, Z.; Wang, H. & Zhu, M. NIR-Laser-Switched In Vivo Smart Nanocapsules for Synergic Photothermal and Chemotherapy of Tumors. *Adv. Mater.* **2016,** *28*, 245-253 https://doi.org/10.1002/adma.201502669

21. Nygren, P. What is cancer chemotherapy *Acta Oncologia* **2001,** *40*, 166-174 https://doi.org/10.1080/02841860151116204

22. Orvig, C. & Abrams, M. J. Medicinal Inorganic Chemistry: Introduction. *Chemical Reviews* **1999**, *99*, 2201-2203 https://doi.org/10.1021/cr980419w

23. Arruebo, M.; Vilaboa, N.; Sáez-Gutierrez, Lambea, J.; Tres, A.; Valladares, M. & González-Fernández, Á. Assessment of the Evolution of Cancer Treatment Therapies. *Cancers* **2011**, *3*, 3279-3330 https://doi.org/10.3390/cancers3033279

24. Falzone, L.; Salomone, S. & Libra, M. Evolution of Cancer Pharmacological Treatments at the Turn of the Third Millennium. *Frontiers in Pharmacology* **2018,** *9,* 1300 https://doi.org/10.3389/fphar.2018.01300

25. Gilman, A. The Initial Clinical Trial of Nitrogen Mustard. *American Journal of Surgery* **1963,** *105,* 574-578 https://doi.org/10.1016/0002-9610(63)90232-0

26. DeVita, V. T. & Chu, E. A History of Cancer Chemotherapy. *Cancer. Res.* **2008,** *68,* 8643-8653 https://doi.org/10.1158/0008-5472.CAN-07-661

27. Szikriszt, B.; Póti, Á.; Pipek, O.;Kryzstanek, M.; Kanu, N.; Molnár, J.; Ribli, D.; Szeltner, Z.; Tusnády, G. E.; Csabi, I.; Szallasi, Z.; Swanton, C. & Szüts, D. A comprehensive survey of the mutagenic impact of common cancer cytotoxics. *Genome Biology* **2016,** *17,* 99 https://doi.org/10.1186/s13059-016-0963-7

28. Jakupec, M. A.; Galanski, M.; Arion, V. B.; Hartiger, C. G. & Keppler, B. K. Antitumor metal compounds: more than theme and variations. *Dalton Trans.* **2008,** *2*, 183-194 https://doi.org/10.1039/b712656p

29. Rosenberg, B. Biological effects of platinum compounds. New agents for the control of tumors *Platinum Metal Reviews* **1971,** *15,* 42-51

30. Kelland, L. The resurgence of platinum-based cancer chemotherapy Lloyd*Nature Reviews* **2007**, *7,* 573-584 https://doi.org/10.1038/nrc2167

31. Szczepaniak, A. & Fichna, J. Organometallic compounds and metal complexes in current and future treatments of inflammatory bowel disease and colorectal cancer-a critical review. *Biomolecules* **2019**, *9*, 398 https://doi.org/10.3390/biom9090398

32. Shtemenko, A. V. & Shtemenko N. I. Rhenium–Platinum antitumor Systems. *Ukr. Biochem. J.* **2017**, *89,* 5-30 https://doi.org/10.15407/ubj89.02.005

33. Frezza, M.; Hindo, S.; Chen, D.; Davenport, A.; Schmitt, S.; Tomco, D. & Dou, P. Novel Metals and Metal Complexes as Platforms for Cancer Therapy *Curr. Pharm. Des.* **2010**, *16*, 1813-1825 https://doi.org/10.2174%2F138161210791209009

34. Hosiner, D.; Gerber, S.; Lichtenberg-Frate, H.; Glaser, W.; Schueller, C. & Edda, K. Impact of acute metal stress in Saccharomyces cerevisiae. *Plos One* **2014**, *9*, e83330 https://doi.org/10.1371/journal.pone.0083330

35. Fuertes, M. A.; Alonso, C.& Perez, J. M. Biochemical Modulation of Cisplatin Mechanisms of Action: Enhancement of Antitumor Activity and Circumvention of Drug Resistance *Chemical Reviews***2003,** *103*, 645-662 https://doi.org/10.1021/cr020010d

36. Florea, A. & Büsselberg, D. Cisplatin as an Anti-Tumor Drug: Cellular Mechanisms of Activity, Drug Resistance and Induced Side Effects *Cancers* **2011**, *3*, 1351-1371 https://doi.org/10.3390/cancers3011351

37. Doval, D. C.; Sekhon, J. S.; Gupta, S. K.; Fuloria, J.; Shukla V. K.; Gupta, S.& Awasthy, B. S. A Phase II study of gemcitabine and cisplatin in chemotherapy-naive, unresectable gall bladder cancer *British Journal of Cancer* **2004,** *90*, 1516-1520 https://doi.org/10.1038/sj.bjc.6601736

38. Karges, J.; Yempala, T.; Tharaud, M.; Gibson, D. & Gasser, G.; A Multi-action and Multi-target RuII–PtIV Conjugate Combining Cancer-Activated Chemotherapy and Photodynamic Therapy to Overcome Drug Resistant Cancers *Angew. Chem. Int. Ed.* **2020,** *59*, 7069-7075 https://doi.org/10.1002/anie.201916400

39. Galluzzi, L.; Vitale, I.; Michels, J.; Brenner, C.; Szabadki, G.; Harel-Bellan, A.; Castedo, M. & Kroemer, G. Systems biology of cisplatin resistance: past, present and future *Cell Death and diseases* **2014,** *5*, e1257 https://doi.org/10.1038/cddis.2013.428

40. Hambley, T. W. The influence of structure on the activity and toxicity of Pt anticancer drugs *Coordination Chemistry Reviews* **1997,** *166,* 181-223 https://doi.org/10.1016/s0010-8545(97)00023-4

41. Galluzzi, L.; Senovilla, L.; Vitale, I.; Michels, J.; Martins, I.; Keep, O.; Castedo, M. & Kroemer, G. Molecular mechanisms of cisplatin resistance *Ocogene* **2012,** *31,* 1869-1883 https://doi.org/10.1038/onc.2011.384

42. Culy, C. R.; Clemett, D. & Wiseman, L. R. Oxaliplatin A Review of its Pharmacological Properties and Clinical Efficacy in Metastatic Colorectal Cancer and its Potential in Other Malignancies *Drugs* **2000,** *60,* 895-924 https://doi.org/10.2165/00003495-200060040-00005

43. Johnstone, T. C.; Suntharalingam, K. & Lippard, S. J. The Next Generation of Platinum Drugs: Targeted Pt(II) Agents, Nanoparticle Delivery, and Pt(IV) Prodrugs *Chemical Reviews* **2016,** *116*, 3436-3486 https://doi.org/10.1021/acs.chemrev.5b00597

44. Gourdon, L.; Cariou, K. & Gasser, G. Phototherapeutic anticancer strategies with first- row transition metal complexes: a critical review *Chem. Soc. Rev.* **2022,** *51,* 1167-1195 https://doi.org/10.1039/d1cs00609f

45. Anthony, E. J.; Bolitho, E. M.; Bridgewater, H. E.; Carter, O. W. L.; Donnelly, J. M.; Imberti, C.; Lant, E. C.; Lermyte, F.; Needham, R. J.; Palau, M.; Sadler, P. J.; Shi, H.; Wang, F.; Zhang, W. & Zhang, Z. Metallodrugs are unique: opportunities and challenges of discovery and development *Chem. Sci.* **2020**, *11*, 12888-128917 https://doi.org/10.1039/d0sc04082g

46. Wen, J.; Yang, K.; Ding, X.; Li, H.; Xu, Y.; Liu, F. & Sun, S. In Situ Formation of Homogeneous Tellurium Nanodots in Paclitaxel-Loaded MgAl Layered Double Hydroxide Gated Mesoporous Silica Nanoparticles for Synergistic Chemo/PDT/PTT Trimode Combinatorial Therapy *Inorg. Chem.***2019,** *58*, 2987-2996 https://doi.org/10.1021/acs.inorgchem.8b02821

47. Wen, J.; Yang, K.; Liu, F.; Li, H.; Xu, Y. & Sun, S. Diverse gatekeepers for mesoporous silica nanoparticle based drug delivery systems *Chem. Soc. Rev.* **2017**, *46*, 6024-6045 https://doi.org/10.1039/C7CS00219J

48. Dai, Z. & Wang, Z. Photoactivatable Platinum-Based Anticancer Drugs: Mode of Photoactivation and Mechanism of Action *Molecules* **2020**, *25*, 5167 https://doi.org/molecules25215167

49. Sternberg, E. D. & Dolphin, D. Porphyrin-based Photosensitizers for Use in Photodynamic Therapy Ethan *Tetrahedron* **1998,** *54*, 4151-4202 https://doi.org/10.1016/S0040-4020(98)00015-5

50. Imberti, C.; Zhang, P.; Huang, H. & Sadler, P. J. New Designs for Phototherapeutic Transition Metal Complexes *Angew. Chem. Int. Ed.* **2020**, *59,* 61-53 https://doi.org/10.1002/anie.201905171

51. Ackroyd, R.; Kelty, C.; Brown, N & Reed, M. The History of Photodetection and Photodynamic Therapy *Photochemistry and Photobiology* **2001,** *74*, 656-669 https://doi.org/10.1562/0031-8655(2001)074%3C0656:thopap%3E2.0.co;2

52. Choi, H. W.; Lim, J. H.; Kim, C. W.; Lee, E.; Kim, J.; Chang, K. & Chung, B. G. Near-Infrared Light-Triggered Generation of Reactive Oxygen Species and Induction of Local Hyperthermia from Indocyanine Green Encapsulated Mesoporous Silica-Coated Graphene Oxide for Colorectal Cancer Therapy *Antioxidants* **2022**, *11*, 174 https://doi.org/10.3390/antiox11010174

53. Wan, W.; Chen, B.; Li, L.; Wang, D.; Shi, S.; Zhang, T.; Wang, Y.; Zhang, L. & Wang, Y. Nanoscaled red blood cells facilitate breast cancer treatment by combining photothermal/photodynamic therapy and chemotherapy *Biomaterials* **2018,** *155,* 25-40 https://doi.org/10.1016/j.biomaterials.2017.11.002

54. Zhen, X.; Xie, C. & Pu, K. Temperature-Correlated Afterglowofa Semiconducting Polymer Nanococktailfor Imaging-Guided Photothermal Therapy *Angew. Chem. Int. Ed.* **2018**, *57*, 3918-3942 https://doi.org/10.1002/anie.201712550

55. Cheng, L.; Wang, C.; Feng, L.; Yang, K. & Liu, Z. Functional Nanomaterials for Phototherapies of Cancer *Chem. Rev.* **2014**, *114,* 10869-10939 https://doi.org/10.1021/cr400532z

56. Mari, C.; Pierroz, V.; Ferrari, S. & Gasser, G. Combination of Ru(II) complexes and light: new frontiers in cancer therapy *Chem. Sci.* **2015,** *6,* 2660-2686 https://doi.org/10.1039/c4sc03759f

57. Lameijer, L. N.; Ernst, D.; Hopkins, S. L.; Meijer, M. S.; Askes, S. H. C.; Dévédec, S. E. L. & Bonnet, S. ARed-Light-Activated Ruthenium-Caged NAMPT Inhibitor Remains Phototoxic in Hypoxic Cancer Cells *Angew. Chem. Int. Ed.* **2017,** *56,* 11549-11553 https://doi.org/10.1002/anie.201703890

58. Tao, W.; Wang, N.; Ruan, J.; Cheng, X.; Fan, L.; Zhang, P.; Lu, C.; Hu, Y.; Che, C.; Sun, D.; Duan, J. & Zhao, M. Enhanced ROS-Boosted Phototherapy against Pancreatic Cancer via Nrf2-Mediated Stress-Defense Pathway Suppression and Ferroptosis Induction *ACS Appl. Mater. Interfaces* **2022,** *14*, 6404-6416 https://doi.org/10.1021/acsami.1c22861

59. Zhang, C.; Gao, F.; Wu, W.; Qiu, W.; Zhang, L.; Li, R.; Zhuang, Z.; Yu, W.; Cheng, H. & Zhang, X. Enzyme-Driven Membrane-Targeted Chimeric Peptide for Enhanced Tumor Photodynamic Immunotherapy *ACS Nano.* **2019,** *13*, 11249-11262 https://doi.org/10.1021/acsnano.9b04315

60. Baskaran, R.; Lee, J. & Yang, S. Clinical development of photodynamic agents and therapeutic applications *Biomaterials Research* **2018,** *22,* 25 https://doi.org/10.1186/s40824-018-0140-z

61. Luby, B. M.; Walsh, C. D. & Zheng, G. Advanced Photosensitizer Activation Strategies for Smarter Photodynamic Therapy Beacons *Angew. Chem. Int. Ed.* **2019**, *58,* 2558-2569 https://doi.org/10.1002/anie.201805246

62. Bolitho, E. M.; Sanchez-Cano, C.; Shi, H.; Quinn, P. D.; Harkiolaki, M.; Imberti, C. & Sadler, P. J. Single-Cell Chemistry of Photoactivatable Platinum Anticancer Complexes *J. Am. Chem. Soc.* **2021**, *143*, 20224-20240 https://doi.org/10.1021/jacs.1c08630

63. Celli, J. P.; Spring, B. Q.; Rizvi, I.; Evans, C. L.; Samkoe, K. S.; Verma, S.; Pogue, B. W. & Hasan, T. Imaging and Photodynamic Therapy: Mechanisms, Monitoring, and Optimization *Chem. Rev.* **2010,** *110,* 2795-2838 https://doi.org/10.1021/cr900300p

64. Cai, X.; Xie, Z.; Ding, B.; Shao, S.; Liang, S.; Pang, M. & Lin, J. Monodispersed Copper(I)-Based Nano Metal–Organic Framework as a Biodegradable Drug Carrier with Enhanced Photodynamic Therapy Efficacy *Adv. Sci.* **2019,** *6,* 1900848 https://doi.org/10.1002/advs.201900848

65. Dabrowski, J. M. & Arnault, L. G. Photodynamic therapy (PDT) of cancer: from local to systemic treatment *Photochem. Photobiol. Sci.* **2015,** *14,* 1765-1780 https://doi.org/10.1039/C5PP00132C

66. Fu, X.; Yang, Z.; Deng, T.; Chen, J.; Wen, Y.; Fu, X.; Zhou, L.; Zhu, Z. & Yu, C. A natural polysaccharide mediated MOF-based Ce6 delivery system with improved biological properties for photodynamic therapy *J. Mater. Chem. B.* **2020,** *8,* 1481-1488 https://doi.org/10.1039/C9TB02482D

67. Gunaydin, G.; Gedik, M. E. & Ayan, S. Photodynamic Therapy for the Treatment and Diagnosis of Cancer–A Review of the Current Clinical Status *Frontiers in Chemistry* **2021,** *9,* 686303 https://doi.org/10.3389/fchem.2021.686303

68. Shi, H. & Sadler, P. J. How promising is phototherapy for cancer? *Br. J. Cancer* **2020**, *123*, 871-873 https://doi.org/10.1038/s41416-020-0926-3

69. Kwiatkowski, S.; Knap, B.; Przystupski, D.; Saczko, J.; Kedzierska, E.; Knap-Czop, K.; Kotlinska, J.; Michel, O.; Kotowski, K. & Kulbacka, J. Photodynamic therapy – mechanisms, photosensitizers and combinations *Biomedicine & Pharmacotherapy* **2018**, *106,* 1098-1107 https://doi.org/10.1016/j.biopha.2018.07.049

70. Chilakamarthi, U. & Giribabu, L. Photodynamic Therapy: Past, Present and Future *Chem. Rec.* **2017**, *17*, 1-29 https://doi.org/10.1002/tcr.201600121

71. Mfouo-Tynga, I. S.; Días, L. D.; Inada, N. M. & Kurachi, C. Features of third generation photosensitizers used in anticancer photodynamic therapy: Review *Photodiagnosis and Photodynamic Therapy* **2021**, *34*, 102091 https://doi.org/10.1016/j.pdpdt.2020.102091

72. Farrer, N. J.; Salassa, L. & Sadler, P. J. Photoactivated chemotherapy (PACT): the potential of excited-state d-block metals in medicine *Dalton Trans.* **2009,** *48,* 10690-10701 https://doi.org/10.1039/b917753a

73. Monro, S.; Colón, K. L.; Yin, H.; Roque III, J.; Konda, P.; Gujar, S.; Thummel, R. P.; Lilge, L.; Cameron, C. G. & McFarland, S. A. Transition Metal Complexes and Photodynamic Therapy from a Tumor-Centered Approach: Challenges, Opportunities, and Highlights from the Development of TLD1433 *Chem. Rev.* **2019,** *199,* 797-828 https://doi.org/10.1021/acs.chemrev.8b00211

74. Kaplan, M.J.; Somers, R. G.; Greenberg, R. H. & Ackler, J. Photodynamic Therapy in the Management of Metastatic Cutaneous Adenocarcinomas: Case Reports From Phase 1/2 studies Using Tin Ethyl Etiopurpurin (SnEt2) *J. Surg. Oncol.* **1998**, *67*, 121-125 https://doi.org/10.1002/(SICI)1096-9098(199802)67:2%3C121::AID-JSO9%3E3.0.CO;2-C

75. Patel, H.; Mick, R.; Finlay, J.; Zhu, T. C.; Rickter, E.; Cengel, K. A.; Malkowicz, S. B.; Hahn, S. M. & Busch, T. M. Motexafin Lutetium-Photodynamic Therapy of Prostate Cancer: Short- and Long-Term Effects on Prostate-Specific Antigen *Clin. Cancer Res.* **2008**, *14,* 4869-4876 https://doi.org/10.1158%2F1078-0432.CCR-08-0317

76. Sokolov, V.V.; Chissov, V. I.; Yakubovskya, R. I.; Aristarkhova, E. I.; Filonenko, E. V.; Belous, T. A.; Vorozhtsov, G. N.; Zharkova, N. N.; Smirnov, V. V.; Zhitkova, M. B. Photodynamic Therapy (PDT) of malignant tumors by photosensitizer Photosens: results of 45 clinical cases *SPIE* **1996**, *2625*, 281-287 https://doi.org/10.1117/12.230943

77. Moore, C. M.; Azzouzi, A.; Barret, E.; Villers, A.; Muir, G. H.; Barber, N. J.; Bott, S.; Trachtenberg, J.; Arumainayagam, N.; Gaillac, B.; Allen, C.; Schertz, A. & Emberton, M. Determination of optimal drug dose and light dose index to achieve minimally invasive focal ablation of localised prostate cancer using WST11-vascular-targeted photodynamic (VTP) therapy *BJU Int.* **2014**, *116*, 888-896 https://doi.org/10.1111/bju.12816

78. McFarland, S. A.; Mandel, A.; Dumoulin-White & Gasser Gilles Metal-based photosensitizers for photodynamic therapy: future of multimodal oncology? *Current Opinion in Chemical Biology* **2020,** *56,* 23-27 https://doi.org/10.1016/j.cbpa.2019.10.004

79. Ouyang, M.; Zeng, L.; Qiu, K.; Chen, Y.; Ji, L. & Chao, H. Cyclometalated Ir[III] Complexes as Mitochondria-Targeted Photodynamic Anticancer Agents *Eur. J. Inorg. Chem.* **2017**, *2017,* 1764-1771 https://doi.org/10.1002/ejic.201601129

80. Zhu, J.; Dominijanni, A.; Rodríguez-Corrales, J. Á.; Prussin, R.; Zhao, Z.; Li, T.; Robertson, J. L. & Brewer, K. J. Visible light-induced cytotoxicity of Ru, Os-polyazine complexes towards rat malignant glioma *Inorganica Chimica Acta* **2017**, *454*, 155-161 https://doi-org/10.1016/j.ica.2016.05.044

81. Naik, A.; Rubbiani, R.; Gasser, G. & Spingler, B. Visible-Light-Induced Annihilation of Tumor Cells with Platinum-Porphyrin Conjugates *Angew. Chem.* **2014,** *126,* 7058-7061 https://doi.org/10.1002/ange.201400533

82. Zhong, F.; Yuan, X.; Zhao, J. & Wang, Q. Visible-Light-harvesting tricarbonyl Re(I) complex: synthesis and application in intracellular photodynamic effect and luminescence imaging *Sci. China Chem.* **2016,** *59,* 70-77 https://doi.org/10.1007/s11426-015-5491-x

83. Wang, Z.; Liu, B.; Sun, Q.; Dong, S.; Kuang, Y.; Dong, Y.; He, F.; Gai, S. & Yang, P. Fusiform-Like Copper(II)-Based Metal–Organic Framework through Relief Hypoxia and GSH-Depletion Co-Enhanced Starvation and Chemodynamic Synergetic Cancer Therapy *ACS Appl. Mater. Interfaces* **2020,** *12,* 17254-17267 https://doi.org/10.1021/acsami.0c01539

84. An, J.; Hu, Y. Cheng, K.; Li, C.; Hou, X.; Wang, G.; Zhang, X.; Liu, B.; Zhao, Y. & Zhang, M. ROS-augmented and tumor-microenviromental responsive biodegradable nanoplatform for enhancing chemo-sonodynamic therapy *Biomaterials* **2020,** *234,* 119761 https://doi.org/10.1016/j.biomaterials.2020.119761

85. Zhang, J.; Ramu, V.; Zhou X.; Frias C.; Ruiz-Molina D.; Bonnet, S.; Roscini, C. & Novio, F. Photoactivable Ruthenium-Based Coordination Polymer Nanoparticles for Light-Induced Chemotherapy *Nanomaterials* **2021,** *11*, 3089 https://doi.org/10.3390/nano11113089

86. Sun, W.; Wen, Y.; Thiramanas, R.; Chen, M.; Han, J.; Gong, N.; Wagner, M.; Jiang, S.; Meijer, M. S.; Bonnet, S.; Butt, H.; Mailander, V.; Liang, X & Wu, S. Red-Light-Controlled Release of Drug–Ru Complex Conjugates from Metallopolymer Micelles for Phototherapy in Hypoxic Tumor Environments *Adv. Funct. Mater.* **2018,** *28*, 1804227 https://doi.org/10.1002/adfm.201804227

87. Mahnken, R. E.; Bina M.; Deibel, R. M.; Luebke, K. & Morrison, H. PHOTOCHEMICALLY INDUCED BINDING OF Rh(phen),Cl,+ TO DNA *Photochemistry and Photobiology* **1989,** 49, 519-522 https://doi.org/10.1111/j.1751-1097.1989.tb09204.x

88. Bonnet, S. Why develop photoactivated chemotherapy? *Dalton Trans.* **2018,** *47,* 10330-10343 https://doi.org/10.1039/c8dt01585f

89. Butler, J. S & Sadler, P. J. Targeted delivery of platinum-based anticancer complexes *Current Opinion in Chemical Biology* **2013,** *17*, 175-188 https://doi.org/10.1016/j.cbpa.2013.01.004

90. Garai, A.; Pant, I.; Banerjee, S.; Banik, B.; Kondaiah, P. & Chakravarty, A. R. Photorelease and Cellular Delivery of Mitocurcumin from its Cytotoxic Cobalt (III) Complex in Visible Light *Inorg. Chem.* **2016**, *55*, 6027-6035 https://doi.org/10.1021/acs.inorgchem.6b00554

91. Cuello-Garibo, J.; James, C. C.; Siegler, M. A. & Bonnet, S. Ruthenium-based PACT compounds based on an N,S non-toxic ligand: a delicate balance between photoactivation and thermal stability *Chem²* **2017,** *1,* 2 https://doi.org/10.28954/2017.csq.12.002

92. Wu, N.; Cao, J.; Wu, X.; Tan, C.; Ji, L. & Mao, Z. Iridium(III) complexes with five-membered heterocyclic ligands for combined photodynamic therapy and photoactivated chemotherapy *Dalton Trans.* **2017,** *46,* 13482-13491 https://doi.org/10.1039/c7dt02477k

93. Leonidova, A.; Pierroz, V.; Rubbiani, R.; Lan, Y.; Schmitz, A. G.; Kaech, A.; Sigel, R. K. O.; Ferrari, S.; Gasser, G. Photo-induced uncaging of specific Re(I) organometallic complex in living cells *Chem. Sci.* **2014**, *5*, 4044-4056 https://doi.org/10.1039/C3SC53550A

94. Rosa, A.; Ricciardi, G.; Baerends, J. & Stufkens, D. J. Density Functional Study of the Photodissociation of $Mn_2(CO)_{10}$ *Inorg. Chem.* **1996,** *35,* 2886-2897 https://doi.org/10.1021/ic950518h

95. Ciesienski, K. L.; Hyman, L. M.; Yang, D. T.; Haas, K. L.; Dickens, M. G.; Holbrook, R. J. & Franz, K. J. A Photo-Caged Platinum(II) Complex That Increases Cytotoxicity upon Light Activation *Eur. J. Inorg. Chem.* **2010,** *15,* 2224-2228 https://doi.org/10.1002/ejic.201000098

96. Paradies, J.; Crudass, J.; MacKay, F.; Yellowlees, L. J.; Montgomery, J.; Parsons, S.; Oswald, I.; Robertson, N. & Sadler, P. J. Photogeneration of titanium(III) from titanium(IV) citrate in aqueous solution *Journal of Inorganic Biochemistry* **2006,** *100,* 1260-1264 https://doi.org/10.1016/j.jinorgbio.2006.02.011

97. Sasmal, P. K.; Saha, S.; Majumdar, R.; Dighe, R. R. & Chakravarty, A. R. Oxovanadium(IV)-based near-IR PDT agents: design to biological evaluation *Chem. Commun.* **2009,** *13,* 1703-1705 https://doi.org/10.1039/b822229k

98. Billadeau, M. A. & Morrsion, H. Photoaquation of cis-Dichlorobis- (1,10-phenanthroline)chromium(III) and the Photochemical and Thermal Reactions of this Complex with Native Calf-Thymus DNA *J. Inorg. Biochem.* **1995,** *57,* 249-270 https://doi.org/10.1016/0162-0134(94)00029-a

99. Motterlini, R.; Clark, J. E.; Foresti, R.; Sarathchandra, P.; Mann, B. E. & Green, C. J. Carbon Monoxide–Releasing Molecules Characterization of Biochemical and Vascular Activities *Circ. Res.* **2002,** *90,* e17-e24 https://doi.org/10.1161/hh0202.104530

100. Maurer, T. D.; Kraft, B. J.; Lato, S. M.; Ellington, A. D. & Zaleski, J. M. Photoactivated DNA cleavage via charge transfer promoted N2 release from tris[3-hydroxy-1,2,3-benzotriazine-4(3H)-one]iron(iii) *Chem. Commun.* **2000,** *4,* 69-70 https://doi.org/10.1039/A908005H

101. Chen Y.; Lei, W.; Jiang, G.; Hou, Y.; Li, C.; Zhang, B.; Zhou, Q. & Wang, X. Fusion of photodynamic therapy and photoactivated chemotherapy: a novel Ru(II) arene complex with dual activities of photobinding and photocleavage toward DNA *Dalton Trans.* **2014,** *43,* 15375-15384 https://doi.org/10.1039/c4dt01755b

102. Renfrew, A. K.; Bryce, N. S. & Hambley, T. Cobalt(III) Chaperone Complexes of Curcumin:Photoreduction, Cellular Accumulation and Light-Selective Toxicity towards Tumour Cells *Chem. Eur. J.* **2015,** *21,* 15224-15234 https://doi.org/10.1002/chem.201502702

103. Kim, M. R.; Morrison, H. & Mohammed, S. I. Effect of a photoactivated rhodium complex in melanoma *Anticancer Drugs* **2011,** *22,* 896-904 https://doi.org/10.1097/CAD.0b013e32834850a5

104. Lutterman, D. A.; Fu, P. K. L. & Turro, C. cis-[Rh2(μ-O2CCH3)2(CH3CN)6]2+ as a Photoactivated Cisplatin Analog *J. Am. Chem. Soc.* **2006,** *128,* 738-739 https://doi.org/10.1021/ja057620q

105. Morales, K.; Samper, K. G.; Peña, Q.; Hernando, J.; Lorenzo, J.; Rodríguez-Diéguez, A.; Capdevila, M.; Figueredo, M.; Palacios, O. & Bayón, P. Squaramide-Based Pt(II) Complexes as Potential Oxygen-Regulated Light-Triggered Photocages *Inorg. Chem.* **2018,** *57,* 15517-15525 https://doi.org/10.1021/acs.inorgchem.8b02854

106. Bednarski, P. J.; Mackay, F. S. & Sadler, P. J. Photoactivatable Platinum Complexes *Anti-Cancer Agents in Medicinal Chemistry,* **2007,** *7,* 75-93 https://doi.org/10.2174/187152007779314053

107. Chen, Y.; Bai, L.; Zhang, P.; Zhao, H. & Zhou, Q. The Development of Ru(II)-Based Photoactivated Chemotherapy Agents *Molecules* **2021**, *26*, 5679 https://doi.org/10.3390/molecules26185679

108. Singh, T. N. & Turro, C. Photoinitiated DNA Binding by *cis*-[Ru(bpy)$_2$(NH$_3$)$_2$]$^{2+}$ *Inorg. Chem.* **2004**, *43*, 7260-7262 https://doi.org/10.1021/ic049075k

109. Garner, R. N.; Gallucci, J. C.; Dunbar, K. R. & Turro, C. [Ru(bpy)$_2$(5-cyanouracil)$_2$]$^{2+}$ as Potential Ligh-Activated Dual-Action Therapeutic Agent *Inorg. Chem.* **2011**, *50*, 9213-9215 https://doi.org/10.1021/ic201615u

110. Howerton, B. S.; Heidary, D. K. & Glazer, E. C. Strained Ruthenium Complexes Are Potent Light-Activated Anticancer Agents *J. Am. Chem. Soc.* **2012**, *134,* 8324-8327 https://doi.org/10.1021/ja3009677

111. Lameijer, L. N.; Ernst, D.; Hopkins, S. L.; Meijer, M. S.; Askes, S. H. C.; Le Dévédec, S. E. & Bonnet, S. A Red-Light-Activated Ruthenium-Caged NAMPT Inhibitor Remains Phototoxic in Hypoxic Cancer Cells *Angew. Chem.* **2017**, *129*, 11707-11711 https://doi.org/10.1002/ange.201703890

112. Knoll, J. D.; Albani, B. A. & Turro, C. New Ru(II) Complexes for Dual Photoreactivity: Ligand Exchange and ^{1}O$_2$ Generation *Acc. Chem. Res.* **2015**, *48*, 2280-2287 https://doi.org/10.1021/acs.accounts.5b00227

113. Sun, W.; Li, S.; Häupler, B.; Liu, J.; Jin, S.; Steffen, W.; Schubert, U. S.; Butt, H.; Liang, X. & Wu, S. An amphilic Ruthenium Polymetallodrug for Combined Photodynamic Therapy and Photochemotherapy In Vivo *Adv. Mater.* **2017**, *29*, 1603702 https://doi-org.1002/adma.201603702

114. Jin, Z.; Qi, S.; Guo, X.; Jian, Y.; Hou, Y.; Li, C.; Wang, X. & Zhou, Q. The modification of a pyrene group makes a Ru(II) complex versatile *Chem. Commun.* **2021**, *57*, 3259-3262 https://doi-org.are.uab.cat/10.1039/D0CC08400J

115. Shi, H.; Imberti, Sadler, P. J. Diazido platinum(IV) complexes for photoactivated anticancer chemotherapy *Inorg. Chem. Fron.* **2019,** *6*, 1623-1638 https://doi.org/10.1039/c9qi00288j

116. Kratochwill, N. A.; Zabel, M.; Range, K.; Bednarski, P. J. Synthesis and X-ray Crystal Structure of trans,cis-[Pt(OAc)$_2$I$_2$(en)]: A Novel Type of Cisplatin Analog That Can Be Photolyzed by Visible Light to DNA-Binding and Cytotoxic Species in Vitro *J. Med. Chem.* **1996,** *39,* 2499-2507 https://doi.org/10.1021/jm9509105

117. Kratochwil, N. A. & Bednarski, P. J. Relationships between Reduction Properties and Cancer Cell Growth Inhibitory Activities of *cis*-Dichloro- and *cis*-Diiodo-Pt(IV)-ethylenediamines *Arch. Pharm. Pharm. Med. Chem.* **1999**, *332*, 279-285 https://doi.org/10.1002/(SICI)1521-4184(19998)332:8%3C279::AID-ARDP279%3E3.0.CO;2-1

118. Müller, P.; Schröder, B.; Parkinson, J. A.; Kratochwill, N. A.; Coxall, R. A.; Parkin, A.; Parsons, S. & Sadler, P. J. Nucleotide Cross-Linking Induced by Photoreactions of Platinum(iv)±Azide Complexes *Angew. Chem. Int. Ed.* **2003,** *42,* 335-339 https://doi.org/10.1002/anie.200390110

119. Kaspárková, J.; Mackay, F. S.; Brabec, V. & Sadler, P. J. Formation of platinated GG cross-links on DNA by photoactivation of a platinum(IV) azide complex *J. Biol. Inorg. Chem.* **2003,** *8,* 741-745 https://doi.org/10.1007/s00775-003-0474-3

120. Mackay, F. S.; Woods, J. A.; Moseley, H.; Ferguson, J.; Dawson, A.; Parsons, S. & Sadler, P. J. A Photoactivated *trans*-Diammine Platinum Complex as Cytotoxic as Cisplatin *Chem. Eur. J.* **2006**, *12*, 3155-3161 https://doi.org/10.1002/chem.200501601

121. Farrer, N. J.; Woods, J. A.; Munk, V. P.; Mackay, F. S. & Sadler, P. J. Phototoxicity *trans*-Diam(m)ine Platinum(IV) Diazido Complexes More Potent than Their *cis* Isomer *Chem. Res. Toxicol.* **2010**, *23*, 413-421 https://doi.org/10.1021/tx900372p

122. Farrer, N. J.; Woods, J. A.; Salassa, L.; Zhao, Y.; Robinson, K. S.; Clarkson, G.; Mackay, F. S. & Sadler, P. J. *Angew. Chem.* **2010**, *122*, 9089-9092 https://doi-org/10.1002/ange.201003399

123. Mackay, F. S.; Farrer, N. J.; Salassa, L.; Tai, H.; Deeth, R. J.; Moggach, S. A.; Wood, P. A.; Parsons, S. & Sadler, P. J. Synthesis, characterisation and photochemistry of Pt^{IV} of pyridyl azido acetate complexes *Dalton Trans.* **2009**, *2009,* 2315-2325 https://doi.org/10.1039/B820550G

124. Lotnner, C.; Bart, K.; Bernhardt, G. & Brunner, H. Hematoporphyrin-Derived Soluble Porphyrin-Platinum Conjugates with Combined Cytotoxic and Phototoxic Antitumor Activity *J. Med. Chem.* **2002**, *45*, 2064-2078 https://doi.org/10.1021/jm0110688

125. Heringova, P.; Woods, J.; Mackay, F. S.; Kasparkova, J.; Sadler, P. J. & Brabec, V. Transplatin is cytotoxic when photoactivated: Enhanced Formation of DNA Cross-Links *J. Med. Chem.* **2006**, *49*, 7792-7798 https://doi.org/10.1021/jm0606692

126. Mlcouskova, J.; Stepankova, J. & Brabec, V. Antitumor carboplatin is more toxic in tumor cells when photoactivated: enhanced DNA binding *J. Biol. Inorg. Chem.* **2012**, *17*, 891-898 https://doi.org/10.1007/s00775-012-0906-z

127. Srivastava, P.; Singh, K.; Verma, M.; Sivakumar, S. & Patra, A. K. Photoactive Platinum(II) complexes of nonsteroidal anti-inflammatory drug naproxen: Interaction with biological targets, antioxidant activity and cytotoxicity *European Journal of Medicinal Chemistry* **2018**, *144*, 243-254 https://doi-org/10.1016/j.ejmech.2017.12.025

128. Mitra, K.; Gautam, S.; Konaiah, P. & Chakravarty, A. R. The *cis*-Diammineplatinum(II) Complex of Curcumin: A Dual Action DNA Crosslinking and Photochemotherapeutic Agent *Angew. Chem.* **2015**, *127*, 14795-14199 https://doi-org/10.1002/ange.201507281

129. Liu, D.; Ma, J.; Zhou, W. He, W. & Guo, Z. Synthesis and photoactivity of Pt(II) complex based on an *o*-nitrobenzyl-derived ligand *Inorganica Chimica Acta* **2012**, *393*, 198-203 https://doi.org/10.1016/j.ica.2012.06.047

130. Morales, K.; Rodríguez-Calado, S.; Hernando, J.; Lorenzo, J.; Rodríguez-Diéguez, A.; Jaime, C.; Nolis, P.; Capdevila, M.; Palacios, O.; Figueredo, M. & Bayón, P. Synthesis and In Vitro Studies of Photoactivatable Semisquaraine-type Pt(II) Complexes *Inorg. Chem.* **2022,** *61,* 7729-7745 https://doi.org/10.1021/acs.inorgchem.1c03957

131. Zhang, Z; Jayakumar, M. K. G.; Zheng, X.; Shikha, S.; Zhang, Y.; Bansal, A.; Poon, D. J. J.; Chu, P. L-; Yeo, E. L. L.; Chua, M. L. K.; Chee, S. K. & Zhang, Y. Upconversion superballs for programmable photoactivation of therapeutics *Nature Communications* **2019**, *10*, 1-12 https://doi.org/10.1038/s41467-019-12506-w

132. Park, Y.; Lee, K. T.; Suh, Y. D. & Hyeon, T. Upconverting nanoparticles: a versatile platform for wide-field two-photon microscopy and multi-modal *in vivo* imaging *Chem. Soc. Rev.* **2015**, *44*, 1302-1317 https://doi-org/10.1039/C4CS00173G

133. Philips, D. The photochemistry of sensitisers for photodynamic therapy *Pure & Appl. Chem.* **1995**, *67*, 117-126 https://doi.org/10.1351/pac199567010117

134. Idris, N. M.; Gnanasammandhan, M. K.; Zhang, J.; Ho, P. C.; Mahendran, R. & Zhang, Y. In vivo photodynamic therapy using upconversion nanoparticles as remote-controlled nanotransducers *Nat. Med.* **2012**, *18,* 1580-1586 https://doi.org/10.1038/nm.2933

135. Auzel, F. Upconversion and Anti-Stokes Processes with f and d Ions in Solids *Chem. Rev.* **2004,** *104,* 139-173 https://doi.org/10.1021/cr020357g

136. Farka, Z.; Mickert, M.; Mikusová, Z.; Hlavacek, A.; Pavla, B.; Xu, W.; Bounchal, P.; Skladal, P. & Gorris, H. H. Surface design of photon-upconversion nanoparticles for high- contrast immunocytochemistry *Nanoscale,* **2020***, 12*, 8303-8313 https://doi.org/10.1039/C9NR10568A

137. Shao, Y.; Liu, B.; Di, Z.; Zhang, G.; Sun L.; Li, L. & Yan, C. Engineering of Upconverted Metal–Organic Frameworks for Near-Infrared Light-Triggered Combinational Photodynamic/Chemo-/Immunotherapy against Hypoxic Tumors *J. Am. Chem. Soc.* **2020,** *142,* 3939-3946 https://doi.org/10.1021/jacs.9b12788

138. Auzel, F. E. Materials and Devices Using Double-Pumped Phosphors with Energy Transfer *Proceedings of The IEE* **1973**. *61*, 758-786 https://doi-org.are.uab.cat/10.1109/PROC.1973.9155

139. Ji, G.; Wang, Y.; Qin, Y.; Peng, Y.; Li, S.; Han, D.; Ren, S.; Qin, K.; Li, S.; Gao, Z. & Han, T. Latest developments in the upconversion nanotechnology for the rapid detection of food safety: A review *Nanotechnology Reviews* **2022**, *11*, 2101-2122 https://doi.org/10.1515/ntrev-2022-0086

140. Mahata, M.; De, R. & Lee, K. T. Near-Infrared-Trigged Upconverting Nanoparticles for Biomedicine Applications *Biomedicines* **2021**, *9*, 756 https://doi.org/10.3390/biomedicines9070756

141. Cheng, L.; Wang, C. & Liu Z. Upconversion nanoparticles and their composite nanostructures for biomedical imaging and cancer therapy *Nanoscale* **2013,** *5*, 23-37 https://doi.org/10.1039/c2nr32311g

142. Haase, M. & Schäfer, H. Upconverting Nanoparticles *Angew. Chem. Int. Ed.* **2011**, *50*, 5808-5829 https://doi-org/10.1002/anie.201005159

143. Xie, X. & Liu, X. Upconversion goes broadband *Nature Materials* **2012**, *11*, 842-843 https://doi.org/10.1038/nmat3426

144. Wang, F. & Liu, X. Recent advances in the chemistry of lanthanide-doped upconversion nanocrystals *Chem. Soc. Rev.* **2009**, *38*, 976-989 https://doi-org/10.1039/B809132N

145. Joubert, M. F. Photon avalanche upconversion in rare earth laser materials *Optical Materials* **1999**, *11*, 181-203 https://doi.org/10.1016/S0925-3467(98)00043-3

146. Wang, F.: Banerjee, D.; Liu, Y.; Chen X. & Liu, X. Upconversion nanoparticles in biological labeling, imaging, and therapy *Analyst* **2010,** *135,* 1839-1854 https://doi.org/10.1039/c0an00144a

147. Dong, N.; Pedroni, M.; Piccinelli, F.; Conti, G.; Sbarbati, A.; Ramírez-Hernández, J. E.; Maestro, L. M.; Iglesias-de la Cruz, M. C.; Sanz-Rodríguez, F.; Juarranz, A.; Chen, F.; Vetrone, F.; Capobianco, J. A.; Solé, J. G.; Bettinelli, M.; Jaque, D. & Speghini, A. NIR-to-NIR Two-Photon Excited CaF_2: Tm^{3+}, Yb^{3+} Nanoparticles: Multifunctional Nanoprobes for Highly Penetrating Fluorescence Bio-Imaging *ACS Nano* **2011**, *5*, 8665-8671 https://doi.org/10.1021/nn202490m

148. Chatterjee, D. K.; Rufaihah, A. J. & Zhang, Y. Upconversion fluorescence imaging of cells and small animals using lanthanide doped nanocrystals *Biomaterials* **2008**, *29*, 937-943 https://doi.org/10.1016/j.biomaterials.2007.10.051

149. Peng, J.; Wang, Y.; Wang, J.; Zhou, X. & Liu, Z. A new biosensor for glucose determination in serum based on up-converting fluorescence resonance energy transfer *Biosensors and bioelectronics* **2011**, *28*, 414-420 https://doi.org/10.1016/j.bios.2011.07.057

150. Niedbala, R. S.; Feindt, H.; Kardos, Vail, T.; Burton, J.; Bielska, B.; Li, S.; Milunic, D.; Bourdelle, P. & Vallejo, R. Detection of Analytes by Immunoassay Using Up-Converting Phosphor Technology *Analytical Biochemistry* **2001**, *293*, 22-30 https://doi.org/10.1006/abio.2001.5105

151. Wang, C.; Cheng, L. & Liu, Z. Drug delivery with upconversion nanoparticles for multi-functional targeted cancer cell imaging and therapy *Biomaterials* **2011**, *32*, 1110-1120 https://doi.org/10.1016/j.biomaterials.2010.09.069

152. Wang, C.; Tao, H.; Cheng, L. & Liu, Z. Near-infrared light induced in vivo photodynamic therapy of cancer based on upconversion nanoparticles *Biomaterials* **2011**, *32*, 6145-6154 https://doi.org/10.1016/j.biomaterials.2011.05.007

153. Zhang, P.; Steelant, W.; Kumar, M. & Scholfield, M. Versatile Photosensitizers for Photodynamic Therapy at Infrared Excitation *J. Am. Chem. Soc.* **2007**, *129,* 4526-4527 https://doi.org/10.1021/ja0700707

154. Guo, H.; Qian, H.; Idris, N. M.; Zhang, Y. Singlet Oxygen-induced apoptosis of cancer cells using upconversion fluorescent nanoparticles as a carrier of photosensitizer *Nanomed., Nanotechnol., Biol., Med.* **2010**, *6*, 486-495 https://doi.org/10.1016/j.nano.2009.11.004

155. Liu, K.; Liu, X.; Zeng, Q.; Zhang, Y.; Tu, L.; Liu, T.; Kong, X.; Wang, Y.; Cao, F.; Lambrechts, S. A. G.; Aalders, M. C. G. & Zhang, H. Covalently Assembled NIR Nanoplatform for Simultaneous Fluorescence Imaging and Photodynamic Therapy of Cancer Cells *ACS NANO* **2012**, *6*, 4054-4062 https://doi.org/10.1021/nn300436b

156. Zhou, A.; Wei, Y.; Wu, B.; Chen, Q. & Xing, D. Pyropheophorbide A and c(RGDyK) Comodified Chistosan-Wrapped Upconversion Nanoparticle for Targeted Near-Infrared Photodynamic Therapy *Mol. Pharmaceutics* **2012**, *9*, 1580-1589

157. Cui, S.; Chen, H.; Zhu, H.; Tian, J.; Chi, X.; Qian, Z.; Achilefu, S. & Gu, Y. Amphiphilic chitosan modified upconversion nanoparticles for *in vivo* photodynamic therapy induced by near-infrared light *J. Mater. Chem.* **2012**, *22*, 4861-4873 https://doi-org.are.uab.cat/10.1039/C2JM16112E

158. Guo, Y.; Kumar, M. & Zhang, P. Nanoparticle-Based Photosensitizers under CW Infrared Excitation *Chem. Mater.* **2007**, *19*, 6071-6072 https://doi.org/10.1021/cm7028454

159. Garcia, J. V.; Yang, J.; Shen, D.; Yao, C.; Li, X.; Wang, R.; Stucky, G. D.; Zhao, D.; Ford, P. C. & Zhang, F. NIR-Triggered Release of Caged Nitric Oxide using Upconverting Nanostructured Materials *Small* **2012**, *24*, 3800-3805 https://doi.org/10.1002/smll.201201213

160. Pierri, A. E.; Huang, P.; Garcia, J. V.; Stanfill, J. G.; Chui, M.; Wu, G.; Zheng, N. & Ford, P. C. A photoCORM nanocarrier for CO release using NIR-light *Chem. Commun.* **2015**, *51*, 2072-2075 https://doi-org.are.uab.cat/10.1039/C4CC06766E

161. Dai, Y.; Xiao, H.; Liu, J.; Yuan, Q.; Ma, P.; Yang, D.; Li, C.; Cheng, Z.; Hou, Z.; Yang, P. & Lin, J. In vivo Multimodality Imaging and Cancer Therapy by Near-Infrared Light-Triggered *trans*-Platinum Pro-Drug-Conjugated Upconversion Nanoparticles *J. Am. Chem. Soc.* **2013**, *135*, 18920-18929 https://doi.org/10.1021/ja410028q

162. Perfahl, S.; Natile, M. M.; Mohamed, H. S.; Helm, C. A.; Schulzke, C.; Natile,G. & Bednarski, P. J. Photoactivation of Diiodido-Pt(IV) Complexes Coupled to Upconverting Nanoparticles *Mol. Pharmaceutics* **2016**, *13*, 2346-2362 https://doi.org/10.1021/acs.molpharmaceut.6b00108

163. Ruggiero, E; Hernández-Gil, J.; Mareque-Rivas, J. C. & Salassa, L. Near Infrared activation of an anticancer Pt(IV) complex by Tm-doped upconversion nanoparticles *Chem. Commun.* **2015**, *51*, 2091-2094 https://doi.org/10.1039/C4CC07960D

164. Dai, Y.; Bi, H.; Deng, X.; Li, C.; He, F.; Ma, P.; Yang, P. & Lin, J. 808 nm near-infrared light controlled dual-drug release and cancer therapy *in vivo* by upconversion mesoporous silica nanostructures *J. Mater. Chem. B.* **2017**, *5*, 20m86-2095 https://doi.org/10.1039/C7TB00224F

165. Dai, Y.; Kang, X.; Yang, D.; Li, X.; Zhang, X.; Li, C.; Hou, Z.; Cheng, Z.; Ma, P. & Lin, J. Platinum (IV) Pro-Drug Conjugated NaYF$_4$:Yb^{3+}/Er^{3+} Nanoparticles for Targeted Drug Delivery and Up-Conversion Cell Imaging *Adv. Healthcare Mater.* **2013**, *2*, 562-567 https://doi.org/10.1002/adhm.201200234

166. Min, Y.; Li, J.; Liu, F.; Yeow, E. K. L. & Xing, B. Near-Infrared Light-Mediated Photoactivation of a Platinum Antitumor Prodrug and Simultaneous Cellular Apoptosis Imaging by Upconversion-Luminescent Nanoparticles *Angew. Chem.* **2014,** *126*, 1030-1034 https://doi.org/10.1002/anie.201308834

167. Ruggiero, E.; Habtemariam, A.; Yate, L.; Mareque-Rivas, J. C. & Salassa, L. Near Infrared photolysis of a Ru polypyridyl complex by upconverting nanoparticles *Chem. Commun.* **2014,** *50*, 1715-1718 https://doi.org/10.1039/C3CC47601D

168. He, S.; Krippes, K.; Ritz, S.; Chen, Z.; Best, A.; Butt, H.; Mailänder, V. & Wu, S. Ultralow-Intensity near-infrared light induces drug delivery by upconverting nanoparticles *Chem. Commun.* **2015**, *51*, 431-434 https://doi.org/10.1039/C4CC07489K

169. Shi, H.; Fang, T.; Tian, Y.; Huang, H. & Liu, Y. A dual-fluorescent nano-carrier for delivering photoactive ruthenium polypyridyl complexes *J. Mater. Chem. B.* **2016**, *4*, 4746-4753 https://doi.org/10.1039/C6TB01070A

170. Zhang, C.; Guo, X.; Da, X.; Yao, Y.; Xiao, H.; Wang, X. & Zhou, Q. UNCP@BSA@Ru nanoparticles with tumor-specific and NIR-triggered efficient PACT activity *in vivo Dalton Trans.* **2021**, *50*, 7715-7724 https://doi.org/10.1039/D1DT00777G

171. Meijer, M. S.; Natile, M. M. & Bonnet, S. 796 nm Activation of a Photocleavable Ruthenium(II) Complex Conjugated to an Upconverting Nanoparticle through Two Phosphonate Groups *Inorg. Chem.* **2020**, *59*, 14807-14818 https://doi.org/10.1021/acs.inorgchem.0c00043

CHAPTER 2

OBJECTIVES

2.   Objectives

Most of the Pt(II)-photosensitive complexes studied for application in PACT are activated by UV or Visible light. However, due to damage to normal tissue and poor tissue penetration, short wavelength lights have limited application *in vivo*. Furthermore, the low solubility that Pt(II) complexes usually present is revealed as an added limitation. To overcome all these limitations at once, a series of objectives were set in this work.

Different efforts have been made to activate the drug with lower energy, near-infrared (NIR) light, which is more penetrating and presents lower damage towards cells. The main objective of this thesis is to synthesise and fully characterize a new platform containing UCNPs bearing photoactivatable Pt(II)-complexes as putative anticancer compounds. This new platform may allow the activation by NIR light, and through the upconversion process the nanoparticles may emit at shorter wavelength and subsequently photoactivate the Pt(II)-complex and release as a bioactive form (see **Scheme 2.1**). In order to increase solubility of the platform in aqueous media, this will be coated with polyethylene glycol methyl ether-octadecylamine (mPEG-ODA).
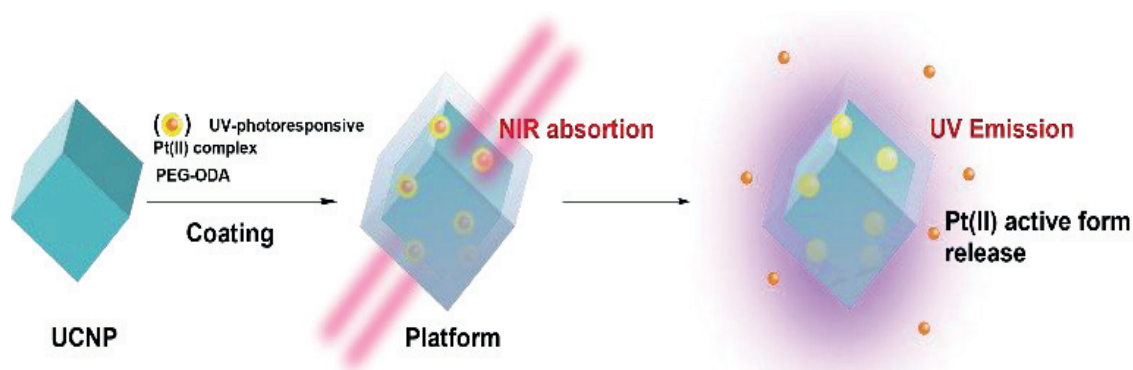
Scheme 2.1: Photoactivation of the platform, containing UCNPs and Pt(II) photoactivated complexes coated with mPEG-ODA, with NIR light which through the upconversion process will activate the Pt(II)-photosensitive complex

To achieve this new system, first, it was proposed to address the following partial objectives:

1) Synthesis and characterization of 2 photoactivatable ligands based on *o*-nitrobenzyl groups bound to 1,2-diaminocyclohexane scaffold.
2) Synthesis and characterization of the corresponding Pt(II) complexes.
3) Synthesis and characterization of Upconversion Nanoparticles containing Y^{3+}, Yb^{3+} and Tm^{3+} elements.
4) Synthesis and characterization of mPEG-ODA as coating.
5) Assessment of the photochemical properties of individual components Pt(II)-complexes and Upconversion Nanoparticles and the full platforms (Pt(II)-complex/UCNPs/mPEG-ODA)
6) Evaluation of the biological response in cell cultures of the individual Pt(II)-complexes and the platforms prepared, in the dark and after irradiation.

CHAPTER 3

SYNTHESIS AND

CHARACTERIZATION OF THE

INDIVIDUAL COMPONENTS AND

THE FULL PLATFORMS

3. Synthesis and characterization of the individual components and the full platforms

3.1. Introduction

Most Pt(II)-photocage complexes studied for their application in cancer phototherapy have several limitations, they require activation by light (in the UV-visible range) that can also damage healthy cells, and frequently, they present low solubility in physiological media. Therefore, new strategies are being studied to selectivity administrate Pt(II) and achieve a spatially and temporally controlled mode of action.

Directly activating the Pt(II)-photosensitive complex with NIR light seems to be problematic, as only one example has been published to our knowledge.[1] Our alternative approach has been to introduce Pt(II)-compounds into a nanoplatform containing UCNPs, so that the UV emission of the nanoparticles resulting from the irradiation by NIR light, can photodegrade and activate the Pt(II)-complex. Thus, activation will be achieved by irradiation at longer wavelengths within the biological window.

In a recent article published by Chen *et. al.*,[2] who investigated a novel method of releasing H_2S for disease treatments. A new photosensitiser called propane-2,2-diylbis((1-(4,5-dimethoxy-2-nitrophenyl)ethyl)sulfane) (**SP**) was synthesised, which upon irradiation with UV light generated H_2S (**Scheme 3.1**):
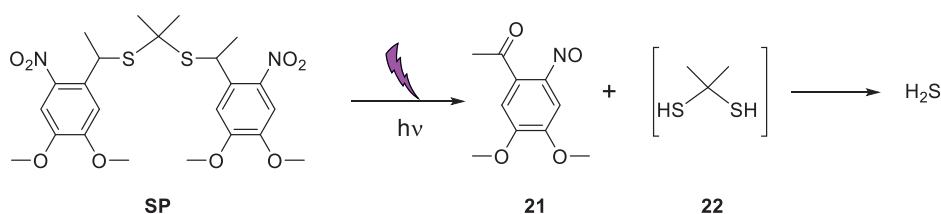
Scheme 3.1: Release of H_2S from the photodegradation of **SP**.[2]

SP was then loaded on the $LiYF_4$; Yb^{3+}; Tm^{3+} UCNPs through a Poly(ethylene glycol) methyl ether-octadecyamine (mPEG-ODA) coating to obtain a water-soluble nanoplatform. Through upconversion of the nanoparticles, NIR light irradiation led to the emission of UV light, which photodegraded **SP**, releasing H_2S in spatially and temporally controlled manner.

In this work, new Pt(II)-photosensitive complexes have been synthesised using as Pt(II) ligand the photocage previous described [2] and a derivative (**Figure 3.2.**). The goal was to form Pt(II) complexes with a (±)-*trans*-1,2-diaminocyclohexane ligand containing the photoremovable group 4,5-dimethoxy2-nitrobenzyl (**C1** and **C2**). These new Pt(II)-complexes,

when irradiated, may photodegrade, yielding the expected photoproducts shown in **Scheme 3.2**, where photoproduct **24** is an analogue of oxaliplatin. In physiological medium both Pt(II)-compounds, oxaliplatin and **24,** may yield the same product: diaquo(1,2-cyclohexanediamine)platinum(II), **25**.
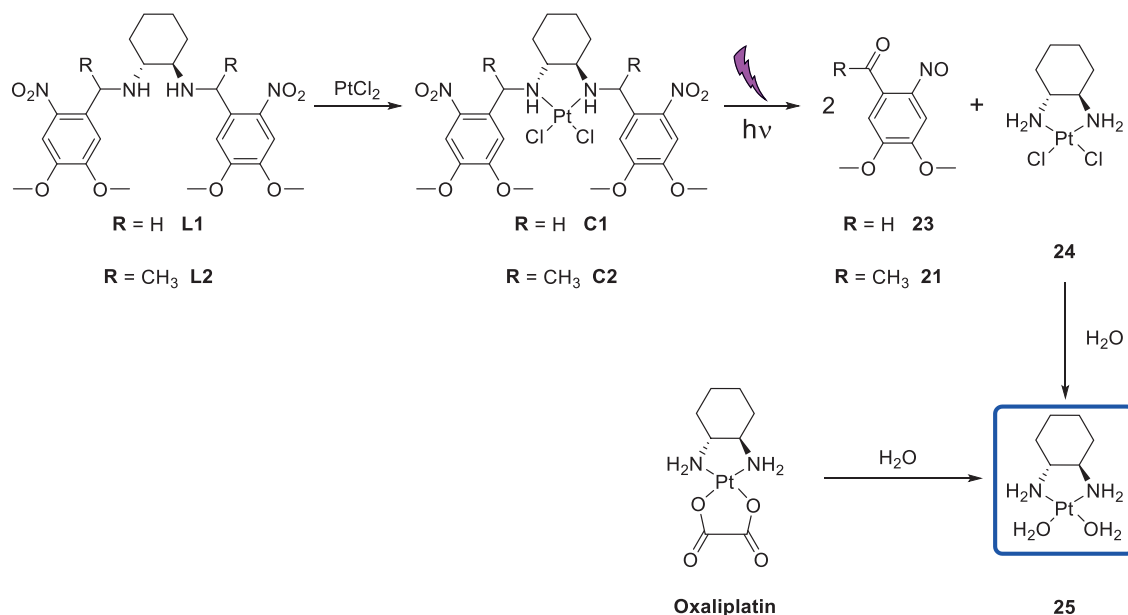
Scheme 3.2: Expected photodegradation of **C1** and **C2** and secondary aquation reaction in physiological medium

Although, in most known cases, the activation of nitrobenzene photocages usually involves the breaking of C-O bonds, the case raised in the present work (C-N breaking) has not been widely spread. Despite this, there are some examples in the literature.[3]

3.2 Synthesis of L1 and L2

First, the corresponding ligands **L1** and **L2** were synthesised (**Schemes 3.3.** and **3.4.**). The difference among them is at the *N*-α position been primary (**L1**) or secondary (**L2**) due to methyl group substitution.
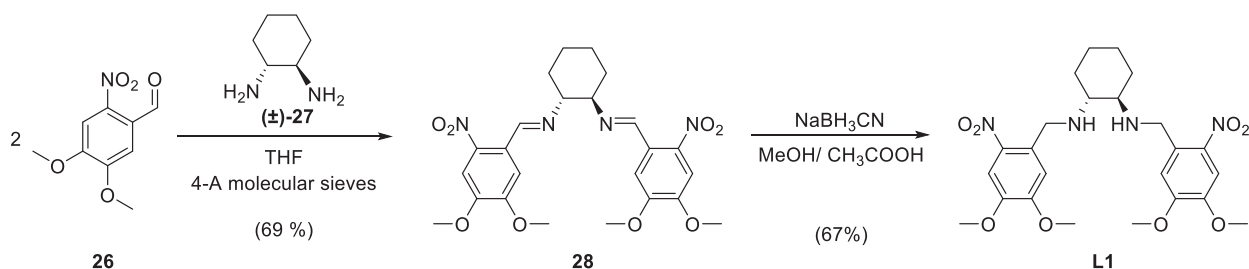
Scheme 3.3: Synthetic strategy to obtain ligand **L1**

The synthetic route towards **L1** comprises two steps. First, diimine **28** is formed through the coupling of the commercially available 6-nitroveratraldeyde (**26**) with (±)-*trans*-1,2-diaminocyclohexane (**±-27**). This reaction was carried out in anhydrous tetrahydrofuran (THF)

and in the presence of molecular sieves, which collect the water generated during the condensation.[4] The [1]H-Nuclear Magnetic Resonance (^{1}H-NMR) spectra demonstrated that the molecule has a C2-symmetry which suggests that the configuration of the two formed imines is identical (*E*). Next step consisted of the reduction of **28** with NaBH$_3$CN to form **L1** in 67% overyield. The obtained products were confirmed by ^{1}H-NMR (**Figure A1 and A4**), ^{13}C-NMR (**Figure A2 and A5**), Infrared (IR) spectroscopy and Electrospray Ionization - Mass Spectrometry (ESI-MS) (**Figures A3 and A6**).

For the synthesis of **L2**, different paths were attempted to obtain the **L2** from the same starting aldehyde **26** (**Scheme 3.4.**):
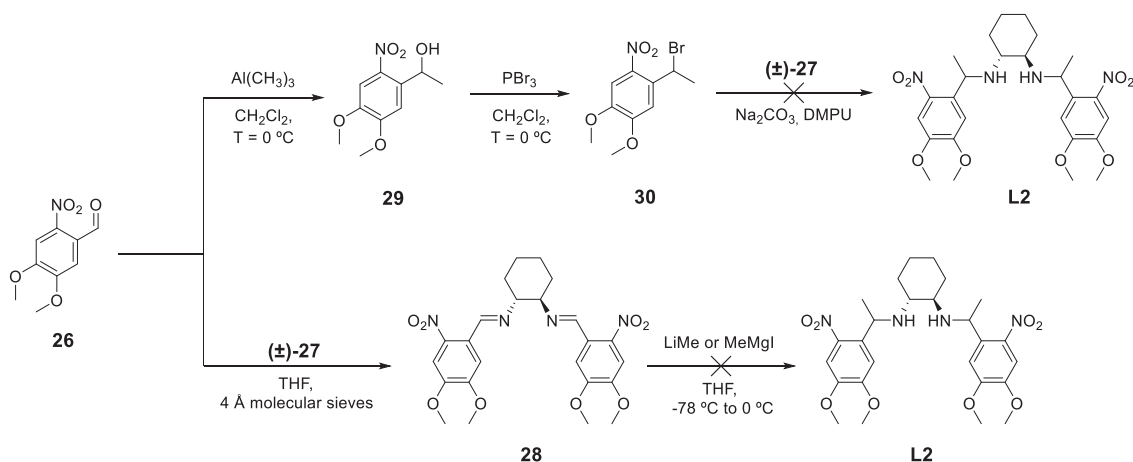
Scheme 3.4: Different synthetic attempts to obtain **L2** from **26**

As a first attempt, to obtain the benzyl bromide **30**, a described procedure was followed.[2] First, addition of methyl group was achieved by treatment of aldehyde **26** with Al(CH$_3$)$_3$ to. Next, benzylbromide **30** was accomplished by treatment of **29** with PBr$_3$. These products were characterised by ^{1}H-NMR (**Figure A.14** and **A.15**). The last step consisted of the doble substitution of bromide in **30** by **(±)-27** through a S$_N$1 mechanism. This last reaction was assayed under different conditions using a variety of solvents (*N,N'*-dimethylpropyleneurea (DMPU), Dimethylformamide (DMF), Toluene, CH$_2$Cl$_2$). Unfortunately, the ^{1}H-NMR spectra of the reaction crudes showed the formation of too many side products, and it was difficult to isolate a pure **L2** sample. Nevertheless, employing DMPU as a solvent seems to produce product **L2** but with a combination of diastereomers. Since in the ^{1}H-NMR (**Figure A.16**) two quadruplets can be observed that must correspond to the benzylic proton. This is because the molecule has four chiral centres, resulting in six diastereomers with three pairs on enantiomers (**Scheme 3.5**). Therefore, a mixture of diastereomers was so obtained. The purification of these products was not possible, although several attempts were made. As a result, an alternative route was sought to have a more stereoselective route.
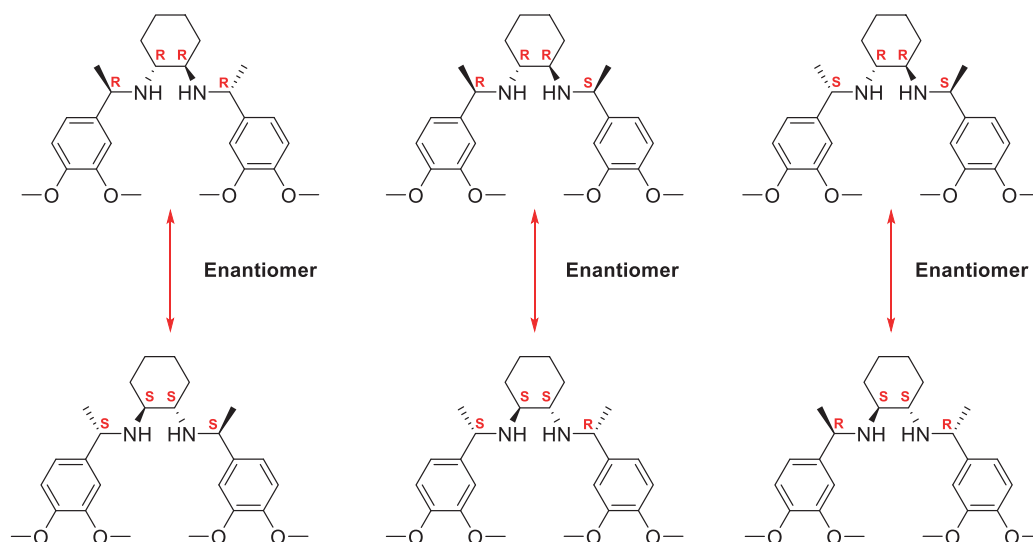
Scheme 3.5: Possible **L2** stereoisomers obtained with DMPU as a solvent.

The second attempt to synthesise **L2** from **26**, require the formation of diimine **28** in presence of **(±)-27** the same used to obtain **L1**. The last step methylation with an organometallic compound was attempted with LiMe and MeMgI in THF. In both cases, the ^{1}H-NMR spectra showed the degradation of the diimine **28**. The nitro group is a strong electron withdrawing group (EWG), when the organometallic reagent reacts with a nitrobenzene it can react via different undesired ways: by reduction of the nitro group,[5,6] the substitution of the nitro group by the alkyl group from the Grignard reagent[7,8] or the ortholihtiation respect the nitro group forming a new organolithium compound.[9]

Due to the reactions between the organometallic reagents and the nitro group it was difficult to introduce a methyl group to the imine moieties, it was decided to change the synthesis route and explore new options by starting with a different reagent. Instead of using an aldehyde as reagent, it was chosen to use the corresponding methyl ketone **31** as starting material (**Scheme 3.6**)
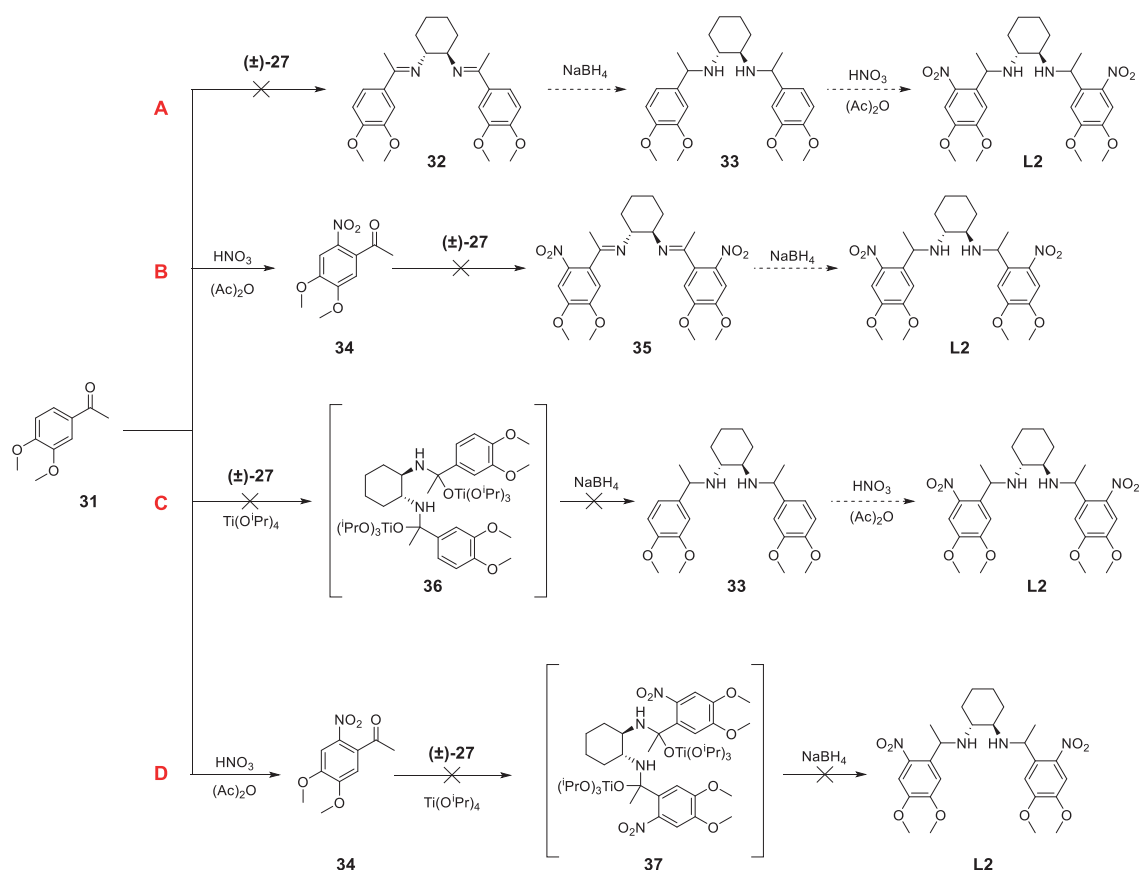
Scheme 3.6: Different synthetic attempts to obtain **L2** from **31**

Four different routes were tested to obtain the product **L2** from the ketone reagent **31** (**Scheme 3.6**).

- Route **A:** an attempt to obtain imine **32,** using several conditions with different conventional solvents (EtOH, THF, etc…). At neat conditions and higher temperature, the corresponding monoamine was formed, instead of the expected diamine **32**. A mixture of monoimine and the starting ketone **31** was obtained. Although the reactions were left to proceed longer time than the initially proposed (24 h), no increase in conversion was observed, thus indicating that an equilibrium was reached. Attempts to isolate the monoimine were also unsuccessful Even the direct reduction of the reaction crude with NaBH$_4$ did not allow the obtention of any pure final product.

- Route **B:** an effort was done to form the diimine **35** by introduction of the nitro group beforehand. Acetophenone **34** was obtained by nitration of ketone **31** in the presence of anhydrous acetic acid. However, in the next step (the double imine formation to **35**) many by-products were formed and, finally **35** could not be isolated.

- Route **C**: Direct double imine formation was carried out between **(±)-27** and **31** using a combination of Ti(O^{i}Pr)$_4$/NaBH$_4$.[10] Ketone **31** reacted with the cyclohexyl diamine

to form the intermediate titanium(IV) complex **36**, which was reduced in presence of NaBH$_4$. This reaction yielded **33** as a complex mixture of stereoisomers.

- Route **D**: In analogy with diaminal **36**, the preparation of dinitro compound **37** was assayed in the same conditions. A variety of compounds were produced when the nitro group was present, probably because Ti(IV) reduces the nitro group to an amine group. [11,12]

At this point and given that the nitro group was revealed as probably an impairment to the formation of diimine, a change of strategy was made. Consequently, the key step of double nitration takes place at the end of the pathway as shown in **Scheme 3.7**.
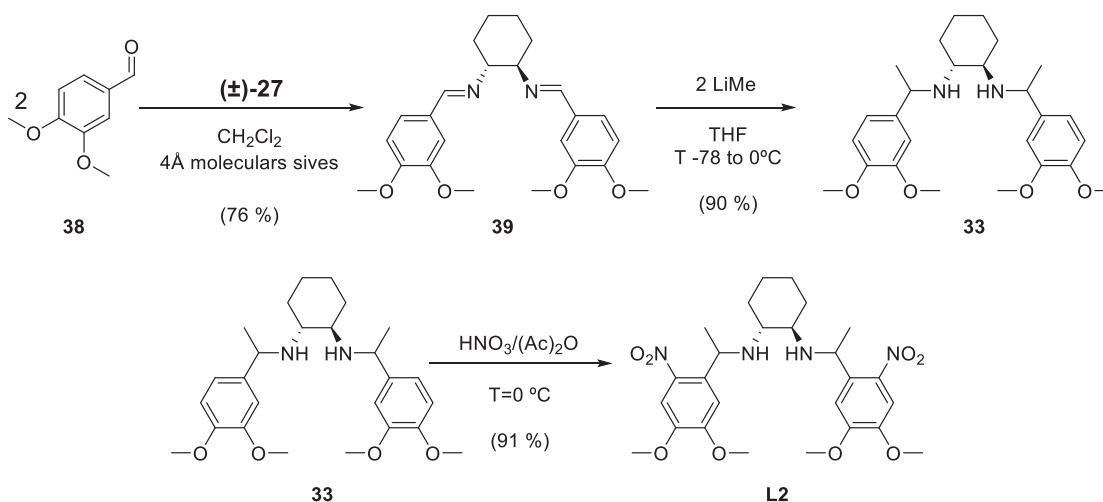
Scheme 3.7: Alternative synthetic route to yield **L2**

For the first step, a procedure already described was followed,[13] in which the commercially reagent 3,4-dimethoxybenzaldehyde (**38**) reacts with **(±)-27** to obtain the diimine (**39**). Next, **39** was methylated by MeLi to yield diamine **33**. Gratifyingly, the presence of a C_2-symmetry, as a revealed by the ^{1}H-NMR, indicated the complete stereoselectivity of this reaction. Finally, **33** was nitrated in the presence of nitric acid under the catalysis of acetic anhydride to achieve **L2** in a 62% overall yield. This synthetic route yields **L2** as pair of enantiomers instead of the multiple diastereomers (**Figure 3.2**). All new compounds involved in this successful synthetic route were full characterized by ^{1}H-NMR (**Figure A17, A18 and A21)**, ^{13}C-NMR **(Figure A19 and A22)**, IR spectroscopy and ESI-MS (**Figure A20 and A23**).

As explained above, there are different pairs of enantiomers that can be obtained. To determine which enantiomer pair was obtained by this synthetic route, **L2** has to be crystallised. Different crystallisation tests were performed, in which finally a crystal was formed by liquid-liquid diffusion between ethyl acetate and isopropanol. The crystal obtained was analysed by

X-Ray Diffraction (XRD) (**Figure 3.2**), which confirmed the structure of the pair of enantiomers yield, these structures are represented in **Schem 3.8**:
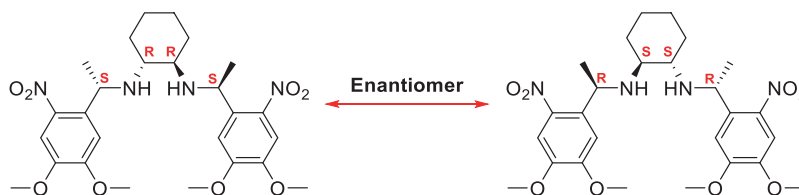
Scheme 3.8: The enantiomers obtained in the synthetic route to yield **L2**, analysed by XRD
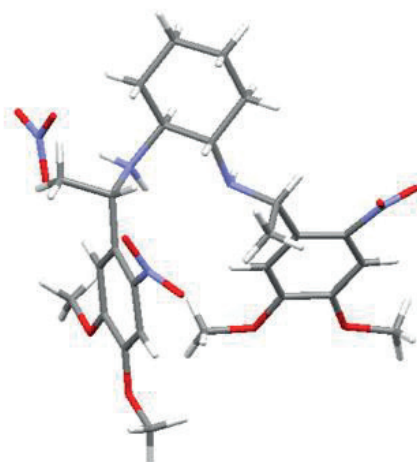
Figure 3.1: MERCURY drawing for **L2**.

3.3 Synthesis of Pt(II)-complexes

After obtaining the pure **L1** and **L2** ligands, the next step was the obtention of the corresponding Pt(II)-complexes. Different methods can be found in the literature to prepare Pt(II)-compounds, but among them, one common trend is the use of the water-soluble salt precursor K_2PtCl_4.[14] Several works have described the coordination of Pt(II) with secondary amines derivatised from the *trans*-**27** using a mixture of water:MeOH (1:1 v/v) and equimolar amounts of Ligand and–Pt precursor.[15–17] However, as both **L1** and **L2** were not soluble in MeOH, THF was used as alternative solvent.

In both cases, the Pt(II)-complex was prepared by slowly adding a solution of the corresponding ligand in THF to a solution of K_2PtCl_4 in water at equal concentrations (**Scheme 3.9**). After 24 hours of reaction, water was added to the action mixture to precipitate the complex formed and subsequently separate it by filtration. The precipitation of [PtL1Cl$_2$] (**C1**) was nicely accomplished and the resulting yellowish solid was further washed with acetone. However, the precipitation of [PtL2Cl$_2$] (**C2**) required the use acetone and Et_2O to obtain a solid product which was finally collected by centrifugation.
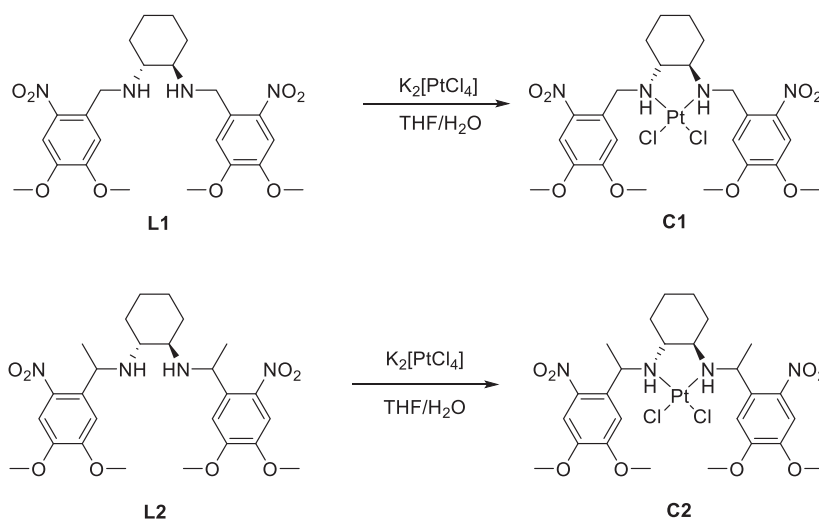
Scheme 3.9: Synthesis of complexes **C1** and **C2** from their corresponding ligands **L1** and **L2**

The successful Pt(II) coordination in **C1** and **C2** was corroborated by ESI-MS (**Figure A12 and A28**), as their spectra showed not only the expected mass peak but also the characteristic isotopic platinum pattern. Furthermore, **C1** and **C2** were characterised by ^{1}H-NMR and ^{13}C-NMR (**Figure A10, A11, A26, A27)** where the loss of symmetry in these complexes by the presence of Pt(II) was observed in both cases. Comparing the recorded NMR data of the ligands and the corresponding Pt(II)-complexes, it can be observed splitting of some signals. These changes were attributed the loss of symmetry due to complexation (**Figure 3.2-3.5**)
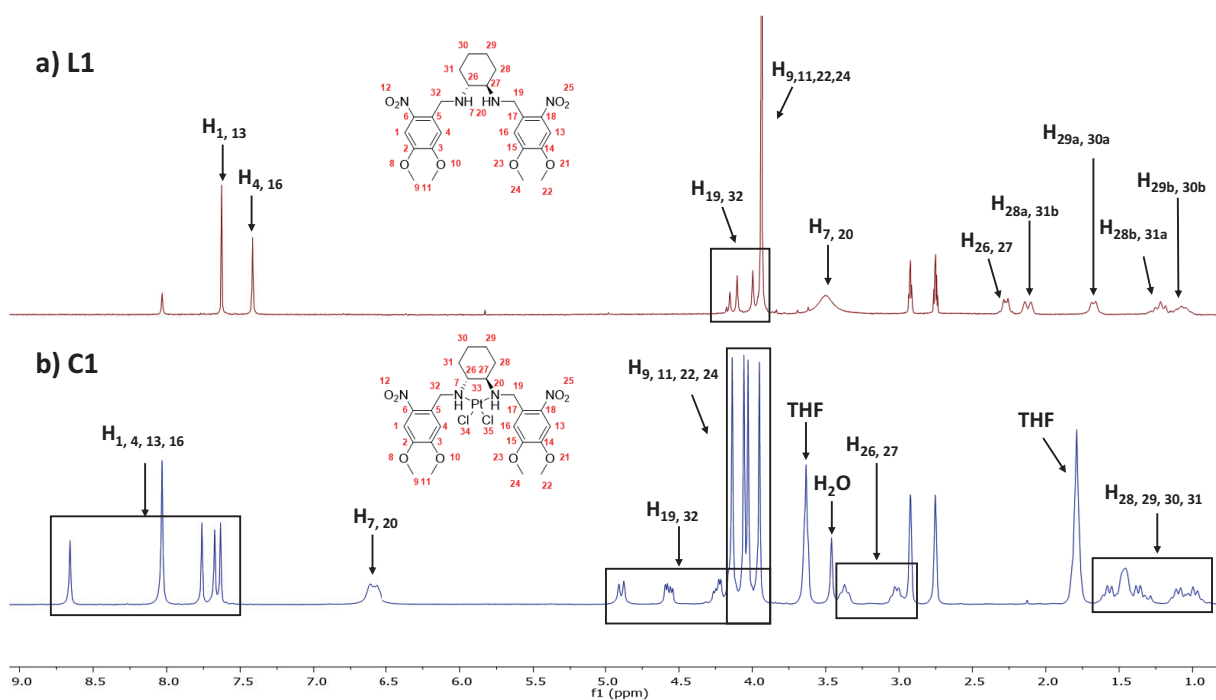
Figure 3.2: ^{1}H-NMR (400 MHz, DMF-d^7) of a) **L1** and b) **C1**
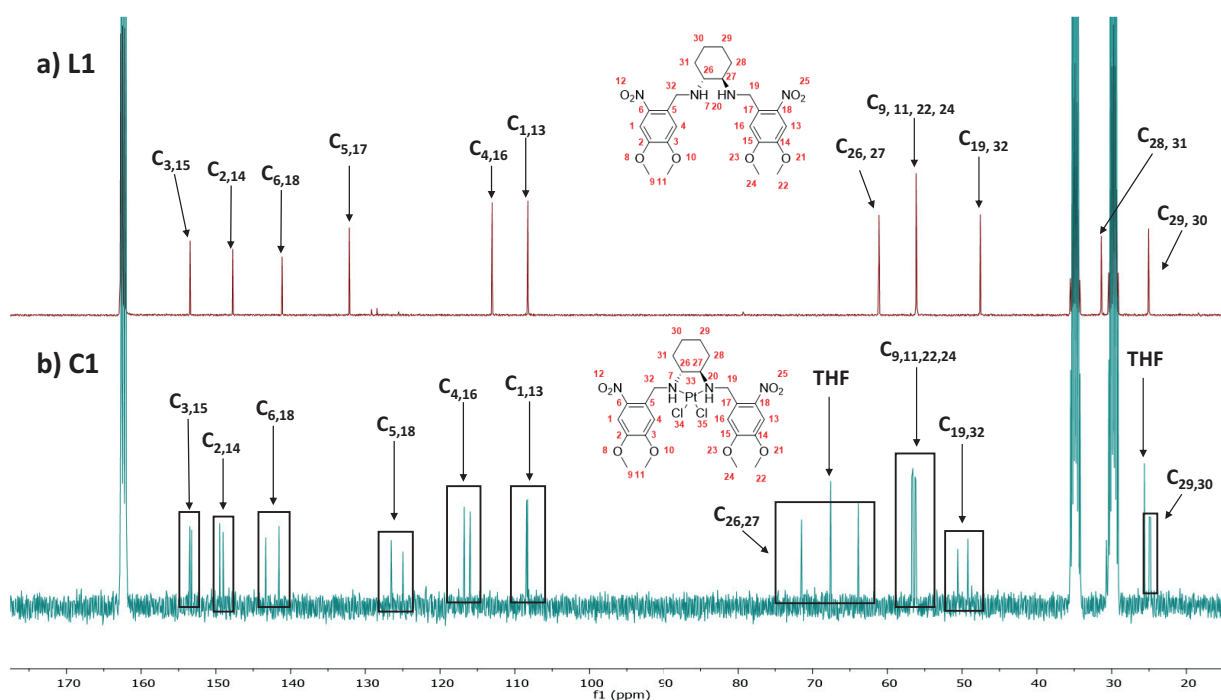
Figure 3.3: ^{13}C-NMR (100 MHz, DMF-d^7) of a) **L1** and b) **C1**
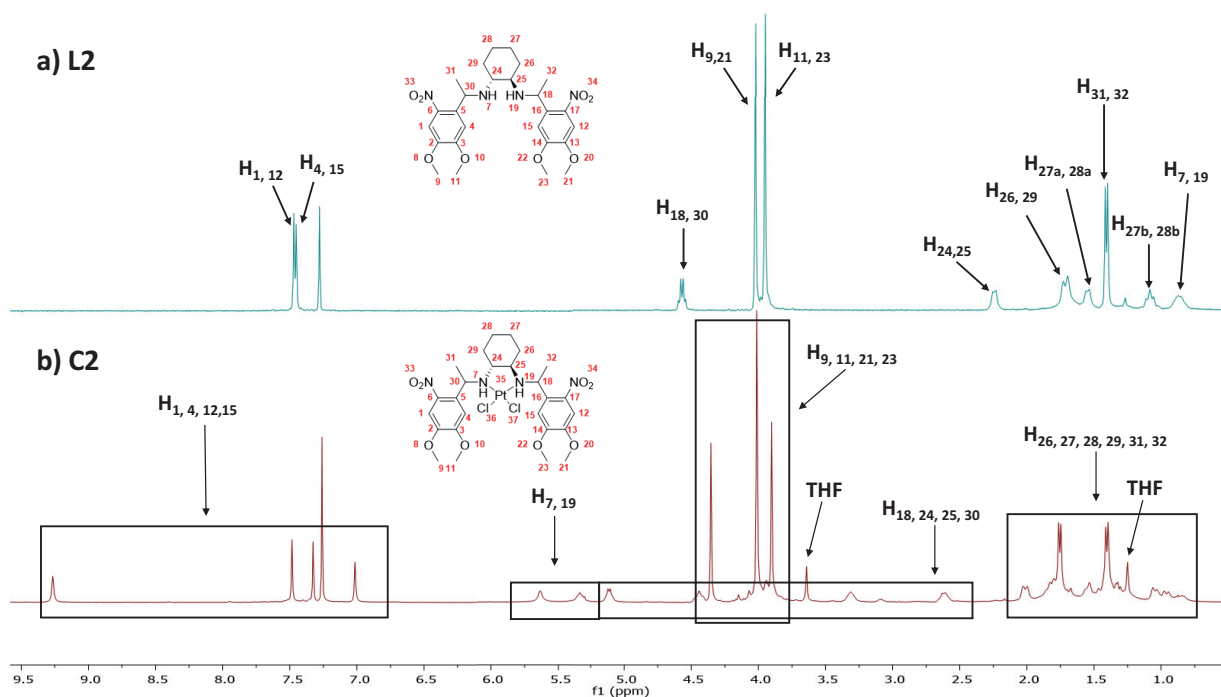
Figure 3.4: ^{1}H-NMR (400 MHz, CDCl$_3$) of a) **L2** and b) **C2**
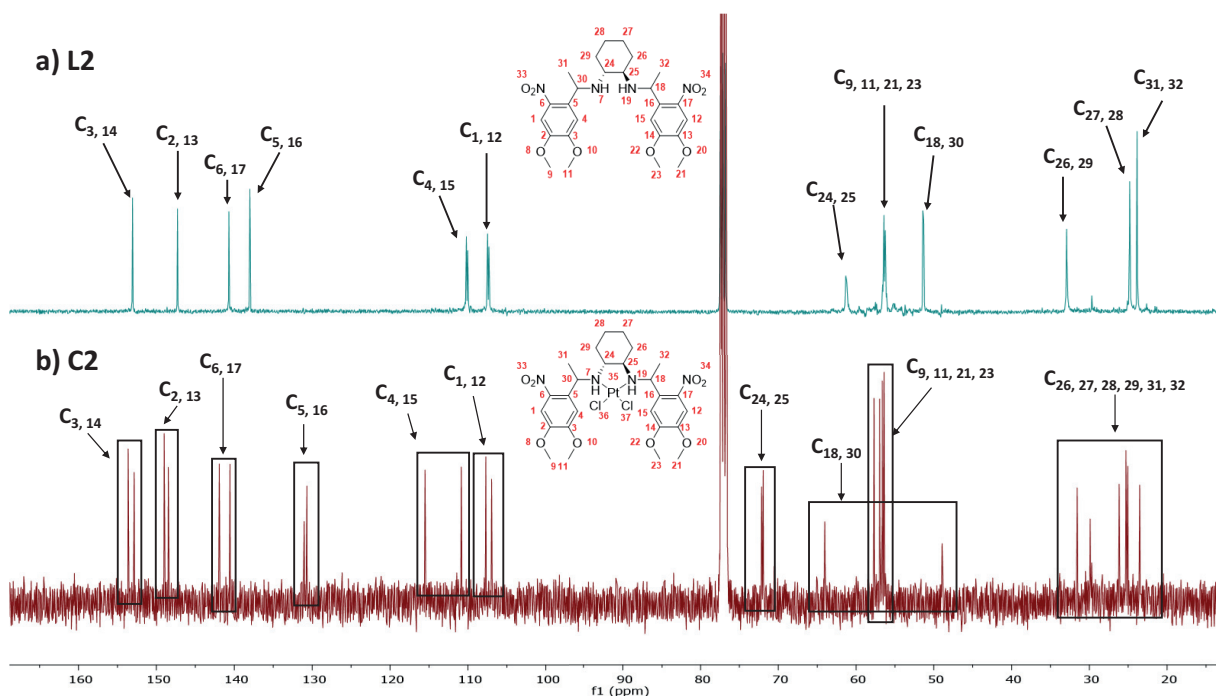
Figure 3.5: ^{13}C-NMR (100 MHz, CDCl$_3$) of a) **L2** and b) **C2**

It should be noted that, even though the only difference between the Pt(II)-complexes is a methyl group at the benzylic position, they are considerably different in terms of solubility. **C1** is insoluble in all solvents except dimethyl sulfoxide (DMSO) and DMF, while **C2** is insoluble in water, alcohols, and non-polar solvents.

3.4 Synthesis of UCNPs

All studies involving nanoparticles have been possible thanks to the collaboration with Dr. Fernando Novio of the *Universitat Autònoma de Barcelona* from the NanosFun group of the Catalan Institute of Nanoscience and Nanotechnology (ICN2).

To synthesise upconversion nanoparticles, we focused on using lanthanides ion-doped because they can absorb in the Near-Infrared and upconvert to emit light into the visible or ultraviolet range.[18] Yb^{3+} and Tm^{3+} doping ions were chosen to synthesise LiYF$_4$ nanoparticles because they have shown to absorb at 980 nm (NIR) and emit in the UV region.[19,20] In addition, the use of fluorides as a host is also advantageous because of their stability and low phonon energy, which reduces the non-radiative relaxation energy and consequently increase the effectiveness of the upconversion emission.[19,21]

There are different ways to obtain monodisperse and crystalline nanoparticles of different sizes, morphology, dispersity, and emissions depending on the application. Thermal decomposition method,[22] hydrothermal method,[23] and co-precipitation method[24] are the most common ones.

Thermal decomposition method was used in this work to synthesise the nanoparticles because it presents the advantage of low cost, short time reaction, obtention of well-shaped particles with narrow size distribution, and high colloidal stability. In this technique, the organic precursors are dissolved in the presence of surfactant and heated to high temperatures.[25]

The synthesis of UCNPs was done following a procedure already published.[26] This synthesis is divided in two parts as shown in **Scheme 3.10**:

$$Ln_2O_3 \xrightarrow[\text{T = 80 °C}]{\text{TFA (50\%)}} Ln(CF_3COO)_3 \xrightarrow[\substack{\text{Oleic acid:1-octadecene (1:1)}\\\text{120 °C to 315 °C}}]{\text{LiCOOCH}_3\cdot 2H_2O} LiYF_4\text{:Yb, Tm}$$

Ln = Y^{3+} (74.5 mol %), Yb^{3+} (25 mol %) and Tm^{3+} (0.5 mol %)
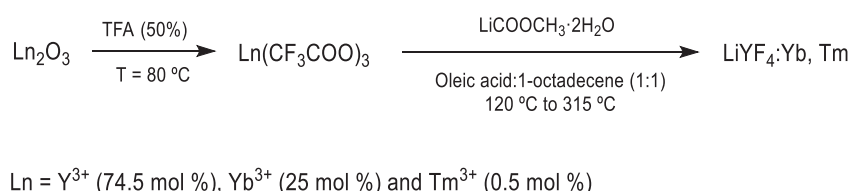
Scheme 3.10: Synthesis of upconverting nanoparticles composed by $LiYF_4$ and doped with Yb^{3+}; Tm^{3+} where Ln = Y^{3+} (74.5 mol %), Yb^{3+} (25 mol %) and Tm^{3+} (0.5 mol %)

The first step was a reaction between the corresponding lanthanide oxides (Y_2O_3, (Y^{3+} (74.5 mol %)), Yb_2O_3 (Yb^{3+} (25 mol %)) and Tm_2O_3 (Tm^{3+} (0.5 mol %))) and trifluoroacetic acid to yield the lanthanide trifluoroacetate precursors. The proportions of the amounts of each lanthanide in this mixture is crucial for the efficiency of the upconversion process, as the ratio of Yb/Tm determines the emission intensity.[20,27] The second step consists of a thermal decomposition: the corresponding amount of lithium acetate was added to a solution of the lantanide acetates in 1-octadecene and oleic acid in equal volumes. This solution was first heated for 30 minutes at 120 °C and degassed under vacuum to remove water and oxygen. Following, the temperature was increased to 315 °C with a ramp-up of 10 °C/min and maintained at that temperature for an hour (the set up for this operation can be found in (**Figure A.42**). When the mixture was cooled down to room temperature, the formed nanoparticles were precipitated with ethanol and isolated by centrifugation.

In this reaction, the presence of oleic acid is necessary as it works as a stabiliser ligand for the nanoparticles. The size of the nanoparticles can be controlled by the ratio of oleic acid/ lanthanide trifluoroacetates. Also, 1-octadecene was used as a solvent with a high boiling point.[28] An important issue for this step is the control of the morphology of the nanoparticles, which depends on the oleic acid/1-octadecene ratio and particularly on the temperature ramp. Scanning transmission electron microscopy (STEM) images allowed to observe the morphology of the nanoparticles. Results obtained show that when the temperature ramp was lower than 10 °C/min, spherical or a mixture of spherical and rhombohedral nanoparticles were obtained, whereas if the temperature ramp was higher than 10 °C/min, rhombohedral nanoparticles were obtained (**Figure 3.6**).
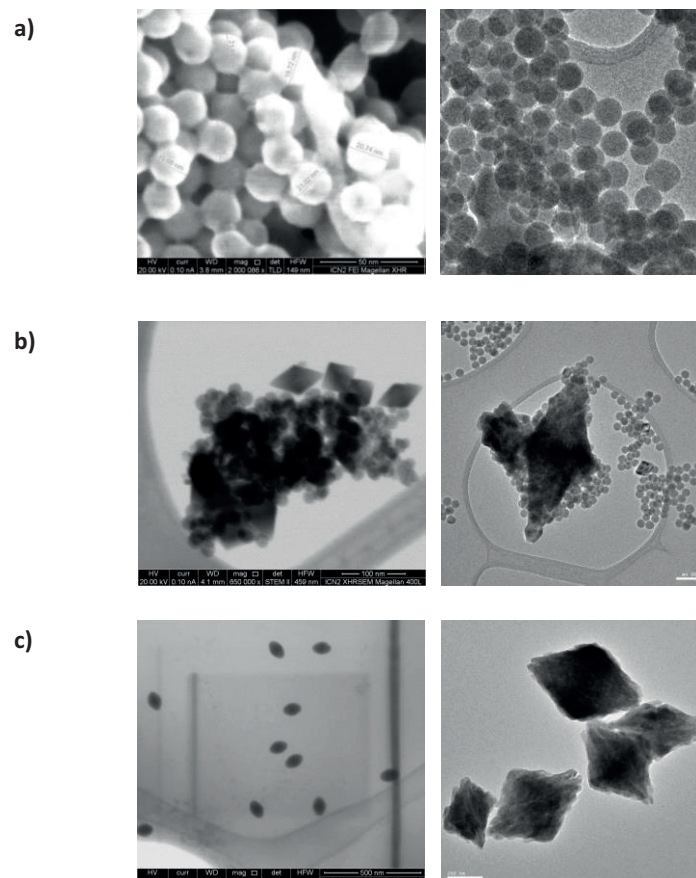
Figure 3.6: STEM images of the LiYF$_4$; Yb^{3+}; Tm^{3+} nanoparticles synthesised under different conditions, showing different morphologies depending on the temperature ramp used (from spherical (ramp temperature < 10 ºC/min) to rhombohedral (ramp temperature > 10 ºC/min)

The rhombohedral nanoparticles were larger than the spherical ones. The large diagonal for rhombohedral nanoparticles measured on average 95 nm whilst 63 nm elongated on the small diagonal, likewise the diameter of the spherical nanoparticles was 20 nm, on average. The composition of the nanoparticles was obtained by Energy-dispersive X-Ray Spectroscopy (EDX), being possible to identify Y^{3+} and the doped elements Yb^{3+} and Tm^{3+} and calculated the molar ratio of each element (Y^{3+} (76 %), Yb^{3+} (23 %), Tm^{3+} (1%)) (**Figure 3.7**)
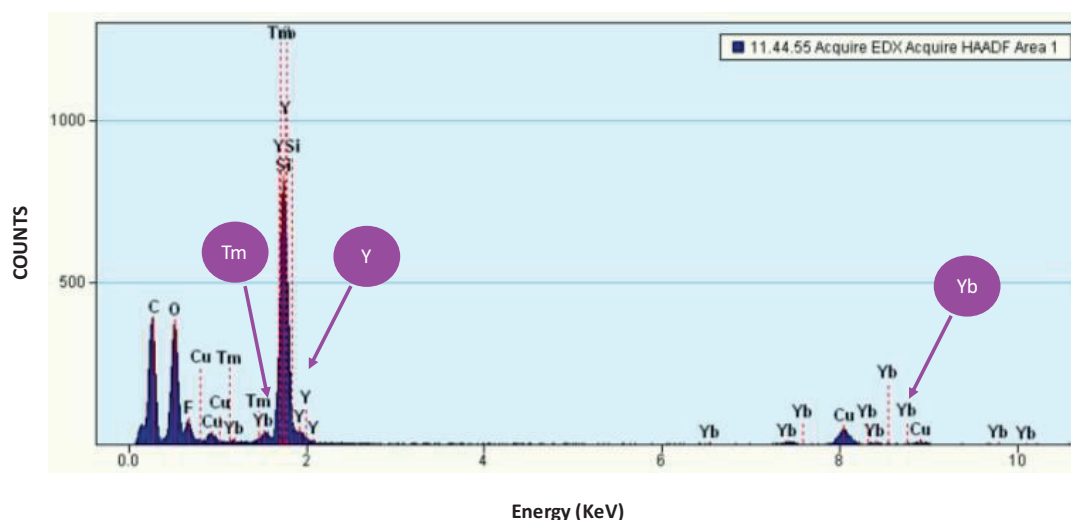
Figure 3.7: EDX analysis of the LiYF$_4$;Yb^{3+};Tm^{3+} synthesised UCNPs. The signals corresponding to Y and the doping lanthanides (Yb and Tm) can be observed.

3.5 Synthesis of mPEG-ODA

The synthesised nanoparticles were shown to be soluble in some organic solvents but not in water as they are stabilised with a hydrophobic coating. These hydrophobic nanoparticles must be transformed into water-soluble in order to be used in biomedical applications.[29] There are three approaches to solubilise the nanoparticles and, in this case, and in this case, to take advantage of it as a container for the photosensitiser(PS), in our case the Pt(II) complexes

- Silica encapsulation: This method consists of coating the PS and nanoparticles with mesoporous silica. The advantages of using silica shell are that it has low cytotoxicity, is very stable, have high adsorption due to the large surface area and volume of the pores, and different functional groups are easy to anchor to the surface.[30,31]

- Non-covalent physical adsorption: This method achieves the attachment of PS to the surface of nanoparticles through hydrophobic interactions between PS and oleic acid layer on the nanoparticle surface. Therefore, an amphiphilic polymer (hydrophilic and hydrophobic properties), such as polyethylene glycol (PEG), is used to coat the nanoparticles and the PS, achieving dispersion in an aqueous solution. The advantage of using this method is that they interactions are weak, the release of the PS will be easier.[32]

- Covalent conjugation: Is the same as physical adsorption but with covalent interactions, which make the interaction between the PS and the nanoparticle more stable, avoiding the release of PS before reaching the target.[33]

In this work the second method was used to coat the nanoparticles, and it involved covering them with the amphiphilic polymer mPEG-ODA. To synthesise the polymer, the procedure described previously was followed (**Scheme 3.11**).[2]
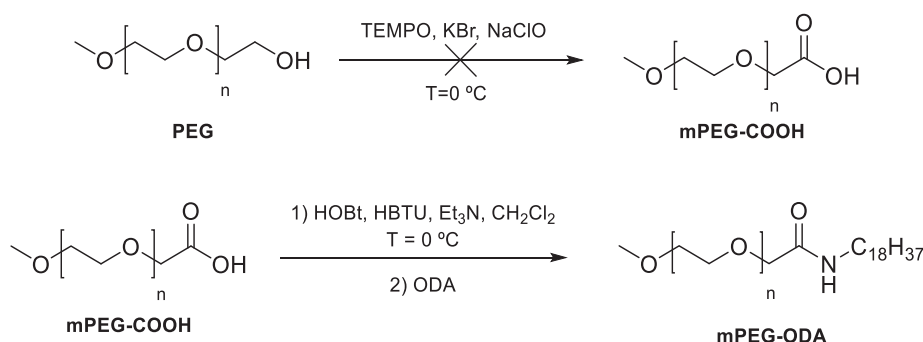
Scheme 3.11: Synthetic route followed to obtain mPEG-ODA

The first reaction consisted of the oxidation of Poly(ethylene glycol) methyl ether (mPEG) to form the corresponding carboxylic acid in the presence of NaClO, (2,2,6,6-Tetramethylpiperidin-1-yl)oxyl (TEMPO) and KBr. Although the experimental procedure of the article was followed, the desired product could not be obtained, as observed by the ^{1}H NMR of the reaction crude, which only showed the peaks corresponding to the PEG reagent.

As the initial step did not work, the oxidation reagents were changed using a solution containing $KMnO_4$ and KOH in water following a described procedure (**Scheme 3.12**).[34]
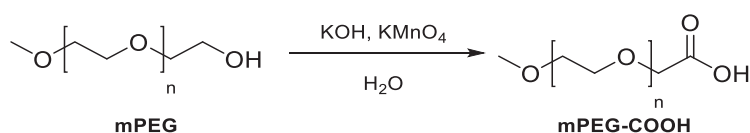
Scheme 3.12: Alternative oxidation reaction to yield mPEG-ODA

The oxidation of mPEG with the $KMnO_4$ in a basic medium rendered mPEG-COOH in excellent yield (96 %). The ^{1}H-NMR data registered confirmed the presence of the expected product (**Figure A38**).

The second step consisted in the formation of the corresponding amide (mPEG-ODA) between mPEG-COOH and octadecyl amine (ODA) (**Scheme 3.11**, second reaction). In order to activate the carboxylic acid, the coupling agents hydroxybenzotriazole (HOBt) and Hexafluorophosphate Benzotriazole Tetramethyl Uronium (HBTU) were initially added to the reaction with mPEG-COOH in a basic medium. Secondly, ODA was added to the reaction and after reacting overnight, the product mPEG-ODA was obtained as confirmed ^{1}H-NMR (**Figure A.39)** and ^{13}C-NMR (**Figure A.40**) data.

3.6 Synthesis of Pt(II)/UCNPs/mPEG-ODA

In this section, once all the components were synthesised and characterised (the Pt(II)-complexes, UCNPs and the polymer mPEG-ODA), the next step was the production of the nanoplatform (**Scheme 3.13**).
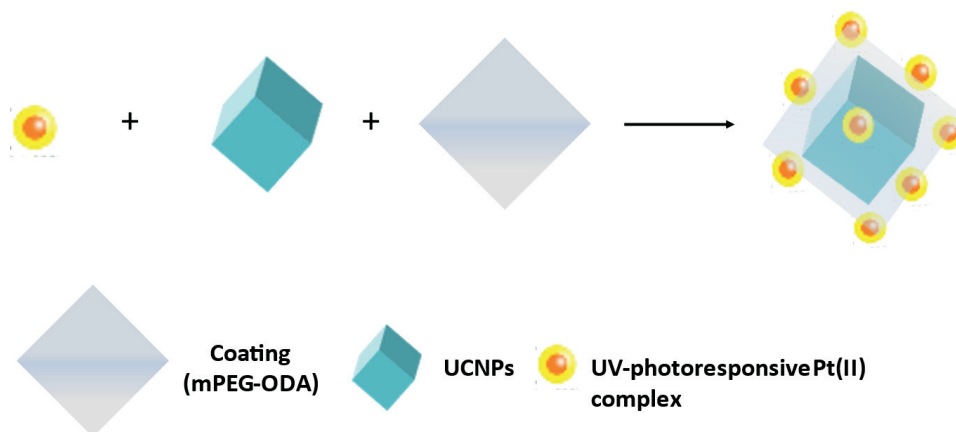
Scheme 3.13: Formation of the Pt(II)/UCNPs/mPEG-ODA platforms from the individual components

As mentioned in the previous section, the amphiphilic polymer mPEG-ODA will coat the nanoparticles in order to convert these hydrophobic nanoparticles into water-soluble ones.

The coating was prepared through sequential emulsion and solvent evaporation.[35] The three components were solved in a mixture of water and organic solvent (chloroform) (3:1), which were immiscible with each other. In the case of coating the sample containing **C1**, THF was also added to increase the solubility of the Pt(II)-complex. Subsequently, the solution was stirred vigorously, and the organic solvent was slowly evaporated. In this way, the nanoparticles were coated in the organic phase and once coated, were transferred to the aqueous phase.

The resulting aqueous solution was centrifuged at 4000 rpm for 10 minutes to remove excess polymer. The nanoparticles previously precipitated were redispersed with water and filtered. For this, two filters were tested one measuring 0.8 µm and the other 0.4 µm. It was observed that filtrating with the bigger-pore filter allowed aggregated nanoparticles to pass through. However, with the 0.4 µm pore filter, only non-aggregated nanoparticles were collected.

Finally, mPEG-ODA-coated nanoparticles doped with Pt(II)-complexes were obtained by removing the solvent by freeze-drying. Removal of water by vacuum evaporation at 60 °C was tried, but it was observed by STEM, that a small portion of the nanoparticles was disaggregated or degraded.

These new platforms (Pt(II)-complex/UCNPs/mPEG-ODA) were characterized by conventional techniques: STEM (**Scheme 3.14**), EDX (**Figure 3.8**), dynamic light scattering (DLS) (**Figure A.43**) and ζ-potential measurements.

STEM showed a thin layer of 4 nm surrounding the nanoparticles, demonstrated that the UCNPs were mPEG-ODA coated (**Scheme 3.14**). In addition, when UCNPs were coated in the presence of the Pt(II) complexes their morphology varied slightly, appearing more ellipsoids and less rhombohedral (**Scheme 3.14**).

UCNPs before coating   UCNPs after coating
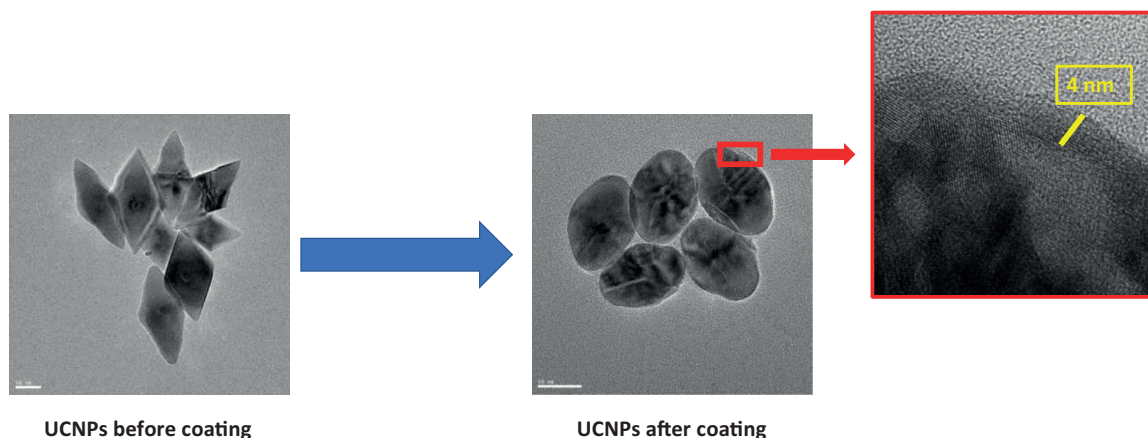
Scheme 3.14: STEM image of the UCNPs with different morphology before coating and after coating

On the other hand, EDX of all the platforms synthesised showed new picks corresponding to the presence of Pt thus confirming the loading of the Pt(II)-complex in the new platform (**Figure 3.8**):
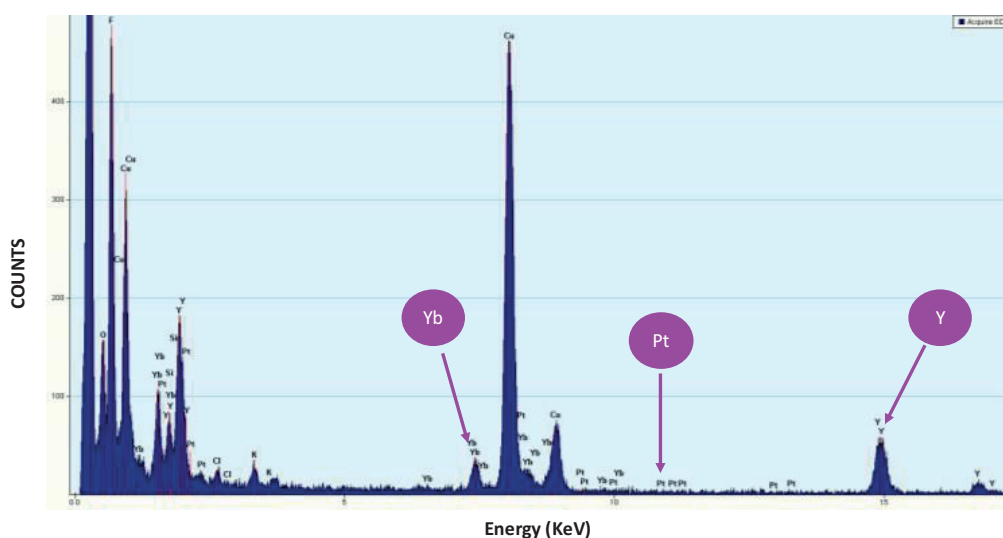
Figure 3.8: EDX of Pt(II)/UCNPs/mPEG-ODA

DLS measurements revelled that Pt(II)/UCNPs/mPEG-ODA platforms prepared had an average size around 124 nm, within the biomedical application range, and ζ-potential of -12 mV. From these results it can be deduced that the carboxylic groups of mPEG-ODA are more positioned towards the outer side (further away from the nanoparticles) and the amino groups are closer to the interior (closer to the nanoparticle).

On the other hand, in order to know the amount of Pt(II) that each platform contained, it was analysed by inductively coupled plasma optical emission spectroscopy (ICP-OES), in which the platform **C2**/UCNPs/mPEG-ODA gave a bigger average value of Pt(II) content (1.7 % Pt(II) (w/w)) than **C1**/UCNPs/mPEG-ODA platform (1,0 % Pt(II) (w/w)).

3.7 Summary of Chapter 3

In this chapter two new Pt(II)/UCNPs/mPEG-ODA platforms have been prepared and characterised. To achieve this, it has been necessary to prepare all the individual components.

Two new compounds used as metal ligands were synthesised and characterised containing 4,5-dimethoxy nitrobenzyl and (±)-*trans*-diaminocyclohexane motifs, the main difference among them is at the benzylic positions as it is primary in **L1** but secondary in **L2**. The corresponding Pt(II)-complexes were also synthesized and characterized (**C1** and **C2**).

On the other hand, the UCNPs of $LiYF_4$;Yb^{3+};Tm^{3+} were synthesised and characterized. First, the corresponding trifluoroacetate precursors for yttrium and the lanthanides were synthesized. A thermal decomposition was then carried out to obtain the UCNPs. Results showed that depending on the speed of the ramp temperature, it was possible to obtain spherical nanoparticles with a diameter of 20 nm of or rhombohedral nanoparticles with a measure 95 nm x 63 or a mixture of both.

Lastly, UCNPs were successfully coated in the presence of the Pt(II)-complexes, using the previous synthesised and characterised mPEG-ODA polymer.

After synthesising and characterising both platforms (**C1**/UCNPs/mPEG-ODA and **C2**/UCNPs/mPEG-ODA), the next step is to carry out a photochemical study of each of them.

3.8. References

1- Mitra, K.; Lyons, C. E. & Hartman, M. C. T. A Platinum(II) Complex of Heptamethine Cyanine for Photoenhanced Cytotoxicity and Cellular Imaging in Near-IR Light *Angew. Chem. Int. Ed.* **2018**, *57*, 10263-10267 https://doi.org/10.1002/anie.201806911

2- Chen, W.; Chen, M.; Zang, Q.; Wang, L.; Tang, F.; Han, Y.; Yang, C.; Deng, L. & Liu, Y. NIR light controlled release of caged hydrogen sulfide based on upconversion nanoparticles *Chem. Commun.* **2015,** *51*, 9193-9196 https://doi.org/10.1039/c5cc02508g

3- Bandara, H. M. D.; Walsh, T. P. & Burdette, S. C. A Second-Generation Photocage for Zn²⁺ Inspired by TPEN: Characterization and Insight into the Uncaging Quantum Yields of ZinCleav Chelators *Chem. Eur. J.* **2011**, *17*, 3932-3941 https://doi.org/10.1002/chem.201001982

4- Karamé, I.; Tommasino, M. L.; Faure, R. & Lemaire, M. Easy synthesis of New Chiral Tetradentate N₄ Schiff Bases and Their Use as Ligands for Metal Complexes *Eur. J. Org. Chem.* **2003**, *2003,* 1271-1276 https://doi.org/10.1002/ejoc.200390182

5- Bianchi, L.; Dll'Erba, C.; Maccagno, M.; Mugnoli, A.; Novi, M.; Petrillo, G.; Severi, E. & Tavani, C. The Reaction of 3,4-Dinitrothiophene with Grignard Reagents: Formation of 2-(3-Amino-4-nitrothiophen-2-yl)phenols *Eur. J. Org. Chem.* **2004,** *16,* 3566-3570 https://doi.org/10.1002/ejoc.200400259

6- Liu, K.; Zhang, F. & Duan, X. 1,2-Addition of Alkyl Grignard Reagents to the Nitro Group: Simple Access to 2-[Alkyl(hydroxy)amino]pyridine N-Oxides and 2-Alkylaminopyridine N-Oxides *Eur. J. Org. Chem.* **2013,** *27,* 6152-6157 https://doi.org/10.1002/ejoc.201300801

7- Gilman, H. & McCracken, R. THE REACTION BETWEEN AROMATIC NITRO COMPOUNDS AND ORGANOMAGNESIUM HALIDES *JACS* **1929,** *51,* 821-830 https://doi.org/10.1021/ja01378a024

8- Barboni, L.; Bartoli, G.; Marcantoni, E. & Petrini, M. N-Allylhydroxylamines from 1,2-Addition of Ally1 Grignard Reagents to Nitro Compounds: Generality and Drawbacks of the Reaction *J. Chem. Soc. Perkin Trans,* **1990,** *7,* 2133-2138 https://doi.org/10.1039/P19900002133

9- Nagaki, A.; Kim, H. & Yoshida, J. Nitro-Substituted Aryl Lithium Compounds in Microreactor Synthesis: Switch between Kinetic and Thermodynamic Control *Angew. Chem. Int.* **2009,** *48*, 8063-8065 https://doi.org/10.1002/anie.200904316

10- Dalai, M. & Periasamy, M. Diastereoselective reductive N-alkylation of (R,R)-trans-1,2-diaminocyclohexane with prochiral ketones using the Ti(OiPr)4/NaBH4 system *Tetrahedron: Asymmetry* **2009,** *20,* 1247-1253 https://doi.org/10.1016/j.tetasy.2009.05.004

11- Suzuki, H. & Hanazaki, Y. Titanium-mediated reduction of nitrobenzenes and benzil with dialkyl telluride *Chemistry Letters* **1986,** *15,* 549-550 https://doi.org/10.1246/cl.1986.549

12- Imamura, K.; Nakanishi, K.; Hashimoto, K. & Kominami, H. Chemoselective reduction of nitrobenzenes having other reducible groups over titanium(IV) oxide photocatalyst under protection-, gas-, and metal-free conditions *Tetrahedron* **2014,** *70,* 6134-6139 https://doi.org/10.1016/j.tet.2014.04.067

13- Bravo, J.; Cativiela, C.; Navarro, R. & Urriolabeitia, E. P. Synthesis, characterization and catalytic activity in Heck-Type reactions of orthometallated Pdᴵᴵ and Ptᴵᴵ complexes derived from (1*R*, 2*R*)-1,2-diaminocyclohexane *Journal of Organometallic Chemistry* **2002,** *650*, 157-172 https://doi-org/10.1016/S0022-328X(02)01148-8

14- Wilson, J. J. & Lippard, S. J. Synthetic Methods for the Preparation of Platinum Anticancer Complexes *Chem. Rev.* **2014,** *114*, 4470-4495 https://doi-org/10.1021/cr4004314

15- Gao, J.; Liu, Y. & Zingaro, R. A. Cytotoxic Activities, Cellular Uptake, Gene Regulation, and Optical Imaging of Novel Platinum (II) Complexes *Chem. Res. Toxicol.* **2009**, *22,* 1705-1712 https://doi.org/10.1021/tx900180v

16- Zhang, H.; Gou, S.; Zhao, J.; Chen, F.; Xu, G. & Liu, X. Cytotoxicity profile of novel sterically hindered platinum(II) complexes with (1*R*, 2*R*)-N¹,N²-dibutyl-1,2-diaminocyclohexane *European Journal of Medical Chemistry* **2015,** *96,* 187-195 https://doi.org/10.1016/j.ejmech.2015.04.019

17- Gao, J.; Liu, Y. G.; Liu, R. & Zingaro, R. A. Herceptin-Platinum(II) Binding Complexes: Novel Cancer-Cell-Specific Agents *Chem. Med. Chem.* **2008,** *3,* 954-962 https://doi.org/10.1002/cmdc.200700349

18- Auzel, F. Upconversion and Anti-Stokes Processes with f and d Ions in Solids *Chem. Rev.* **2004,** *104,* 139-173 https://doi.org/10.1021/cr020357g

19- Mahalingam, V.; Vetrone, F.; Naccache, R.; Speghini, A. & Capobianco, J. A. Colloidal Tm^{3+}/Yb^{3+} - Doped $LiYF_4$ Nanocrystals: Multiple Luminescence Spanning the UV to NIR Regions via Low-Energy Excitation *Adv. Mater.* **2009,** *21,* 4025-4028 https://doi.org/10.1002/adma.200901174

20- Zhang, Y.; Shi, Y.; Liu, L.; Song, M. & Qin, Z. Synthesis of Tetragonal Phase $LiYF_4$: Yb and Tm Microcrystals with Strong UV Upconversion Fluorescence *Journal of Nanomaterials* **2018,** *2018,* 3091607 https://doi.org/10.1155/2018/3091607

21- Kueny, A. W.; Case, W. E. & Koch, M. E. Infrared-to-ultraviolet photon-avalanche-pumped upconversion in $Tm:LiYF_4$ *J. Opt. Soc. Am. B.* **1993,** *10,* 1834-1839 https://doi.org/10.1364/JOSAB.10.001834

22- Yi, G. S. & Chow, G. M. Synthesis of Hexagonal-Phase $NaYF_4$:Yb,Er and $NaYF_4$:Yb,Tm Nanocrystals with Efficient Up-Converson Fluorescence *Adv. Funct. Mater.* **2006**, *16*, 2324-2329 https://doi.org/10.1002/adfm.200600053

23- Wang, M.; Liu, J.; Zhang, Y.; Hou, W.; Wu, X. & Xu, S. Two-phase conventional synthesis of rare-earth doped $NaYF_4$ upconversion fluorescent nanocrystals *Materials Letters* **2009**, *63*, 325-327 https://doi.org/10.1016/j.matlet.2008.10.028

24- Yi, G.; Lu, H.; Zhao, S.; Ge, Y.; Yang, W.; Chen, D. & Guo, L. Synthesis, Characterization, and Biological Applications of Size-Controlled Nanocrystalline $NaYF_4$:Yb,Er Infrared-to-Visible Up-Conversion Phosphors *Nano Lett.* **2004**, *4*, 2191-2196 https://doi.org/10.1021/nl048680h

25- Odularu, A. T. Metal nanoparticles: Thermal Descomposition, Biomedical Applications to Cancer Treatment, and Future Perspectives *Bioinorganic Chemistry and Application* **2018**, *2018*, 9354708 https://doi.org/10.1155/2018/9354708

26- Meijer, M. S.; Rojas-Gutierrez, P. A.; Busko, D.; Howard, I. A.; Frenzel, F.; Würth, C.; Resch-Genger, U.; Richards, B. S.; Turshatov, A.; Capobianco, J. A. & Bonnet, S. Absolute upconversion quantum yields of blue-emitting $LiYF_4$:Yb^{3+}, Tm^{3+} upconverting nanoparticles *Phys. Chem. Chem. Phys.* **2018**, *20,* 22556-22562 https://doi.org/10.1039/c8cp03935f

27- Braud, A.; Girald, S.; Doualan, L.; Thuau, M. & Moncorge, R. Energy-Transfer process in Yb:Tm-doped KY_3F_{10}, $LiYF_4$, and BaY_2F_8 single crystals for laser operation at 1.5 and 2.3 μm *Phys. Rev. B* **2000**, *61,* 5280-5292 https://doi.org/10.1103/PhysRevB.61.5280

28- Li, D.; Lai, W.; Shao, Q. & Huang, W. A facile methodology for regulating the size of hexagonal $NaYF_4$:Yb^{3+},Er^{3+} upconversion nanocrystals *New J. Chem* **2017,** *41,* 11521-11524 https://doi.org/10.1039/C7NJ02744C

29- Basiruddin, S. K.; Saha, A.; Pradhan, N. & Jana, N. R. Advances in Coating Chemistry in Deriving Soluble Functional Nnaoparticles *J. Phys. Chem. C.* **2010,** *114,* 11009-11017 https://doi.org/10.1021/jp100844d

30- Lee, J. E.; Lee, N.; Kim, T. & Hyeon T. Multifunctional Mesoporous Silica Nanocomposite Nanoparticles for Theranostic Applications *Acc. Chem. Res.* **2011,** *44,* 893-902 https://doi.org/10.1021/ar2000259

31- Liu, J.; Bu, W. & Shi, J. Silica Coated Upconversion Nanoparticles: A Versatile Platform for the Development of Efficient Theranostics *Acc. Chem. Res.* **2015,** *48,* 1797-1805 https://doi.org/10.1021/acs.accounts.5b00078

32- Wang, C.; Cheng, L.; Liu, Z. Drug delivery with upconversion nanoparticles for multi-functional targeted cancer cell imaging and therapy *Biomaterials* **2011**, *32*, 1110-1120 https://doi.org/10.1016/j.biomaterials.2010.09.069

33- Liu, K; Liu, X.; Zeng, Q.; Zhang, Y.; Tu, L.; Liu, T.; Kong, X.; Wang, Y.; Cao, F.; Lambrechts, S. A. G.; Aalders, M. C. G. & Zhang, H. Covalently Assembled NIR Nanoplatform for Simultaneous Fluorescence Imaging and Photodynamic Therapy of Cancer Cells *ACS Nano* **2012**, *6*, 4054-4062 https://doi.org/10.1021/nn300436b

34- Malisova, B.; Tosatii, S.; Textor, M.; Gademann, K. & Zürcher, S. Poly(ethylene glycol) Adlayers Immobilized to Metal Oxide Substrates Through Catechol Derivatives: Influence of Assembly Conditions on Formation and Stability *Langmuir* **2010,** *26,* 4018-4026 https://doi.org/10.1021/la903486z

35- Quintanar-Guerrero, D.; Allémann, E.; Fessi, H. & Doelker, E. Preparation Techniques and Mechanisms of Formation of Biodegradable Nanoparticles from Preformed Polymers *Drug Dev. Ind. Pharm.* **1998,** *24,* 1113-1128 https://doi.org/10.3109/03639049809108571

CHAPTER 4

PHOTOCHEMICAL STUDY

4: Photochemical study

At this point, when **L1**, **L2**, **C1**, **C2**, UCNPs (LiYF$_4$; Yb^{3+}, Tm^{3+}), mPEG-ODA, **C1**/UNCPs/mPEG-ODA, and **C2**/UNCPs/mPEG-ODA were synthesised and characterized, the following step was to assess their behaviour under irradiation.

All the photochemical studies in this thesis have been possible thanks to the collaboration with Dr. Jordi Hernando from the *Grup d' Electroquímica, Fotoquímica y Reactivitat Orgànica (GEFRO)* at the *Universitat Auntònoma de Barcelona.*

4.1 Photochemical study of L1, L2, C1 and C2

4.1.1 Introduction

As can be seen, the ligands contain the nitroveratryl group acting as Photolabile Protecting Group (PPG) (also known as photoreleasable, photocleavable, or photoactivatable protecting group). PPG are chemical motifs added to molecules forming a photocage. In photocages, PPGs are removed with light. PPGs are chromophore groups that are transformed after irradiation provoking the release of part of this molecule. This changes in the molecules allow to control spatial, temporally release of the active forms and thus to control their concentration with light.[1]

Among all the numerous known PGGs the *o*-nitrobenzyl (*o*-NB) motif and its derivatives are well known. The first case in which *o*-NB was described as PPG was reported by Schofield and co-workers in 1966.[2] Further on, it was found that the addition of functional groups such as two methoxides to the aromatic ring in the *meta* and *para* position respect to the nitro group (Nitroveratryl group) results in an increase in the wavelength of maximum absorption (bathochromic effect).[3] The photomechanism for the release of the *o*-NB group (**Scheme 4.1**) consists of photodegradation upon absorption with UV-light, which yields the byproduct *o*-nitrosobenzaldehyde.[4,5]
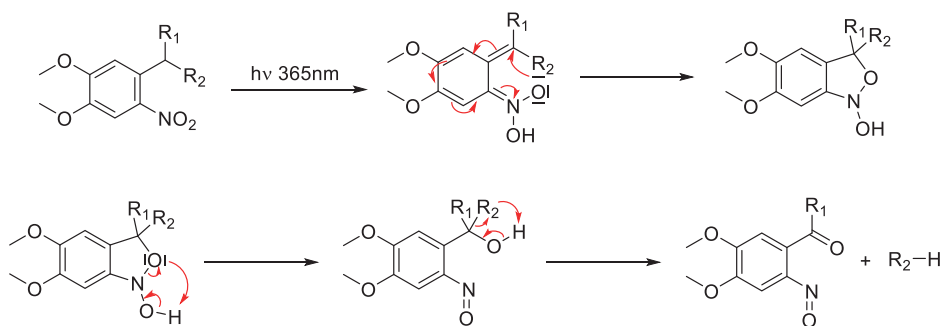
Scheme 4.1: Mechanism for photorelease of *o*-NB group as PPG under UV-light (365 nm)

The photocage is irradiated to form the *aci*-nitro, subsequently an isoxazolidine ring is form through cyclisation at the benzylic position. Finally, the ring is reopened by means of a proton transfer process provoking the breaking of the bond at the benzylic position. Thus, liberating a nitrosobenzaldehyde unit.

Over the years, *o*-NB and derivative groups have been applied as PPGs in biomedicine. These photocages have been bonded with different compounds to release carboxylic acids,[6] amines,[7] hydroxyl groups,[8] and thiols[9] resulting a photocleavage upon UV-light (approx. 365 nm).

In view of this, it is proposed that the Pt(II)-complexes **C1** and **C2** containing 4,5-dimethoxy-2-nitrophenyl as photocage, will degrade when irradiated with the corresponding excitation light, forming the corresponding nitroso photoproduct and the complex dichloro-(±)-*trans*-(1,2-diaminocyclohexane)platinum(II) (**24**) (**Scheme 4.2**). Eventually, if irradiation is performed in aqueous media, the chloride ligands of the corresponding Pt(II) photoproduct will be substituted forming the diaquo-(±)-*trans*-1,2-diaminocyclohexane platinum(II) which in turn, is the active form of oxaliplatin.
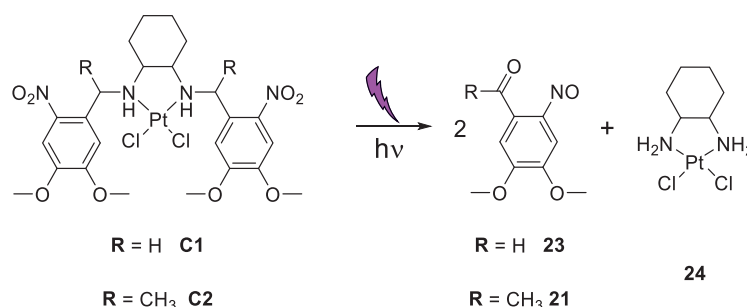
Scheme 4.2: Expected photodegradation of complexes **C1** and **C2**

As already explained, the difference between the two Pt(II)-compounds is a methyl group in the benzyl position (**Scheme 4.2**). When there is no substitution in the benzyl position (primary α-*N* position) of the PPG group, a nitrosobenzaldehyde is formed, and this photoproduct can further react itself to form an azo compound as a by-product, which absorbs at the UV (**Scheme 4.3**). The formation of this secondary photoproduct can reduce the effectiveness of the photolysis as it acts as a filter.[10,11]
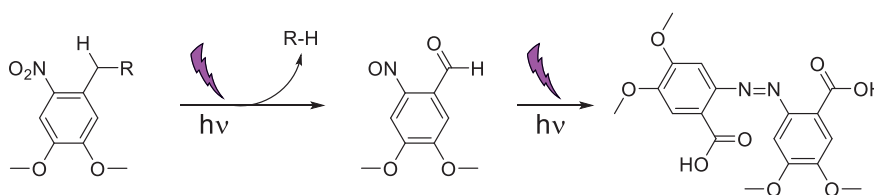
Scheme 4.3: Formation of the azo-compound during the photolysis of a nitrosobenzaldehyde

Taking into consideration all these, the photochemical behaviour of the ligands and the corresponding Pt(II)-complexes was studied.

4.1.2 Photochemical study of L1 and C1

The evolution of the photodegradation of **L1** and **C1** was followed under UVirradiation (365 nm) for both compounds' spectroscopy.

Both the ligand and the Pt(II)-complex absorb in the UV range (**Figure 4.1**). Both spectra are very similar, showing three bands, two of them are around 245 nm and 350 nm, that can be related to the presence of the 6-nitroveratryl group.[12,13]
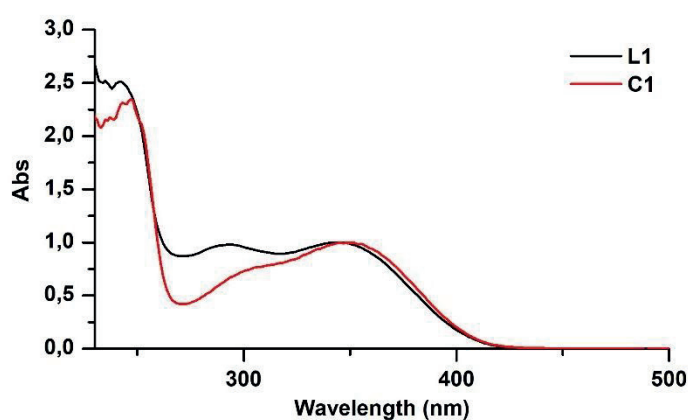
Figure 4.1: UV-Vis absorption spectra the initial of **L1** and **C1** in Acetonitrile
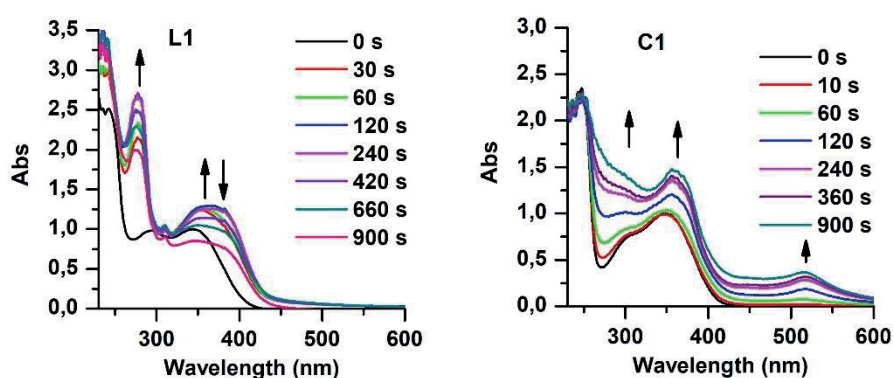
Figure 4.2: a) Evolution of photodegradation for **L1** and **C1** at λ_{exc} = 365 nm in acetonitrile

The UV-Vis spectra recorded for **L1** and **C1** show that the photodegradation with continuous UV light irradiation (λ_{exc} = 365 nm) occurs for each compound through different mechanism (**Figure 4.2**). In the case of **L1** two steps can be observed. First, two bands at 277 nm and about 355 nm increase their intensity. When irradiation continues at the same wavelength, the new band appeared at 355 nm starts to decrease while the 277 nm band

continues to increase. This suggest a self-reaction of the photoproducts formed in the first step to form a different species or to be degraded.

On the other hand, when **C1** is continuously irradiated at 365 nm in the UV region a band is observed at 290 nm and there is a bathochromic effect from the 350 nm to 356 nm band and in the visible range a new absorption band appears at 517 nm. These data suggest a maintenance of the initial structure of the complex in relation to the 6-nitroveratyl group surroundings, while a new species is formed.

4.1.3 Photochemical study of L2 and C2

As already stated, the main difference among **L1** and **L2** (and consequently their corresponding Pt(II) complexes) is the presence of a methyl group in the benzylic position.
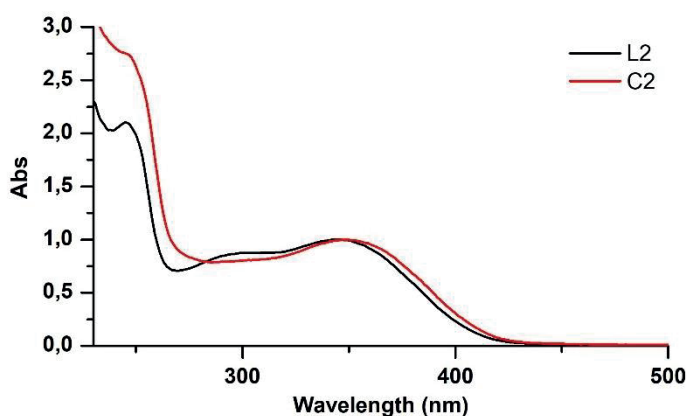
Figure 4.3: UV-Vis absorption spectra of **L2** and **C2** in acetonitrile before irradiation

The UV-Vis absorption spectra recorded for **L2** shows three UV-absortion bands while **C2** exhibits only two UV-absortion bands (**Figure 4.3**) those related with the PPG present in the molecules, as suggested by the similarity in both spectra as well as in the case of **L1** and **C1** The photodegradation of **C2** and **L2** excited to 365 nm radiation, followed by UV-Vis spectroscopy shows only one step for both compounds(**Figure 4.4**)
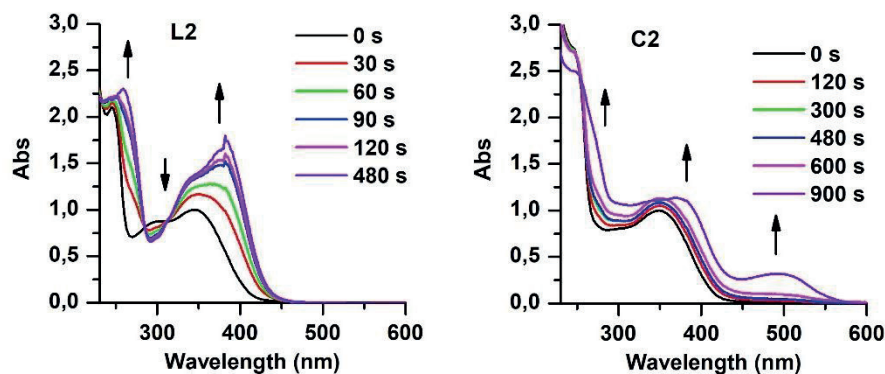
Figure 4.4: UV-Vis spectra photolysis of **L2** and **C2** in Acetonitrile under irradiation at 365 nm

In the case of **L2,** there are two increasing absorption bands while one is decreases. In addition, C2 irradiation causes a decrease of the 247 nm band and, as in the case of C1, a bathochromic effect from the 349 nm to 364 nm band and the appearance of a new band in the visible range (495 nm).

By comparing the photodegradation processes for **L2** and **C2**, the bands increasing in the same region for **L2** and **C2** (260 nm and 380 nm) suggest that in both cases there is a photoproduct in common and moreover, they must have similar photolysis mechanism.

Interestingly, all the compounds under study (**L1**, **C1**, **L2** and **C2, Figure 4.1** and **Figure 4.3**), present some absorption reaching the visible range (> 400nm). It was found that by irradiation with a 450 nm LED it was possible to photodegrade each product at longer irradiation times. The possibility of photodegradation with less energetic radiation such as visible radiation can be advantageous for working in the biological field.

4.1.4 Quantum yields of the photodegradation processes

To deepen in the photodegradation process, the quantum yield of the process for each compound was determined. The efficiency of a particular photoprocess is normally lower than 100% because not all photons that are absorbed by a luminescent material are directed to a particular process, some are diverted to other paths. The quantum yield (Φ) is a measure that indicates the number of times a particular process occurs for photon absorbed by the system. In the context of this work, it indicates how many molecules are degraded per absorbed photon.

$$\Phi = \frac{\text{number of molecules degraded}}{\text{number of photons absorbed}}$$

The quantum yields were determined using the 1,2-bis(2-methyl-5-trifluoroactylthien-3-yl)cyclopentene (DTE-(COCF$_3$)$_2$) as a reference.[14] This molecule has an absorption band at

approximately 350 nm, and when exposed to UV light, it undergoes a photodegradation from colourless (open ring) to coloured (closed ring).

DTE-(COCF$_3$)$_2$ Open ring   **DTE-(COCF$_3$)$_2$ Closed ring**
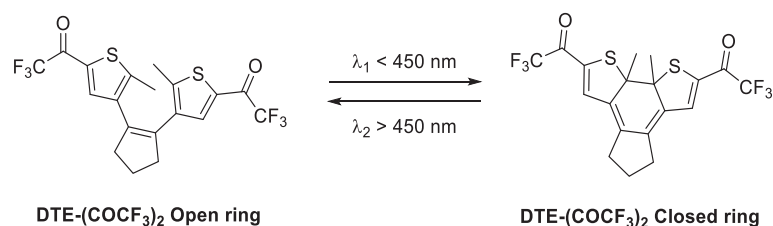
Scheme 4.4: Photocyclization of DTE-(COCF$_3$)$_2$

All the quantum yield determinations were done in acetonitrile and irradiated with a pulsed laser at 355 nm and followed up with the UV-Vis spectrometer. In the case of **L1**, which contains two degradation processes, the quantum yield was calculated until the first degradation process is complete.

Table 4.1: Quantum yields calculated for **L1**, **L2**, **C1** and **C2** taking as reference the known system DTE-(COCF$_3$)$_2$. Molar extinction coefficients are also indicated.

Compound	Φ_{ph}	ε (M$^{-1}\cdot$cm^{-1})
DTE-(COCF$_3$)$_2$	0.320	5411
L1	0.406	10041
C1	0.015	10025
L2	0.147	7424.3
C2	0.028	7995.9

The values calculated (**Table 4.1**) show that the quantum yields are higher for the ligands (**L1** and **L2**) than for the corresponding Pt(II)-complexes (**C1** and **C2**). This seems reasonable as it has been experimentally observed that Pt(II)-compounds take longer to photodegrade. Interestingly, **C2** has a quantum yield almost twice as **C1**.

4.1.5 Investigation of L1 and C1 photoproducts

To learn more about the photomechanism and the structure of the photoproducts, the same photodegradation processes were carried out followed by NMR and mass spectrometry.
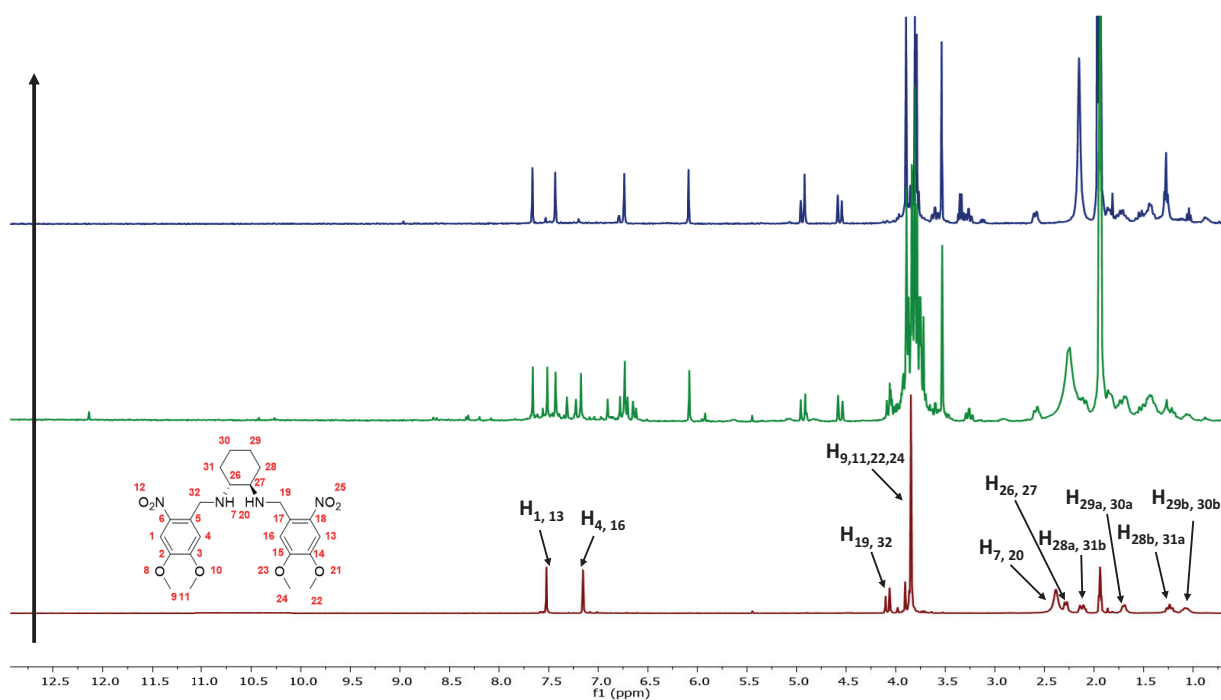
Figure 4.5: ^{1}H-NMR spectra (Acetonitrile-d_3) of the evolution of photodegradation of **L1** irradiating continuously at 365 nm (Red, (t = 0 min), Green (t = 50 min), Blue (t = 110 min))

When **L1** is irradiated at 365 nm during 50 min (**Figure 4.5, green spectra**), new ^{1}H-NMR peaks appear in the recorded spectra, in comparison with the initial spectrum of the ligand, including a singlet 12.1 ppm corresponding to the aldehyde proton of the photoproduct **23**. The mass data recorded at this point confirmed the presence of this species in solution ([M+H⁺] = 196.0607 Da, **Figure A.8**)

As irradiation continued, some of these peaks disappeared while others were maintained in position and intensity. The two initial signals of the aromatic zone in two (δ = 7.57, 7.10 ppm) gave rise to four signals (δ = 7.71, 7.42, 6.80, 5.93 ppm), where two of them appear at downfield and the other two at up field. The signals corresponding to the benzylic protons (δ = 4.12, 3.94 ppm) shift to downfield (δ = 4.91, 4.80 ppm). Four peaks (δ = 3.97, 3.88, 3.80, 3.58 ppm), result from the signal assigned to the methoxides protons (δ = 3.94, 3.93 ppm). In addition, it is noticeable that the signals of the protons at the α-*N* position (δ = 2.30 ppm) in the cyclohexane are also shifted to downfield at different ppm for each peak (δ = 3.27, 2.73 ppm).

The analysis of this by mass spectrometry, revealed the presence of three peaks: 150.1045, 274.1543, 469.2088 (**Figure A.9**). None of these peaks were correlating with the expected products, thus, further investigation would be needed to identify the resulting photoproducts.

As it was difficult to identify the photoproducts formed, a structurally simplified analogue of **L1** was synthesised, which consisted of keeping the same photocage but changing the (±)-*trans*-DACH group for an isopropylamine group (**40**) (**Scheme 4.5**), in this way the amine group would be bonded to a secondary carbon as in **L1**.
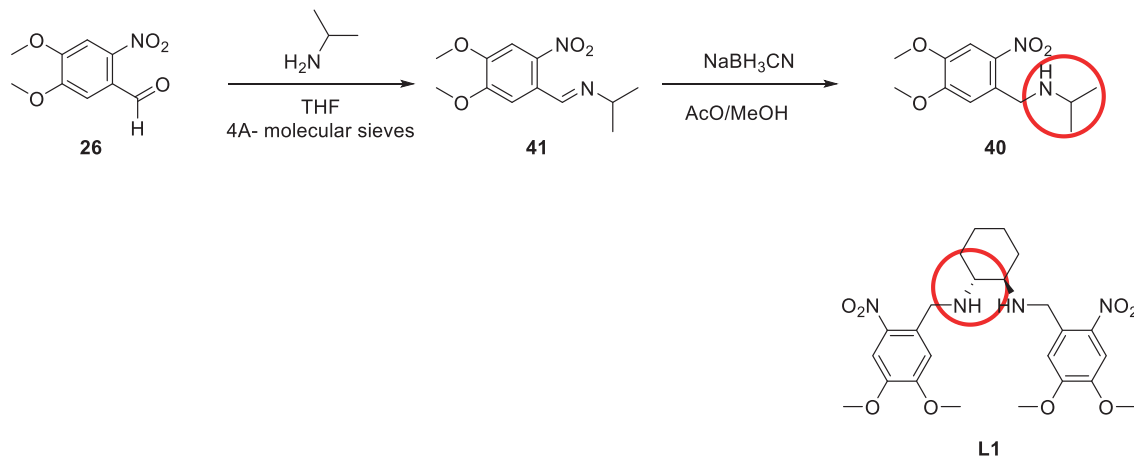
Scheme 4.5: Synthesis of **40** to change of functional group (±)-*trans*-(DACH) to isopropylamine to do a photochemical study of a simplified analogue of **L1**

To synthesis of compound **40** (**Scheme 4.5**), followed the same synthetic route as for **L1**. First, the 6-nitroveraltraldehyde (**26**) reacted with isopropylamine in the presence of 4 Å molecular sieves to yield the imine **41**. Subsequently this imine was reduced with NaBH$_3$CN to obtain the desired product **40** (75 % overall yield).

The UV-Vis spectrum of compound **40** (**Figure 4.6 A**) shows three absorption bands: at 244 and 348 nm corresponding to 6-nitroveratryl, and a band at 306 nm. This spectrum closely resembles more to the one recorded for **C1** spectrum than for **L1** (**Figure 4.1**)
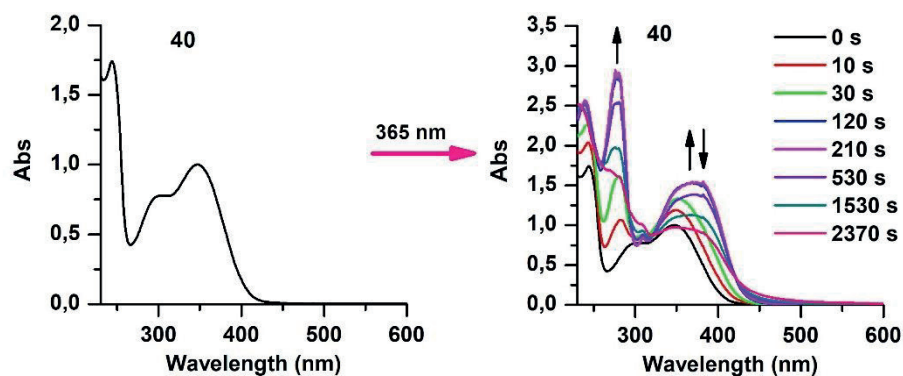
Figure 4.6: a) Photodegradation evolution of **40** at λ_{exc} = 365 nm in acetonitrile **b)** Evolution of **40** photodegradation

When irradiating at 365 nm (**Figure 4.6 B**), a similar process to that observed in **L1** occurs. At the initial steps two new bands appear around 275 nm and 365 nm, but as the irradiation progresses, these bands are reduced, unlike **L1** (where only one of the two bands was decreasing intensity). These results confirm a similar photochemical process for compound **40** and **L1** when irradiated at 365 nm, even is not identical probably due by the lack the (±)-*trans*-DACH group.
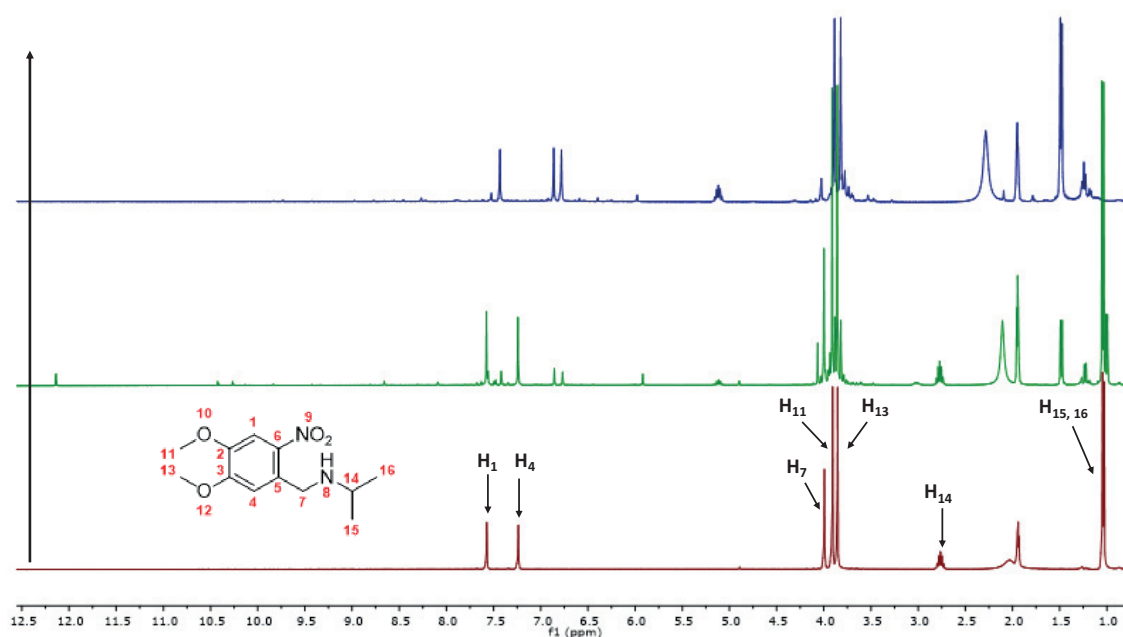
Figure 4.7: ^{1}H-NMR spectra (Acetonitrile-d_3) of the photodegradation of **40** at 365 nm during 210 min (Red t = 0 min, Green t = 80 min, Blue t = 210 min)

Irradiation of **40** at 365 nm followed by ^{1}H-NMR suggests the formation of compound **23** due to the appearance of a singlet peak at 12.1 ppm characteristic of an aldehyde proton. This was also confirmed by mass spectrophotometry ([M+H$^+$] = 196.0608 (**Figure A.36**)

When **40** was irradiated for longer time, a stable photoproduct was formed, which shows that in the aromatic zone there were two singlets (7.63, 7.13 ppm), and in the photoproduct, there are three (7.22, 6.96, 6.71 ppm). It can also be observed that the septet signal, corresponding to the α-*N* proton, is clearly shifted to higher field from 2.77 ppm to 5.1 ppm. MS data rendered a set of peaks, one which correlated the mass of the imine **43** ([M+H$^+$] = 237.1242, **Figure A.37**). With these results it can be concluded that when compound **40** was irradiated with UV light it initially formed the photoproducts **23** and isopropylamine, and later, they both react to form the imine **43** (**Scheme 4.6**)
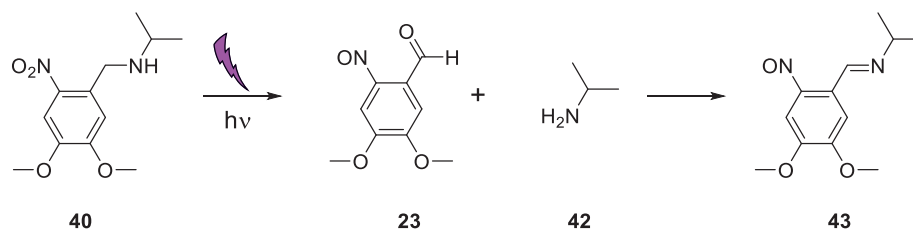
Scheme 4.6: Photodegradation of **40** when irradiated with UV light, which yields **23** and **42** as photoproducts that react with each other to form imine **43**.

Unfortunately, the formation of an imine coming from the resulting photoproducts, as observed in the case on compound **40**, cannot be considered with **L1,** as ^{1}H-NMR signals do not match with the production of an imine.

Finally, after many attempts, it was possible to obtain a crystal of the photoproduct from the irradiation of **L1**, by means of liquid-liquid fusion, between DMF and MeOH, which was analysed by XRD to study the structure. The XRD results (**Figure 4.8**) revealed that when **L1** is irradiated during long time with UV light, a pyrazole ring was formed (**45**). At short irradiation time in acetonitrile one of the photocleaves desegregated and yields and the amine **44** the aldehyde **23** which was confirmed by MS (**Figure A.8**) and NMR (**Figure 4.5**), in which they react with each other by the Davis-Beirut-type reaction[15] leading the formation of the pyrazole ring and yielding photoproduct **45** (**Schem 4.7**). This structure agreed with the information obtained from the NMR and MS (**Figure A.7** and **Figure A.9**).
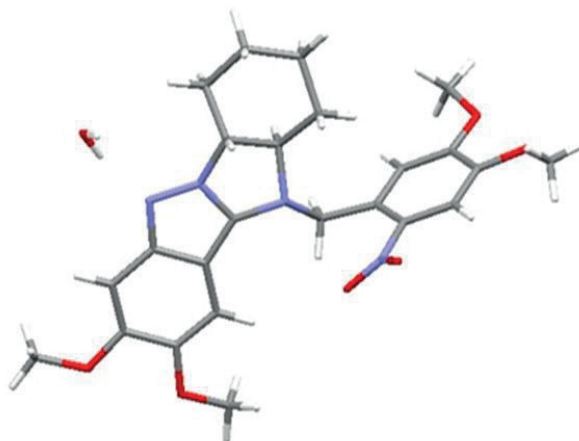
Figure 4.8 3D model of the XRD resolved structure for photoproduct **45**
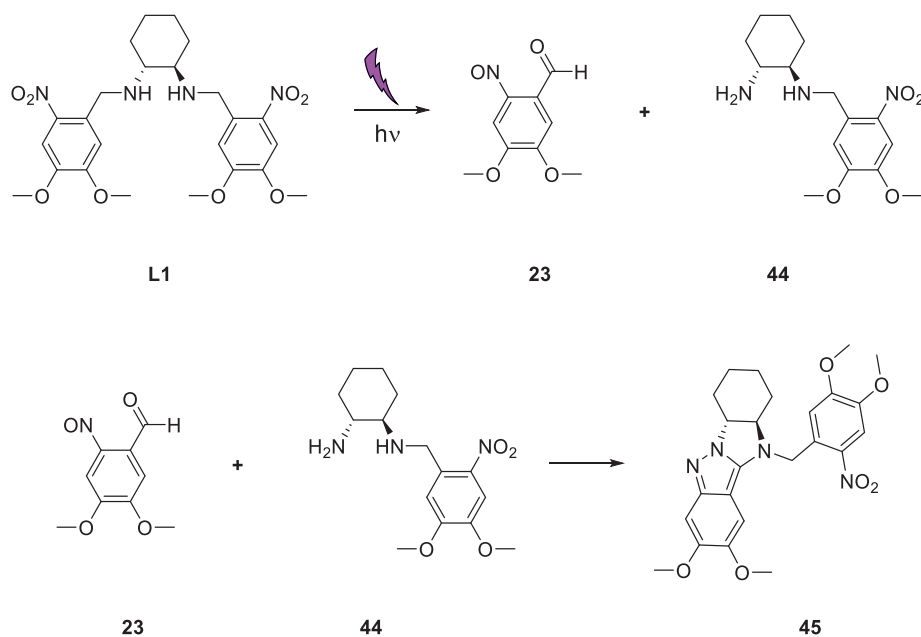
Scheme 4.7: Photodegradation of **L1** when irradiated with UV light, which yields **45**. The structure was confirmed by XRD.

The photodegradation of **C1** followed by ¹H-NMR was performed with DMF-d_7. With this compound it was possible to detect the signal corresponding to the aldehyde proton of the photoproduct **23** (**Figure 4.9**).
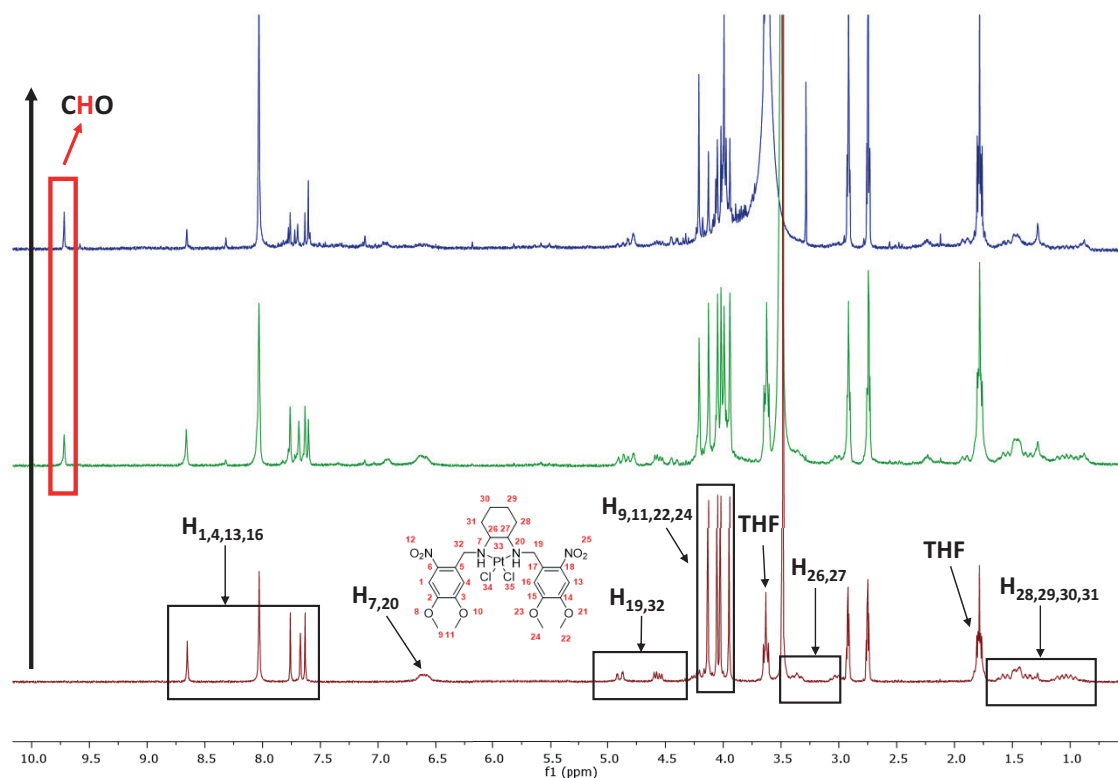
Figure 4.9: ¹H-NMR spectra (DMF-d_7) of **C1** photodegradation over time under 365 nm (Red t = 0 min, Green t = 60 min, Blue t = 120 min)

As **C1** was irradiated, some new peaks were appeared. A singlet peak at 9.72 ppm could be identified as corresponding to the aldehyde proton from the photoproduct **23**. Although countless attempts were made with chromatography and/or crystallizations, in no case could any photoproduct be isolated.

ESI-MS data recorded allowed the identification the photoproduct **23** ($[M+Na]^+$ 217.1 Da, **Figure A.13**). Additional peak at 598.1 Da suggest the formation of species related with the partial photolysis of **C1,** forming expected compound **46** (theoretical $[M+Na]^+$ 598.1 Da, **Figure A.13**) (**Scheme 4.8).**
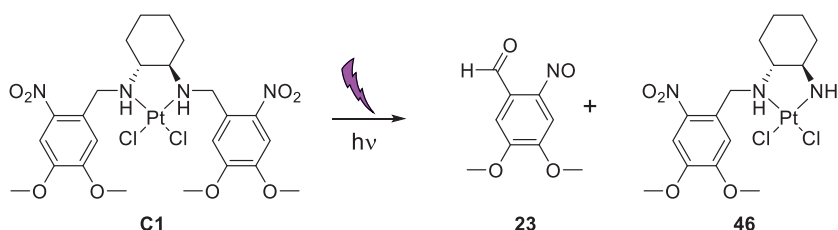
Scheme 4.8: Suggested photolysis of **C1** when irradiated with UV light, based on experimental data collected.

When comparing the ^{1}H-NMR spectra of the photoproducts obtained after irradiation of **L1** and **C1** (**Figure 4.10**) it can be observed that the signals, and consequently the products formed, are quite different. Thus, it can be concluded that the presence of Pt(II) bound to **L1** promotes a different behaviour of the ligand under irradiation by UV light. To determine the exact nature of these photo products more research must be done.
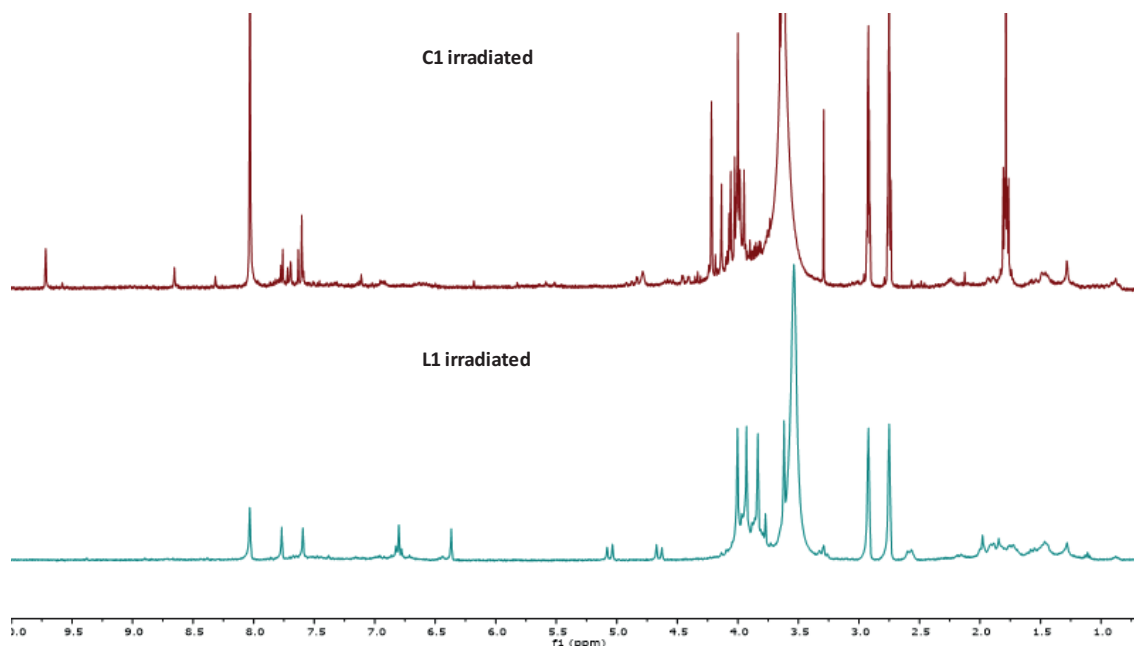
Figure 4.10: ^{1}H-NMR spectra (DMF-d_7) of **C1** and **L1** after irradiated at 365 nm

4.1.6 Investigation of L2 and C2 photoproducts
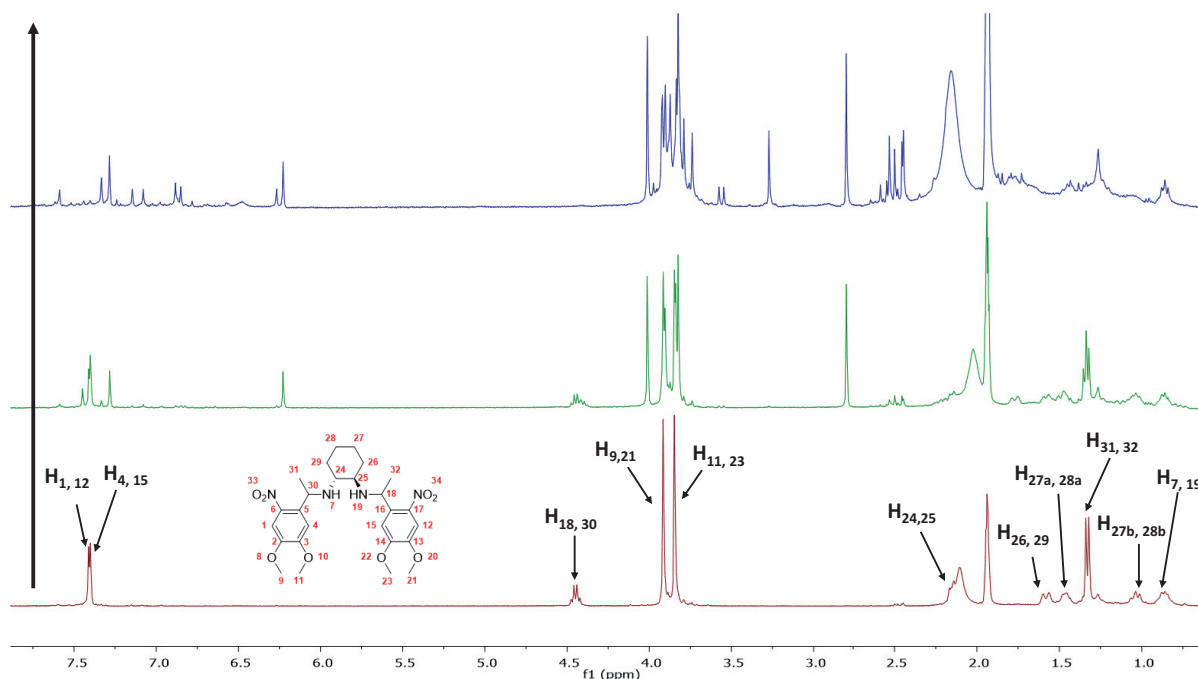
Figure 4.11: ^{1}H-NMR spectra (Acetonitrile-d_3) of the photolysis of **L2** irradiated during 80 min at 365 nm (Red t = 0 min, Green t = 20 min, Blue t = 80 min of irradiation)

The ^{1}H-NMR spectra recorded before and after irradiation of **L2** showed that just 20 min after irradiation, a new singlet appeared at 2.79 ppm which was assigned to the methyl group of the suggested photoproduct acetone **21** (**Scheme 4.8**). The relative intensity of this signal increases up to a maximum value. This suggests is that part of the formed photoproduct **21**, at certain moment reacts with a secondary photoproduct to form another species.

Further irradiation resulted in the appearance of a new singlet at 3.72 ppm. This new singlet could provide proof that photoproduct **21** does not stabilise and react with another compound. However, more research would have to be done to reach a solid conclusion. In addition, an attempt was made to separate the photoproducts by column chromatography, but this was unsuccessful.

The final mixture obtained after irradiation was also analysed by mass spectrometry, as previously. By analysing the mass spectrum (**Figure A.25**), two peaks one related to compound **21** ([M+H$^+$] (210.076 Da)) and the other related with the partial photolysis of the ligand ([M+H$^+$] (324.19 Da)), suggesting the formation of **47** (**Scheme 4.9**), as similarly observed in the case of **C1** (**Scheme 4.8**)
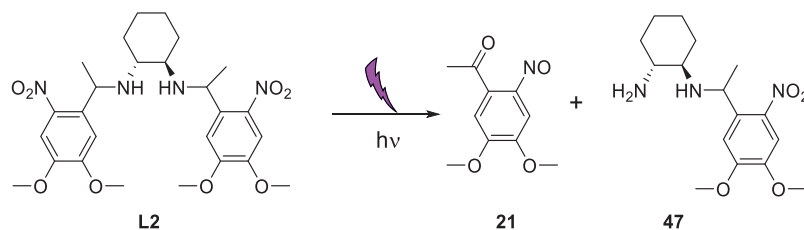
Scheme 4.9: Suggested photodegradation of **L2** irradiated at 365 nm based on experimental data collected.

Next, irradiation at 365 nm of the corresponding Pt(II)-complex **C2** was followed by ^{1}H-NMR in DMF-d_7 solvent (**Figure 4.12**)
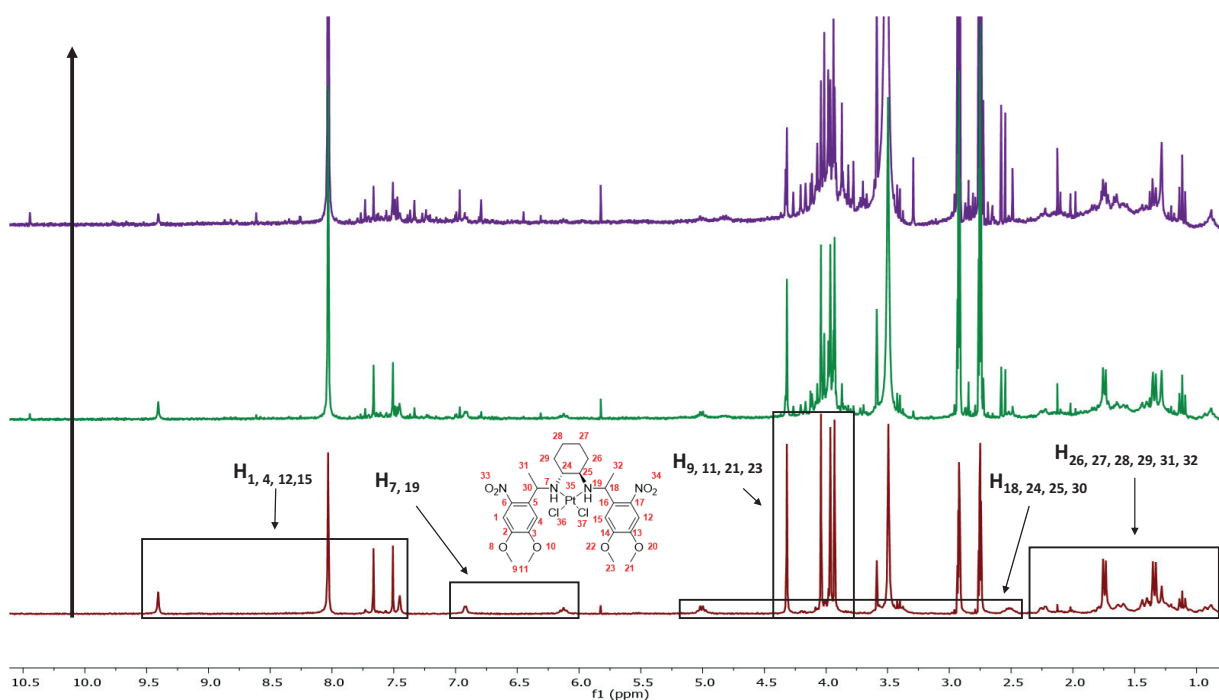
Figure 4.12: ^{1}H-NMR spectra (DMF-d_7) of the photolysis of **C2** irradiated at 365 nm for 150 min (Red t = 0 min, Green t = 30 min, Purple t = 150 min)

After irradiation of **C2**, many new signals appeared. Among these peaks, three singlets appeared at 2.84, 2.58 and 2.55 ppm, one of which could correspond to the methyl ketone **21** that is probably formed. It was challenging to draw any assignation due to the high number of signals appearing, although it is important to note that the more time the Pt(II)-complex was irradiated, the benzylic proton (δ = 4.80 ppm) disappeared, and a new quadruplet signal appeared next to it (δ = 4.88 ppm). This suggest the hypothesis that if the photolysis of **C2** is similar to **L2**, where only one part of the molecule is photocleaved.

The comparison of the ^{1}H-NMR analysis spectra of the ligand and Pt(II)-complex when are exposed to UV light with the same irradiation time (**Figure 4.13**) clearly confirmed it.
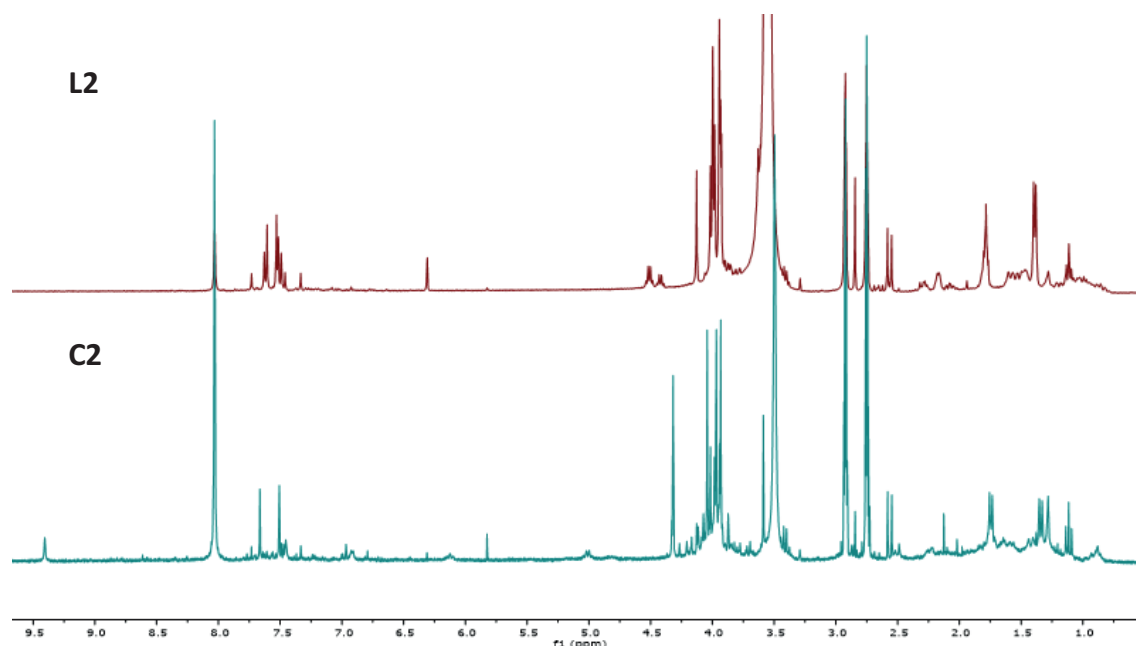
Figure 4.13: Comparison of ^{1}H-NMR (DMF-d_7) signals obtained for **L2** and **C2** when irradiated for 50 minutes at 365 nm.

Both ^{1}H-NMR spectra (**Figure 4.13**) contain some identical peaks, for example the three singlets at 2.84, 2.58, and 2.55 ppm, and a new quadruplet next to the benzylic proton signal (δ = 4.80 ppm for **C2**, δ = 4.40 ppm for **L2**)

Mass data recorded after UV exposure of **C2** (**Figure A.28**) also leads to a similar process in both cases. A peak with 210.0748 Da was identified [M+H⁺] mass corresponding to the photoproduct **21** (theoretical 210.077 Da), and the peak at 554.1158 Da correlates with the photoproduct **48** after releasing a [Cl⁻] ion ([M-Cl⁻] = 553.118 Da, theoretical mass). The last product, that exhibits the typical isotopic Pt pattern, matches with the release of only one of the two PPG of complex **C2** (**Scheme 4.10**).

All this data allows to conclude that both molecules (**L2** and **C2**) most likely follow the same mechanism of photodegradation with common photoproducts, and it seems that only one part of the molecule (one of the PPG) is photocleaved.
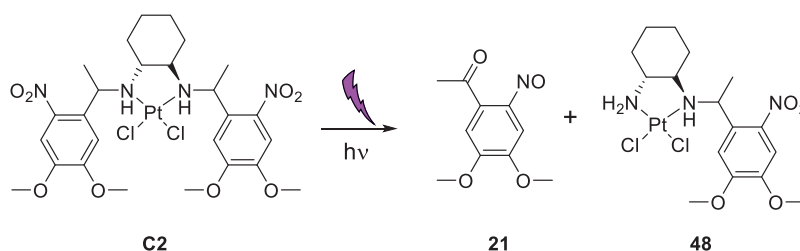
Scheme 4.10: Photodegradation of **C2** irradiated with UV light.

With the results obtained, it can be determined that **C1**, **L2**, and **C2** do not completely degrade as expected, as only one of the two photocages group is removed. On the other hand, it has not been possible to elucidate how **L1** photodegrades because it follows an unexpected mechanism. Further research needs to be done to shed light into its photodegradation.

4.2 Photochemical study of UCNPs

. As already mentioned, our ligands and their corresponding complexes absorb efficiently in the UV-vis range and therefore could act as photosensitizers. Nevertheless, activating these photosensitizers at those wavelengths would not be clinically applicable. Ideally, it would be better to activate them with lower energy light and higher tissues penetration, such as NIR light.

The use of UCNPs has been the alternative here proposed to overcome this drawback. UCNPs have a fundamental optical characteristic that allow them to convert NIR light into visible o UV light and, therefore, may allow photodegration of UV photosensible motifs by NIR irradiation.

Initially, the $LiYF_4$ nanoparticles doped with Yb^{3+} and Tm^{3+} (UCNPs) were synthesised and characterised, and mainly two different morphologies of nanoparticles (rhombohedral and spherical) were obtained.

Figure 4.14: UV-vis absorption spectrum for $LiYF_4$; Yb^{3+}; Tm^{3+} UCNPs in solid the solid state (powder)

The absorption spectrum of the UCNPs was measured in solid powder because it was difficult to detect the absorption band in solution due to their small absorption. The spectrum shows the absorption band at 960 nm within the NIR light range.

As two different morphologies of nanoparticles (rhombohedral and spherical) were obtained depending on the synthetic conditions, a study of their excitation at 980 nm was carried out to determine the difference among them (**Figure 4.15**)

Figure 4.15: Emission spectra of spherical *vs* rhombohedral UCNPs measured as solid powders under NIR irradiation (λ_{exc} = 980 nm, power density = 3.8 W/cm^2, $\lambda_{detection}$ = 320 − 730 nm). The thulium emission transitions giving rise to each of the luminescence bands registered are indicated in the figure.

Both rhombohedral and spherical nanoparticles were irradiated at 980 nm at the same power intensity during the same time, and the emission spectra in the visible rang confirm that both batches have the same emissions bands. The main difference was that rhombohedral UCNPs have much higher emission intensities than the spherical ones. For this reason, it was decided to continue with the study using UCNPs with a rhombohedral shape.

The emission spectrum of the rhombohedral UCNPs excited at 980 nm laser (**Figure 4.15**), show different band than without the filter. The bands in the emission spectrum can be coorelated to the energy levels in the diagram of energy transfer upconversion (ETU) between Yb^{3+} and Tm^{3+} (**Figure A.41**). The bands in the visible range at 650 nm, 510 nm, 475 nm, 450 nm correspond to transitions $^1G_4 \rightarrow {}^3F_4$, $^1D_2 \rightarrow {}^3H_5$, $^1G_4 \rightarrow {}^3H_6$, $^1D_2 \rightarrow {}^3F_4$, respectively. The two bands in the UV range at 360 nm and 345 nm correspond to $^1D_2 \rightarrow {}^3H_6$ and $^1I_6 \rightarrow {}^3F_4$ transitions, respectively.[16]

The quantum yield of the upconversion process of the nanoparticles was also measured as previously done with the complexes and ligands and resulted in a 0.053 % when irradiated at a power of 580 W/cm^2.

4.3 Pt(II)-release through UCNPs

It has been proven that when irradiated with NIR light there was an emission in the UV range, coinciding with the absorption range of Pt(II)-complexes **C1** and **C2**. Therefore, the next step was to perform a photochemical study of the **C1**/UNCPs/mPEG-ODA and **C2**/UCNPs/mPEG-ODA platforms and determine if the Pt(II)-compounds are degraded and thus, platinum could be released by the platforms upon irradiation with NIR light.

Initially, the photoresponse of the complexes inserted into the platforms **C1**/UCNPs/mPEG-ODA and **C2**/UCNPs/mPEG-ODA was studied. To do this, the platforms were dispersed in PBS medium and irradiated under UV and NIR light irradiation and the behaviour was compared to that observed in the dark.

The procedure was carried out preparing dispersions of each platform at a concentration of 220 µM in Pt(II), in a phosphate saline buffer (PBS). The resulting dispersions were introduced into a porous cuvette recovered with a dialysis bag (3 nm pore). This cuvette was placed in a PBS bath at 37 °C and irradiated over the top of the cuvette at the corresponding wavelength, using a setup made on purpose (**Figure 4.16**).
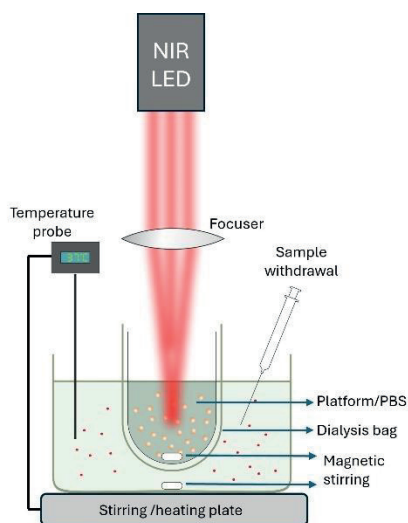
Figure 4.16: Setup employed in the study of Pt(II) release of the **C1/**UCNPs/mPEG-ODA and **C2/**UCNPs/mPEG-ODA platforms

Aliquots from the PBS bath were collected at different times and analysed by ICP-MS to determine the amount of Pt(II) released. The results obtained for each preparation at the three different conditions (dark, irradiating with UV, and irradiating with NIR light) show interesting behaviours. (**Table A.1** and **Figure 4.17**)
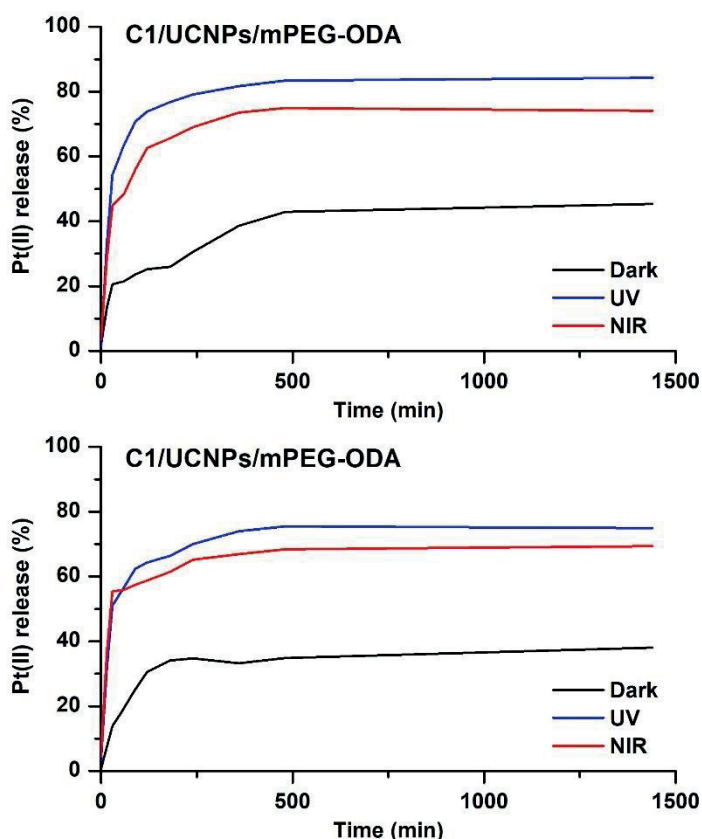
Figure 4.17: Pt(II) release profile obtained for **C1**/UCNPs/mPEG-ODA and **C2**/UCNPs/mPEG-ODA platforms (data showing average of the 2 tests done for each sample), comparing the three conditions assayed: in the dark, under irradiation at 365 nm (UV) and at 980 nm (NIR)

The release curves representing the amount of delivered Pt(II) determined by ICP over the irradiation time (**Figure 4.17**). As shown, in the absence of light, Pt(II) was moderately released in both preparations. With time (~ 400 min) the Pt(II) release was stabilized at 45%, in the case of platform containing **C1** and less than 40 % for **C2** platform after 200 min. When irradiating with NIR and UV light, Pt(II) delivery was clearly improved. Even if the Pt(II) was more efficient for the direct UV radiation than the NIR, in both cases the curves recorded are close enough to considered that the upconversion process was satisfactorily efficient. To our delight, these results indicated that this new platform can therefore activate Pt(II)-UV photoresponsive complexes when exposed to NIR light.

It has been shown that the upconversion process, using the synthesised platforms, has the capacity to photoactivate Pt(II)-photosensitizer complexes. This finding has prompted further investigation into the effectiveness of this process in biomedical applications.

4.4. Summary and conclusions for Chapter 4

In this chapter a general photochemical study of different previously synthesised components in chapter 3 has been carried out.

First, the photochemical study of the ligands **L1** and **L2** and their corresponding Pt(II)-complexes **C1** and **C2** was performed. All compounds absorb mostly at the UV range, although they can absorb some visible light.

A photodegradation study was carried out for each compound to investigate which photoproducts were produced when irradiated at 365 nm. The changes and the products formed were characterised by UV, NMR and mass spectrometry. When **L2**, **C1** and **C2** were irradiated, it turns out that only one of the photocleavage (4,5-dimethoxy-2-nitrobenzyl) was photodissociated instead of the expected double photocleavage. Besides, **L1** photodegraded differently than the other compounds, as it follows a different photomechanism than the expected, it turns out that one of the photocleavage forms an pyrazole ring between the aldehyde **23** and the amine **44**.

Moreover, the synthesised UCNPs absorb in the NIR region with the maximum absorbance at 960 nm. When observing the behaviour of the different shaped nanoparticles, it could be concluded that the morphology plays an important role in the efficacy of the upconversion process, since the emission bands of the excited nanoparticles at 980 nm are more intense for rhombohedral than for spherical UCNPs. Also, it has been observed that the emission bands for the UCNPs in the UV coincides with the absorption bands for the Pt(II) complexes. Therefore, indicating that UCNPs can activate complexes **C1** and **C2**.

Finally, a photochemical study of both platforms **C1**/UCNPs/mPEG-ODA and **C2**/UCNPs/mPEG-ODA were carried out. Interestingly, the Pt(II) release in the dark was poor compared to under the presence of light. The Pt(II) release curves when the platform was irradiated with UV or NIR light are similar, allowing to conclude that the upconversion process to degrade the Pt(II) complex when irradiated with NIR light is effective enough to promote the Pt(II) delivery after the upconversion process takes place.

4.5. References

1. Klán, P.; Solomek, T.; Bochet, C. G.; Blanc, A.; Givens, R.; Rubina, M.; Popik, V.; Kostikov, A. & Wirz, J. Photoremovable Protecting Groups in Chemistry and Biology: Reaction Mechanism and Efficacy *Chem. Rev.* **2013**, *113*, 119-191 https://doi.org/10.1021/cr300177k

2. Barltrop, J. A.; Plant, P. J. & Schofield, P. Photosensitive Protective Groups *Chem. Commun.* **1966**, *22*, 822-823 https://doi.org/10.1039/C19660000822

3. Adams, S. R.; Kao, P. Y. & Tsien, R. Y. Biologically Useful Chelators That Take Up Ca^{2+} upon Illumination *J. Am. Chem. Soc.* **1989**, *111*, 7957-7968 https://doi.org/10.1021/ja00202a042

4. Pelliccioli, A. P. & Wirz, J. Photoremovable protecting groups: reaction mechanisms and applications *Photochem. Photobiol. Sci.* **2002**, *1*, 441-458 https://doi-org/10.1039/B200777K

5. Il'ichev, Y. V.; Schwörer, M. A. & Wirz, J. Photochemical Reaction Mechanisms of 2-Nitrobenzyl Compounds: Methyl Ethers and Caged ATP *J. Am. Chem. Soc.* **2004**, *126*, 4581-4595 https://doi.org/10.1021/ja039071z

6. Russell, A. G.; Ragoussi, M.; Ramalho, R.; Wharton, C. W.; Carteau, D.; Bassani, D. M. & Snaith, J. S. α-Carboxy-6-Nitroveratryl: A Photolabile Protecting Group for Carboxylic Acids *J. Org. Chem.* 2010, *75*, 4648-4651 https://doi.org/10.1021/jo100783v

7. Álvarez, M.; Alonso, J. M.; Filevich, O.; Bhagawati, M.; Etchnique, R.; Piehler, J. & del Campo, A. Modulating Surface Density of Proteins via Caged Surfaces and Controlled Light Exposure *Langmuir* 2011, *27*, 2789-2795 https://doi.org/10.1021/la104511x

8. Corrie, J. E. T. Synthesis, Photochemistry and Enzymology of 2-*O*-(2-Nitrobenzyl)-D-glucose, a Photolabile Derivative of D-Glucose *J. Chem. Soc. Perkin. Trans.* 1993, *1*, 2161-2166 https://doi-org/10.1039/P19930002161

9. Kotzur, N.; Briand, B.; Beyermann, M. & Hagen, V. Competition between cleavage and decarboxylation in photolysis of α-carboxy-2-nitrobenzyl protected cysteine derivates *Chem. Commun.* **2009**, 3255-3257 https://doi-org./10.1039/B900865A

10. Patchornik, A.; Amit, B. & Woodward, R. B. Photosensitive protecting group *J. Am. Chem. Soc.* **1970**, *92*, 6333-6335 https://doi.org/10.1021/ja00724a041

11. Giralt, E.; Eritja, R.; Pedroso, E.; Granier, C. & Rietschoten, J. V. Convergent solid phase peptide synthesis-III: Synthesis of the 44-52 protected segment of the toxin II of androctonus australis hector *Tetrahedron* **1986**, *42*, 691-697 https://doi-org.are.uab.cat/10.1016/S0040-4020(01)87472-X

12. Blanc, A. & Bochet, C. G. Wavelength-Controlled Orthogonal Photolysis of Protecting Groups *J. Org. Chem.* **2002**, *67*, 5567-5577 https://doi-org/10.1021/jo025837m

13. Neranon, K.; Aslund, M.; Yan, M.; Xu, H.; Fu, Y.; Petermann, I.; Björk, P. & Ramström, O. Laser-induced, Surface Plasmon-enhanced Two-photon Excitation for Efficient Chemical Functionalization of Nanostructured Gold Surfaces *Chem. Rxiv.* **2021**, *12* https://doi.org/10.26434/chemrxiv.13695994.v1

14. Villabona, M.; Wiedbrauk, S.; Feist, F.; Guirado, G.; Hernando, J. & Barner-Kowollik, C. Dual-Wavelength Gated *oxo*-Diels-Alder Photoligation *Org. Lett.* **2021**, *23*, 2405-2410 https://doi.org/10.1021/acs.orglett.1c00015

15. Conrad, W. E.; Fukazawa, R.; Haddadin, M. J. & Kurth, M. J. The Davis-Beirut Reaction: N^1, N^2-Disubstituted-1*H*-Indazolones via 1,6-Electrophilic Addition to 3-Alkoxy-2H-Indazoles *Organic Letters* **2011**, *13*, 3138-3141 https://doi.org/10.1021/ol2010424

16. Maurizio, S. L.; Tessitore, G.; Mandl, G. A. & Capobianco, J. A. Luminescence dynamics and enhancement of the UV and visible emissions of Tm^{3+} in $LiYF_4$:Yb^{3+}, Tm^{3+} upconverting nanoparticles *Nanoscale Adv.* **2019**, *1*, 4492-4500 https://doi-org/10.1039/C9NA00556K

CHAPTER 5

BIOLOGICAL STUDIES

5. Biological studies

After confirming the ability of the new platforms to release Pt(II) when exposed with NIR light, the next step was to assess their cytotoxicity against cancer cells when irradiated with NIR light.

Before going to to the cell cultures, it was planned to evaluate the *in vitro* reactivity of the single complexes **C1** and **C2** towards DNA to check the responses under different conditions. This reactivity was followed by circular dichroism (CD) and UV-vis absorbance spectroscopies.

5.1 Interaction with DNA studied by Circular Dichroism

First, the interaction of DNA with the Pt(II)-complexes (**C1**, **C2**) and the corresponding photoproducts (**C1 IR**, **C2 IR**) was observed by CD.

CD is a technique that is highly sensitive to any small change in the structure of the DNA.[1] It is well known that when Pt(II) compounds bind to DNA they can provoke structural changes in the nucleic acid, impairing the replication of the cells, thus acting as cytotoxic agents. CD is widely used to study the interaction between metal-complexes and DNA.[2–5] DNA presents two bands in the CD spectra at the UV range, base stacking causes a positive band at 275 nm, and one negative band at 245 nm caused by the right-handed helicity of β-DNA.[6]

In this case, to see if the Pt(II) products can interact and perturb the DNA strands, replicates of a 50 μM *ct*-DNA solution were incubated with each of the complexes at different molar ratio (r = 0 to 2) along 24 h at 37 °C (**Figure 5.1**)
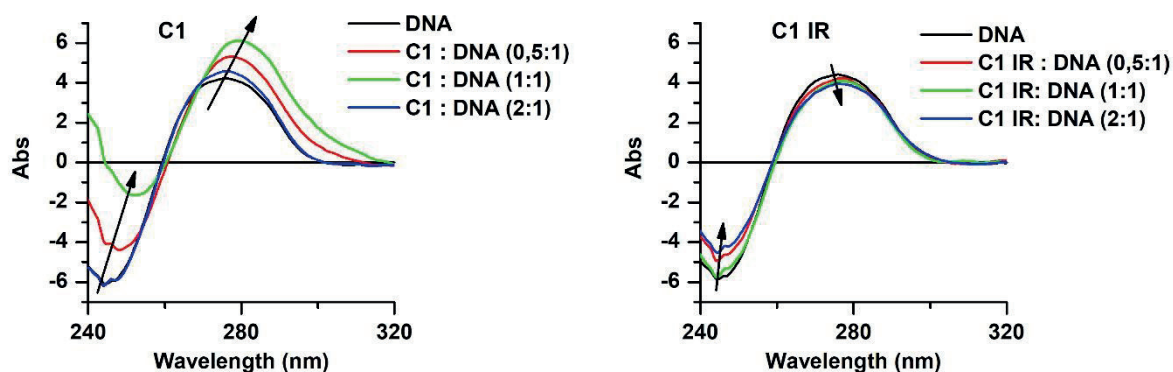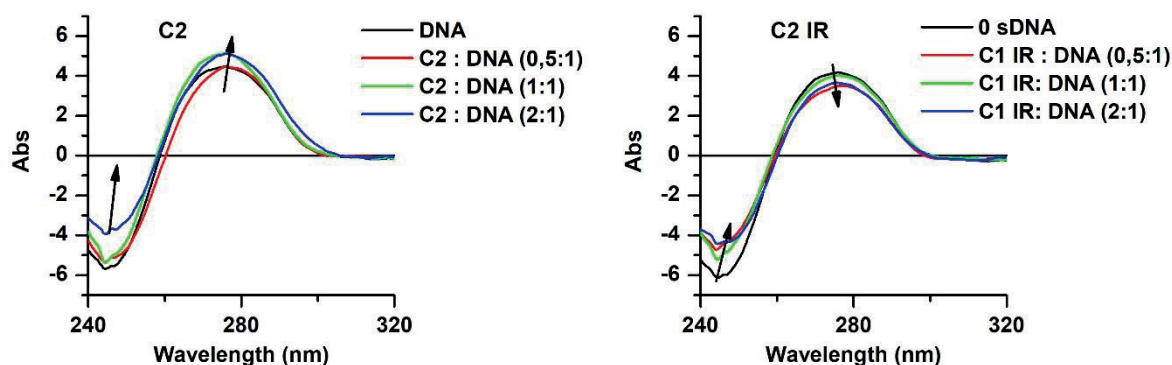
Figure 5.1: CD spectra recorded for the interaction of **C1, C1 IR, C2** and **C2 IR** at 50 µM of *ct*-DNA and at 0.5:1, 1:1 and 2:1 (DNA:Complex) ratios in Tris·HCl at pH 7.2, incubated at 37 °C for 24 h

The CD data recorded shown slight interactions between the *ct*-DNA and each complex. For the non-irradiated Pt(II)-complexes, **C1** and **C2** there is an increase in both, the positive and negative band, which it is worth noting that **C1** present a large bathochromic shift. On the other hand, the spectra of the photoproducts also show an increase and a bathochromic shift of the band at 245 nm, but the band at 275 nm decreases with a bathochromic shift for each case. These results indicate that the Pt(II)-complexes before and after irradiation bound to DNA destabilise the base stacking, even if each compound does it differently.

5.2 Electronic absorption spectral study

Similarly, to the previous experiments, the interaction of the complexes with *ct*-DNA was observed by UV-Vis spectroscopy. Unlike those previous CD experiments, in this study the concentration of the Pt(II)-complexes was constant, while DNA concentration was increasing.

These experiments provide a better understanding of the reactivity between DNA and the compound. The addition of DNA to the drug solution allows the interaction between the DNA and the compound to be evaluated. On the one hand, I f the reaction is highly selective and specific or poorly reactive, the signals associated with the complex would gradually decrease with each addition of DNA. On the other hand, if the reaction is non-specific, fast, and strong, the signal of the complex would disappear from the first addition. In either case, the binding constant can be estimated.[7–9]

The absorbance of each compound alone was recorded at 50 µM and as *ct*-DNA (0 – 100 µM) was added, the changes in absorbances were monitored (**Figure 5.2**)
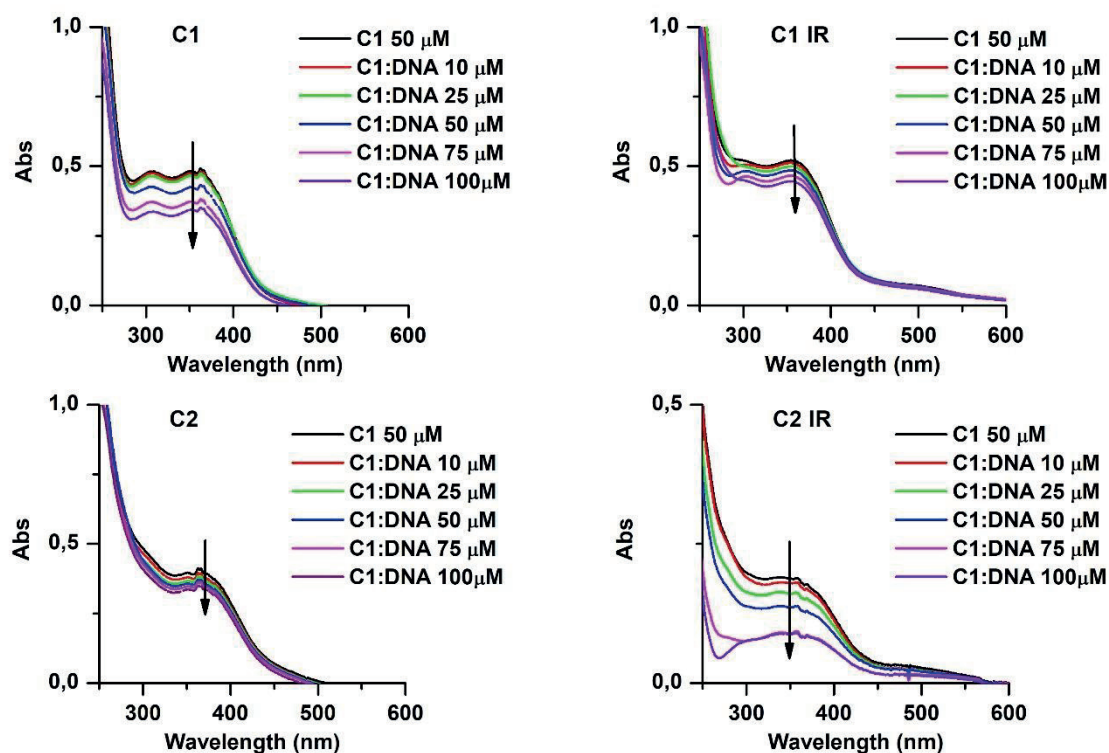
Figure 5.2: UV-Vis spectra of **C1, C1 IR, C2** and **C2 IR** at 50 µM treated with *ct*-DNA from 0-100 µM in Tris-HCl buffer at pH 7.2. Each spectrum was recorded after 10 minutes of stabilization time.

For each compound there an hypochromic effect was observed as the concentration of *ct*-DNA increased. Usually, the hypochromic effect is accompanied by a bathochromic effect. When there is a strong intercalation between metal complex and DNA, it can lead to an energetic decrease of π-π* as the π orbitals of the ligands can intercalate with π orbitals of the DNA base pairs.[10] However, in neither of these cases a these band shifts were observed, this means that the interaction between the metal complex and the DNA is weak and gives rise to electrostatic interaction or groove binding interaction.[11,12]

Changes in UV spectra revealed specific for each compound. While for **C1 IR** and **C2** the variation revealed soft, with a gradual decrease of the signal, for **C1** and **C2 IR** the variations were sharper.

Then, using plots of the Benesi-Hildebrand host-guest equation (**Equation 1**), the intrinsic binding constant (K_b) was calculated, where the value of the constant reflects the strength of the interaction between each compound and DNA. High values are normally reflecting strong intercalation in the DNA bases, while low K_b value denote poor intercalating capacity of the complex.

$$\frac{A_0}{A-A_0} = \frac{\varepsilon_G}{\varepsilon_{H-G}-\varepsilon_G} + \frac{1}{k_b[DNA]}$$

Equation 1: Benesi-Hildebrand host-guest equation

A_0 is the absorbance of the metal complex in the absence of DNA, A is the absorbance at any given DNA concentration, and ε_G and ε_{H-G} are the molar extinction coefficients of the complex and the complex-DNA respectively.[11,13] In this case, it is not necessary to know the values ε_G and ε_{H-G}.

K_b can be determined for each compound by the variation of absorbance ($A_0/(A-A_0)$) *vs* the inverse of the DNA concentration ($1/[DNA]$), when plotting both magnitudes, the slope obtained can be used to calculate the value of the constant (**Table 5.1**)

Table 5.1: K_b values and the % hypochromic effect obtained for the interaction of *ct*-DNA and with each Pt(II)-complex preparation: **C1**, **C1 IR**, **C2** and **C2 IR**. K_b was calculated from the ratio of the intercept to the slope, according to the Benesi-Hildebrand equation (**Equation 1**) after the fitting of the UV-Vis data from **Figure 5.2**

Complex	K_b (M^{-1})	log K_b	% hypochromic effect (λ in nm)
C1	2.4×10^3	3.38	29 % (358 nm)
C1 IR	1.8×10^3	3.25	14 % (354 nm)
C2	5.6×10^3	3.75	15 % (363 nm)
C2 IR	4.0×10^3	3.60	52 % (348 nm)

The range of K_b values obtained is between 1×10^3 to 6×10^3 M^{-1} resulting in a binding affinity of moderate strength, when compared to K_b of classical intercalators such as ethidium ($K_b = 7 \times 10^7$ M^{-1})[14] and proflavine ($K_b = 4.1 \times 10^5$ M^{-1})[15], which are 2-4 orders of magnitude higher. On the other hand, if it is compared to the oxaliplatin drug (4.12×10^4 M^{-1}), there is only one order of magnitude difference.[16]

These results confirm that the interaction with DNA takes place in most of the cases studied, but the metallic complex must act more as DNA bonding by means of covalent interaction than intercalator.

5.3. Cytotoxicity assays A375 cancer cell line

All these studies done with the A375 cancer cell line have been possible thanks to the collaboration with Dr. Helena Oliveira from the Cell Culture and Cyto/Genotoxicity Lab (3C's Lab) group of the Biology and CESAM Department at the University of Aveiro.

A375 is a cancer cell line that comes from 54 years old female with malignant melanoma. Melanoma is the most serious skin cancer; it comes from the transformation of the melanocytes and has a high probability of spreading and producing metastases.[17] Since 1970, there have been more and more new cases of this type of cancer year and the mortality rate has increased, according to the World Health Organization (WHO) in 2020 there were about 325000 new cases of melanoma cancer Worldwide, of which 57000 died.[18] The main cause of melanoma cancer is UV radiation from the sun, together with skin type and genetics.[19] Many treatments have been applied to avoid this dispersion such as surgery, chemotherapy, PDT, immunotherapy, radiotherapy and other form of targeted, but no treatment has been sufficiently effective.[20]

In order to have a clear idea about the toxicity of each compound (ligands, complexes and platforms), the assays were carried out for each individual component, without (in the dark) and with irradiation at the corresponding wavelength.

5.3.1 Cytotoxicity evaluation of L1, L2, C1, C2

First, the cytotoxicity of ligands (**L1**, **L2**), and the corresponding Pt(II) complexes (**C1**, **C2**) was studied.

As none of the compounds are soluble in culture media, they had to be diluted with DMF beforehand. Therefore, a previous study had to be done to determine the % of DMF that A375 cell cultures can tolerate. The cells were exposed to different % of DMF in the usual culture medium and the cell viability was determined by MTT assays (**Figure 5.3**).
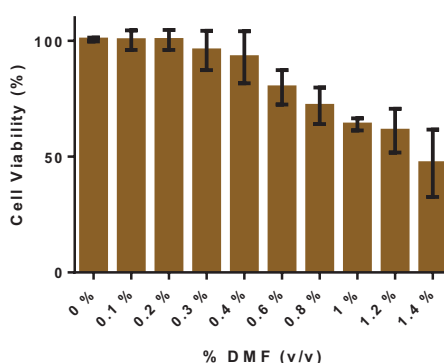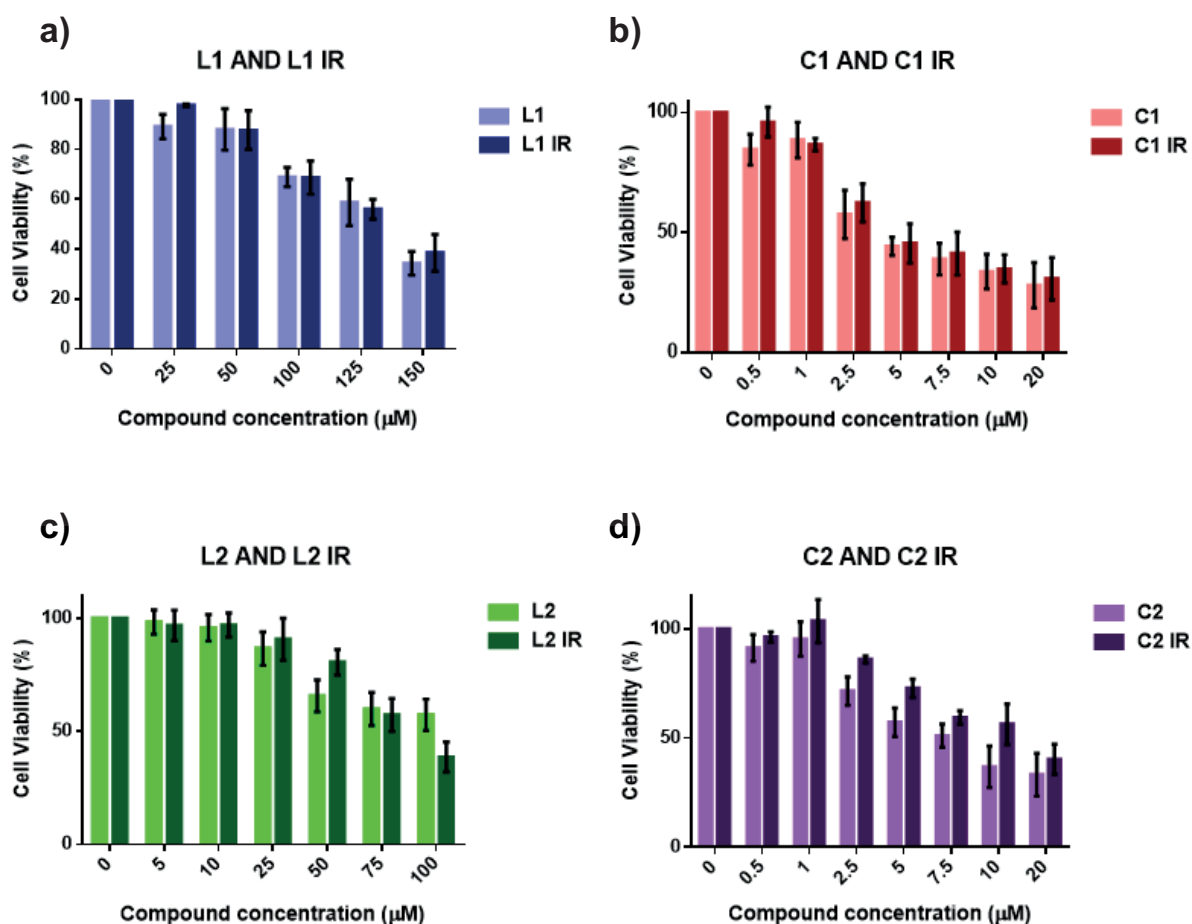

Figure 5.3: Effect of DMF on the viability of A375 cells. Cell viability was determined after 24 h of post-incubation at 37 °C, using MTT for the quantification with 3 independent experiments for triplicate.

As expected, cell viability decreased as DMF concentration increased. Consequently, ~~only~~ 0.4 %(v/v) DMF was determined as the maximum amount of DMF to be used in further assays.

Knowing the maximum % of DMF that can be used, a study was made to compare the cytotoxicity of ligands and Pt(II)-complexes and their respective photoproducts after irradiation at 365 nm.

To carry out the experiments, for each compound, a stock solution of known concentration in DMF was prepared and then divided into two equal volumes: one used as it was prepared, and the other was irradiated at 365 nm. Thus, compounds and mixture of photoproducts were obtained in the same conditions.

The effect of **L1**, **L2**, **C1**, **C2** and the respective photoproducts (**L1 IR**, **L2 IR**, **C1 IR**, **C2 IR**) in cell viability was evaluated in front the A375 cancer cell line after 24 h of exposure by MTT assay (**Figure 5.4**). IC_{50} values were also determined (**Table 5.2**).

Figure 5.4: Effect of a) **L1** and **L1 IR** b) **C1** and **C1 IR** c) **L2** and **L2 IR** d) **C2** and **C2 IR** on the cell viability of A375 cell line. Cells were exposed to different concentration of each compound for 24 hours and cell viability was determined using MTT assays with 3 independent experiments for triplicate.

Table 5.2: Calculated IC_{50} values for **L1**, **L1 IR**, **L2**, **L2 IR**, **C1**, **C1 IR**, **C2** and **C2 IR** in front of A375 after 24 hours of incubation.

| Entire	Compound	IC_{50} (µM)
1	L1	130 ± 1.0
	L1 IR	131 ± 1.0
2	L2	111 ± 1.1
	L2 IR	84.6 ± 1.5
3	C1	4.7 ± 1.1
	C1 IR	5.3 ± 1.1
4	C2	4.1 ± 1.1
	C2 IR	6.2 ± 1.4

Fortunately, the IC_{50} values obtained clearly show that the complexes are more cytotoxic than the corresponding ligands. In the case of **C1** and **C1 IR** exhibit half maximal inhibitory concentration (IC_{50}) around 5 µM, while both **L1** and **L1 IR** have an IC_{50} of approximately 130 µM, about 26 times higher. On the other hand, **L2** and **L2 IR** which have an IC_{50} around 100 µM is 20 times higher than **C2** and **C2 IR** which has an IC_{50} of about 5 µM. From these results it can be concluded that cytotoxicity of the Pt(II) complexes is far higher than those related to the ligands. The values obtained in the case of the complexes, before and after irradiation, if considering the errors associated, are significantly the same values, which indicates that irradiation is not altering the cytotoxicity of the compounds.

An important point to note after considering the cell viability graphs of the ligands is that **L2** and **L2 IR** are more cytotoxic than **L1** and **L1 IR**, this means that the methyl group in the benzyl position provides higher cytotoxicity to the ligand. This is not reflected in the complexes, at least from the toxicological point of view.

The results just discussed have shown that the mixture of photoproducts obtained when the Pt(II)-complexes are irradiated with UV light exhibit cytotoxicity at low concentrations. The next step was to study the cytotoxicity of both **C1** and **C2** platforms under the same conditions assayed.

5.3.2 Evaluation of C1/UCNPs/mPEG-ODA and C2/UCNPs/mPEG-ODA

The cytotoxicity of both platforms synthesised was evaluated against A375 cancer cell line in the dark, using different incubation times before washing, at 1, 2 and 4 hours at 37 °C, and measuring the cell viability after 24 h **(Figure 5.5)**. These data allow to provide an idea about the internalization of the platforms.
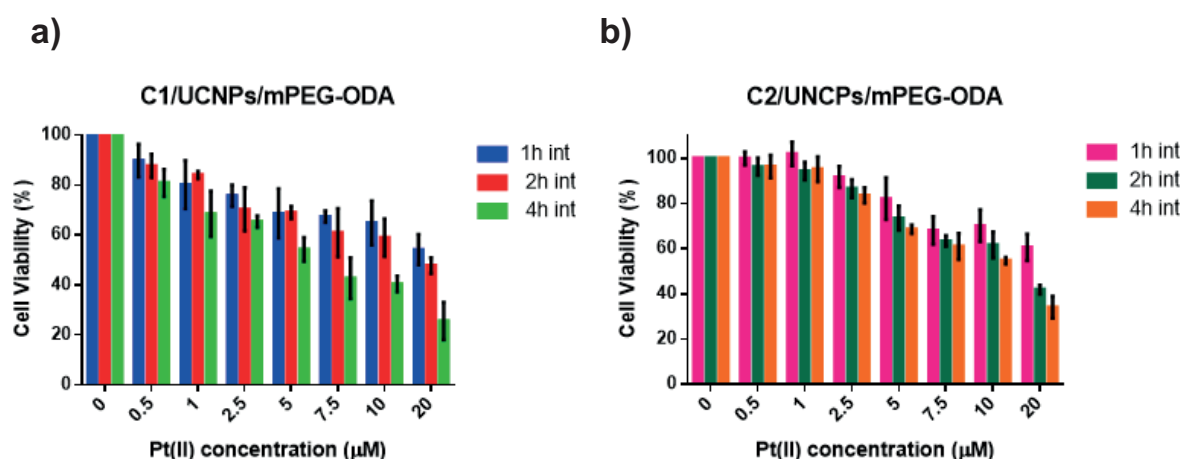
Figure 5.5: Cell viability of A375 cancer cell line in front a) **C1**/UCNPs/mPEG-ODA, and b) **C2**/UCNPs/mPEG-ODA. Cells were exposed to different concentrations of each platform with 1, 2, 4 hours of internalization, then cell culture was washed and left to incubate during 24 h. The cell viability was determined using MTT assays with 3 independent experiments with 3 technical replicates.

The cell viability data recorded show that platform **C1**/UCNPs/mPEG-ODA was a little more cytotoxic than **C2**/UCNPs/mPEG-ODA. If assuming that the differences in cytotoxicity among both platforms are mainly due to the different internalization, when considering the highest concentration assayed 20 µM, the main difference is observed after 2 h of incubation. Also, for the irradiation tests, two concentrations (0.5 and 2.5 µM for **C1**/UCNPs/mPEG-ODA and 1 and 5 µM for **C2**/UCNPs/mPEG-ODA) were selected that corresponds to IC_{10} and IC_{30} for each platform. These specific concentrations were selected because under these conditions the platforms exhibit poor cytotoxicity in absence of light and test if in the presence of light its cytotoxicity increases.

Next step was irradiation in the NIR range. A significant issue with 980 nm radiation is that water is also absorbing at this energy, what provokes heating the cell medium and causing cell death when using conventional methodologies. Therefore, it was necessary to find the best conditions of power irradiation in which the upconversion process can take place at maximum possible time without causing cell death. After extensive research, it was found that the best conditions were doing cycles of 1 min irradiation at 4.5 W/cm^2 intensity power and 2 min break.

Once the conditions were established, the definitive test was carried out. The concentrations corresponding to IC_{10} and IC_{30} (0.5 µM and 5 µM of Pt(II) for **C1**/UCNPs/mPEG-ODA and 2.5 µM and 7.5 µM of Pt(II) for **C2**/UCNPs/mPEG-ODA) were used to study the effect of each platform. Samples with the same concentration were placed on different wells, some were irradiated, and the others were kept in the dark, as a blank with the same concentrations for comparison. Cells were treated with the different concentrations of each platform for 2 h.

After this time, the medium was washed to remove the non-internalised platforms. Subsequently, each selected well was irradiated at 980 nm at 4.5 W/cm^2 with cycles of 1 min laser on and 2 min off for 1 hour, the setup employed for irradiating the cells is depicted in **Figure 5.6 a.** After 24 h, the cell viability was determined by MTT assay and compared to results obtained in the dark (**Figure 5.6 b and c**)
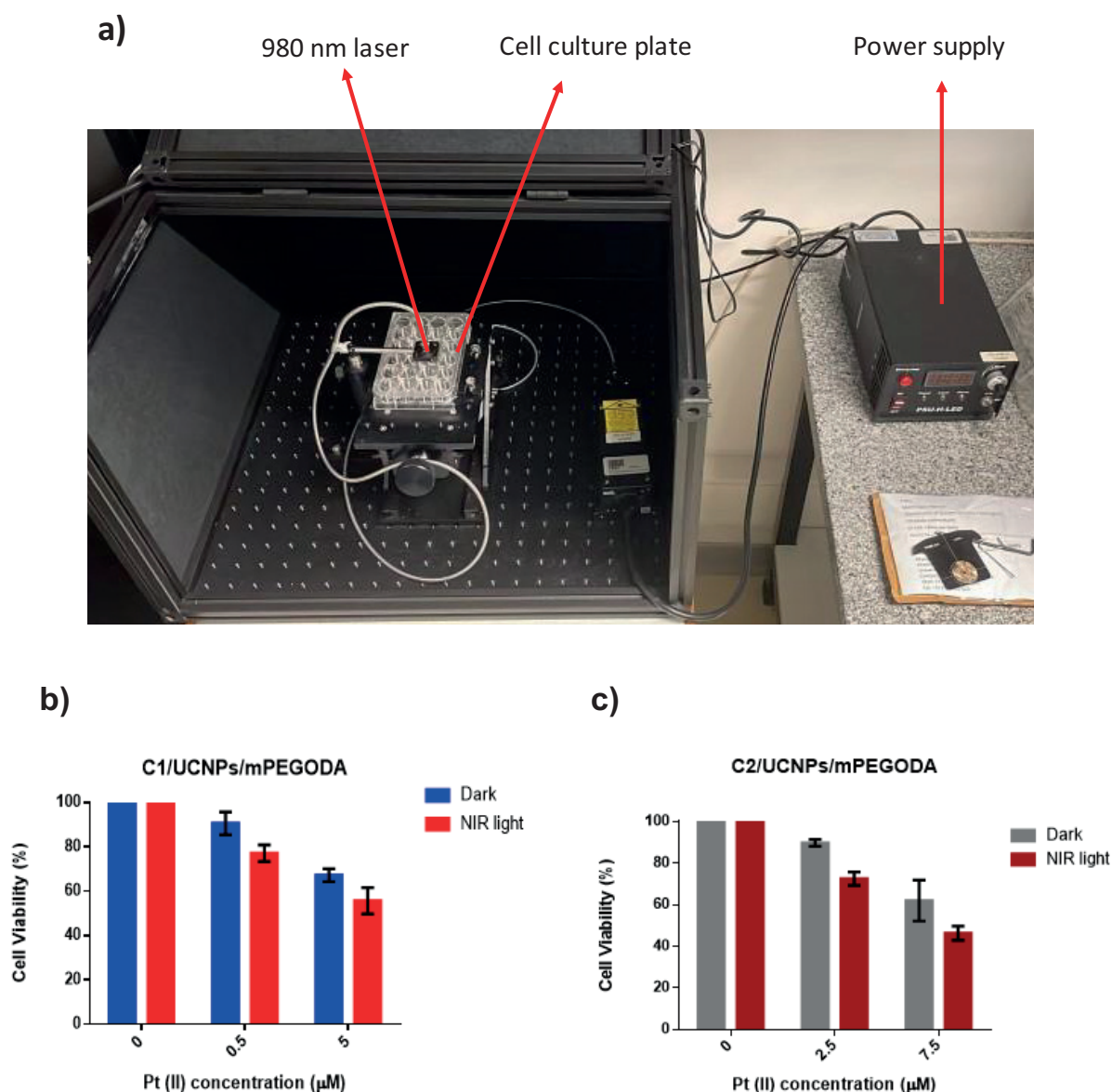
Figure 5.6: a) Setup irradiation for the cell culture plate with the 980 nm laser controlled by a power supply and cell viability plots with or without NIR light irradiation after 24 h incubation (2 h internalization) at two different concentrations in A375 cancer cell line with **b) C1**/UCNP/mPEG-ODA and **c) C2**/UCNPs/mPEG-ODA

The cell viability graphs recorded for both platforms show similar results: an increase of the toxicity as raising the concentration of Pt(II) and significant improvement of cytotoxicity after

irradiation. Also, these results confirm that the upconversion process to release Pt(II)-complex works.

Table 5.3: Cell viability for each platform assayed after 24 h of incubation (2 h of internalization) after irradiation of NIR light and in the dark, using A375 cancer cell line.

Entry	Platform	Concentration (µM)	Cell Viability (%)	
			Dark	**NIR light**
1	**C1**/UCNPs/mPEG-ODA	0.5	91 ± 5,1	77 ± 3,8
2		5	67 ± 2,9	56 ± 5,9
3	**C2**/UCNPs/mPEG-ODA	2.5	80 ± 1,6	73 ± 3,3
4		7.5	62 ± 9,8	46 ± 3,2

The cell viability calculated at the different concentrations assayed (**Table 5.3**) show that in the case of **C1**/UCNPs/mPEG-ODA, the difference in the presence of light or in the dark for each concentration was smaller than **C2**/UCNPs/mPEG-ODA. If considering the similar toxicity observed for both complexes before and after irradiation, these slight differences can be explained by the different internalization.

To our knowledge, this is the first work presenting the control of the activity of Pt(II)-complexes by transforming deeply penetrating NIR light into UV light through UCNPs as nanotransducers. When **C1**/UCNPs/mPEG-ODA and **C2**/UCNPs/mPEG-ODA were exposed to 980 nm radiation showed increased their inhibitor efficiency. Although the values obtained are, for the moment, restrained, the results presented here represent a very promising first step in the future development of anticancer systems activated by UCNPs.

5.4 Cytotoxicity assays with HCT-116 cancer cell line

To further explore the cytotoxicity of the Pt(II) compounds here studied, another cancer cell line was included in the assessment plan: HCT-116. This is a colon cancer cell line, which is usually treated with Pt(II) compounds, among others. Colon cancer is the second most common cancer diagnosed worldwide, this cancer is found from the beginning of the large intestine to the end of the digestive system.[21,22] Among all cancerous tumours, colon cancer has one of the highest death rates.[23] According to the Global Cancer Observatory in 2020, there were 1.15 million new cases of colon cancer, and 0.57 million deaths from this cancer. It is predicted that those numbers will rise, and by 2040 it is estimated to increase to 1.82 million new cases causing and increasing the number of deaths to 0.99 million.[24] Oxaliplatin alone or in combination with other anticancer drugs such as fluorouracil or leucovorin has shown good results against colon cancer, although it is not 100% effective.[25–28]

All the cytotoxicity studies done with the HCT-116 cancer cell line have been possible thanks to the collaboration with Dr. Julia Lorenzo and Dr. David Montpeyó from the Protein Engineering and Nanomedicine Group of the *Institut de Biotecnologia i de Biomedicina* (IBB) at the UAB.

5.4.1 Cytotoxicity evaluation of L1, L2, C1, C2

The first step was studying the cytotoxicity of the ligands and the corresponding Pt(II) complexes, before and after irradiation **L1**, **L1 IR**, **L2**, **L2 IR**, **C1**, **C1 IR**, **C2**, **C2 IR** (**Figure 5.7**)
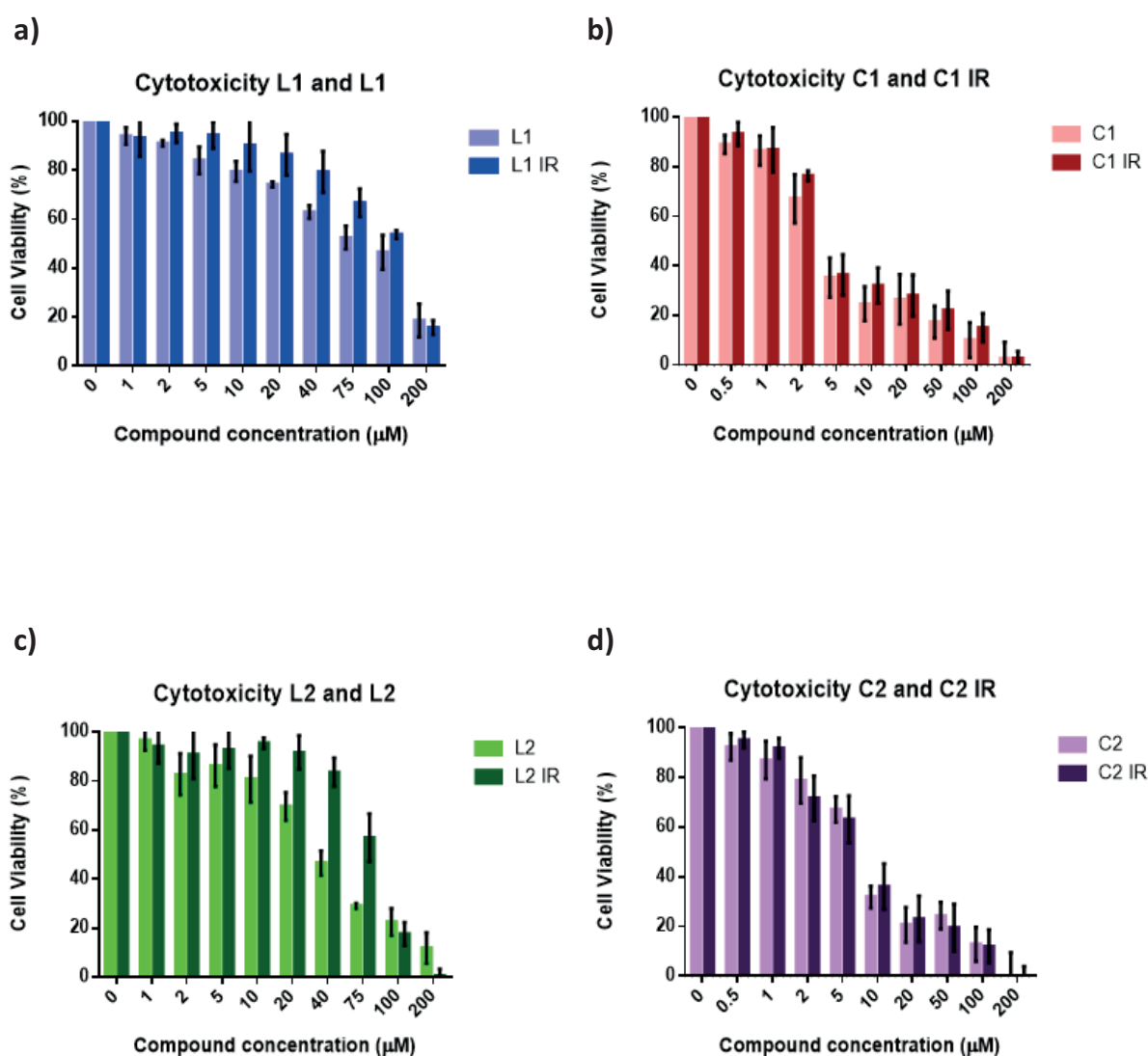
Figure 5.7 Effect of a) **L1** and **L1 IR** b) **C1** and **C1 IR** c) **L2** and **L2 IR** d) **C2** and **C2 IR** on the cell viability of HCT-116. Viability of HCT-116 were evaluated after 24 h and was determined using Presto Blue assays with 3 independent experiments for triplicate.

Table 5.4: IC$_{50}$ calculated for **L1**, **L1 IR**, **L2**, **L2 IR**, **C1**, **C1 IR**, **C2** and **C2 IR** in front of HCT-116 cell line after 24 hours.

Entire	Compound	IC$_{50}$ (µM)
1	L1	67 ± 1.1
	L1 IR	99 ± 1.1
2	L2	34 ± 1.1
	L2 IR	74 ± 1.1
3	C1	4.1 ± 1.1
	C1 IR	5.5 ± 1.1
4	C2	7.1 ± 1.1
	C2 IR	6.9 ± 1.1

As can be seen in the cytotoxicity graphs (**Figure 5.7**) and the corresponding IC$_{50}$ calculated values (**Table 5.4**) for each compound, similar behaviour as that observed in the A375 cell line is observed.

In the case of the ligands, **L2** and **L2 IR (**that contain the methyl group in the benzyl position) show higher cytotoxicity than **L1** and **L1 IR**. In contrast, with the Pt(II)-complexes, **C1** and **C1 IR** exhibit slightly lower IC$_{50}$ than **C2** and **C2 IR**.

5.4.2 Evaluation of C1/UCNPs/mPEG-ODA and C2/UCNPs/mPEG-ODA

The next step was the cytotoxicity against HCT-116 cancer cell line of the two platforms used in this work (**C1**/UCNPs/mPEG-ODA and **C2**/UCNPs/mPEG-ODA). First, a study was done in the dark to find the best concentration conditions for NIR exposure (**Figure 5.8**).
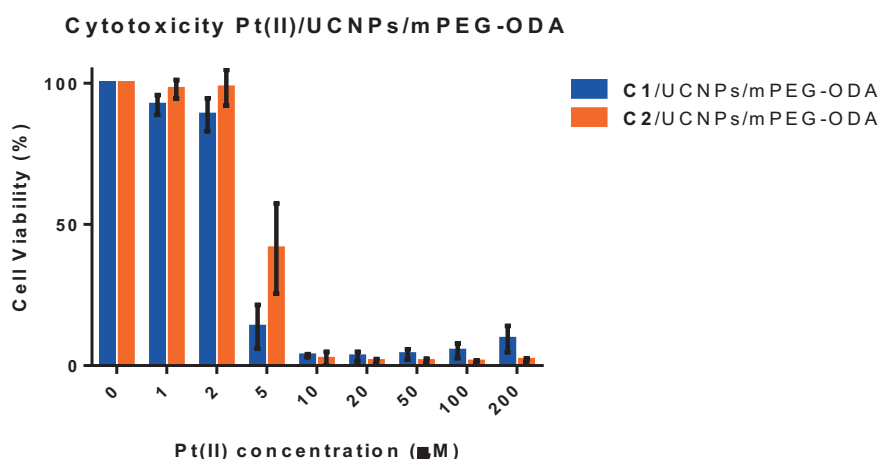
Figure 5.8: Effect of **C1/UCNPs/mPEG-ODA** and **C2/UCNPs/mPEG-ODA** on the cell viability of HCT-116. Viability of HCT-116 was evaluated after 24 h and was determined using Presto Blue assays with 3 independent experiments for triplicate.

As shown in **Figure 5.8** at low platform concentrations ~~of~~ the cell viability is very low. IC_{50} are shown in **Table 5.5**

Table 5.5: IC_{50} for **C1**/UCNPs/mPEG-ODA and **C2**/UCNPs/mPEG-ODA against HCT-116 cells after 24 hours.

Entire	Platform	IC_{50} (µM)
1	**C1**/UCNPs/mPEG-ODA	3.2 ± 1.1
2	**C2**/UCNPs/mPEG-ODA	4.7 ± 1.0

As both platforms exhibited high cytotoxicity, the next step will involve reducing the internalisation time, for example, by 2 hours as was done with A375, to enable work with higher concentrations.

Due to time limitations, in this thesis, it was not possible to evaluate the effect of irradiation under NIR for HCT-116 cells. The next steps should consist of determining the best conditions for irradiation with NIR light, as well as finding the necessary internalization time, the highest possible concentrations to work with, the optimal irradiation time, the power, and the number of irradiation cycles.

5.5. General remarks and future perspectives of chapter 5

In this chapter a study of the activity of the compounds and platforms previously synthesised was carried out. First, the interaction with DNA of the Pt(II)-complexes and their respective photoproducts was followed by CD and UV-Vis spectroscopy. The results obtained by CD reveal when the photosensitive Pt(II) complexes are bounded to DNA, they destabilise the base stacking differently before and after irradiated with UV light. On the other hand, UV studies revealed that these interactions are non-covalent, giving rise to electrostatic interaction or groove binding interaction.

Cytotoxic studies were performed with two different cancer cell lines: A375 (malignant melanoma) and HCT-116 (colon cancer).

In both cancer cell lines, the Pt(II)-complexes before and after irradiation are more cytotoxic than the respective ligands and their photoproducts, leading to the conclusion that Pt(II) plays an important role in preventing cell division.

The platforms **C1**/UCNPs/mPEG-ODA and **C2**/UCNPs/mPEG-ODA were assessed against the A375 cancer cell line. After screening different settings, the best irradition conditions with NIR light were an internalization for two hours and then irradiation at 980 nm with cycles of 1 min of irradiation and 2 min break for 1 hour at 4.5 W/cm^2. Under these conditions, there was a decrease in the cell viability for each platform irradiating with NIR light with a significant difference compared to that in the dark. These results demonstrate an alternative way of activating UV-photoresponsive Pt(II) complexes under NIR light by means of an upconversion process. In addition, the mPEG-ODA coating provides a solution to the common issue for Pt(II) species of low solubility in water.

Besides, these two platforms are still being studied with HCT-116 cancer cell line. Investigations of the best conditions to activate the platforms with NIR light is underway and it is expected that with NIR light exposure, cell viability will be lower compared to dark conditions.

5.6. References

1. Ivanov, V. I.; Minchenkova, L. E., Schyolkina, A. K. & Poletayev, A. I. Different Conformations of Double-Stranded Nucleic Acid in Solution as Revealed by Circular Dichroism *Biopolymers* **1973**, *12*, 89-110 https://doi.org/10.1002/bip.1973.360120109

2. Naing, K.; Takahashi, M.; Taniguchi, M. & Yamagishi, A. Interactions of Enantiomeric Ruthenium(II) Complexes with Polynucleotides As Studied by Circular Dichroism, Electric Dichroism Measurements, and Photolysis *Inorg. Chem.* **1995**, *34*, 350-356 https://doi.org/10.1021/ic00105a054

3. Figueroa-DePaz, Y.; Resendiz-Acevedo, K.; Dávila-Manzanilla, S. G.; García-Ramos, J. C.; Ortiz-Frade, L.; Serment-Guerrero, J. & Ruiz-Azuara, L. DNA, a target of mixed chelate-copper (II) compounds (Casiopeina®) studied by electrophoresis, UV-Vis circular dichroism techniques *Journal of Inorganic Biochemistry* **2022**, *231*, 111772 https://doi-org.are.uab.cat/10.1016/j.jinorgbio.2022.111772

4. Polyanichko, A. M.; Andrushchenko, V. V.; Chikhirzhina, E. V.; Vorob'ev, V. I. & Wieser, H. The effect of managanese(II) on DNA structure: electronic and vibrational circular dichroism studies *Nucleic Acids Research* **2004**, *32*, 989-996 https://doi.org/10.1093%2Fnar%2Fgkh242

5. Tamburro, A. M.; Celotti, L.; Furlan, D. & Guantieri,V. Interaction of Pt(II) complexes with DNAs from various sources. A circular dichroism study *Chem. Biol. Interactions* **1977**, *16*, 1-11 https://doi.org/10.1016/0009-2797(77)90149-1

6. Veeralakshmi, S.; Nehru, S.; Sabapathi, G.; Arunachalam, S.; Venuvanalingam, P.; Kumar, P.; Anusha, C. & Ravikumar, V. Single and double chain surfactant-cobalt(III) complexes: the impact of hydrophobic on the interactions with calf thymus DNA, and their biological activities *RSC Adv.* **2015**, *5*, 31746-31758 https://doi.org/10.1039/C5RA02763B

7. Shahabadi, N. & Heidari, L. Synthesis, characterization and multi-spectroscopic DNA interaction studies of a new platinum complex containing the drug metformim *Spectrochimica Acta Part A: Molecular and Biomolecular Spectroscopy* **2014**, *128*, 377-385 https://doi.org/10.1016/j.saa.2014.02.167

8. Shahabadi, N.; Kalar, Z. M. & Moghadam, N. H. DNA interaction studies of platinum (II) complex containing an antiviral drug, ribavirin: The effect of metal on DNA binding *Spectrochimica Acta Part A: Molecular and Biomolecular Spectroscopy* **2012**, *96*, 723-728 https://doi.org/10.1016/j.saa.2012.07.020

9. Li, Q.; Yang, P.; Wang, H. & Guo, M. Diorganotin(IV) Antitumor Agent. $(C_2H_5)_2SnCl_2(Phen)$/ Nucleotides Aqueous and Solid-State Coordination Chemistry and its DNA Binding Studies *Journal of Inorganic Biochemistry*, **1996**, *64*, 181-195 https://doi-org/10.1016/0162-0134(96)00039-6

10. Rajesh, J.; Kesavan, M. P.; Ayyanaar, S.; Karthikeyan, K.; Rjagopal, G. & Athappan, P. DNA interaction and cleavage studies of ancillary chiral ligand and N,N-donor ligands coordinated platinum(II) complexes *Appl. Organometal. Chem.* **2017**, *31*, e3868 https://doi.org/10.1002/aoc.3868

11. Peña, Q.; Lorenzo, J.; Sciortiono, G.; Rodríguez-Calado, S.; Maréchal, J.; Bayón, P.; Simaan, A. J.; Iranzo, O.; Capdevila, M.; Palacios, O. Studying the reactivity of "old" Cu(II) complexes for "novel" anticancer purpose *Journal of Inorganic Biochemistry* **2019**, *195*, 51-60 https://doi-org/10.1016/j.jinorgbio.2019.03.011

12. Sankarganesh, M.; Jose, P. R. A.; Raja, J. D.; Solomon, R. V.; Sheela, C. D. & Gurusamy, S. Bioactive Platinum complex of ligand bearing pyrimidine skeleton: DNA/BSA binding, molecular docking, anticancer, antioxidant and antimicrobial activities *Journal of Biomolecular structure and dynamics* **2020**, *40*, 6683-6696 https://doi.org/10.1080/07391102.2021.1889667

13. Querino, A. L.; Enes, K. B.; Chaves, O. A.; Ditzz, D.; Couri, M. R. C.; Diniz, R. & Silva, H. Modified pyrazole platinum(II) complex can circumvent albumin and glutathione: Synthesis, structure and cytotoxic activity *Bioorganic Chemistry* **2020**, *100*, 103936 https://doi.org/10.1016/j.bioorg.2020.103936

14. Waring, M. J. Complex formation between Ethidium Bromide and Nucleic Acids *J. Mol. Biol.* **1965**, *13*, 269-282 https://doi-org.are.uab.cat/10.1016/S0022-2836(65)80096-1

15. Shahabadi, N.; Mohammadi, S. & Alizadeh, R. DNA Interaction Studies of a New Platinum(II) Complex Containing Different Aromatic Dinitrogen Ligands *Bioinorganic Chemistry and Applications* **2011**, *2011*, 492241 https://doi.org/10.1155/2011/429241

16. Ray, B.; Gupta, B. & Mehrotra, R. Binding of Platinum Derivative, Oxaliplatin to Deoxyribonucleic Acid: Structural Insight into Antitumor Action *Journal of Biomolecular Structure and Dynamics* **2019**, *37*, 3838-3847 https://doi.org/10.1080/07391102.2018.1531059

17. Houghton, A. N. & Polsky, D. Focus on melanoma *Cancer Cell* **2002**, *2*, 275-278 https://doi.org/10.1016/s1535-6108(02)00161-7

18. WHO (World Health Organization), https://gco.iarc.fr/today/fact-sheets-cancers [Accessed March 2023]

19. De Vries, E. & Coebergh, J. W. Cutaneous malignant melanoma in Europe *European Journal of Cancer* **2004**, *40*, 2355-2366

20. Domingues, B.; Lopes, J. M.; Soares, P. & Pópulo, H. Melanoma treatment in review *ImmunoTargets and Therapy* **2018**, *7*, 35-49 https://doi.org/10.2147/ITT.S134842

21. GBD 2016 Disease and Injury Incidence and Prevalence Collaborators. Global, regional, and national incidence, prevalence, and years lived with disability for 328 diseases and injuries for 195 countries, 1990-2016: a systematic analysis for the Global Burden of Disease Study 2016 *Lancet* **2017**, *390*, 1211-1259 https://doi.org/10.1016/s0140-6736(17)32154-2

22. Makhdoomi, R. H.; ul Khurshid, S.; Shah, B.M.; Pathology in Colorectal Maligancy. In New treatment Modalities in Rectal Cancer; *Springer* **2020**, 76-96, Berlin/Heidelberg, Germany

23. El-Hazek, R. M. M.; Zaher, N. H.; Emam, H. E. S.; El-Gazzar, M. G. & Khalil, A. Pyrazole-Sulfonamide scaffold featuring dual-tail strategy as apoptosis inducers in colon cancer *Scientific Reports* **2023**, *13*, 5782 https://doi.org/10.1038/s41598-023-32820-0

24. World Health Organization-Global Cancer Observatory https://gco.iarc.fr [Accessed July 2023]

25. De Gramont, A.; Figer, A.; Seymour, M.; Homerin, M.; Hmissi, A.; Cassidy, J.; Boni, C.; Cortes-Funes, H.; Cervantes, A.; Freyer, G. Papamichael, D.; Le Bail, N.; Louvet, C.; Hendler, D.; de Braud, F.; Wilson, C.; Morvan, F. & Bonetti, A. Leucovorin and Fluorouracil with or without oxaliplatin as First-Line Treatment in Advanced Colorectal Cancer *Journal of Clinical Oncology* **2000**, *18*, 2938-2947 https://doi.org/10.1200/jco.2000.18.16.2938

26. Giacchetti, S.; Perpoint, B.; Zidani, R.; Le Bail, N.; Focan, F. C.; Chollet, P.; Llory, J. F.; Letourneau, Y.; Coudert, B.; Bertheaut-Cvitkovic, F.; Larregain-Fournier, D.; Le Rol, A.; Walter, S.; Adam, R.; Misset, J. L. & Lévi, F. Phase III Multicentre Randomized Trial of Oxaliplatin Added to Chronomodulated Fluorouracil-Leucovorin as First-Line Treatment of Metastatic Colorectal Cancer *Journal of Clinical Oncology* **2000**, *18*, 136-147 https://doi.org/10.1200/jco.2000.18.1.136

27. Goldberg, R. M.; Sargent, D. J.; Morton, R. F.; Fuchs, C. S.; Ramanthan, R. K.; Williamson, S. K.; Findlay, B. P.; Pitot, H. C. & Alberts, S. R. A Randomized Controlled Trial of Fluorouracil Plus Leucovorin, Inrinotecan, and Oxaliplatin Combinations in Patients With Previously Untreated Metastatic Colorectal Cancer *Journal of Clinical Oncology* **2004**, *22*, 23-30 https://doi.org/10.1200/jco.2004.09.046

28. André, T.; Boni, C.; Mounedji-Boudiaf, L.; Navarro, M.; Tobernero, J.; Hickish, T.; Topham, C.; Zaninelli, M.; Clingan, P.; Bridgewater, J.; Tabah-Fisch, I. & de Gramont, A. Oxaliplatin, Fluorouracil, and Leucovorin as Adjuvant Treatment for Colon Cancer *N. Eng. J. Med.* **2004**, *350*, 2343-2351 https://doi.org/10.1056/nejmoa032709
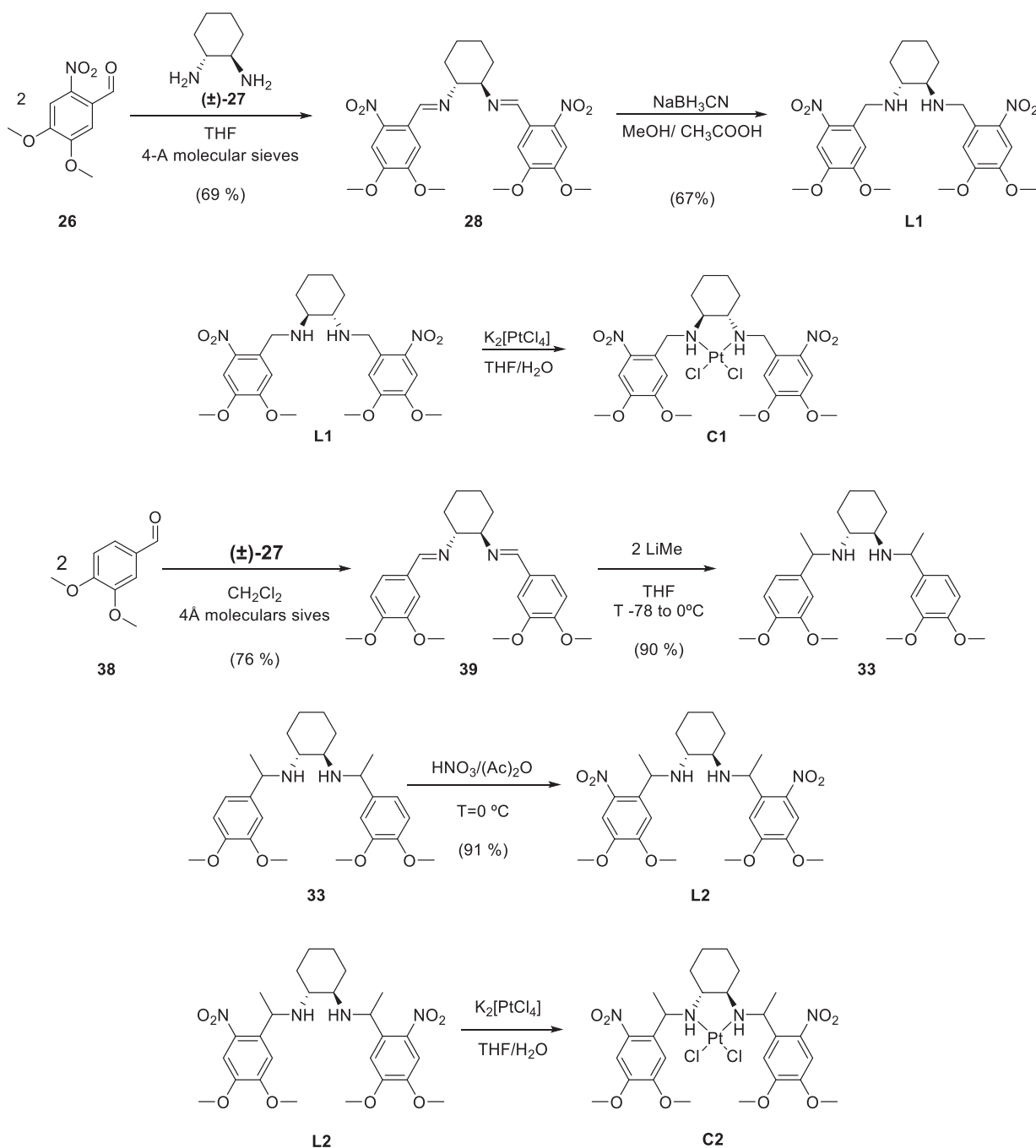
CHAPTER 6

SUMMARY AND CONCLUSIONS

6. Summary and Conclusions

In this thesis, two new ligands containing two 4,5-dimethoxy-2-nitrobenzyl groups as photocage, bonded to 1,2-diaminocyclohexane (**L1**, **L2**), and their corresponding Pt(II)-complexes (**C1**, **C2)** were synthesised and characterised, the difference between them being a methyl group in the benzyl position (**Scheme 6.1**).


**Scheme 6.1:** The two ligands and their corresponding Pt(II)-complexes synthesised in this thesis

The photochemical properties of both ligands and Pt(II)-complexes have been studied, they have been shown to photodegrade in both UV and visible light.

Photoproducts derived from both ligands and complexes have been characterized and their structure and formation mechanisms have been discussed (**Scheme 6.2**).

a)
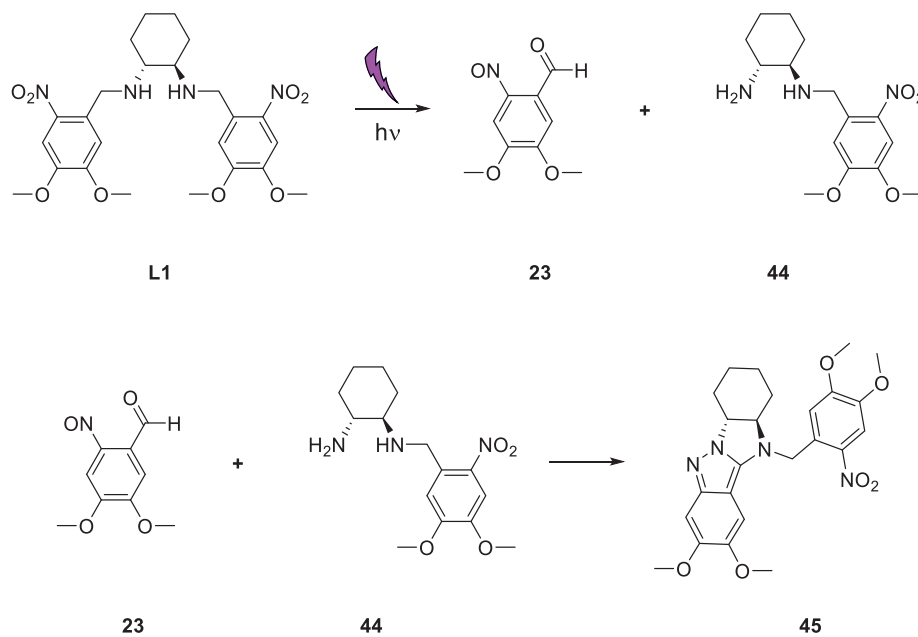
b)
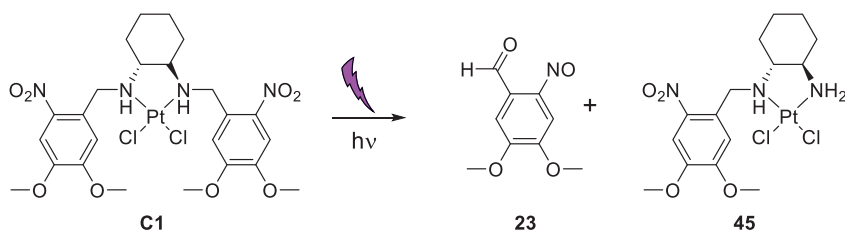
c)
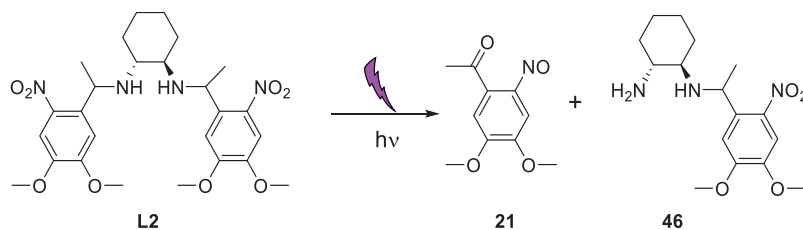
d)
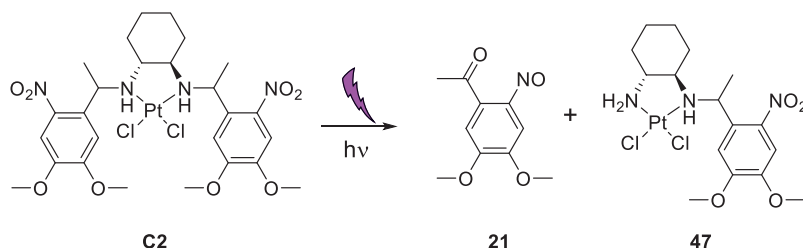
Scheme 6.2: Photodegradation of a) **L1,** b) **C1**, c) **L2** and d) **C2** irradiated with UV light.

Also, UCNPs composed by LiYF$_4$;Yb^{3+},Tm^{3+} were synthesised and characterised. Depending on the temperature ramp conditions two different morphologies were obtained: rhombohedral and spherical. Upconversion process occurred in both shapes, giving rise to more intense emission with the rhombohedrons. Furthermore, it was confirmed the overlap between the UCNPs emission and the Pt(II) absorption. This coincidence in emission and absorption values is necessary to activate the complexes with the nanoparticles efficiently.

Two new platforms were synthesised where the Pt(II)-complexes could be stabilized in mPEG-ODA coated UCNPs (**C1**/UCNPs/mPEG-ODA and **C2**/UCNPs/mPEG-ODA). Both platforms were capable to activate the Pt(II) releasing. The similarity of the release values under UV and NIR of Pt(II) for both platforms has served to corroborate the efficiency of the upconversion phenomenon.

The cytotoxicity assessment for ~~the~~ platforms **C1**/UCNPs/mPEG-ODA and **C2**/UCNPs/mPEG-ODA showed higher cell toxicity when irradiated with NIR light than in the dark. This demonstrates that these platforms could release the active form of the Pt(II)-complexes through NIR light by the upconversion process.

In summary, a series of results have been presented in this thesis that show the viability to release of Pt(II) species in a physiological medium through UCNPs. For the specific case of Pt(II), this is the first time this strategy has been used. We have been able to demonstrate that the two platforms presented display a differentiated ability to release Pt(II) among dark conditions or under NIR illumination. Although the difference observed between these releases has not been very large, we believe that the results presented here suggest great possibilities validating the strategy. For this reason, this thesis has served as an incentive to start a long project in the group where it was carried out.

CHAPTER 7

EXPERIMENTAL SECTION

7. Experimental section

7.1. General Procedures

Reagents and solvents

The commercially reagents were used without any modifications. Solvents were dried by distillation over the appropriate drying agents: CH_2Cl_2 (CaH_2), THF (Na^0). When required, the reactions were carried out following standard procedures, carefully avoiding moisture, and conducted under a nitrogen or argon atmosphere.

Physical Measurements. Instruments and experimental procedures

a) NMR spectroscopy

NMR experiments were recorded in *Servei de Ressonància Magnètica* at the UAB using BRUKER DPX-250, 300, 360, and 400 MHz instruments. Proton chemical shifts (δ) are reported in ppm with non-deuterated residual solvent as internal references ($CDCl_3$, 7.26 ppm, CD_3CN, 1.94 ppm, DMSO-d_6, 2.50 ppm, and DMF-d_7, 8.03, 2.92, 2.75 ppm). ^{13}C-NMR spectra were recorded with complete proton decoupling on DPX360 (91 MHz), and Bruker AR430 (101 MHz). Carbon chemical shifts are reported in ppm with the non-deuterated residual solvent as internal reference ($CDCl_3$ 77.16 ppm, DMSO-d_6, 39.52 ppm and DMF-d_7, 163.15, 34.89, 29.76 ppm). NMR signals were assigned with the help of COSY, HSQC and HMBC experiments. All spectra have been registered at 298 K otherwise noticed.

The abbreviations used to describe signal multiplicities are: s (singlet), d (doublet), dd (doublet doublet), t (triplet), q (quadruplet), and m (multiplet) and J to indicate the coupling constants.

b) Total quantification by ICP-OES/ICP-MS

Inductively coupled plasma mass spectrometry (ICP-MS) was performed on an Agilent apparatus, model 7500ce. Inductively coupled plasma optical emission spectrometry (ICP-OES) was carried out in a Perkin-Elmer, model Optima 4300 DV

Measurements of Pt content was performed at *Servei d'Análisi Química* in the *Universitat Autònoma de Barcelona*

c) Infrared Spectrometry

Infrared Spectra (IR) were recorded on a Bruker Tensor 27 Spectrophotometer equipped with a Golden Gate Single Refraction Diamond Attenuated Total Reflectance (ATR) accessory at *Servei d' Anàlisi Química* in the *Universitat Autònoma de Barcelona.* Peaks are reported as transmitance in cm^{-1}

d) Elemental analysis

Elemental quantification of C, H, and O were performed with a Flash EA 2000 CHNS, Thermo Fisher Scientific equipment with a TCD and a MAS 200 R autosampler for solid samples at *Servei d'Anàlisi Química* in the *Universitat Autònoma de Barcelona.*

e) ESI-MS measurements

Mass spectrometry (MS) and high-resolution mass spectrometry (HRMS) spectra were recorded in a MicroTOF-Q (Brucker Daltonics GmbH, Bremen, Germany) instrument equipped with an electrospray ionization source (ESI) in positive mode at the *Servei d' Anàlisi Qímica* in the *Universitat Autònoma de Barcelona.*

f) UV-Vis studies

All electronic spectra in the UV-Vis range were recorded on HP8453 Spectrophotometer using 1-cm thick quartz cuvettes and HPLC-quality solvents.

Non-covalent DNA-complex interactions were recorded in the same instrument. Solution of complexes **C1**, **C2**, **C1 IR**, **C2 IR** were prepared in 5 mM Tris-HCl buffer (pH 7.2), containing maximum 2 % of DMF to solubilize them. *Ct*-DNA stock solutions were prepared from its corresponding sodium salt and the concentration determined from its absorbance at 260 nm (ε = 6600 cm^{-1}). Blank and dilution effects were corrected.

g) Circular Dichroism

Circular Dichroism (CD) were recorded on a JASCO 715 spectropolarimeter. Measurements were carried out at a constant temperature of 20 °C. CD spectra were measured in 5 mM Tris-HCl buffer (pH 7.2). *Ct*-DNA concentration was 50 µM. Different samples with increasing amount of the complexes to study (25, 50, 100 µM) were incubated at 37 °C for 24 h, coating maximum of 2 % DMF to solubilize them. *Ct*-DNA stock solutions were prepared form its corresponding sodium salt (Sigma Adrich) and the concentration determined from its absorbance at 260 nm (ε = 6600 cm^{-1})

h) STEM and EDX

Scanning Transmission Electron Microscopy (STEM) and Energy Dispersive X-Ray (EDX) scan profiles were obtained with a FEI Tecnai G2 F20 coupled to an EDAX detector.

The observation was performed at room temperature at a voltage of 200 kV. The sample were prepared by dispersion and dilution with ethanol. A couple of drops were place on copper TEM grid which is coated with holey carbon. Then let the solvent evaporated

i) Emission

The emission of the UCNPs were recorded by a USB-portable spectrometer (Maya 2000 pro, Ocean Optics) coupled to an optical fiber (QP450-1-XSR, Oceans Optics) excited with a laser of 980 nm (MDL-H-980-5W)

j) Quantum Yield of UCNPs

Quantum Yield of UCNPs were measured at room temperature using a Quantaurus-QY Plus C13534 (Hamamatsu) system with a 150 W xenon lamp coupled to monochromator, an integrating sphere, and two multichannel analysers to record the emission intensity, excited with a laser of 980 nm (MDL-H-980-5W)

k) DLS

Dynamic light scattering (DLS) using a ZetasizerNano 3600 instrument (Malvern Instruments, UK), the size range limit of which is 0.6 nm to 6 mm. Note: the diameter measured by DLS is the hydrodynamic diameter. The samples are comprised of aqueous dispersions of the nanoparticles in distilled water, or, in buffer. All samples are diluted to obtain an adequate nanoparticle concentration (0.5 – 1 mg/mL).

l) Melting Point

Melting point (mp) were determined using a Koffler-Reichert hot stage melting point apparatus and are not corrected.

m) Chromatography

All the reactions were monitored by analytical thin-layer chromatography (TLC) using silica gel 60 F254 pre-coated aluminium plates (0.25 mm thickness). Compounds were visualized using a 254 nm UV lamp and/or developing with $KMnO_4$/NaOH aqueous solution.

Flash column chromatography was performed using silica gel (pore size: 40-63 µm) or neutral aluminium oxide (pore size: 58 Å) as stationary phase. Eluents are indicated in each case.

7.2. Experimental description

Synthesis of ***N*,*N'*-(cyclohexane-1,2-diyl)bis(1-(4,5-dimethoxy-2-nitrophenyl)methanimine) (28)**
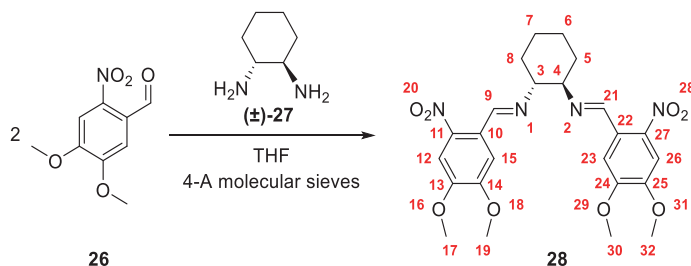
(±)-*trans*-1,2-diaminocyclohexane (604 µL, 4.63 mmol) was added to a solution of 3,4-Dimethoxy-6-nitrobenzaldehyde (**26**) (2000 mg, 9.44 mmol) and 4 Å molecular sieves in anhydrous THF (20 mL). The mixture was stirred overnight at room temperature under argon. DCM was added, and the resulting mixture was filtered through a pad of silica. The solvent of the filtrate was evaporated under reduced pressure to give a yellow solid. This crude solid was recrystallized from absolute ethanol to yield **28** (1618 mg, 3.23 mmol, 69%) as yellow solid.

^{1}H-NMR (400 MHz, CDCl$_3$): δ = 8.72 (s, 2H: H-9,21), 7.49 (s, 2H: H-12,26), 7.42 (s, 2H: H-15,23), 3.96 (s, 6H: H-17,32), 3.93 (s, 6H: H-17,30), 3.61-3.49 (m, 2H: H-3,4), 2.0-0.7 (m, 4H: H-5,6,7,8)

^{13}C NMR (100 MHz, CDCl$_3$): δ = 156.95 (C-9,21), 153.32 (C-14,24), 150.11 (C-13,25), 141.85 (C-11,27), 126.40 (C-10,212), 110.32 (C-15,23), 107.10 (C-12,26), 74.16 (C-3,4), 56.69 (C-17,19,30,32), 32.91 (C-5,8), 24.49 (C-6,7)

MS (ESI$^+$): calculated for [C$_{24}$H$_{28}$N$_4$O$_8$]: 501.199 [M + H]$^+$, found: 501.199 [M + H]$^+$

IR (ATR): 2938, 2857, 1501, 1322, 1276, 1217, 1065, 994, 880, 795, 750 cm^{-1}

m.p.: 175-177 °C

Synthesis of *N^1*,*N^2*-bis(4,5-dimethoxy-2-nitrobenzyl)cyclohexane-1,2-diamine (L1)
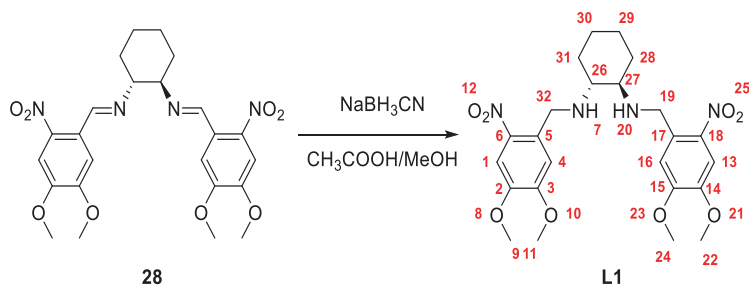
Diimine **28** (700 mg, 1.39 mmol) and sodium cyanoborohydride (220 mg, 3.49 mmol) with glacial acetic (6.5 mL) were stirred at room temperature for 5 minutes. After 5 minutes, MeOH (7 mL) were added and stirring was continued for 1 hour. The solution was evaporated under reduced pressure. A solution of potassium hydroxide was added to achieve basic pH and extracted with DCM. The organic layer was dried over anhydrous Na_2SO_4, filtered, and evaporated under reduced pressure to give a yellow solid. The solid was purified by flash column chromatography (silica gel, DCM:MeOH (9.5:0.5) + 2 % of TEA) to yield **L1** (683 mg, 1.36 mmol, 97 %) as a yellow solid.

¹H-NMR (400 MHz, CDCl$_3$): δ = 7.57 (s, 2H: H-1,13), 7.09 (s, 2H: H-4,16), 4.18-4.06(d, J=14.1 Hz, 2H: H-19,32), 3.94 (s + d, 14H: H-9,11,19,32,22,24), 2.32-2.29 (d, J=8.8 Hz, 2H: H-26,27), 2.20-2.17 (d, J=11.6 Hz, 2H: H-28a,31b), 1.86 (s, 2H: 7,20) 1.76-1.74 (d, J=8.5 Hz, 2H: H-29ª,30a), 1.22 (m, 2H: H-28b,31a), 1.05 (m, 2H: H-29b,30b)

¹³C-NMR (100 MHz, CDCl$_3$): δ = 153.37 (C-3,15), 147.71 (C-2,14), 141.11 (C-6,18), 131.71 (C-5,17), 112.88 (C-4,16), 108.16 (C-1,13), 61.62 (C-26,27), 56.57(C-9,11,22,24), 48.63 (C-19,32), 31.77 (C-28,31), 25.10 (C-29,30)

MS (ESI⁺): calculated for [$C_{24}H_{32}N_4O_8$]: 505.230 [M + H]⁺, found: 505.230 [M + H]⁺

IR (ATR): 2927, 2855, 1516, 1324, 1270, 1064, 796 cm⁻¹

m.p.: 127-129 °C

Synthesis of C1

A solution of **L1** (65 mg, 0.130 mmol) in THF (2 mL) was added to an aqueous solution that contained the equivalent amount of K_2PtCl_4 (54 mg, 0.130 mmol). THF was added to the resulting mixture until everything was dissolved, the resulting solution wa stirred at room temperature overnight. After this time, an orange solid precipitated which was filtered and washed with acetone. (61 mg, 0.07 mmols, 61 %).

¹H-NMR (400 MHz, DMF-*d7*) δ = 8.65 (s, 1H), 7.75 (s, 1H), 7.66 (s, 1H), 7.62 (s, 1H), 6.61-6.55 (s, 2H), 4.90-4.85 (d, 1H, J = 13.42), 4.59-4.52 (dd, 1H, J = 13.69, J = 6.15), 4.26-

4.19 (dd, 1H, J = 13.69, J = 6.15), 4.13 (s + d, 4H), 3.90 (s, 3H), 4.05 (s, 3H), 4.01 (s, 3H), 3.94 (s, 3H), 2.36 (m, 1H), 2.98 (m, 1H), 1.68-0.68 (m, 8H)

^{13}**C-NMR** (100 MHz, DMF-d_7) δ = 153.23, 153.00, 149.25, 148.79, 143.07, 141.31, 126.28, 124.72, 116.52, 115.72, 108.19, 108.05, 71.22, 63.64, 56.48, 56.35, 56.05, 55.95, 50.34, 48.97, 24.73, 24.54

MS (ESI$^+$): calculated for [$C_{24}H_{32}Cl_2N_4O_8Pt$]: 788.1572 [M + NH$_4$]$^+$, found: 788.1592 [M + NH$_4$]$^+$, 813.1686 [M – Cl$^-$ + dmso]$^+$, found 813.1703 [M – Cl$^-$ + dmso]$^+$

EA calculated for $C_{24}H_{32}Cl_2N_4O_8Pt$ + THF (%): C, 39.91; H, 4.79; N, 6.65. Found: C, 40.08; H, 4.93; N, 6.78

IR (ATR): 2940, 2862, 1521, 1450, 1325, 1275, 1222, 1064. 801 cm^{-1}

m.p.: > 230 °C

Synthesis of 1-(4,5-dimethoxy-2-nitrophenyl)ethan-1-ol (29)[1]
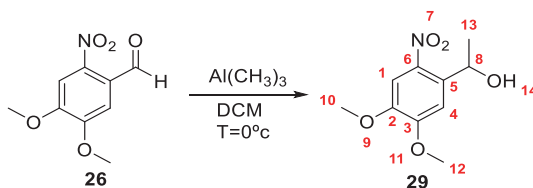
3,4-Dimethoxy-6-nitrobenzaldehyde (**26**) (750 mg, 3,5 mmols) was dissolved in dry DCM (15 mL) and treated dropwise with trimethyl aluminium in toluene (2M, 5,3 mL) at 0 °C. After 4 h of reaction, the mixture was treated with ice-cold aqueous hydrochloric acid. The product was extract with DCM (Dichloromethane): Potassium sodium tartrate solution and purified by flash chromatography (EtOAc/ Hexane, 1:1, v/v) to give compound **29** (417 mg, 1.44 mmol, 43%).

^{1}**H-NMR** (250 MHz, CDCl$_3$): δ = 7.57 (s, 1H: H-1), 7.31(s, 1H: H-4), 5.62–5.52(q, J=6.3 Hz, 1H: H-8), 4.00 (s, 3H: H-10), 3.94 (s, 1H: H-12), 1.58-1.53 (d, J=6.3 Hz, 3H: H-13)

Synthesis of 1-(1-bromoethyl)-4,5-dimethoxy-2-nitrobenzene (30)[1]
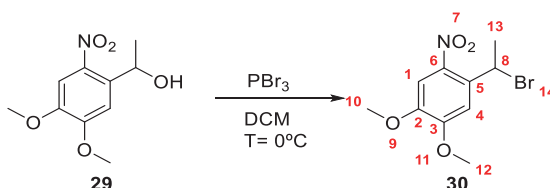
29 (328 mg, 1,4 mmols) was dissolved in 25 mL of DCM at 0 ºC, followed by PBr$_3$ (789 mg, 2.8 mmols) addition. After stirring for 3 h at 0 ºC, the mixture was dropped into ice-cold water, followed by extraction and solvent removal. The crude product was purified by flash chromatography (EtOAc:Hexane, 1:1, v/v) to give **30** (310 mg, 1.07 mmol, 74%) as a brown oil **30**, (310 mg, 1.07 mmol, 74%)

^{1}H-NMR (250 MHz, CDCl$_3$): δ = 7.46 (s, 1H: H-1), 7.27(s, 1H: H-4), 6.07–5.99 (q, J=6.8 Hz, 1H: H-8), 4.01 (s, 3H: H-10), 3.94 (s, 1H: H-12), 2.09-2.05 (d, J=6.8 Hz, 3H: H-13)

Syntheisis of N^1,N^2-bis(1-(3,4-dimethoxyphenyl)ethyl)cyclohexane-1,2-diamine (33)

31 **36** **33**
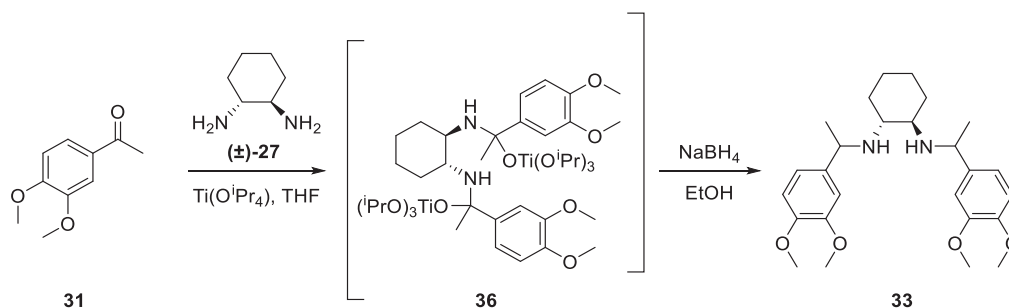
A mixture of the (±)-*trans*-1,2-diaminocyclohexane (61 µL, 0.504 mmols), 1-(3,4-dimethoxyphenyl)ethan-1-one (**31**) (200, 1.111 mmols) and Ti(O^{i}Pr$_4$) (600 µL, 2.016 mmols) in dry THF (2.5 mL) was stirred for 12 h at room temperature. Then a solution of NaBH$_4$ (95 mg, 2.52 mmols) in absolute EtOH (2.5 mL) were added at 0 °C and the resulting mixture was stirred for 12 h more at room temperature. The mixture was then quenched with water. The solvent was evaporated under pressure and the residue was stirred with Et$_2$O for 15 minutes and filtrated. The precipitate was washed with Et$_2$O. Next, the filtrate was added to a Brine solution and the organic layer was separated and dried with Na$_2$SO$_4$, and the solvent was removed under pressure (220 mg, 0.50 mmol, 99 %)

Synthesis of N,N'-(cyclohexane-1,2-diyl)bis(1-(3,4-dimethoxyphenyl)methanimine) (39)[2]

38 **39**
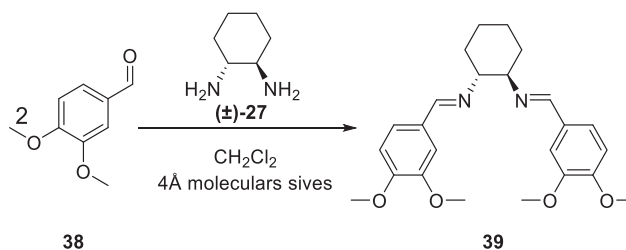
To a solution of benzaldehyde **8** (20300 mg, 12 mmol) in DCM (4 mL) with 4 Å molecular sieves at room temperature was added (±)-1,2-diaminocyclohexane (680 mg, 5.96 mmol). The reaction mixture was stirred for 2 hours and then filtered. The solvent of the filtrate was evaporated under reduced pressure. The resulting solid was purified by a recrystallization from absolute ethanol to give diimine **39** (1861 mg, 4.53 mmol, 76 %) as yellow solid.

^{1}H-NMR (360 MHz, CDCl$_3$): δ = 8.09 (s, 2H: H-9,20), 7.24 (d, J = 1.3 Hz, 2H, H-11,26), 7.02-6.99 (dd, J = 8.1 Hz, J = 1.3, 2 H: H-15,22), 6.78-6.76 (d, J = 8.1 Hz, 2H: H-12,25), 3.87 (s, 6H: H-19,28), 3.86 (s, 6H: H-17,30), 3.36-3.34 (d, 2H: H-3,4), 1.95-1.43 (m, 8H)

Synthesis of N^1,N^2-bis(1-(3,4-dimethoxyphenyl)ethyl)cyclohexane-1,2-diamine (33)
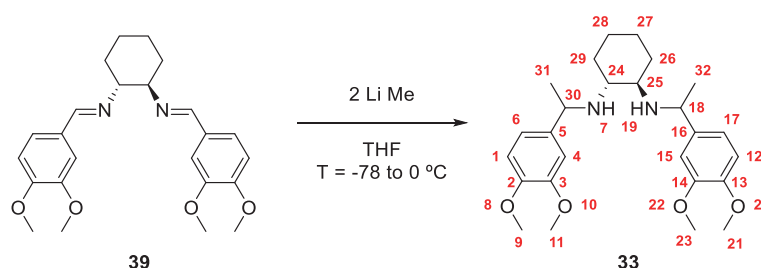
Methyllithium (1.6 M in Et$_2$O, 4.10 mmols, 2.56 mL) was added to magnetically stirred solution of the diimine **39** in THF (15 mL) which was previously cooled at -78 ºC. After 30 min, the reaction mixture was slowly warmed at 0 ºC, stirred for a further 2 h, and then quenched with a saturated aqueous solution of NaHCO$_3$. The organic phase was extracted with EtOAc and the organic layer were collected, dried over anhydrous Na$_2$SO$_4$ and evaporated under vacuum to leave the curde product. Flash column chromatography (alumina, *n*-hexane /EtOAc (1:1)), gave the product **33** (403 mg, 0.91 mmol, 90 %) as a yellow oil.

^{1}H-NMR (360 MHz, CDCl$_3$): δ = 6.95 (d, J = 1.8 Hz, 2H: H-4,12), 6.87 (dd, J = 8.2 Hz, J = 1.8 Hz, 2H: H-6,17), 6.80 (d, J = 8.2 Hz, 2 H: H-1,12), 3.89 (s, 6H: H9,21), 3.87 (s, 6H: H-11,23), 3.80 (q, J = 6.5 Hz, 2H: H-18,30), 2.24 (m, 2H: H-24,25), 1.76 (m, 4H: H-7,19,26b,29a), 1.56 (m, 2H: H-27ª,28a), 1.31 (d, J = 6.5 Hz, 6H: H-31,32, 1.10 (m, 2H: H-27b,28b), 0.89 (m, 2H: H-26ª,29b)

^{13}C-NMR (100 MHz, CDCl$_3$): δ = 148.87 (C-2,13), 147.78 (C-3,14), 140.40 (C-5,16), 118.47 (C-6,17), 110.91 (C-1,12), 109.75 (C-4,15), 60.54 (C-24,25), 56.01 (C-7,15), 55.96 (C-9,21), 55.89 (C-11,23), 32.83 (C-26,29), 25.07 (C-27,28), 24.24 (C-31,32)

MS (ESI$^+$): calculated for [C$_{26}$H$_{38}$N$_2$O$_4$]: 443.2904 [M + H]$^+$, found: 443.2897 [M + H]$^+$

IR (ATR): 2927, 2834, 1509, 1462, 1258, 1231, 1138, 1028, 759, 632 cm^{-1}

Synthesis of *N¹,N²*-bis(1-(4,5-dimethoxy-2-nitrophenyl)ethyl)cyclohexane-1,2-diamine (L2)
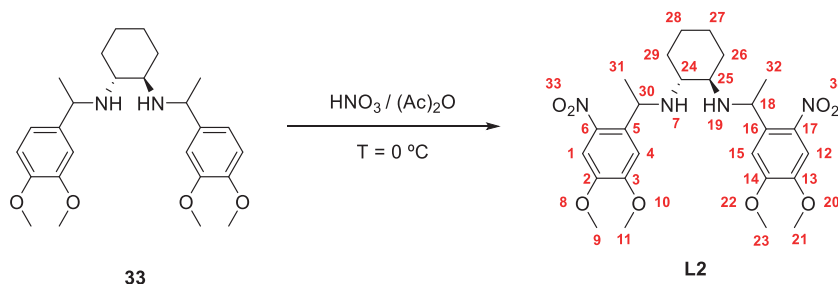
To a solution of 5.80 mL of HNO₃ 60% in an ice-bath, acetic anhydride (0.984 mL) was added and stirred during 10 min. To that solution, **33** (2.091 g, 4.73 mmol) was added. The reaction was stirred for another 3 hours and then poured into water. A solution of potassium hydroxide was added to arrive basic pH and extracted with DCM. The organic phase was dried over anhydrous Na₂SO₄ and dried under reduced pressure. Flash column chromatography (silica gel, DCM:AcOEt (1:1) + 2% TEA) gave **L2** (2.287 g, 4.29 mmol, 91%) as yellow solid.

¹H-NMR (400 MHz, CDCl₃): δ = 7.45 (s, 2H: H-1,12), 7.43 (s, 2H: H-4,15), 4.55 (q, J = 6.3 Hz, 2 H: H-18,30), 4.00 (s, 6H: H-9,21), 3.93 (s, 6H: H-11,23), 2.22 (m, 2H: H-24,25), 1.69 (m, 2H: H-26,29), 1.53 (m, 2H: H-27a,28a), 1.39 (d, J = 6.3 Hz, 6H: H-31,32), 1.06 (m, 2H: H-27b,28b), 0.85 (m, 2H: H-7,19)

¹³C-NMR (100 MHz, CDCl₃): δ = 153.03 (C-3,14), 147.29 (C-2,13), 140.69 (C-6,17), 138.00 (C-5,16), 110.20 (C-4,15), 107.47 (C-1,12), 61.28 (C-24,25), 56.30 (C-9,11,21,23), 51.32 (C-18,30), 32.90 (C-26,29), 24.80 (C-27,28), 23.85 (C-31,32)

MS (ESI⁺): calculated for [C₂₆H₃₆N₄O₈]: 533.2606 [M + H]⁺, found: 533.2591 [M + H]⁺

IR (ATR): 2932, 2854, 1510, 1459, 1330, 1265, 1214, 1058, 793 cm⁻¹

m.p.: 72-74 °C

Synthesis of C2
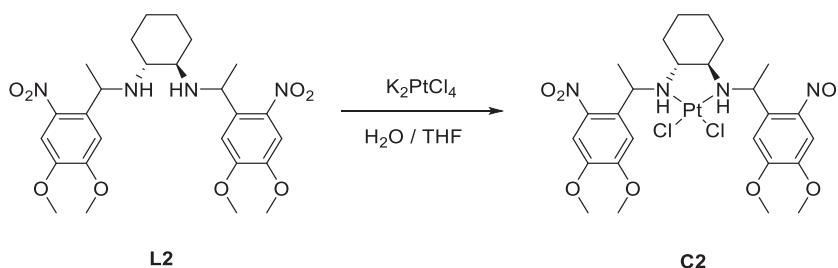
A solution of **L2** (50 mg, 0.094 mmol) in THF (2 mL) was added to an aqueous solution that contained the stoichiometric amount of K_2PtCl_4 (39 mg, 0.094 mmols). THF was added to the resulting mixture until everything was dissolved, the resulting mixture was stirred at room temperature overnight. After this time a brown solid precipitate, which was filtered. The solid was purified by precipitation Acetone/Et_2O to obtain **C2** (21 mg, 0.03 mmol, 28 %).

¹H-NMR (400 MHz, CDCl₃) δ = 7.45 (s, 2H), 7.43 (s, 2H), 4.55 (q, J = 6.3 Hz, 2 H), 4.00 (s, 6H), 3.93 (s, 6H), 2.22 (m, 2H), 1.69 (m, 2H), 1.53 (m, 2H), 1.39 (d, J = 6.3 Hz, 6H), 1.06 (m, 2H), 0.85 (m, 2H)

¹³C-NMR (100 MHz, CDCl₃): δ = 153.63, 152.86, 149.00, 148.47, 141.92, 140.55, 131.03, 130.67, 115.50, 110.86, 107.70, 106.96, 72.14, 71.94, 64.01, 57.67, 56.94, 56.62, 56.40, 48.94, 31.57, 29.89, 26.16, 25.29, 25.06, 23.52

MS (ESI⁺): calculated for [$C_{26}H_{36}Cl_2N_4O_8Pt$]: 821.1439 [M + Na]⁺, found: 821.1461 [M + Na]⁺

IR (ATR): 2948, 2841, 1519, 1456, 1341, 1261, 1207, 1073, 1010, 876, 796, 725 cm⁻¹

m.p.: > 230 °C

Synthesis of (*E*)-1-(4,5-dimethoxy-2-nitrophenyl)-*N*-isopropylmethanimine (41)
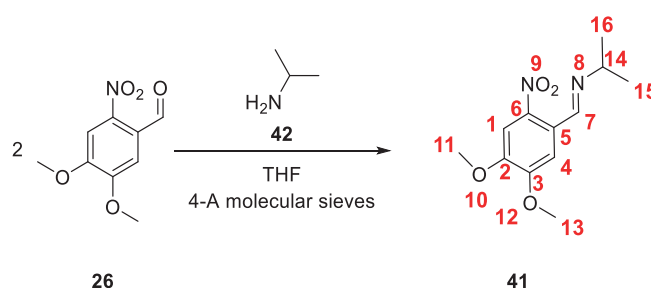
To a solution of **26** (2000 mg, 12 mmol) in CH_2Cl_2 (4 mL) at room temperature (±)-1,2-diaminocyclohexane (680 mg, 5.96 mmol) and 4 Å molecular sieves were added. The reaction mixture was stirred for 2 hours and then filtered. The resulting solution was evaporated under pressure. The resulting solid was purified by a recrystallization with absolute ethanol which give **41** (1861 mg, 7.38 mmol, 76 %) as a yellow solid.

¹H-NMR (400 MHz, CDCl₃) δ = 8.78 (s, 1H: H-7), 7.58 (s, 1H: H-1), 7.47 (s, 1H: H-4), 4.03 (s, 3H: H-11), 3.98 (s, 3H: H-13), 3.65 (hepta, 1H, J = 6.3 Hz: H-14), 1.28 (d, 6H, J = 6.3 Hz: H-15,16).

¹³C-NMR (100 MHz, CDCl₃): δ = 154.96 (C-7), 153.44 (C-3), 150.05 (C-2), 141.89 (C-6), 126.83 (C-5), 110.42 (C-4), 107.27 (C-1), 61.55 (C-14), 56.73 (C-11-13), 24.15 (C-15-16)

MS (ESI$^+$): calculated for [$C_{12}H_{16}N_2O_4$]: 253.1171 [M + H]$^+$, found: 253.1183 [M + H]$^+$

m.p.: 146-147 °C

Synthesis of *N*-(4,5-dimethoxy-2-nitrobenzyl)propan-2-amine (40)
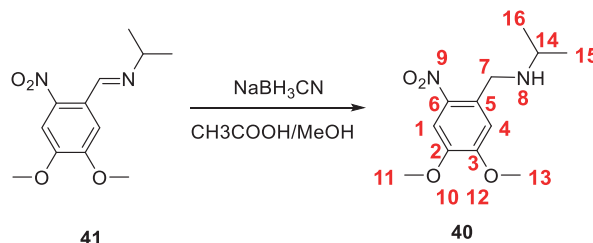
41 (250 mg, 0.971 mmols) and sodium cyanoborohydride (153 mg, 2.43 mmols) with glacial acetic (4.5 mL) were stirred at room temperature for 5 minutes. After 5 minutes, MeOH (5 mL) were added and stirring was continued for 1 hour. The solution was evaporated at vacuum. A solution of potassium hydroxide was added to arrive basic pH and extracted with DCM. The organic phase was dried over anhydrous Na_2SO_4, filtered, and evaporated under reduced pressure to give a yellow solid. The solid was purified with flash column chromatography (silica gel, DCM:MeOH (9.5:0.5) + 2 % of TEA) to give **40** (244 mg, 0.879 mmol, 99 %)as a yellow solid (244 mg, 99 %)

^{1}H-NMR (400 MHz, CDCl$_3$) δ = 7.63 (s, 1H: H-1), 7.12 (s, 1H: H-4), 4.01 (s, 3H: H-7), 3.99 (s, 3H: H-11), 3.93 (s, 3H: H-13), 2.87 (hepta, 1H, J = 6.3 Hz: H-14), 1.12 (d, 6H, J = 6.3 Hz: H-15,16)

^{13}C-NMR (100 MHz, CDCl$_3$): δ = 151.11 (C-3), 147.42 (C-2), 140.77 (C-6), 131.59 (C-5), 112.60 (C-4), 108.00 (C-1), 56.19 (C-11,13), 48.97 (C-7), 48.54 (C-14), 22.86 (C-15,16)

MS (ESI$^+$): calculated for [$C_{12}H_{16}N_2O_4$]: 255.1344 [M + H]$^+$, found: 255.1339 [M + H]$^+$

m.p.: 66-68 °C

Synthesis of LiYF$_4$; Yb; Tm nanoparticles[3]

LiYF$_4$;Yb^{3+};Tm^{3+} UCNPs were synthesized *via* thermal decomposition, which was comprised of a two-step process. In the first step, a mixture of water/trifluoroacetic acid (1:1) (10 mL), was added to a 2-neck round-bottom flask containing Tm$_2$O$_3$ (0.0024 g, 6.25 x 10^{-6} mol, 0.5 mol% Tm^{3+}), Yb$_2$O$_3$ (0.1232 g, 3.13 x 10^{-4} mol, 2.5 mol% Yb^{3+}) and Y$_2$O$_3$ (0.2103 g, 9.31 x 10^{-4} mol). The cloudy solution was heated (80 ºC) under reflux until it was clear. The resulting solution was then dried at 60 ºC for 5 hours to form the trifluoroacetate lanthanide precursor, then the solvent was evaporated under pressure. In the second step, LiCOOCH$_3$ · 2

H_2O (0.160 g, 0.016 mols) was added to the dried precursor $Ln(CF_3COO)_3$ (655 mg), with oleic acid (10 mL) and 1-octadecene (10 mL) and the mixture was degassed for 30 minutes at 120 ºC. The temperature was increased at a rate of 10 ºC·min^{-1} to 315 ºC. The reaction mixture was maintained at 315 ºC under stirring for 1 hour. After cooling to room temperature absolute ethanol was added to the reaction mixture to precipitate the $LiYF_4$; Yb^{3+}; Tm^{3+} UCNPs, which were subsequently isolated via centrifugation (3000 rpm, 15 minutes). The pellet was washed with a 1:3 hexane/ethanol mixture twice to remove any impurities.

Synthesis of *m*-PEG-COOH[4]

m-PEG-OH (2.000 g, 1 mmol), KOH (1.408 g, 25.1 mmol), $KMnO_4$ (0.553 g, 3.5 mmol) were dissolved in 15 mL of water. The reaction was stirred overnight. The resulting brown suspension (MnO) was filtered over celite and concentrated HCl (37 %) was added to the filtrate until acidic pH. The product was extracted into CH_2Cl_2 followed by drying with anhydrous Na_2SO_4. The organic phase was evaporated under pressure.

Thereafter, CH_2Cl_2 was added until all the solid was dissolved, then Et_2O was added until the solution became turbid. The solution was stored in the freezer overnight and the white precipitate was filtered, washed with cold diethyl ether, and dried under high vacuum (1.936 g, 0.96 mmol, 96%)

^{1}H-NMR (360 MHz, CDCl$_3$) δ = 4.14 (s, 2 H: H$_c$), 3.64 (s, 176 H: H$_b$), 3.38 (s, 1 H: H$_c$)

Synthesis of *m*PEG-ODA[1]

To a solution of mPEG-COOH (1008 mg, 0.540 mmols) in 3 mL of DCM were added Et_3N (0.098 mL, 0.972 mmols), HOBt (73 mg, 0.540 mmols) and HBTU (205 mg, 0.540 mmols). The mixture was stirred for 1 h at 0 ºC. Subsequently, ODA (146 mg, 0.540 mmols) was added, and the reaction was transferred to room temperature and kept for 20 h. When the reaction was completed, the mixture was extracted with Brine and the organic phase was dried with anhydrous Na_2SO_4 and evaporate under reduced pressure. The crude product was purified by chromatography (silica gel, DCM/MeOH, 9:1) to give a yellowish solid. The resulting solid was

recrystallized at low temperature from DCM/Et$_2$O to yield mPEG-ODA (544 mg, 0.25 mmol, yield 44 %).

^{1}H-NMR (400 MHz, CDCl$_3$): δ = 3.97 (s, 2H: H$_c$), 3.85-3.43 (m, 176 H: H$_b$), 3.38 (s, 3H: H$_a$), 3.26 (dd, J = 13.71, J = 6.62, 2H: H$_d$), 1.51 (m, 2H: H$_e$), 1.26 (m, 30 H: H$_f$), 0.87 (t, J = 6.67 Hz, 3H: H$_g$)

^{13}C-NMR (100 MHz, CDCl$_3$): δ = 169.76 (C$_d$), 77.48-70.29 (C$_{b,c}$), 59.06 (C$_a$), 38.95 (C$_e$), 31.95 (C$_f$), 29.72 – 22.71 (C$_g$), 14.96 (C$_h$)

Preparation of UCNPs/*m*-PEG-ODA

mPEG-ODA (110 mg) was mixed with UCNPs (20 mg) in CHCl$_3$ (1 mL). The mixture was sonicated for 5 minutes. After this time, 6 mL of water was added to the mixture and sonicated for 3 hours to evaporated CHCl$_3$.

After that, the solution was added to a falcon and centrifuged at 4000 rpm for 2 hours, excess mPEG-ODA in supernatant was removed. The nanoparticles were re-dispersed with water and filtered through a 0.45 µm syringe filter to remove large aggregates.

Then, the solvent was removed by evaporation at vacuum or by freezer – dying.

Synthesis of C1/UCNPs/mPEG-ODA

mPEG-ODA (110 mg), of **C1** (10 mg) and UCNPs (20 mg) were mixed in CHCl$_3$ (2 mL). The mixture was sonicated for 5 min and then THF (1 mL) was added to the solution. After 5 min of sonification, water (6 mL) was added to the mixture and the resulting mixture was sonicated for 3 h to evaporate CHCl$_3$ and THF, keeping the water bath of the sonicator below 50 ºC.

After that, the solution was transferred to a falcon tube and centrifuged at 4000 rpm for 2 h, where excess mPEG-ODA in supernatant was removed. The nanoparticles were re-dispersed in water and filtered through a 0.45 µm syringe filter to remove large aggregates. Then, the solvent was removed by evaporation by freezer-–dying overnight.

Synthesis of C2/UCNPs/mPEG-ODA

mPEG-ODA (110 mg), **C2** (11 mg) and UCNPs (20 mg) were mixed in CHCl3 (2 mL). Then the mixture was sonicated for 5 min. After this time, water (6 mL) was added to the mixture and the resulting mixture was sonicated for 3 h to evaporate CHCl$_3$, keeping the water bath below 50 ºC.

After that, the solution was added to a falcon tube and centrifuged at 4000 rpm for 2 h, excess mPEG-ODA in supernatant was removed. The nanoparticles were re-dispersed in water and filtered through a 0.45 µm syringe filter to remove large aggregates.

Then, the solvent was removed by freezer–drying overnight.

Pt (II)-release experiment

Pt(II)/UCNPs/mPEG-ODA (80 µg Pt(II)) were diluted in 2 mL of PBS solution. This solution was introduced in a cuvette dialysis with holes surrounded by a dialysis bag (6 KDa). The cuvette was placed in 65 mL of PBS bath already heated at 37 °C. In this experiment it was irradiated above the cuvette (dark, UV-light and NIR-light), where 1 mL aliquots were collected from the PBS bath at different times and replaced with the same volume of PBS.

The aliquots were analysed by ICP-MS, these samples were diluted with HCl 1 % (v/v) and HNO_3 1 % (v/v).

Photoreaction monitorization

Each compound (**L1, L2**, **C1** and **C2**) was irradiated at λ_{exc} = 365 nm and 3 mW/cm^2. UV-vis absorption measurements of the photoreaction were conducted in $1.0 \ 10^{-5}$ M solutions in DMF and ACN until no more spectral changes were observed. Additional analyses of the photoreaction were performed by ^{1}H NMR for 0.01 M solutions in CD_3CN and DMF-d_7 until the reagent peaks disappeared. On the other hand, the studies of the photodegradation by NMR were done at 0.01 M in CD_3CN and DMF-d_7 until the reagent picks disappear.

Photodegradation quantum yields

The photoreaction quantum yields in acetonitrile were determined by monitoring UV-vis absorbance changes at different irradiation times at λ_{exc} = 355 nm (3rd harmonic of a Nd:YAG pulsed laser, Brilliant, Quantel). Measurements were done relative to the reference compound 1,2-bis(2-methyl-5-trifluoroactylthien-3-yl)cyclopentene (DTE-(COCF$_3$)$_2$) (Φ_{o-c} = 0.37 in toluene).[5] To this data, equations 6.1 and 6.2 were applied as described[6] to obtain the Φ_{ph} values for **L1**, **L2**, **C1** and **C2**.

$$\ln\left(\frac{C_R}{C_R^0}\right) = \alpha \int_{t_0}^{t} \frac{1-10^{-Abs^{tot}}}{Abs^{tot}} \, dt \quad \textbf{(Eq 6.1)}$$

Where:

$$\alpha = -\Phi_{ph} \cdot I_0 \cdot \varepsilon_R \cdot b \qquad \textbf{(Eq. 6.2)}$$

In these equations, c_R is the concentration of the starting material (R) at different irradiation times t, I_0 is the incident light intensity, b is the cell path length, and Abs^{tot} and ε_R are the total absorbance and molar absorptivity of R at the irradiation wavelength, respectively.

Cell Viability Assays with A375 cell line

Human melanoma cell line A375 was routinely maintained in Dulbecco's Modified Eagle Medium (DMEM) supplemented with 10 % fetal bovine serum (FBS), 2 mM L-glutamine, 1 % pen/strep (100 U/mL penicillin, 100 µg/mL streptomycin) and 2.5 µg/mL fungizone. Cells were cultured at 37 °C with 5 % CO_2 and confluence and morphology were frequently monitored. Cells were subculture at 75-80 % confluence.

Stock solutions were freshly prepared in DMF for **L1, L2, C1, C2**. To prepare **L1 IR**, **L2 IR**, **C1 IR** and **C2 IR** stocks, half of volume of stock of each compound (**L1, L2, C1, C2**) was taken and irradiated with UV lamp at 365 nm for 2 hours. Each stock solutions were diluted in the culture medium for working concentrations (maximum 0.2 % DMF in biological experiments).

A375 cells were seeded in 96-well plates at 40000 cells/mL for 24 h of exposure. After 24 h, medium was replaced with fresh medium (100 µL) containing: (i) **L1** and **L1 IR** (0, 25, 50, 100, 125, 150 µM), (ii) **L2** and **L2 IR** (0, 5, 10, 25, 50, 75, 100 µM), (iii) **C1** and **C1 IR** (0, 0.5, 1, 2.5, 5, 7.5, 10, 20 µM), (iv) **C2** and **C2 IR** (0, 0.5, 1, 2.5, 5, 7.5, 10, 20 µM) and incubate for 24 hours more.

At the end of the incubation time, the wells were emptied, and fresh medium (100 µL) was placed in each well. After that, 50 µL of MTT (1 mg/mL in PBS) was added to each well and incubated for 4 h at 37 °C in a 5% CO_2 humified atmosphere. Thereafter, the culture medium with MTT was removed and replaced by 150 µL of DMSO to dissolve the formazan crystals. The absorbance was measured with a plate reader (Synergy HT Multi-Mode, BioTek, Winoski, VT) at 570 nm with blank corrections.

Stock solutions were freshly prepared in water for **C1**/UCNPs/mPEG-ODA and **C2**/UCNPs/mPEG-ODA. Each stock solution was diluted in the culture medium for working concentrations.

In vitro cytotoxicity of **C1**/UCNPs/mPEG-ODA and **C2**/UCNPs/mPEG-ODA were assayed against A375 cancer cells. A375 cells were seeded in 96-well plate with a density of 40000 cells/mL and cultured at 5 % CO_2 at 37 °C for 24 h. Then, the medium was replaced with fresh medium containing **C1**/UCNPs/mPEG-ODA (0, 0.5, 5 µM of Pt(II)) or **C2**/UCNPs/mPEG-ODA (0, 2.5, 7.5 µM of Pt(II)) and incubated for 2 h. After the incubation time, the supernatant

was removed to discard what has not been internalised and new medium was added. Subsequently, it was irradiated at 980 nm with a power intensity of 4.5 W/cm^2 for 60 min (1 min of irradiation after 2 min break). Then the cells were incubated for another 24 h. At the end, the medium was renewed again, and the cells were treated with MTT protocol.

Cell Viability Assays with HCT-116 cell line

Human coloreactal carcinoma cells (HCT-116) were obtained from American Type Culture Collection (ATCC, Manassas, VA, USA). HCT-116 cells were routinely cultured in Dulbecco's modified eagle medium (DMEM, Invitrogent) containing 10 % heat-inactivated fetal bovine serum and 1 % antibiotic-antimycotic solution at 37 °C in a humidified 10 % CO_2 atmosphere.

Stock solutions were freshly prepared in DMF for **L1, L2, C1, C2**. To prepare **L1 IR**, **L2 IR**, **C1 IR** and **C2 IR** stocks, half of volume of stock of each compound (**L1, L2, C1, C2**) was taken and irradiated with UV lamp at 365 nm for 2 hours. Each stock solutions were diluted in the culture medium for working concentrations (maximum 0.2 % DMF in biological experiments).

Stock solutions were freshly prepared in water for **C1**/UCNPs/mPEG-ODA and **C2**/UCNPs/mPEG-ODA. Each stock solution was diluted in the culture medium for working concentrations.

HCT-116 cells were plated in 96-well plates at a density of 5 x 10^3 cells/well in 100 µL of culture medium and were allowed to grown overnight. After this time, cells were treated with different concentrations of each sample (0, 1, 2, 5, 10, 20, 50, 100, 200 µM) during 24 h and then 10 µL of PrestoBlue reagent was added following the standard protocol.[7] The fluorescence was measured exciting at 531 nm (emission at 572 nm) using Victor3 multiwell microplate reader (Perkin Elmer). The relative cell viability (%) for each sample related to the control cells without treatment was calculated. Each sample was tested in triplicate.

7.3. References

1. Chen, W.; Chen, M.; Zang, Q.; Wang, L.; Tang. F.; Han, Y.; Yang, C.; Deng, L. & Liu, Y. NIR light controlled release of caged hydrogen sulfide based on upconversion nanoparticles *Chem. Commun.* **2015,** *51,* 9193-9196 https://doi.org/10.1039/C5CC02508G

2. Bravo, J.; Cativiela, C.; Navarro, R. & Urriolabeitia, E. P. Synthesis, characterization and catalytic activity in Heck-type reactions of orthometallated Pd^{II} and Pt^{II} complexes derived from (1*R,2R*)-1,2-diaminocyclohexane *Journal of Organometallic Chemistry* **2002,** *650,* 157-172 https://doi.org/10.1016/S0022-328X(02)01148-8

3. Meijer, M. S.; Rojas-Gutierrez, P. A.; Busko, D.; Howard, I. A.; Frenzel, F.; Würth, C.; Resch-Genger, U.; Richards, B. S.; Turshatov, A.; Capobianco, J. A. & Bonnet, S. Absolute upconversion quantum yields of blue-emitting LiYF$_4$:Yb^{3+},Tm^{3+} upconverting nanoparticles *Phys. Chem. Phys.* **2018,** *20*, 22556-22562 https://doi-org/10.1039/C8CP03935F

4. Malisova, B.; Tosatti, S.; Textor, M.; Gademann, K. & Zürcher, S. Poly(ethylene glycol) Adlayers Immobilized to Metal Oxide Substrates Through Catechol Derivatives: Influence of Assembly Conditions on Formation and Stability *Langmuir* **2010,** *26,* 4018-4026 https://doi.org/10.1021/la903486z

5. Villabona, M.; Wiedbrauk, S.; Feist, F.; Guirado, G.; Hernando, J. & Barner-Kowollik, C. Dual-Wavelength Gated oxo-Diels-Alder Photoligation Org. Lett. **2021**, 23, 2405-2410 https://doi.org/10.1021/acs.orglett.1c00015

6. Lees, A. J. A Photochemical Procedure for Determining Reaction Quantum Efficiencies in Systems with Multicomponent Inner Filter Absorbances *Anal. Chem.* **1996**, *68*, 226-229 https://doi.org/10.1021/ac9507653

7. Xu, M.; McCanna, D. J. and Sivak, J. G. *Journal of Pharmacological and Toxicological Methods* **2015**, *71*, 1-7 https://doi.org/10.1016/j.vascn.2014.11.003

ANNEX

ANNEX
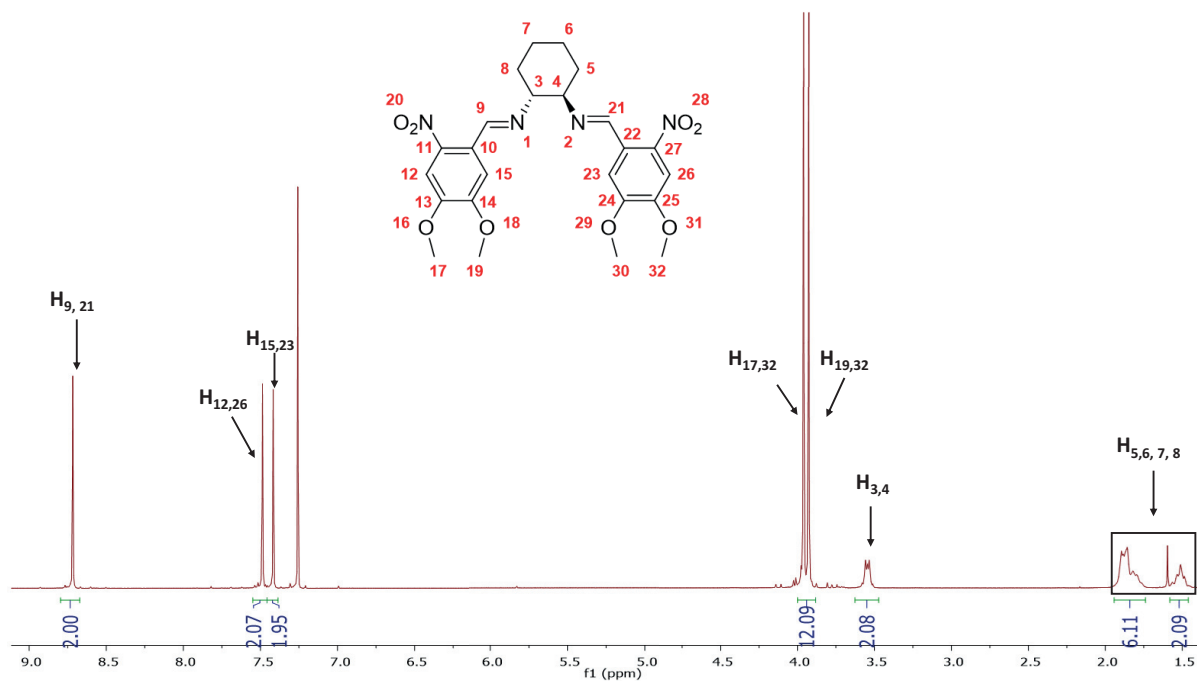
Figure A1: ^{1}H-NMR (400 MHz, CDCl$_3$) of **28**
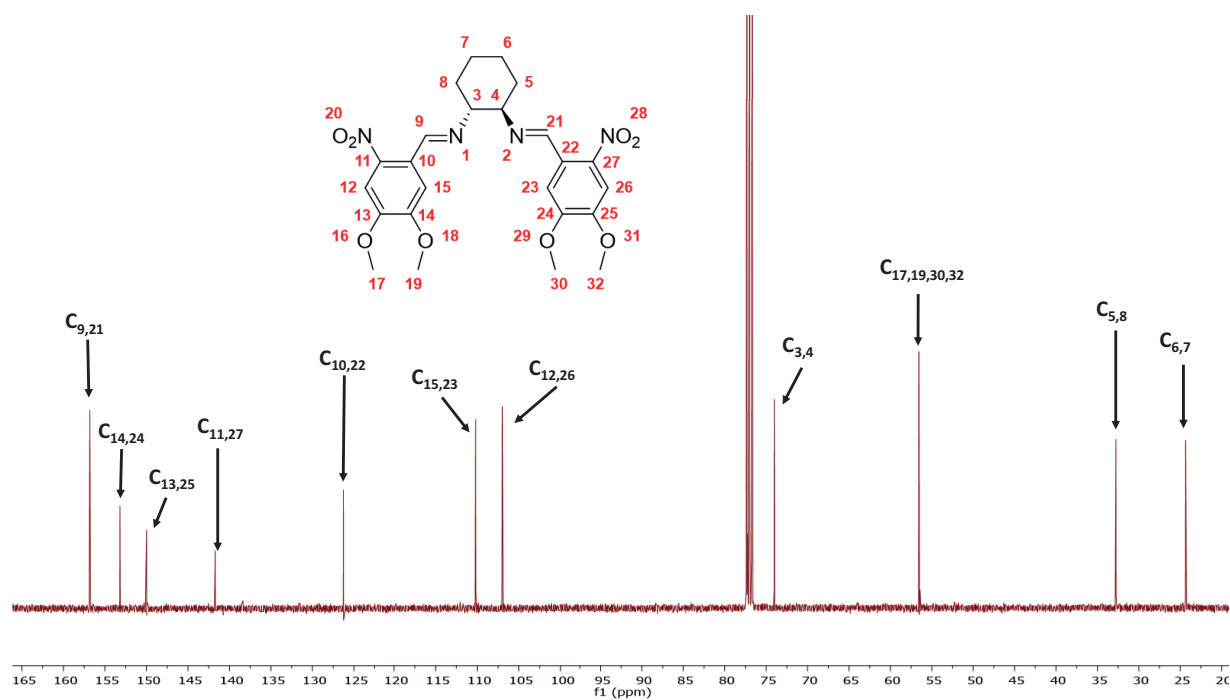
Figure A2: ^{13}C-NMR (100 MHz, CDCl$_3$) of **28**
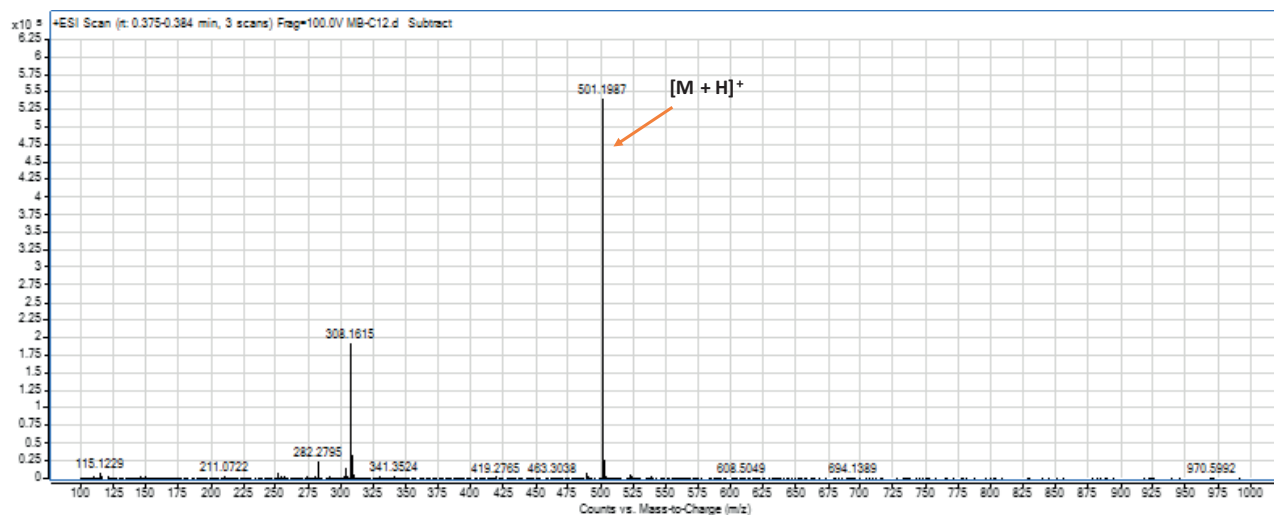
Figure A3: ESI-HRMS spectrum of **5**
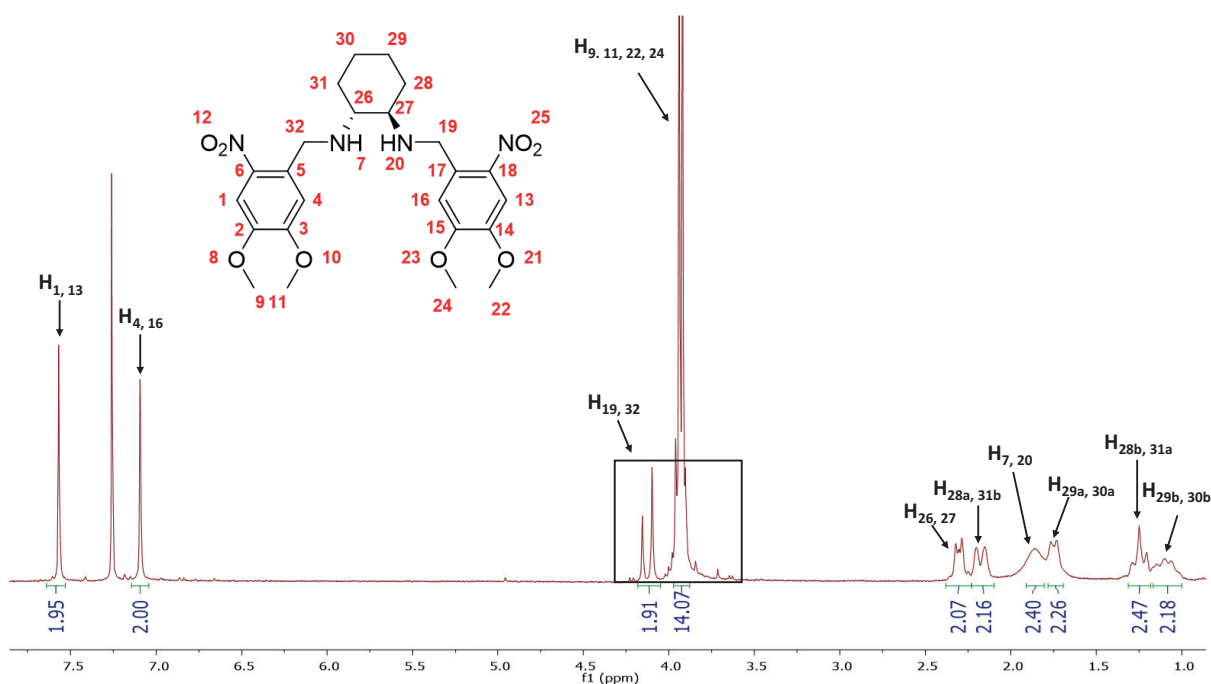
Figure A4: ^{1}H-NMR (400 MHz, CDCl$_3$) of **L1**
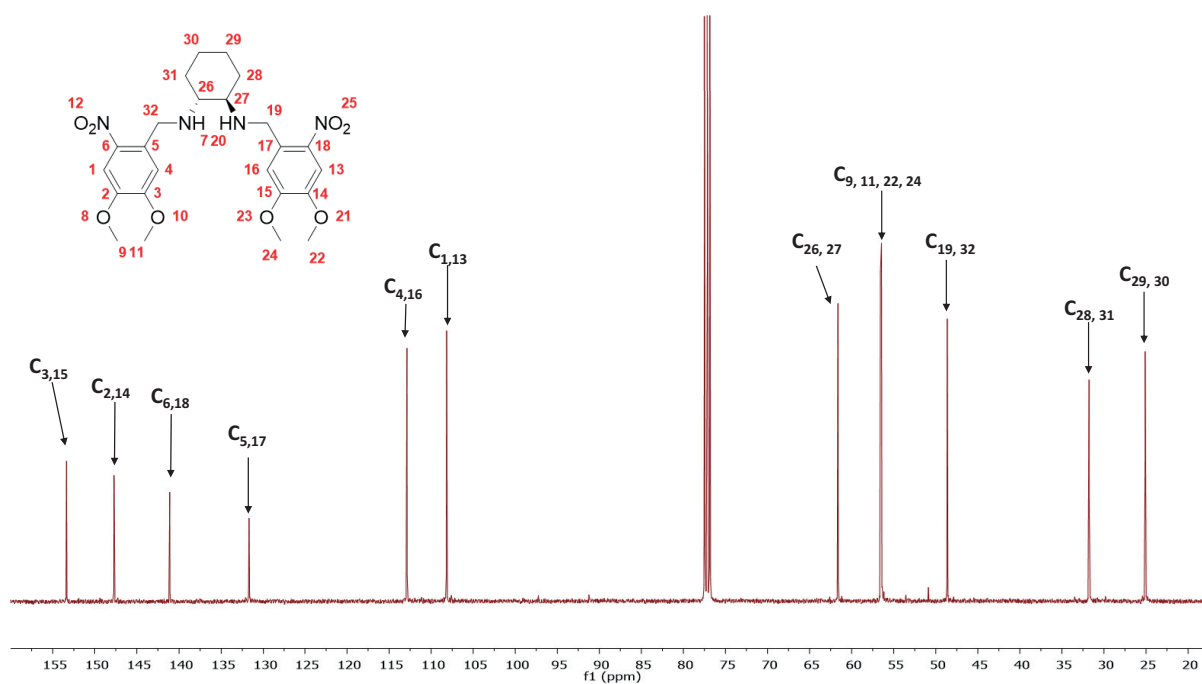
Figure A5: ^{13}C-NMR (100 MHz, CDCl$_3$) of **L1**
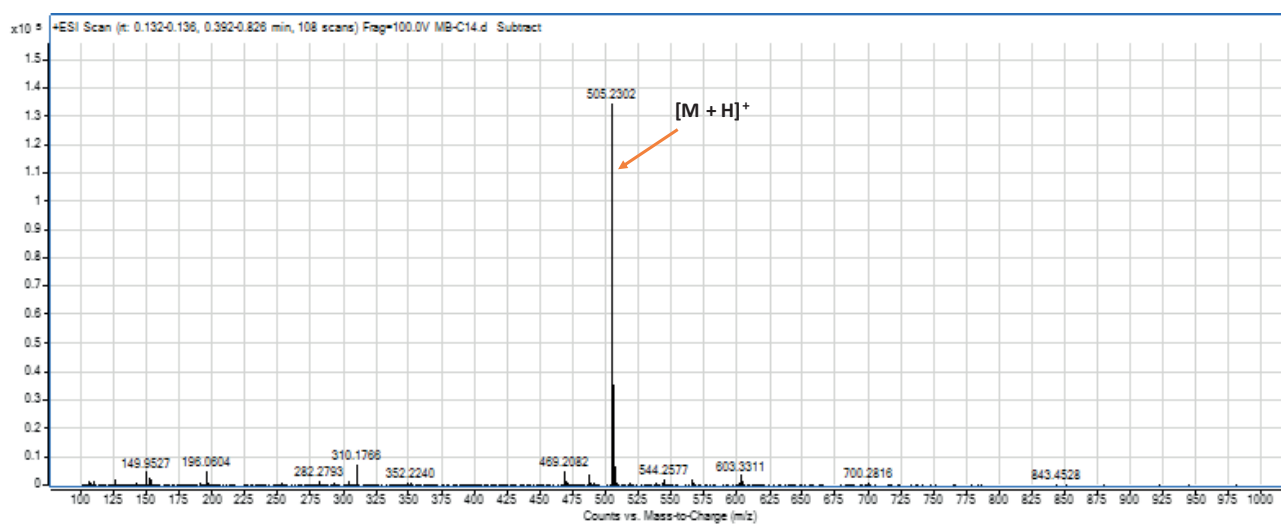
Figure A6: ESI-HRMS spectrum of **L1**
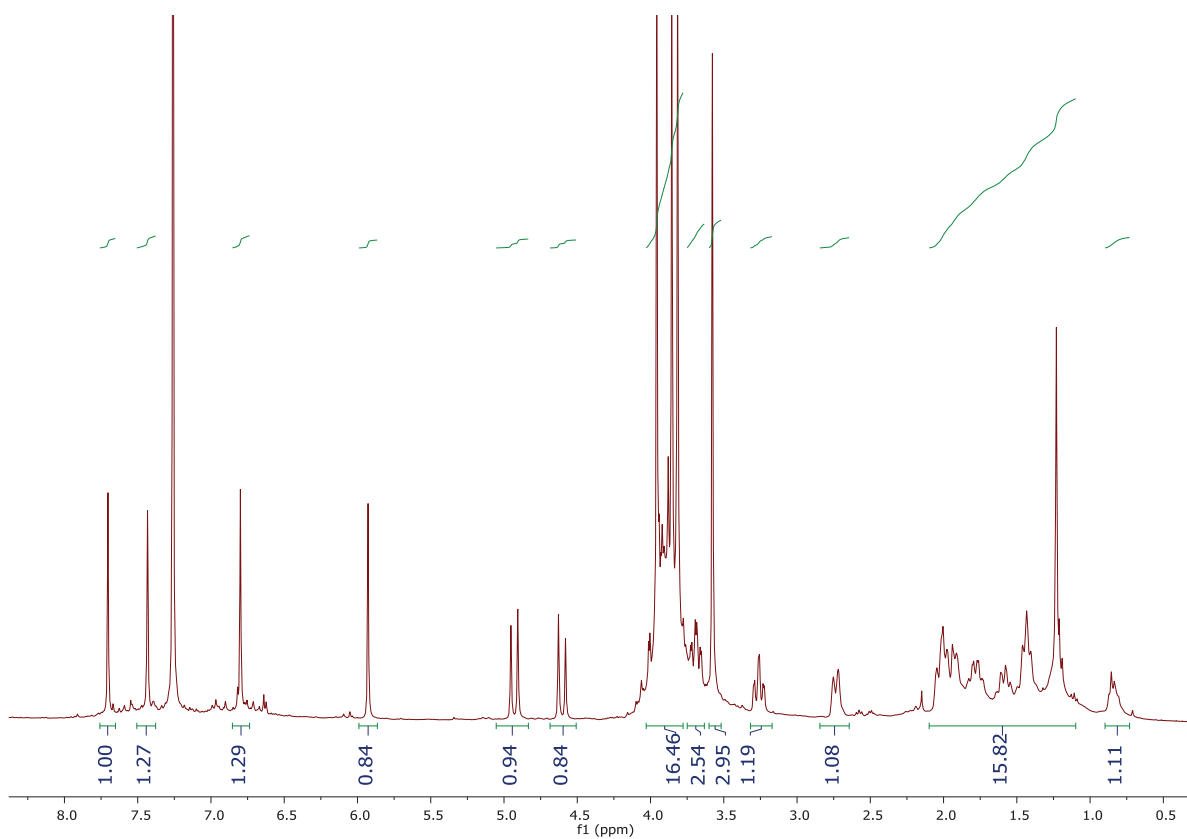
Figure A7: ^{1}H-NMR (400 MHz, CDCl$_3$) of the photoproduct obtained when **L1** is irradiated with UV light
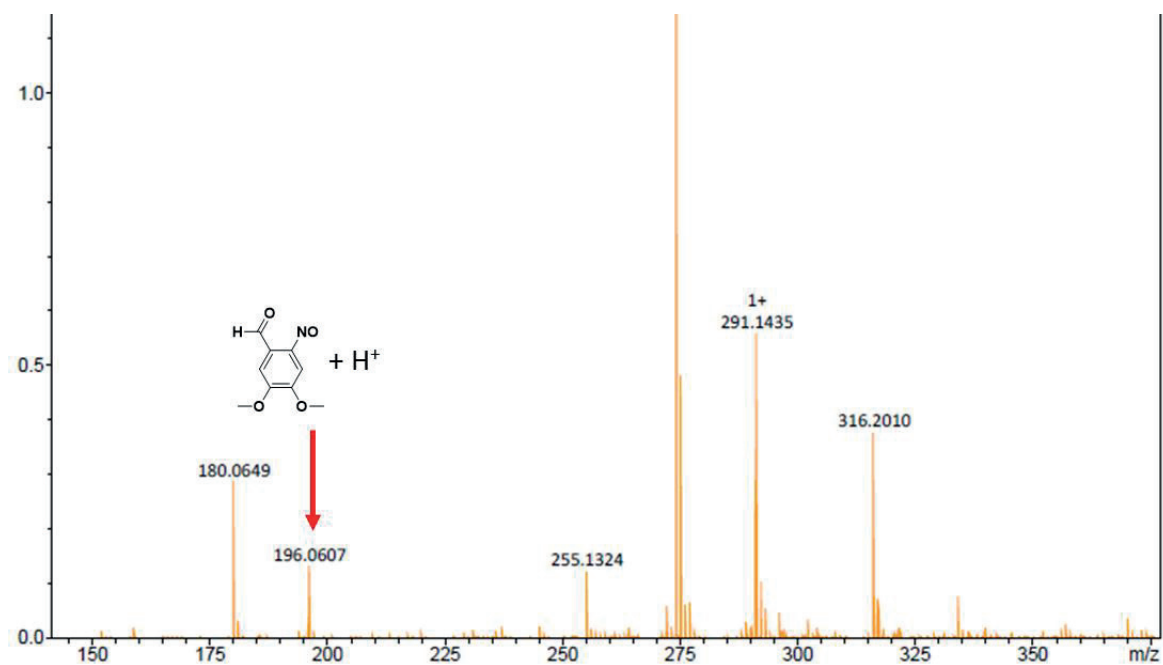
Figure A8: ESI-HRMS spectrum of photodegradation of **L1** after irradiating during 50 min at 365 nm
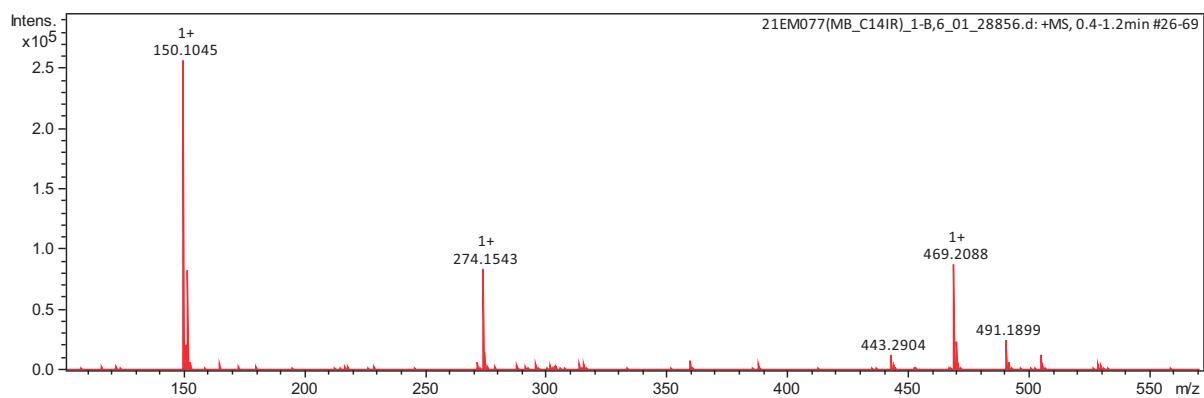
Figure A9: ESI-HRMS spectrum of photodegradation of **L1** after irradiating during 110 min at 365 nm
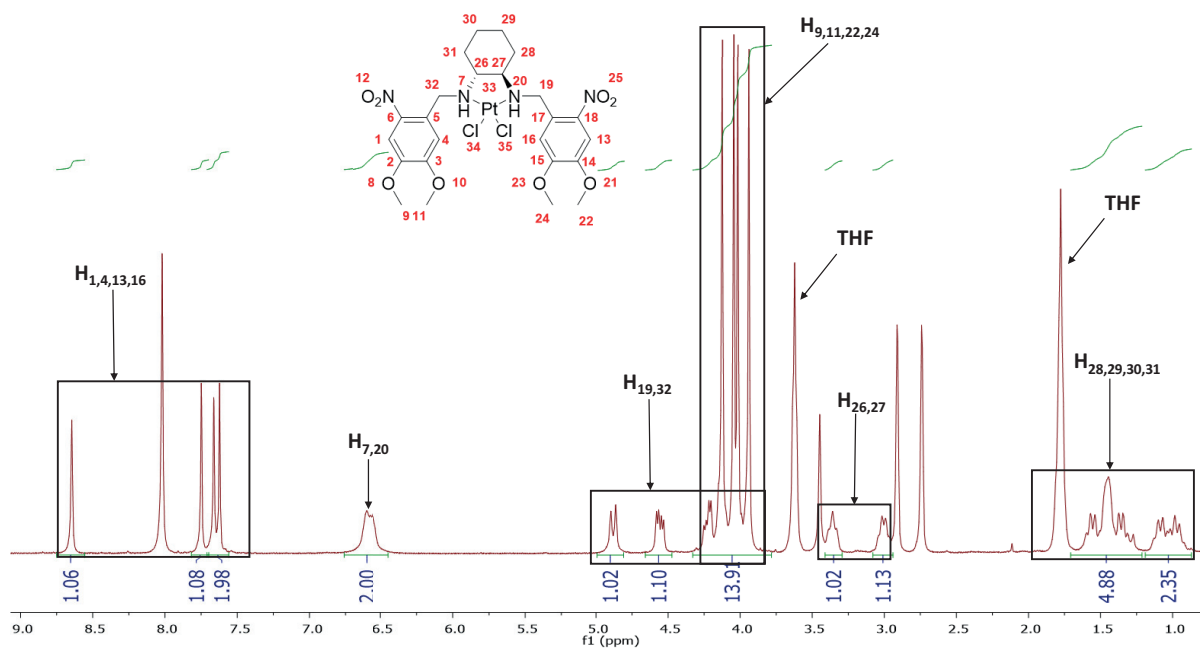
Figure A10: ^{1}H-NMR (400 MHz, DMF-d_7) of **C1**

Figure A11: ^{13}C-NMR (100 MHz, DMF-d_7) of **C1**
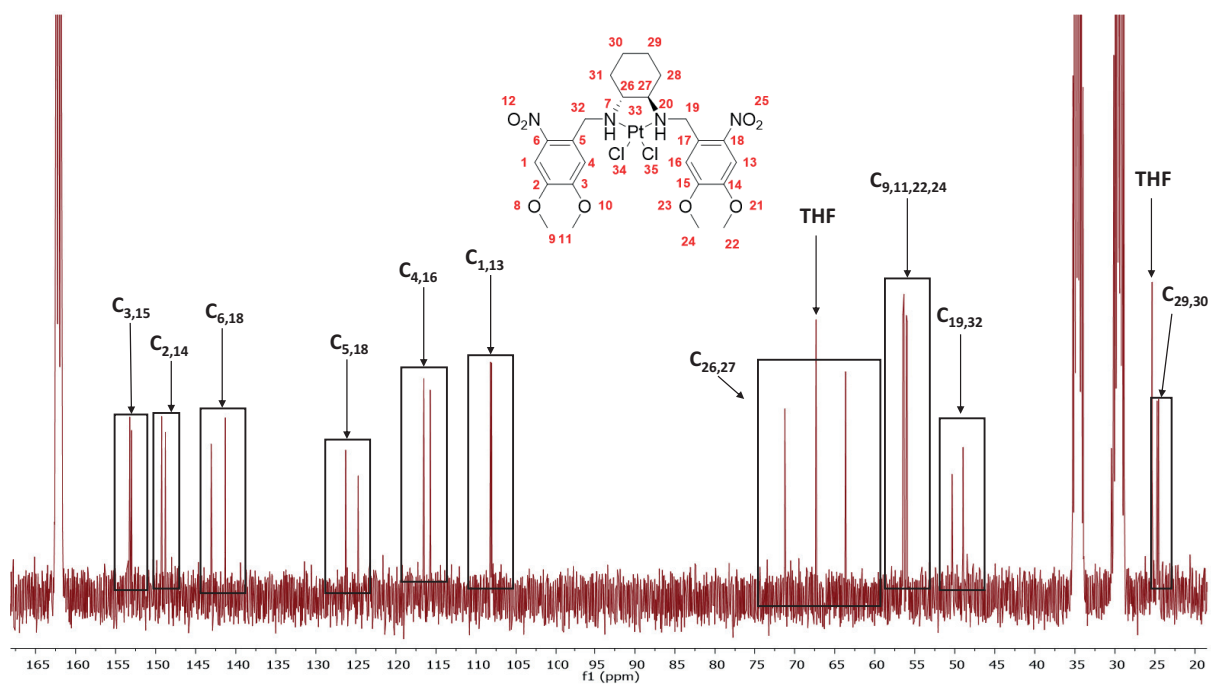
[M + NH₄]⁺
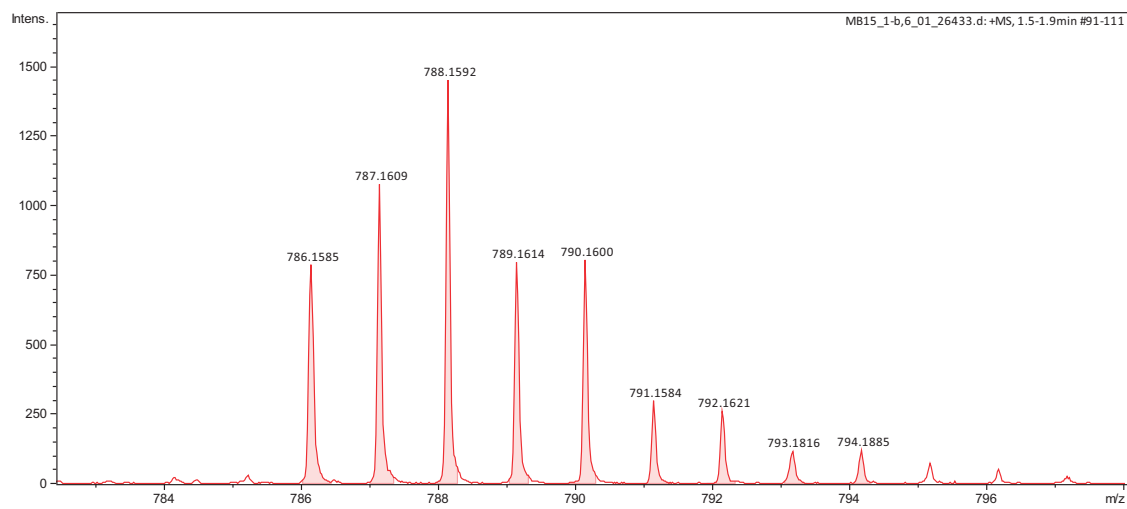
[M – Cl⁻ + dmso]⁺
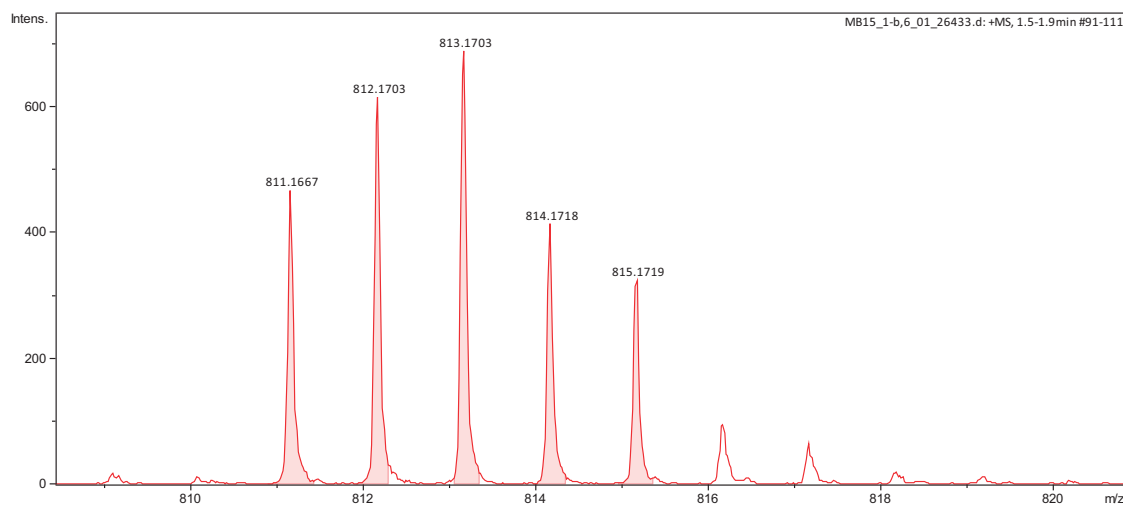
Figure A12: ESI-HRMS spectrum of **C1**
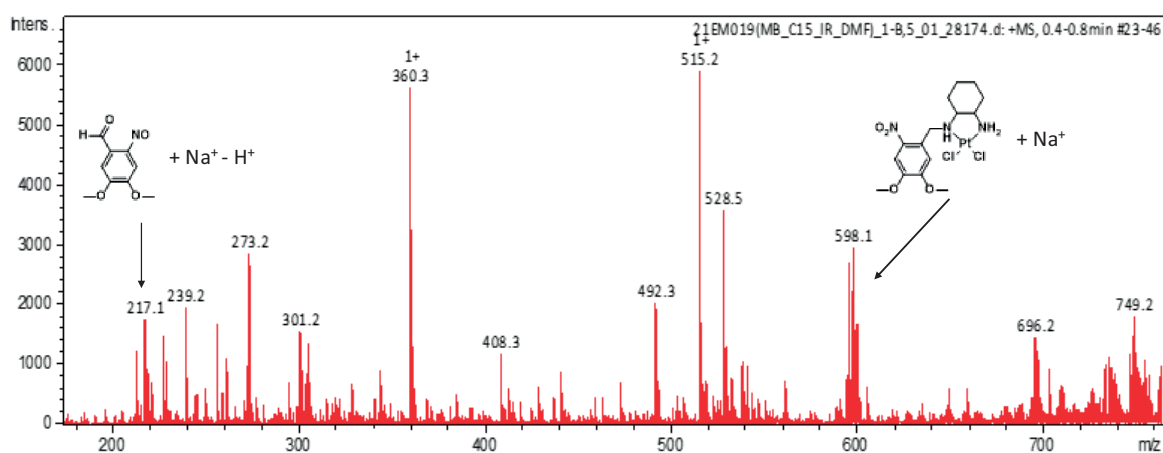
Figure A13: ESI-HRMS spectrum of **C1 IR**
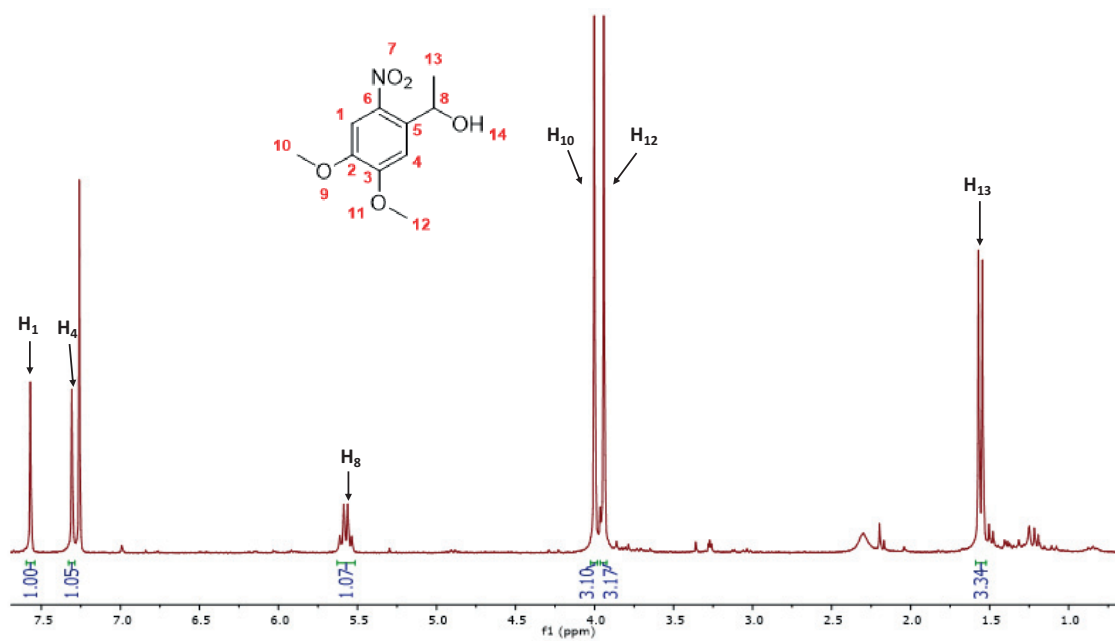
Figure A14: ^{1}H-NMR (250 MHz, CDCl$_3$) of **29**
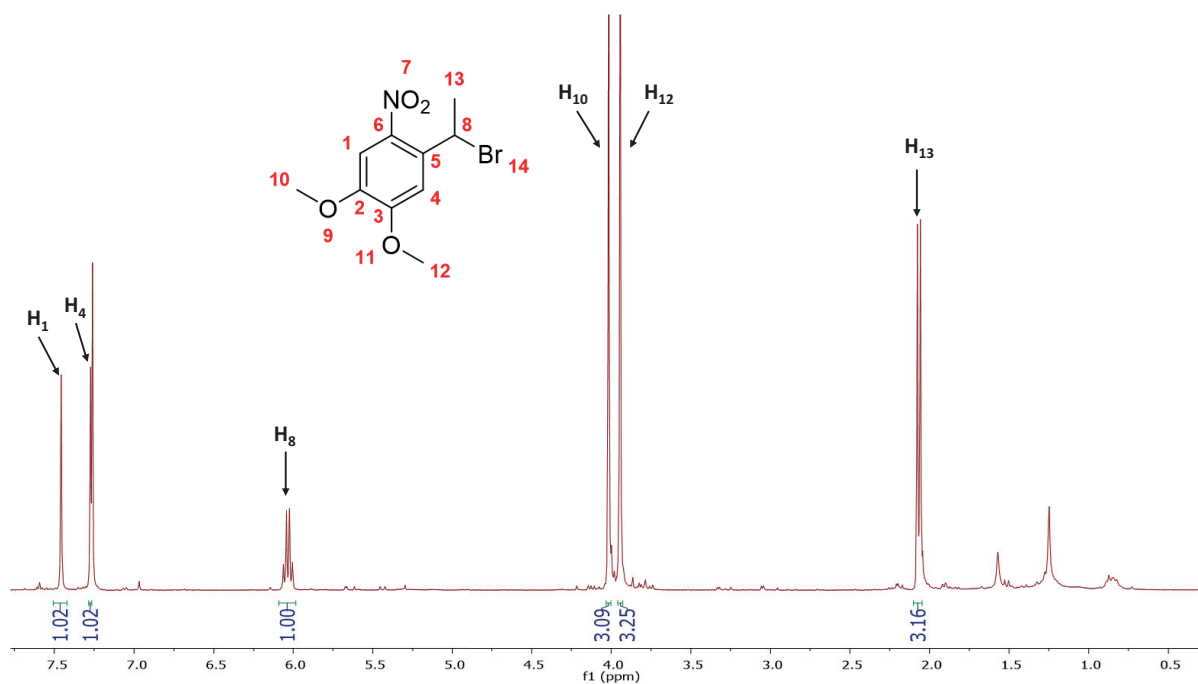
Figure A15: ^{1}H-NMR (250 MHz, CDCl$_3$) of **30**
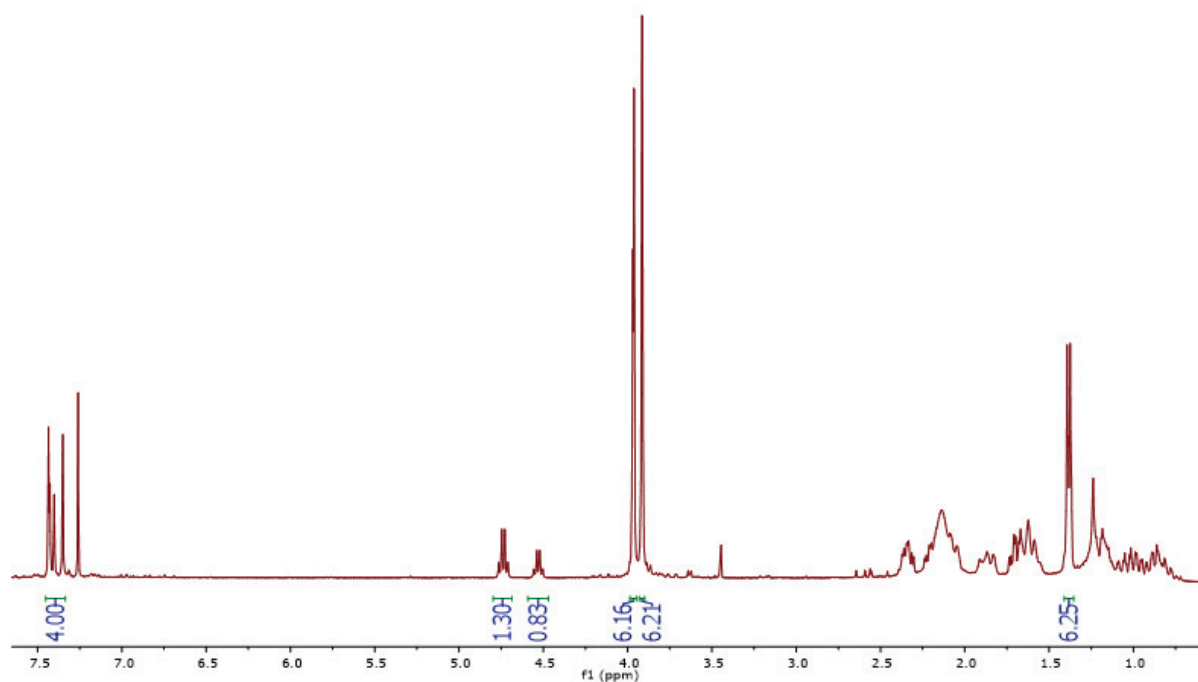
Figure A16: ^{1}H-NMR (250 MHz, CDCl$_3$) of possible diastereomers that can be obtained when reacting compound 30 with (±)-*trans*-DACH in presence of DMPU to form **L1.**
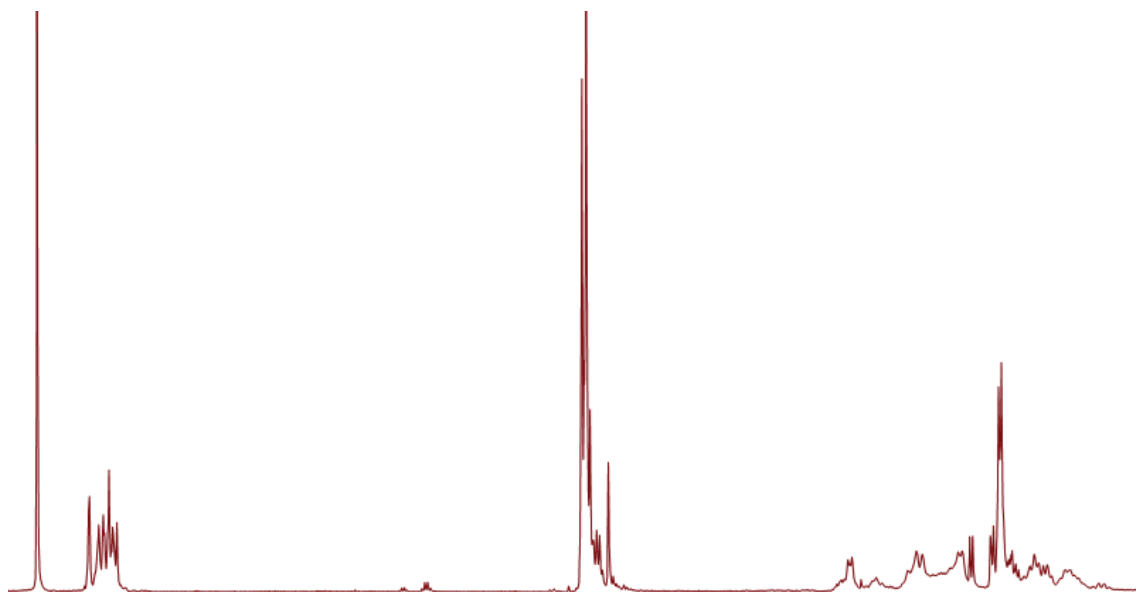
Figure A.17: ^{1}H-NMR (360 MHz, CDCl$_3$) of a mixture of diastereomers of product **33** when reacted **31** with (±)-*trans*-DACH in presence of Ti(O^{i}Pr)$_4$
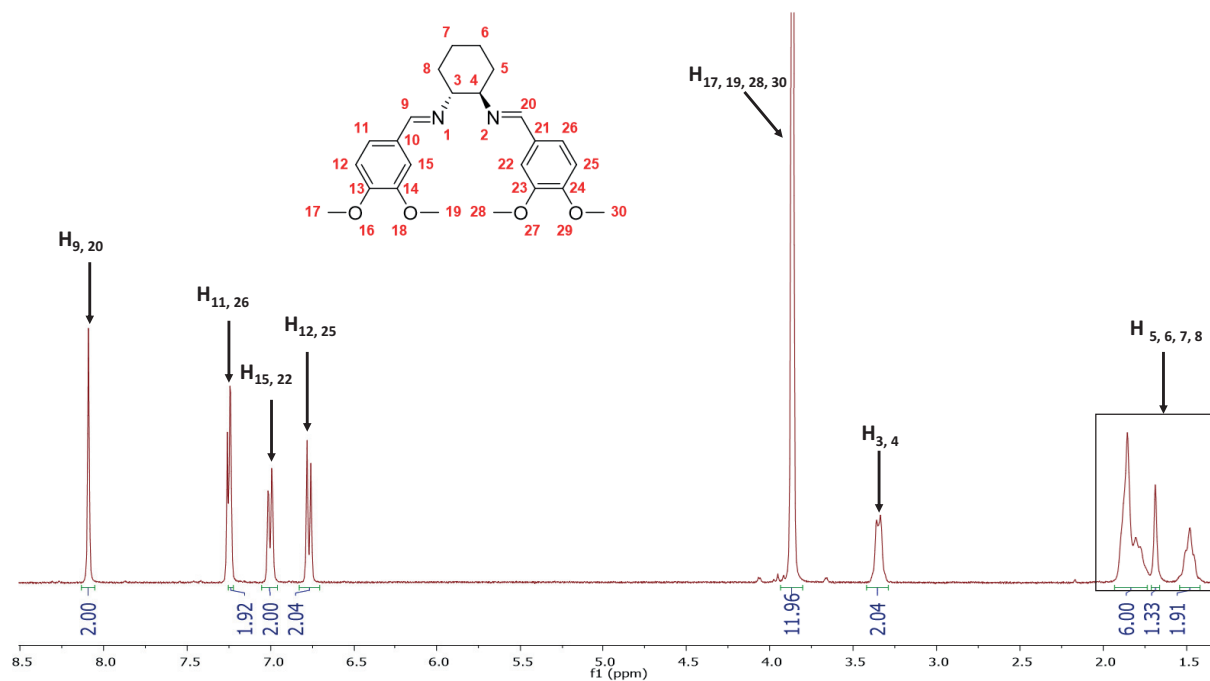
Figure A18: ^{1}H-NMR (360 MHz, CDCl$_3$) of **28**
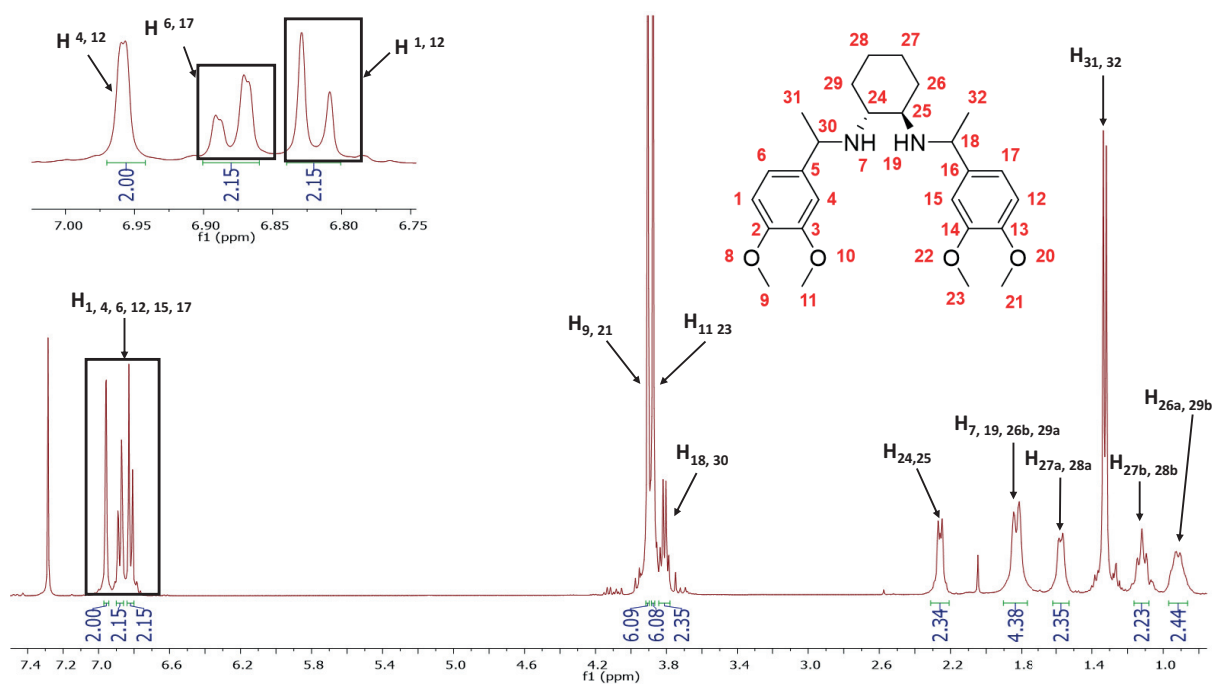
Figure A19: ^{1}H-NMR (360 MHz, CDCl$_3$) of **33**
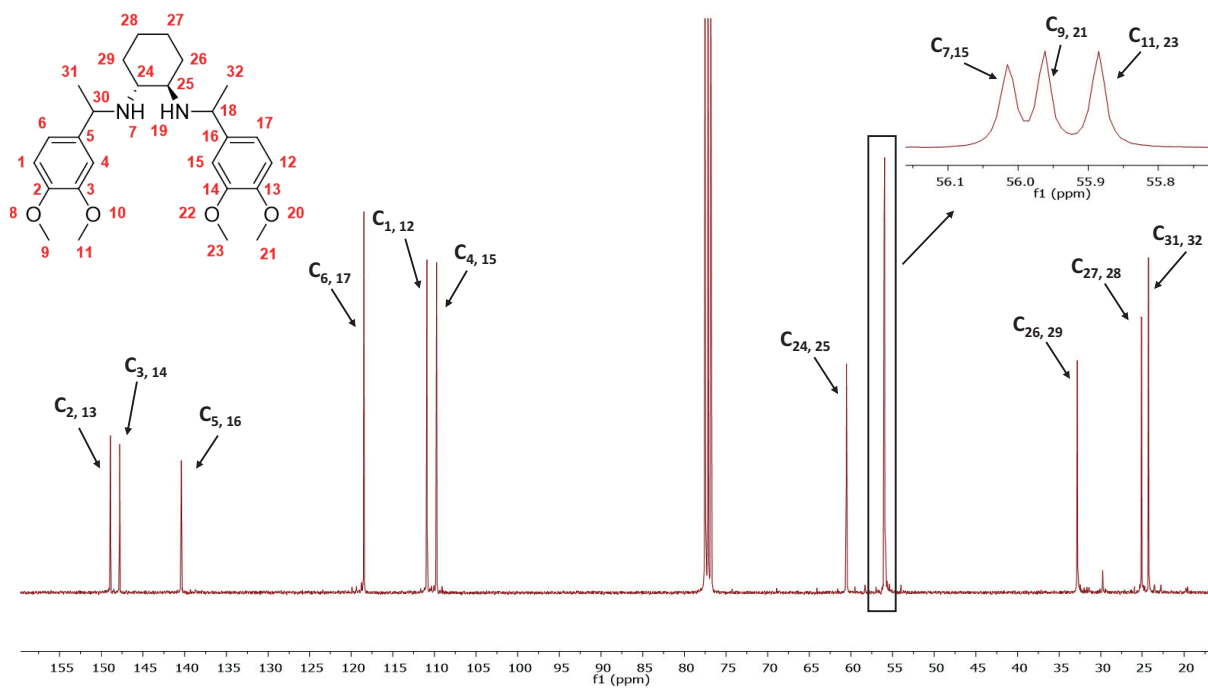
Figure A20: ^{13}C-NMR (100 MHz, CDCl$_3$) of **33**
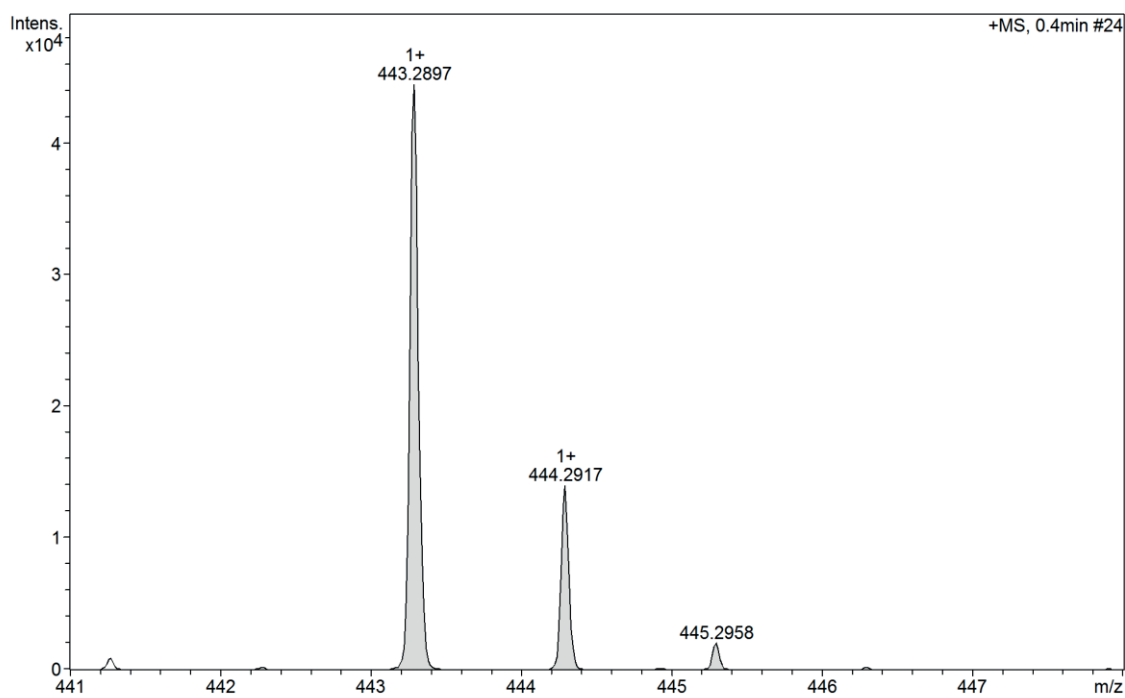
Figure A21: ESI-HRMS spectrum of **33**
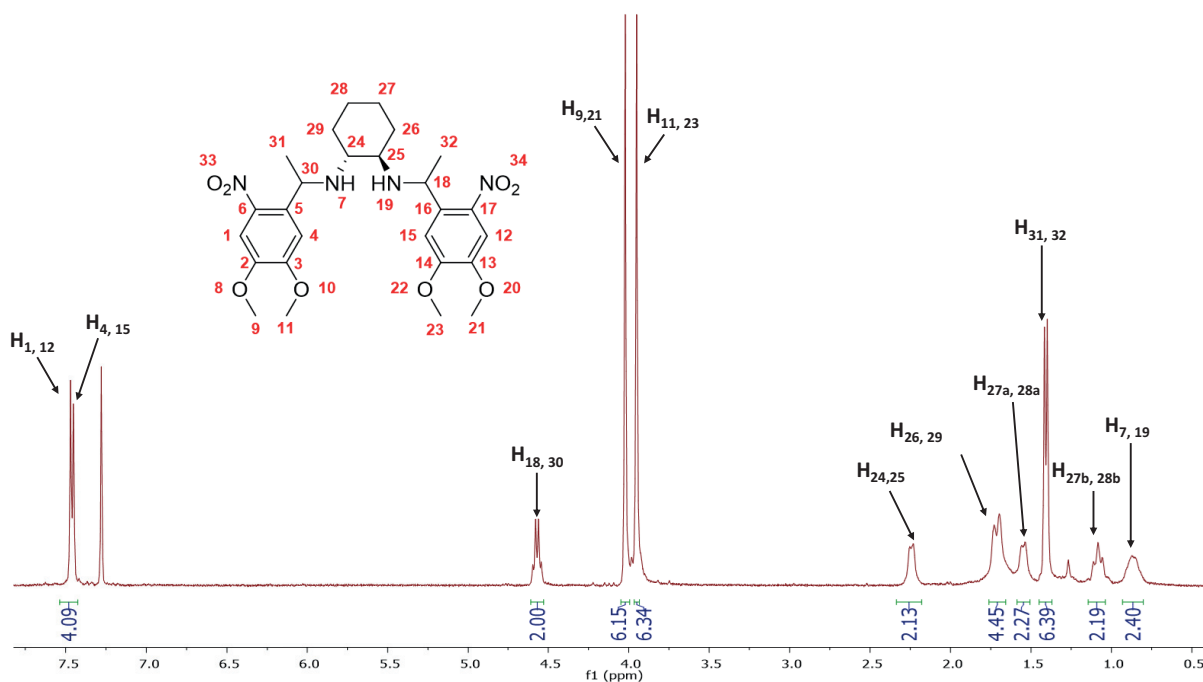
Figure A22: ^{1}H-NMR (360 MHz, CDCl$_3$) of **L2**
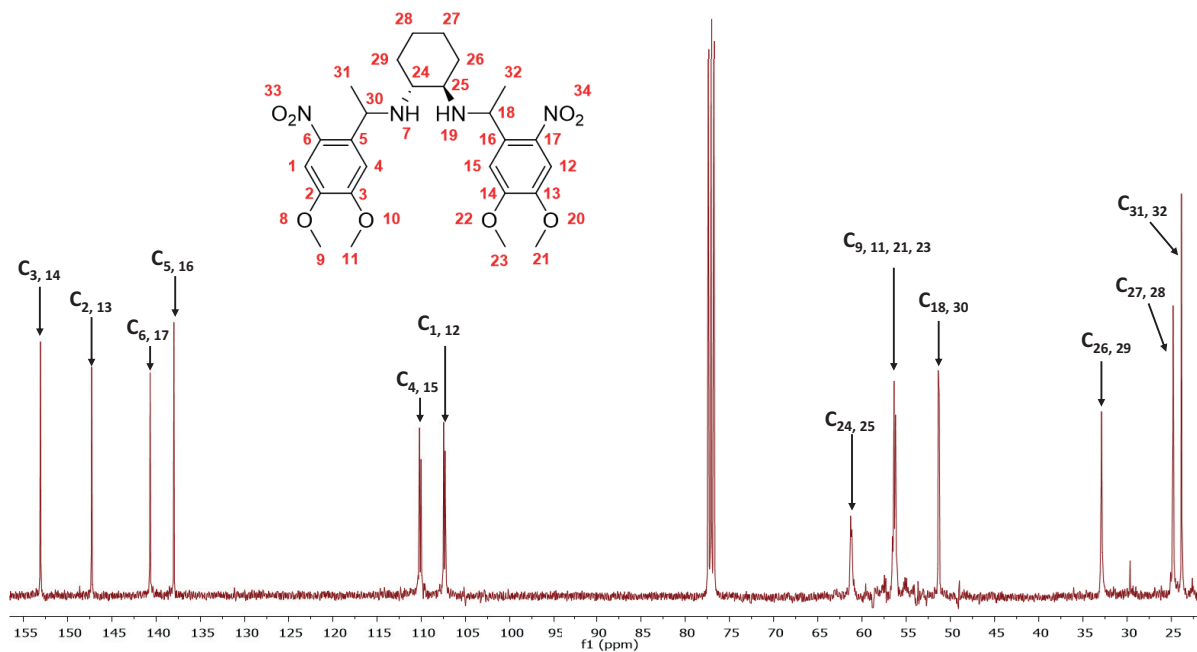
Figure A23: ^{13}C-NMR (100 MHz, CDCl$_3$) of **L2**
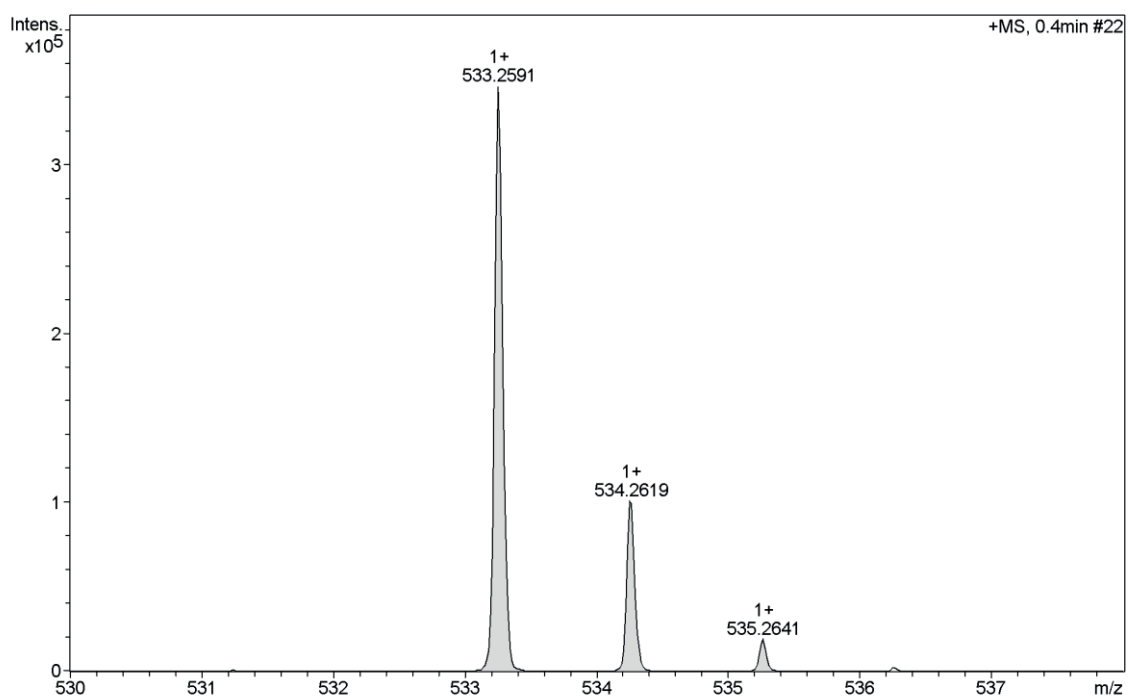
Figure A24: ESI-HRMS spectrum of **L2**
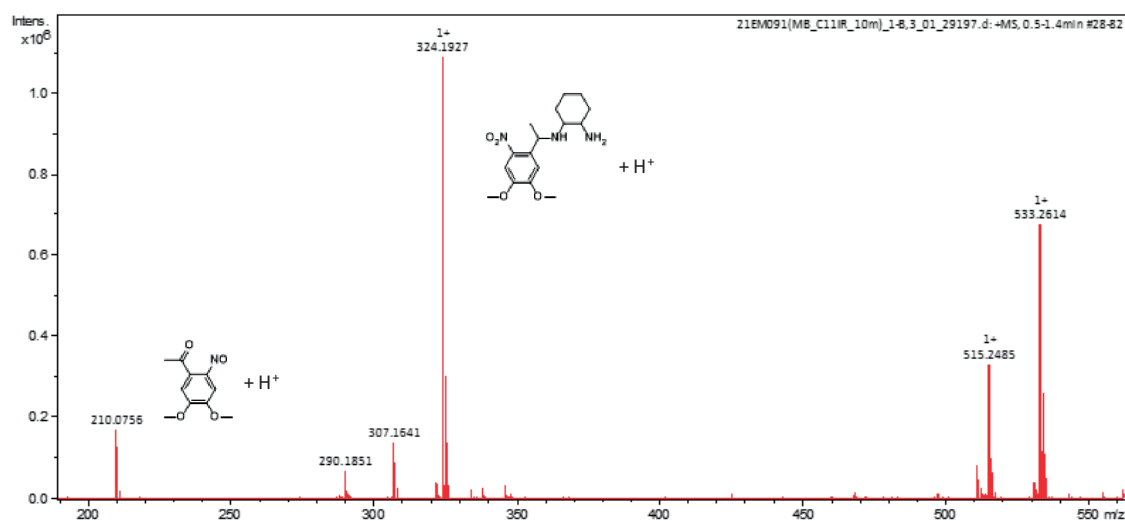
Figure A25: ESI-HRMS spectrum of **L2 IR**
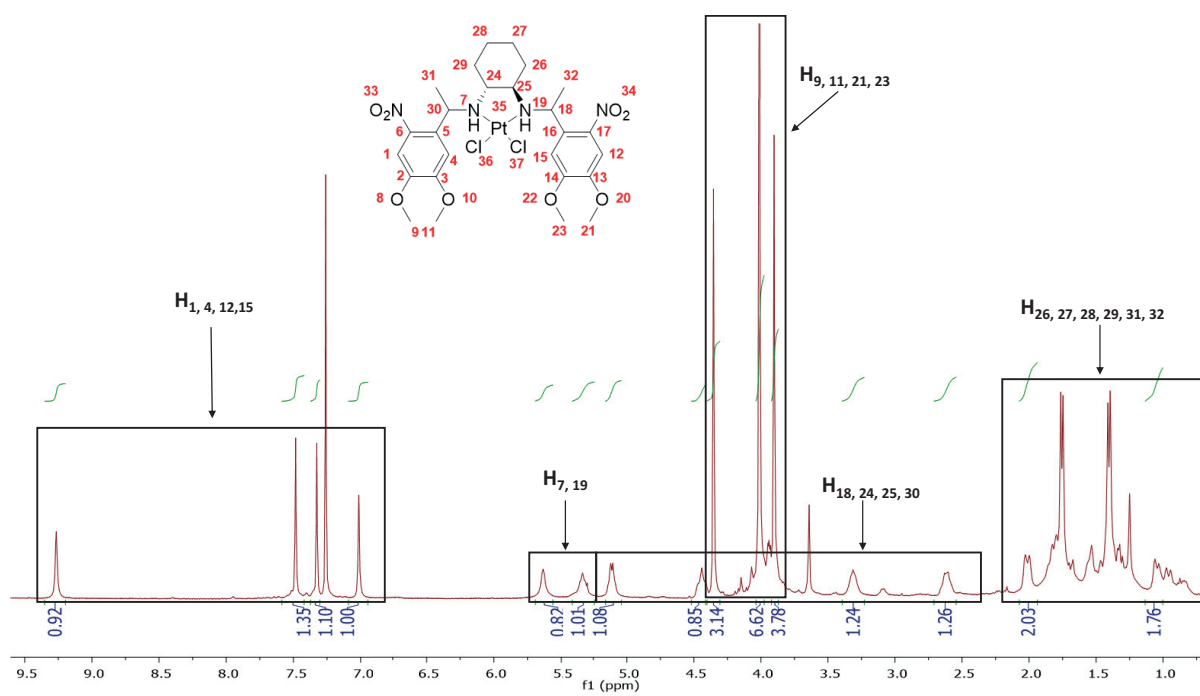
Figure A26: ^{1}H-NMR (400 MHz, CDCl$_3$) of **C2**
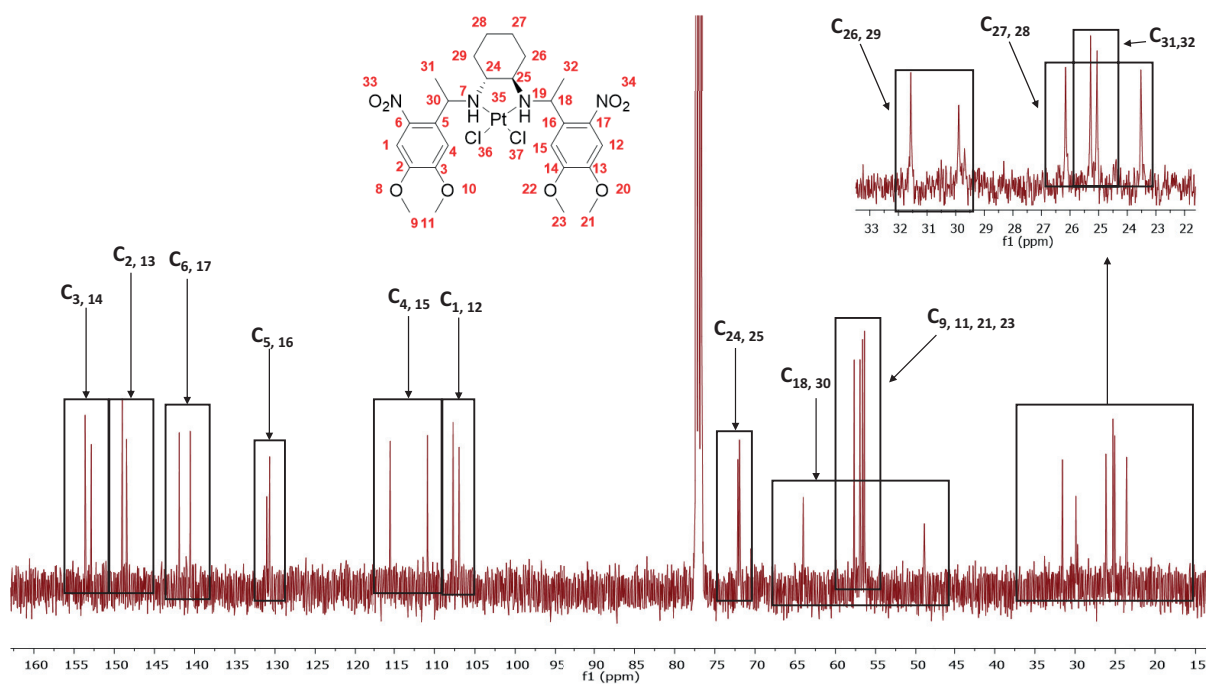
Figure A27: ^{13}C-NMR (100 MHz, CDCl$_3$) of **C2**
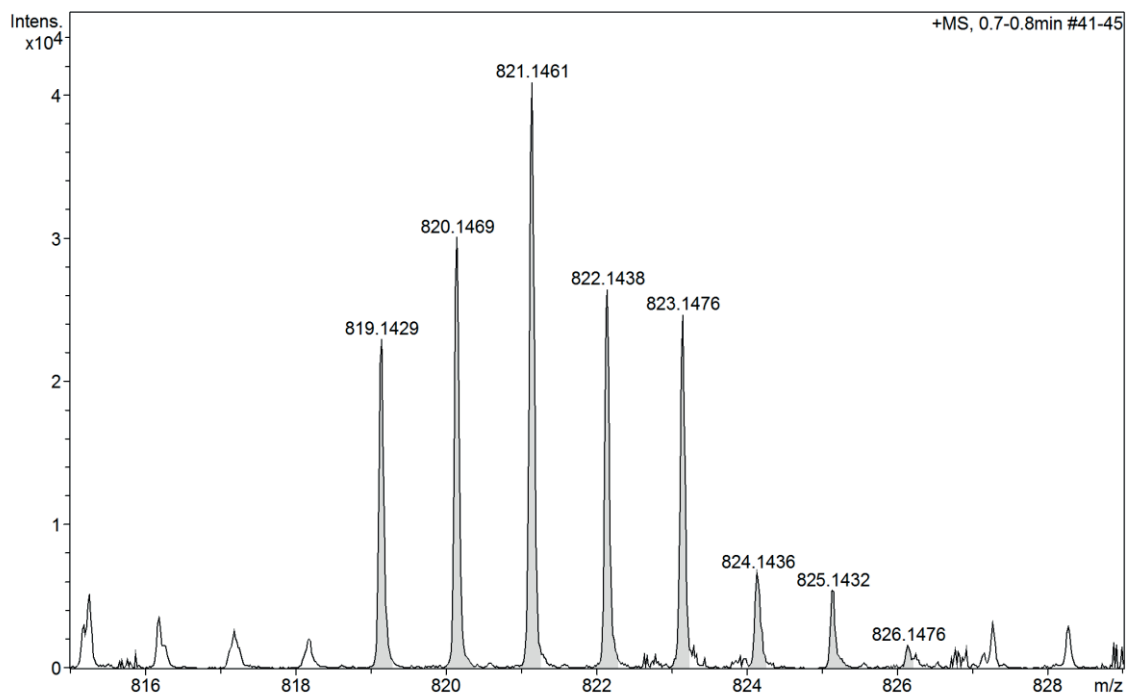
Figure A28: ESI-HRMS spectrum of **C2**
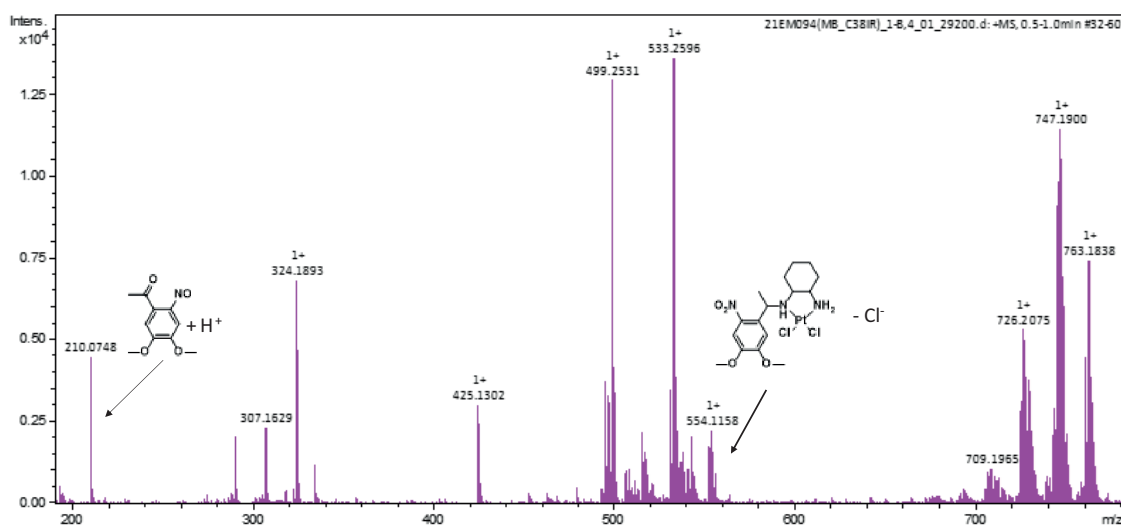
Figure A29: ESI-HRMS spectrum of **C2**
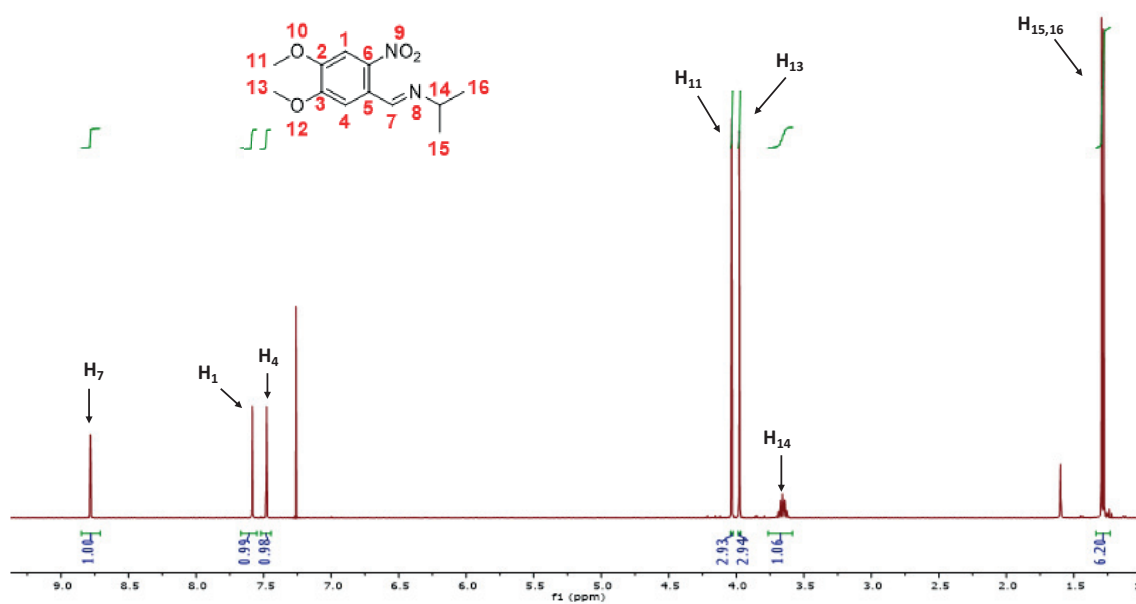
Figure A30: ^{1}H-NMR (400 MHz, CDCl$_3$) of **41**
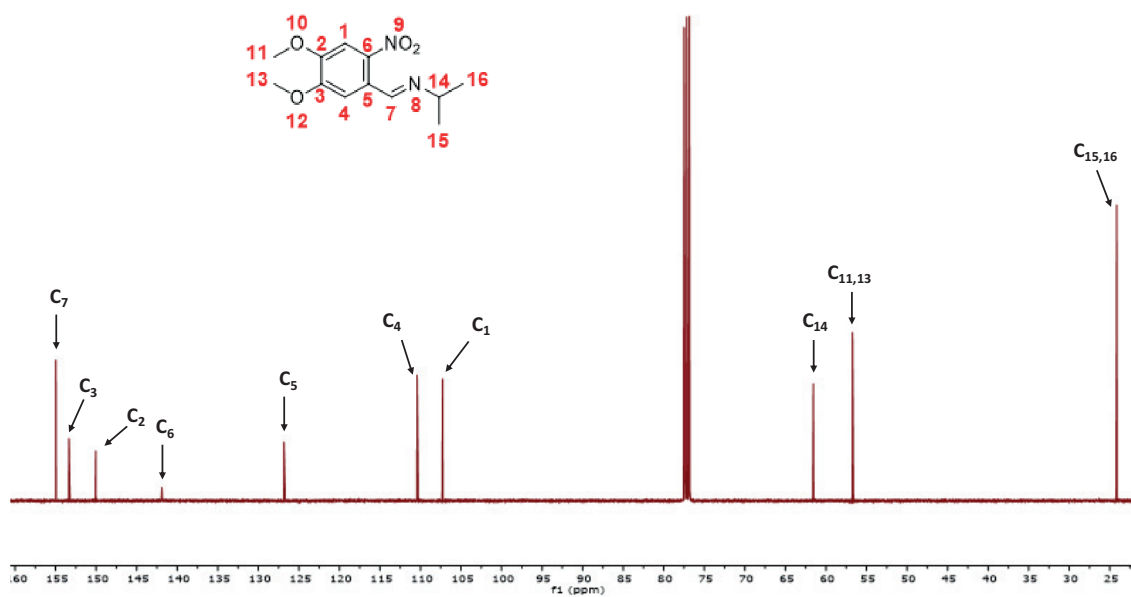
Figure A31: ^{13}C-NMR (100 MHz, CDCl$_3$) of **41**
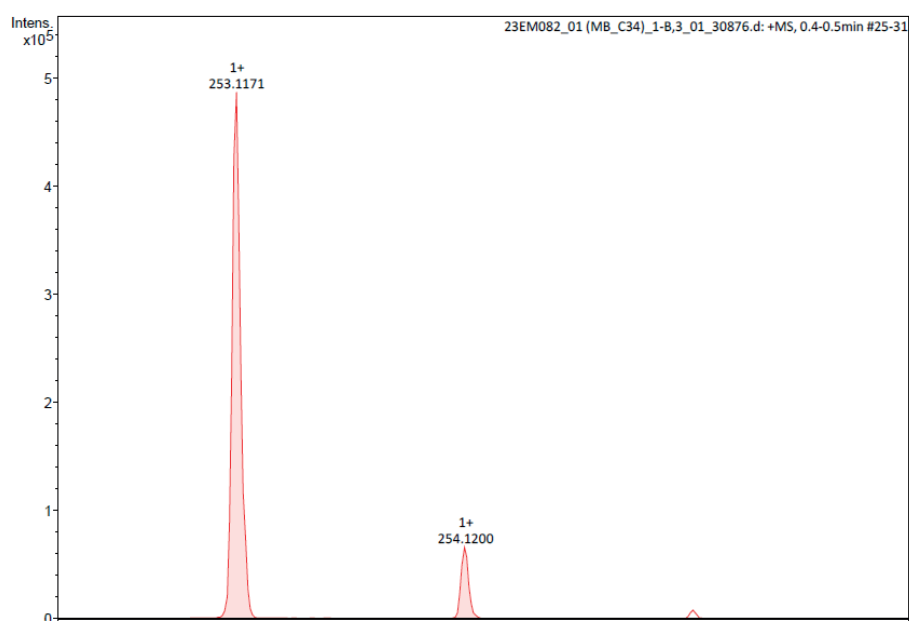
Figure A32: ESI-HRMS spectrum of **41**
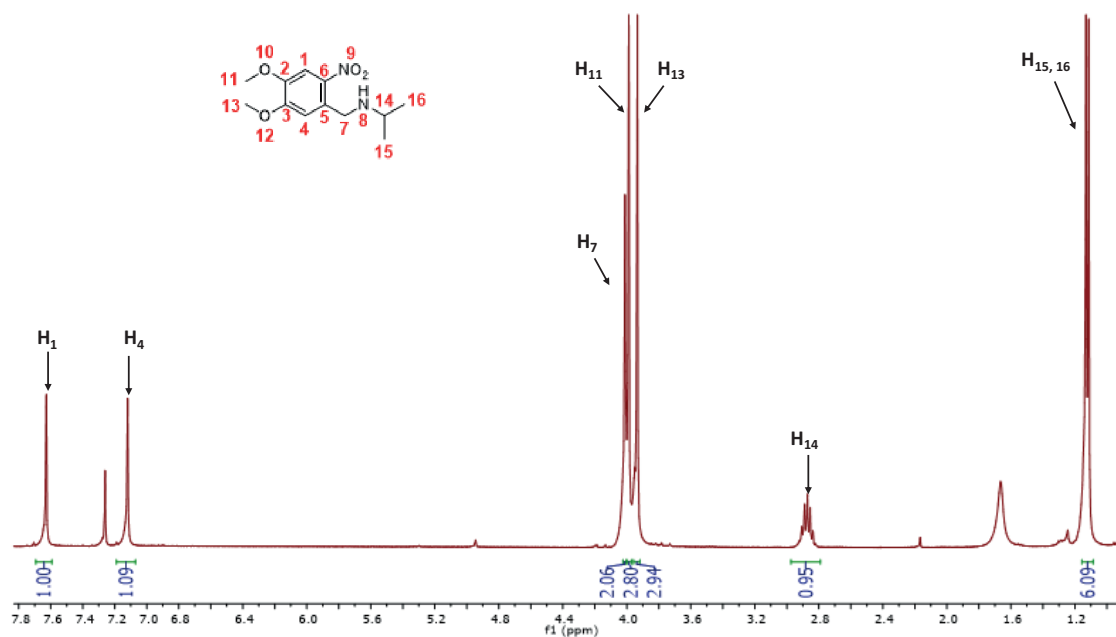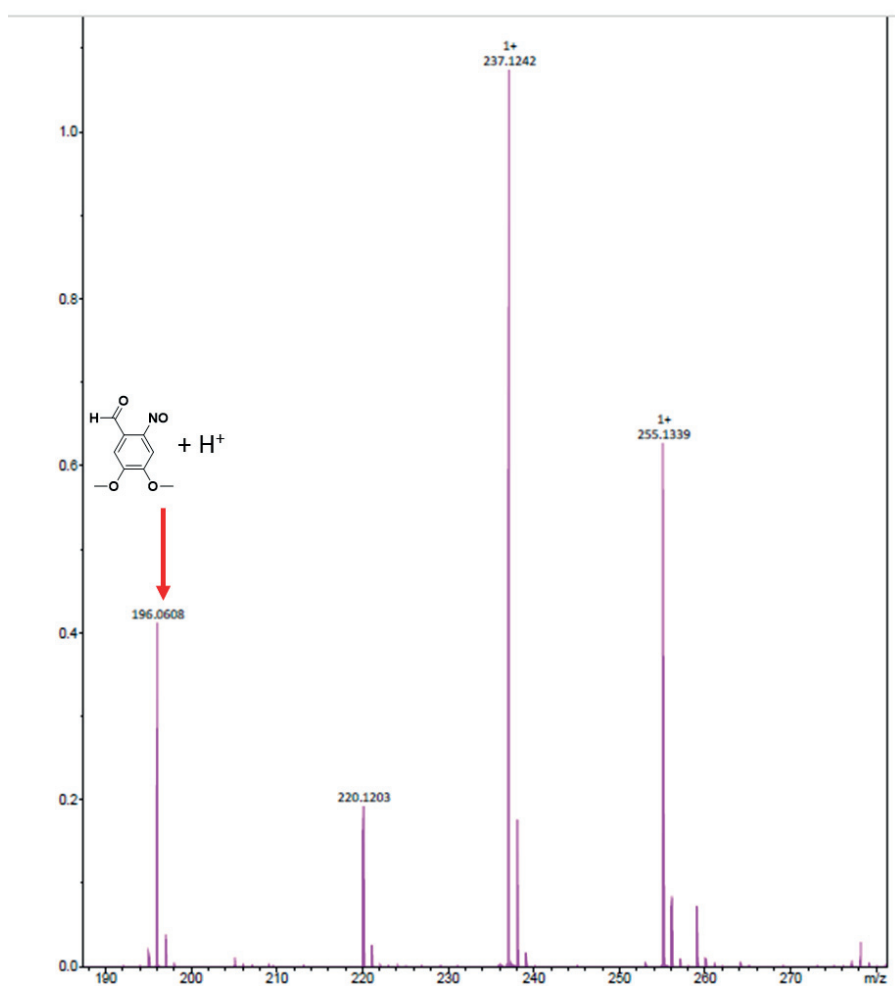
Figure A33: ^{1}H-NMR (400 MHz, CDCl$_3$) of **40**
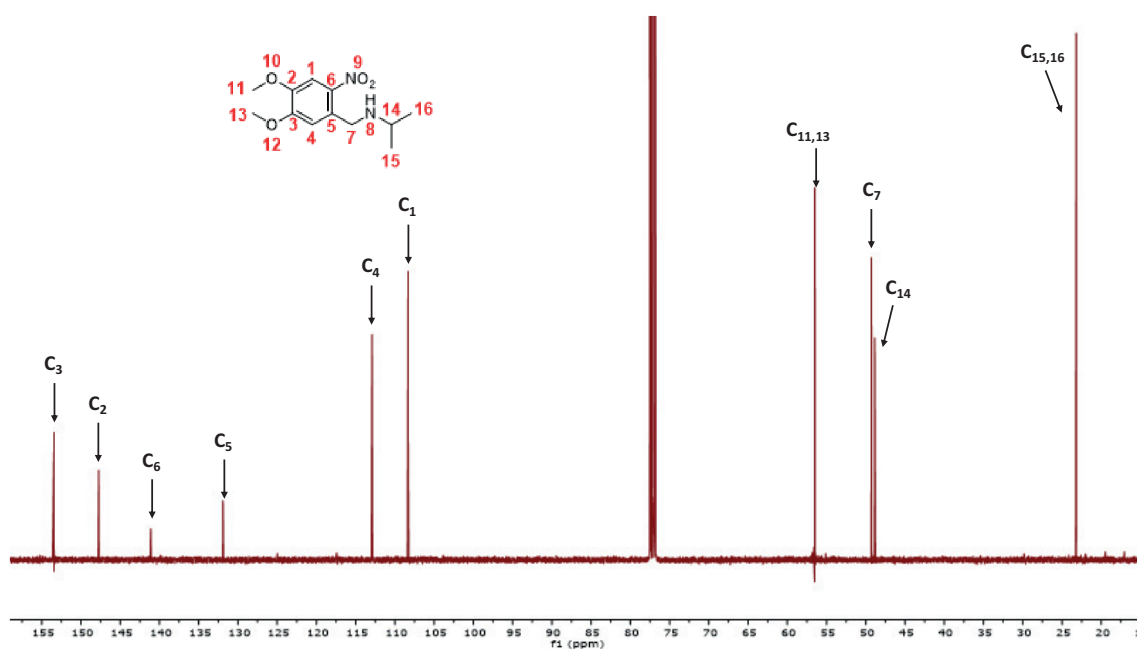
Figure A34: ^{13}C-NMR (100 MHz, CDCl$_3$) of **40**
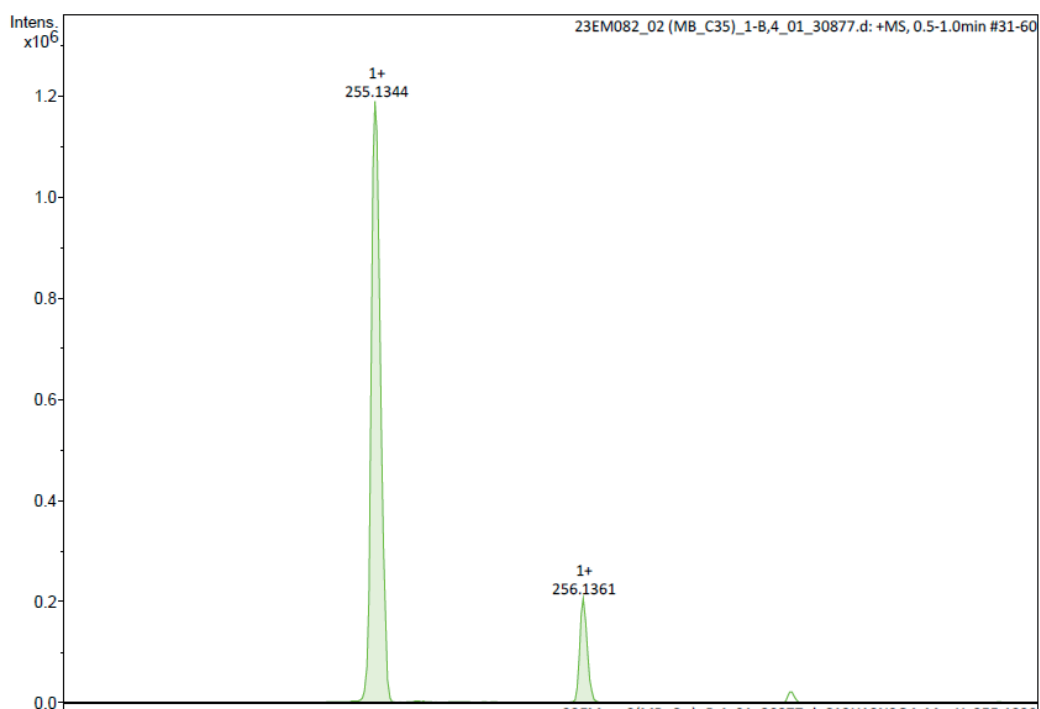
Figure A35: ESI-HRMS spectrum of **40**

Figure A36: ESI-HRMS spectrum of **40** after irradiating for 80 min at 365 nm.
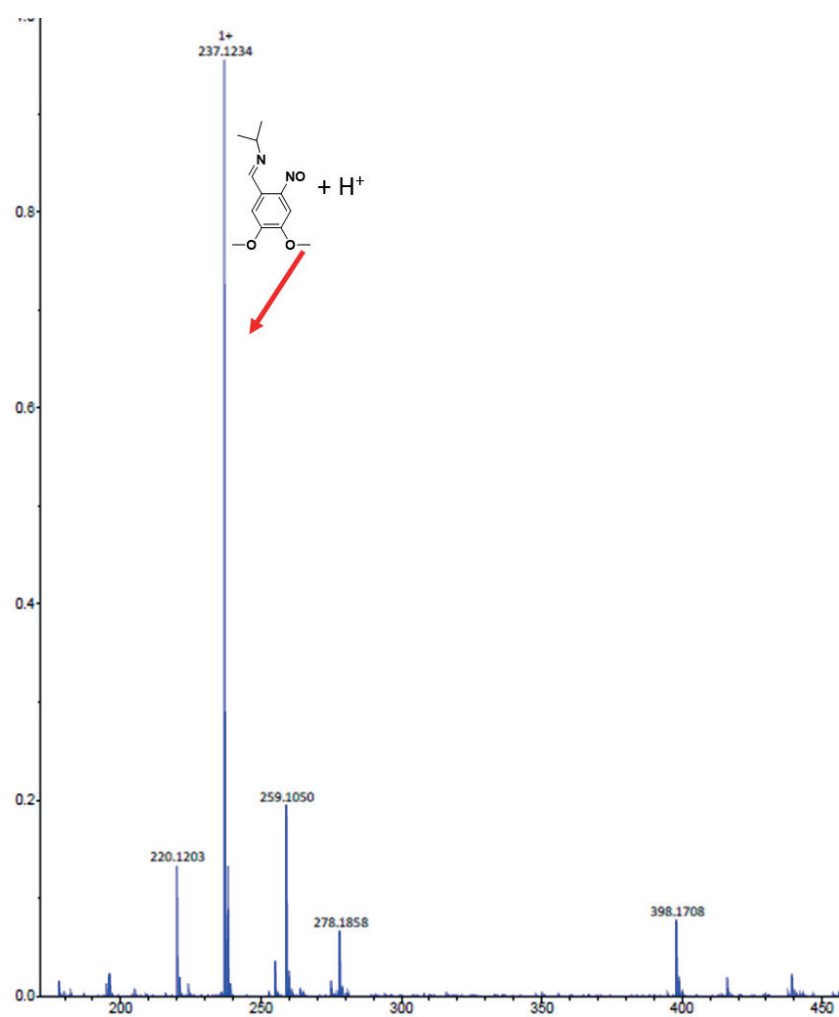
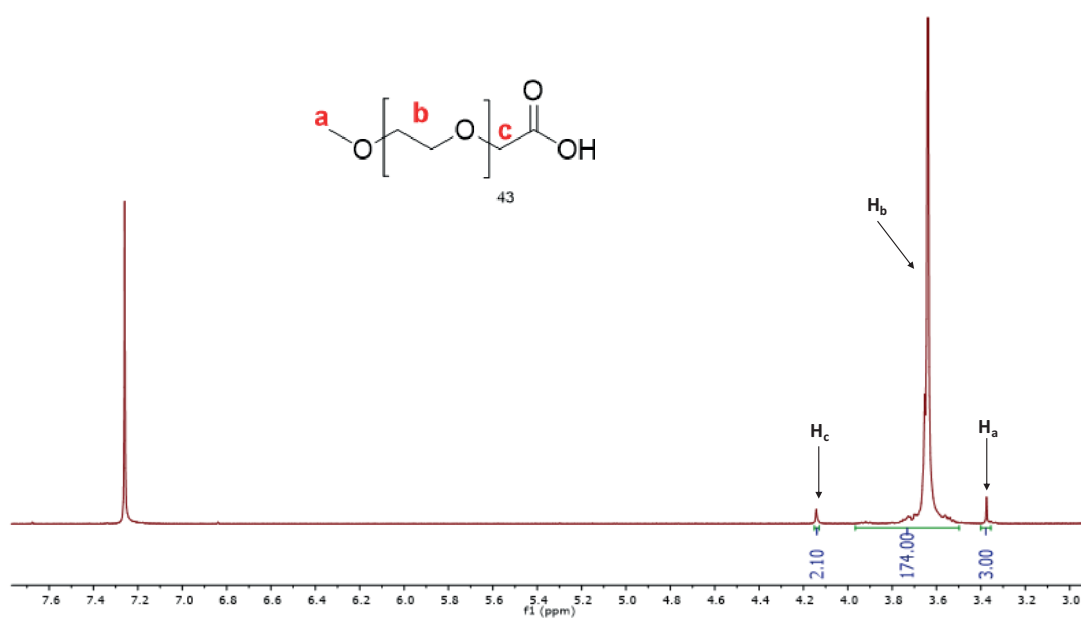**Figure A37:** ESI-HRMS spectrum of **40** after irradiating for 210 min at 365 nm.
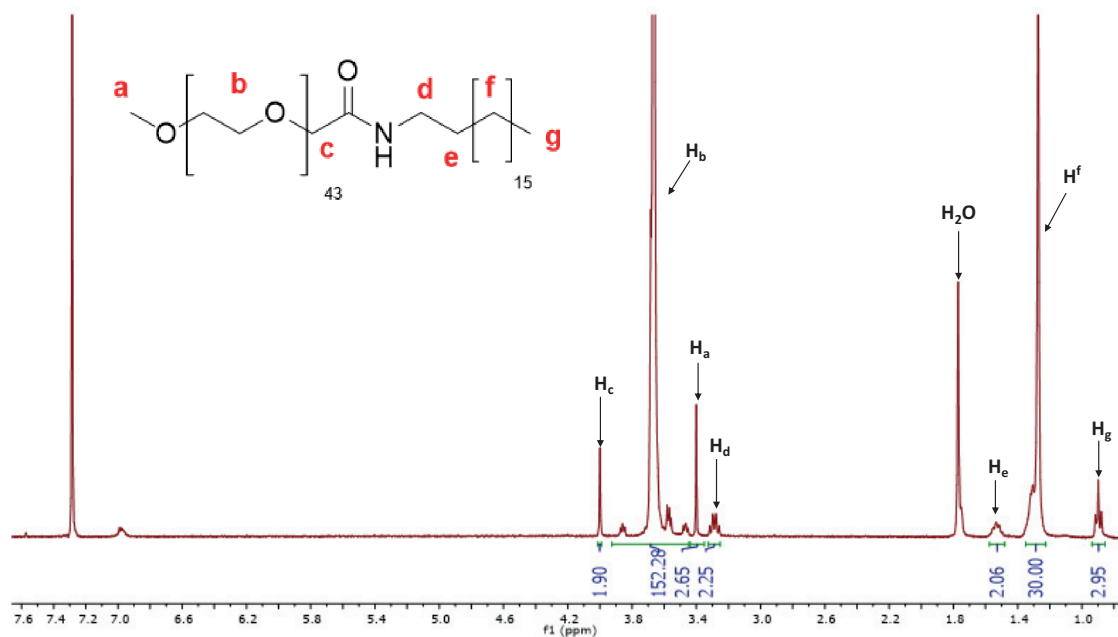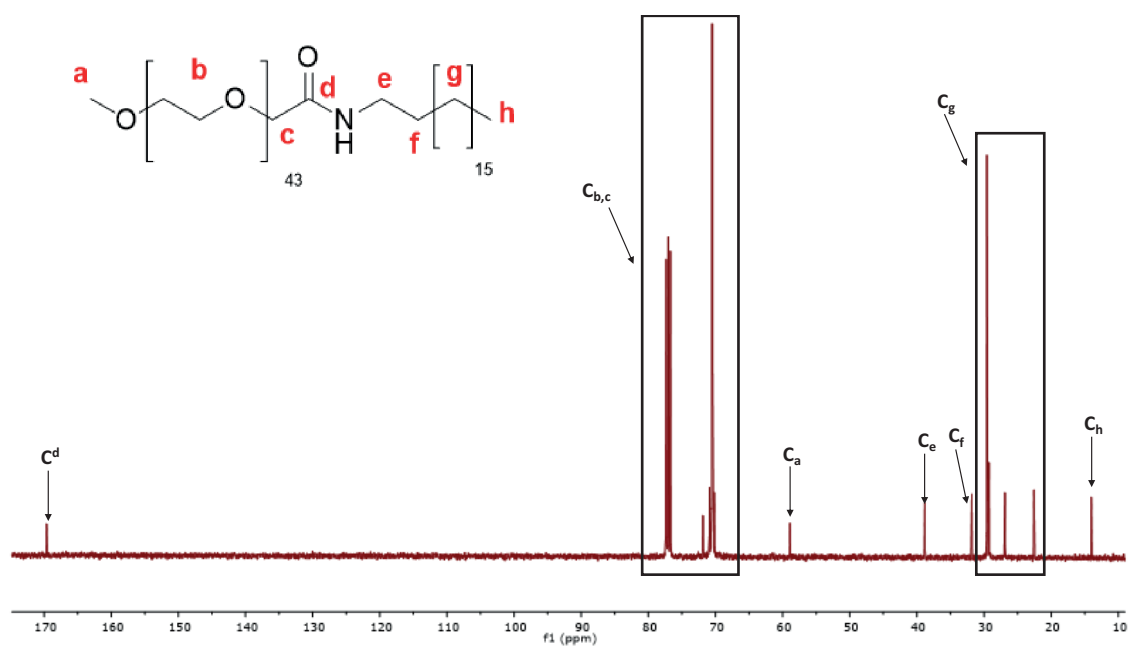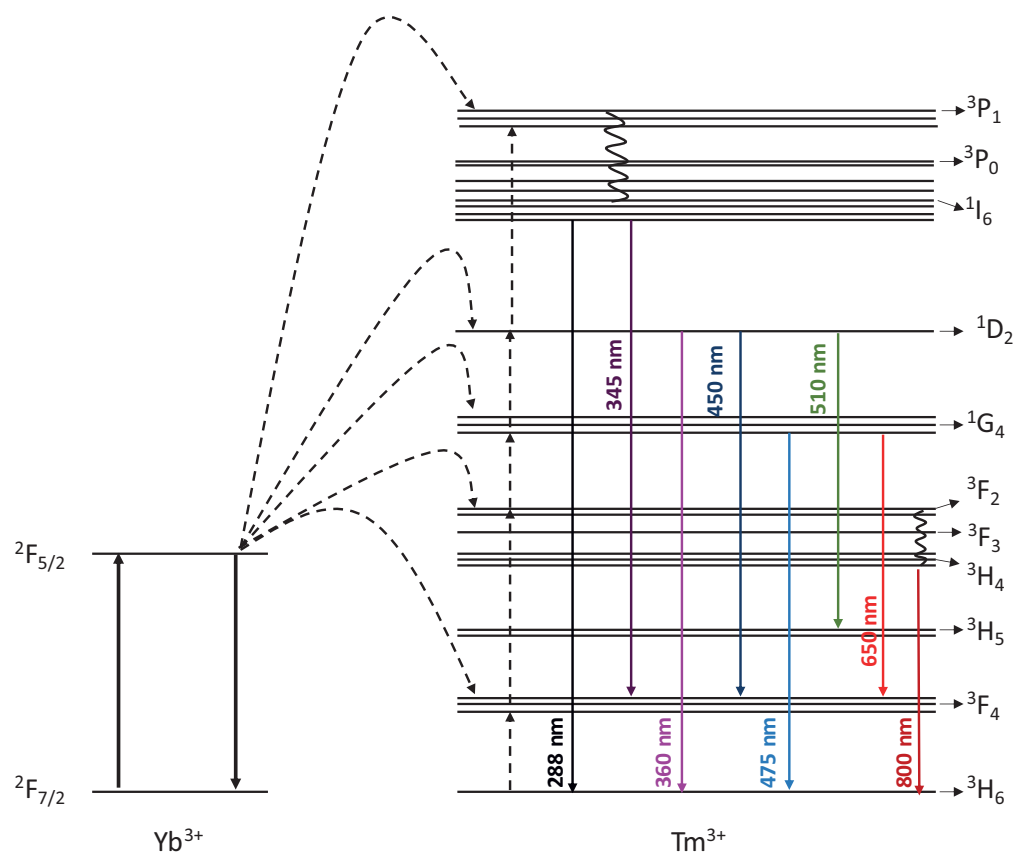
Figure A38: ^{1}H-NMR (360 MHz, CDCl$_3$) of **mPEG-COOH**

Figure A39: ^{1}H-NMR (360 MHz, CDCl$_3$) of **mPEG-COOH**

Figure A40: ^{13}C-NMR (100 MHz, CDCl$_3$) of **mPEG-COOH**

Fig A41: Energy level diagram of ETU between Yb^{3+} and Tm^{3+}

Figure A42: Assembly for the second step of LiYF$_4$;Yb^{3+};Tm^{3+} synthesis
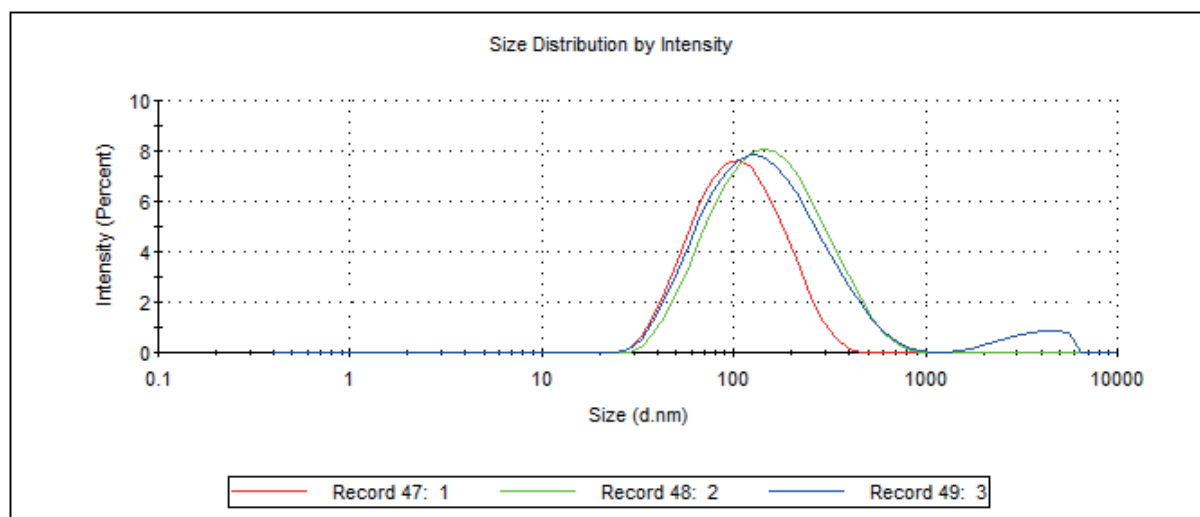
Figure A43: DLS of the platforms Pt(II)/UCNPs/mPEG-ODA synthesised

Table A.1: Evaluation of Pt(II) released at different times for each platform under different conditions: in the dark, under UV and NIR light irradiation

| | % Pt(II) released of C1/UCNPs/mPEG-ODA | | | | | | % Pt(II) released C2/UCNPs/mPEG-ODA | | | | | |
| | Test 1 | | | Test 2 | | | Test 1 | | | Test 2 | | |
Time (min)	Dark	UV	NIR	Dark	UV	NIR	Dark	UV	NIR	Dark	UV	NIR
0	0,00	0,00	0,00	0,00	0,00	0,00	0,00	0,00	0,00	0,00	0,00	0,00
15	-0,12	12,25	33,83	34,68	59,37	38,64	2,58	17,20	39,29	14,58	61,50	54,82
30	-0,05	40,35	41,82	38,56	63,95	42,85	4,43	31,35	45,53	22,99	63,57	56,66
60	0,59	62,23	44,64	42,09	69,53	52,18	5,93	45,60	51,20	31,51	69,95	62,35
90	1,06	63,82	56,45	46,33	71,50	53,93	18,60	53,16	51,82	32,87	70,83	63,13
120	1,46	76,25	72,61	49,16	76,74	55,01	25,89	53,11	47,18	34,55	76,60	68,27
180	2,44	72,35	70,22	50,81	78,85	61,46	30,07	54,16	55,88	38,15	77,19	68,80
240	3,58	70,24	69,38	53,67	86,18	64,82	31,62	56,08	54,62	39,67	83,48	74,41
360	23,91	75,42	70,57	55,62	92,42	80,32	25,32	55,21	51,36	39,82	94,39	84,13
480	34,51	69,27	67,50	56,06	93,13	83,53	25,56	54,21	49,23	41,43	96,39	85,91
1440	30,85	75,05	61,07	57,10	94,88	85,97	29,51	52,96	53,05	48,16	96,75	86,23